UAB
Universitat Autònoma de Barcelona

Role of Plant Fibrillin 6 and Alternative Oxidase during Carotenoid Biosynthesis and Stress Response

Ariadna Iglesias Sanchez

ADVERTIMENT. L'accés als continguts d'aquesta tesi queda condicionat a l'acceptació de les condicions d'ús establertes per la següent llicència Creative Commons:  https://creativecommons.org/licenses/?lang=ca

ADVERTENCIA. El acceso a los contenidos de esta tesis queda condicionado a la aceptación de las condiciones de uso establecidas por la siguiente licencia Creative Commons:  https://creativecommons.org/licenses/?lang=es

WARNING. The access to the contents of this doctoral thesis it is limited to the acceptance of the use conditions set by the following Creative Commons license:  https://creativecommons.org/licenses/?lang=en

UAB
Universitat Autònoma
de Barcelona

CRAG
CENTRE FOR RESEARCH
IN AGRICULTURAL GENOMICS

UNIVERSITAT AUTÒNOMA DE BARCELONA
Facultat de Biociències
Programa de Doctorat en Biologia y Biotecnologia Vegetal

Role of Plant Fibrillin 6 and Alternative Oxidase during Carotenoid Biosynthesis and Stress Response

Dissertation presented by Ariadna Iglesias Sanchez for the degree of Doctor of Biology and Plant Biotechnology by the *Universitat Autònoma de Barcelona*.
This work was performed at the Center for Research in Agricultural Genomics.

Dr. Igor Florez Sarasa
Thesis director

Dr. Manuel Rodríguez Concepción
Thesis director

Ariadna Iglesias Sanchez
Ph. D. Candidate

Index

Abbreviations **11**

Summary **17**

General Introduction **19**

1. Plant carotenoids: biosynthesis and functions 21
2. Plant plastoglobules and fibrillins: roles in carotenoid accumulation and stress 23
3. Plant mitochondria and their energy-bypass systems 26
4. Plastid-mitochondria interactions 29

Objectives 35

Chapter 1: Arabidopsis FIBRILLIN6 influences carotenoid biosynthesis by directly promoting phytoene synthase activity **37**

Introduction 39

Materials and methods 40

Plant material and growth conditions 40

Gene constructs 41

Microscopy 41

Co-immunoprecipitation and immunoblot assays 42

Gene expression and metabolite analysis 42

Statistical analyses 42

Accession numbers 42

Results and discussion 43

Arabidopsis FBN6 and PSY physically interact in particular subplastidial locations 43

FBN6 promotes PSY activity 46

Genetic evidence confirms the functional relevance of FBN6 for PSY activity 47

An alternative connection between FBNs and carotenoids 49

Supplemental Data 53

Chapter 2. The Lack of Alternative Oxidase 1a Restricts in vivo Respiratory Activity and Stress-Related Metabolism for Leaf Osmoprotection and Redox Balancing Under Sudden Acute Water and Salt Stress in *Arabidopsis thaliana* **57**

Introduction 59
Materials and methods 61
Plant Material and Growth Conditions 61
Leaf Water Status 62
Respiration Measurements 62
Photosynthetic Measurements 62
Metabolite Profiling 63
Western Blot Analysis 64
Gene Expression Analysis 64
Statistical Analyses 65
Results 65
The Alternative Oxidase Capacity and Expression in aox1a and Wild-Type Plants Under Control and Stress Conditions 65
Leaf Phenotype and Water Status in *aox1a* and Wild-Type Plants Under Control and Stress Conditions 67
Photosynthetic Parameters in *aox1a* and Wild-Type Plants Under Control and Stress Conditions 68
Metabolite Profiling in *aox1a* and Wild-Type Plants Under Control and Stress Conditions 71
Gene Expression of Other Alternative Respiratory Components in *aox1a* and Wild-Type Plants Under Control and Stress Conditions 73
Discussion 74
The Lack of *AOX1a* Does Not Impair Alternative Oxidase Pathway *in vivo* Activity Under Control Conditions but Restricted Its Response to Stress 75
The Lack *in vivo* Alternative Oxidase Pathway Response Under Stress Altered the Accumulation of Stress-Related Metabolites Involved in Leaf Osmoregulation and Redox Balance 78
Conclusion 82
Supplemental Data 83
Chapter 3: The in vivo post-translational activation of alternative oxidase triggers climacteric respiration in tomato 90
Introduction 91
Material and Methods 93
Plant material and growth conditions 93
Respiration and oxygen isotope discrimination analysis 93

Gene Expression analysis 95
Primary metabolite and carotenoids profiling 95
Statistical Analyses 96
Results 96
Measurements of oxygen consumption in tomato fruit tissues 96
Measurements of oxygen isotope discrimination in tomato fruit tissues 98
Respiration and electron partitioning between AOX and COX during ripening 99
Transcript levels of AOX and ripening-related genes during tomato fruit ripening 100
Metabolite profiles in WT and *ghost* fruits during ripening 102
Discussion 105
^{18}O discrimination analyses in WT and *ghost* mutants: new opportunities and future perspectives 105
In vivo regulation of fruit respiration and consequences for energy metabolism during tomato fruit ripening. 107
Coordinated changes in primary metabolism and electron partitioning to AOX allows for the accumulation of key ripening-related metabolic precursors 108
Conclusion 111
Supplemental Data 112
Chapter 4: Lack of alternative oxidase 1a restricts carbon supply for carotenoid and ethylene biosynthesis during tomato fruit ripening 118
Introduction 119
Material and methods 121
Plant material and growth conditions 121
Constructs and tomato transformation 122
Plant growth and development characterization 122
Respiration analysis 122
Gene expression analysis 123
Primary metabolite profiling 124
Carotenoids and chlorophylls analysis 124
Statistical and data analyses 125
Results and discussion 125
Generation of *AOX1a* knock-out lines 125
Mutant *aox1a* lines show alterations in growth and development 126
Inhibition of fruit AOX *in vivo* delays the onset of ripening 128

Lack of AOX1a disturbs the peak of climacteric respiration and carotenoid accumulation 132

Lack of AOX1a strongly restricts the synthesis of primary metabolite precursors for ethylene biosynthesis 136

Conclusions 143

Supplemental data 145

General Discussion 155

1. Ensuring supply of carotenoid precursors: a major challenge with multiple regulatory checkpoints 156

2. FIBRILLIN6 (FBN6) modulates PSY activity and carotenoid biosynthesis. . 157

3. The role of alternative oxidase (AOX) pathway in primary metabolism during stress 159

4. The role of AOX during fruit ripening 162

Conclusions 166

References 170

Annex 1 196

Annex 2 218

Annex 3 242

Annex 4 268

Index of Figures and Tables

Figure I-1. Schematic representation of the carotenoid biosynthesis pathway. 22

Figure I-2. Illustration of the physical link between the thylakoid membrane and the plastoglobule (PG).....23

Figure I-3. Representation of the respiratory pathways in the mitochondrial electron transport chain (mETC) and ATP synthase in the inner membrane of plant mitochondria. 28

Figure I-4. Simplified metabolic interactions between chloroplasts and mitochondria in photosynthetic tissues.....30

Figure I-5: Interactions between chromoplasts and mitochondria. 33

Figure C1-1. FBN6 and PSY can be immunoprecipitated together. N. benthamiana leaves were co-agroinfiltrated with the indicated combinations of proteins with C-terminal myc or GFP tags.....44

Figure C1-2. FBN6 and PSY co-localize in chloroplasts.....45

Figure C1-3. FBN6 promotes phytoene and downstream carotenoid production. 47

Figure C1-4. FBN6 is required for carotenoid production in Arabidopsis.....51

Figure C2-1. Alternative oxidase (AOX) pathway capacity (Valt) and expression analysis.....67

Figure C2-2. Visual phenotype and relative water content. 68

Figure C2-3. Photosynthetic activity and capacity under different light intensities.....70

Figure C2-4. Metabolite profiles showing relative changes in primary metabolism. 72

Figure C2-5. Gene expression analyses of alternative respiratory components.....74

Figure C2-6. Schematic overview illustrating the impact of in vivo AOP restriction on leaf cell physiology and metabolism in aox1a plants after A) salt and B) mannitol treatments. 80

Figure C3-1. Wild-type (WT) and ghost mutant visual phenotypes. 97

Table C3-1. Oxygen isotope discrimination (‰) in the absence of inhibitors (Δn), in the presence of 20 mM SHAM (Δc-SHAM), 5 mM KCN (Δa) and 1 mM OGAL (Δc-OGAL) 99

Figure C3-2. Respiratory pathways in wild-type (WT) fruits at different ripening stages. 100

Figure C3-3. Relative transcript levels of AOX- and ripening-related genes in WT and ghost mutant fruits at different ripening stages. 101

Figure C3-4. Metabolite profiles showing relative changes in primary metabolism in WT and ghost fruits at different ripening stages. 103

Figure C3-5. Levels of individual carotenoids (phytoene, lycopene, lutein and b-carotene) as well as total carotenoids and chlorophylls in fruits of WT and ghost mutant at different ripening stages. 104

Figure C3-6. Metabolic model showing changes in respiratory and associated metabolism at the climacteric peak of WT tomato fruit ripening (BR stage). 110

Figure C4-1. Tomato *aox1a* mutants 126

Figure C4-2. Wild-type and *aox1a* mutant lines 128

Figure C4-4. Visual phenotypes and ripening stages of tomato fruits from wild-type (WT) and *aox1a* mutant (a1.1 and a2.3) lines. 131

Figure C4-5. Respiration analyses on fruits of WT and *aox1a* mutant lines harvested at MG, MG+1, MG+2, MG+3, MG+5, MG+7, MG+9, MG+11, and MG+13 ripening stages. 134

Figure C4-6. Relative transcript levels of AOX- and ripening-related genes in WT and *aox1a* mutant fruits at different ripening stages. 135

Figure C4-7. Heatmap showing relative changes in primary metabolism in WT and *aox1a* mutant fruits at different ripening stages. 138

Figure C4-8. Levels of individual carotenoids (phytoene, lutein, lycopene, and b-carotene) as well as total carotenoids and chlorophylls in fruits of WT and *aox1a* mutant lines at different ripening stages. 139

Figure C4-9. Metabolite profiles showing relative changes in primary metabolism in WT and *aox1a* mutant fruits during ripened stages (MG +5, MG+7, MG+9, MG+11 , and MG+13). 141

Figure C4-10. Metabolite profiling showing relative changes in primary metabolism in WT and *aox1a* mutant fruits during non-ripened stages (MG, MG+1, MG+2, and MG+3). 143

Figure D-1: Schematic overview illustrating the impact of AOX pathway restriction on leaf cell physiology and metabolism in *Arabidopsis thaliana* (Chapter 2; Del-Saz et al., 2022; Annex 3) and Medicago truncatula (Del-Saz et al., 2016) plants after 1 day of salt stress treatment. 160

Figure D-2. Schematic overview illustrating the impact of in vivo AOP restriction on tomato fruit metabolism in A) breaker (BR) and B) red ripe (RR) stage. 165

Index of Supplemental Figures

Supplemental Table C1-1. Primers used in this work. 53

Supplemental Table C1-2. Phytoene levels in control and NFZ-treated N. benthamiana leaves agroinfiltrated with FBN6 and/or PSY constructs.....53

Supplemental Table C1-3. Photosynthetic pigment levels in N. benthamiana leaves agroinfiltrated with FBN6, PSY and/or crtB constructs.....54

Supplemental Table C1-4. Photosynthetic pigment levels in etiolated and deetiolated WT and fbn6 Arabidopsis seedlings.....54

Supplemental Table C1-5. Photosynthetic pigment levels in WT and fbn6 Arabidopsis seedlings exposed to high light. 54

Supplemental Table C2-1. Overview of the metabolite reporting list.....83

Supplemental Table C2-2. Relative metabolite levels in leaves of WT and aox1a plants under control conditions and after 1 day of severe (300 mM) NaCl and Mannitol treatments 84

Supplemental Table C2-3. Absolute metabolite levels in leaves of WT and AOX1a plants under control conditions and after 1 day of severe (300 mM) NaCl and Mannitol treatments 85

Supplemental Table C2-4. Primers used in the qPCR analyses performed in this study86

Supplementary Figure C2-1. Gene expression analyses of alternative respiratory components under control conditions.....87

Supplementary Figure C2-2. Metabolite profiles showing absolute changes in primary metabolism. Coloured table showing the absolute levels (μmol gDW–1) of the GC-MS-analysed metabolites in leaves of wild-type Col 0 (WT) and *aox1a A. thaliana* plants untreated with NaCl or Mannitol (Control), and after 1 day of severe NaCl or Mannitol treatments (300 mM).....88

Supplemental Figure C3-1. Photographs of the sliced pericarp tissue at MG and R stages of different sizes placed at the DI-IRMS cuvette, and effects on the 18O discrimination. 112

Supplementary Figure C3-2. Changes in respiratory and associated metabolism at the climacteric peak of ghost tomato fruit ripening (BR stage). 113

Supplemental Table C3-1. Primers used in qPCR studies performed in this work.....114

Supplemental Table C3-2. Parameters used for peak annotation of all detected metabolites. 115

Supplemental Table C3-3. Relative metabolite levels detected by GC-MS in WT tomato fruits 116

Supplemental Table C3-4. Relative metabolite levels detected by GC-MS in ghost tomato fruits. 117

Supplemental Table C4-1. Primers used in this work 145

Supplemental Table C4-2. Parameters used for peak annotation of all detected metabolites. 146

Supplemental Table C4-3. Relative metabolite levels from MG+5 to MG+13 stages detected by GC-MS in tomato WT and *aox1a* mutant fruits.....147

Supplemental Table C4-4. Relative metabolite levels from MG to MG+3 detected by GC-MS in tomato WT and *aox1a* mutant fruits.....148

Supplemental Figure C4-1. Relative expression levels of AOX-encoding genes in tomato (AOX1a, AOX1b, AOX1c, and AOX2) at different tissues and fruit developmental stages. 149

Supplemental Figure C4-2. Representative image of MicroTom fruits infiltrated on vine with A) Norfluorazon, B) Water and DMSO and C) Non-infiltrated fruits. 150

Supplemental Figure C4-3. Script used to perform Heatmap and clusters for R 151

Supplemental Figure C4-4. Representative images from top- and front-view pictures of WT and *aox1a* mutant lines (*a1.1* and *a2.3*) at 15, 30, 50, 65, and 80 days after transplanting to 0,5 L pots.....152

Supplemental Figure C4-5. Relative levels of individual metabolites that displayed statistically significant (P<0.05) differences between WT and *aox1a* mutant fruits during ripened stages. 153

Supplemental Figure C4-6. Relative levels of individual metabolites that displayed statistically significant (P<0.05) differences between WT and *aox1a* mutant fruits during non-ripened stages.....154

Abbreviations

2-OG: 2-Oxoglutarate

2-PG: 2-Phosphoglycolate

3-PG: 3-Phosphoglycerate

AA: Amino Acids

ACS2: Aminocyclopropane-1-Carboxylate Synthase 2

AOX: Alternative Oxidase

AOX1a: Alternative Oxidase 1a

AOX1b: Alternative Oxidase 1b

AOX1c: Alternative Oxidase 1c

AOX1d: Alternative Oxidase 1d

AOX2: Alternative Oxidase 2

Asc: Ascorbic Acid

Asp: Aspartate

Asn: Asparagine

ATP: Adenosine Triphosphate

BR: Breaker Stage

CCD4: Carotenoid Cleavage Dioxygenase 4

Cit: Citrate

CO_2: Carbon Dioxide

COP: COX Pathway

COX: Cytochrome c Oxidase

crtB: Gene Coding for Phytoene Synthase in Bacteria

Cyt: Cytochrome

DAT: Days After Transfer

DW: Dry Weight

E: Irradiance (Light Intensity)

E8: 2-Oxoglutarate-Dependent Dioxygenase

ETR: Electron Transport Rate

ETRmax: Maximum Electron Transport Rate

FBN: Fibrillin

Fd2: Ferredoxin Protein in Arabidopsis

Fm: Maximum Fluorescence

Fo: Initial Fluorescence

Fum: Fumarate

Fv: Variable Fluorescence (Fm - Fo)

Fv/Fm: Maximum Efficiency of PSII

GAP: Glyceraldehyde 3-Phosphate

GFP: Green Fluorescent Protein

GGPP: Geranylgeranyl Diphosphate

Gly: Glycine

Glyc: Glycolate

Glu: Glutamate

GOGAT: Glutamine Oxo-glutarate Aminotransferase

His: Histidine

HL: High Light

HrpN: Harpin Protein N

Ile: Isoleucine

Isocit: Isocitrate

KCN: Potassium Cyanide

L-Gal-L: L-Galactono-1,4-lactone

Mal: Malate

Met: Methionine

MG: Mature Green

mETC: Mitochondrial Electron Transport Chain

MEP: Methylerythritol 4-Phosphate Pathway

MS: Murashige and Skoog Medium

Myc: Myelocytomatosis Oncogene Product

NADH: Nicotinamide Adenine Dinucleotide

NADPH: Nicotinamide Adenine Dinucleotide Phosphate

NASC: Nottingham Arabidopsis Stock Centre

NDA1: NAD(P)H Dehydrogenase A1

NDA2: NAD(P)H Dehydrogenase A2

NDB3: NAD(P)H Dehydrogenase B3

NDext: External NAD(P)H Dehydrogenase

NDH: NAD(P)H Dehydrogenase

NDint: Internal NAD(P)H Dehydrogenase

NFZ: Norfluorazon

NH_4^+: Ammonium

NL: Normal Light

O_2: Oxygen

OAA: Oxaloacetate

OGAL: Octyl-gallate

OR: Orange Stage

Orn: Ornithine

PDS: Phytoene Desaturase

PG: Plastoglobule

PG2A: Polygalacturonase

PQ: Plastoquinone

Pro: Proline

PSII: Photosystem II

PSY: Phytoene Synthase

PTOX: Plastid Terminal Oxidase

Pyr: Pyruvate

rETR: Relative Electron Transport Rate

RFP: Red Fluorescent Protein

ROS: Reactive Oxygen Species

RR: Red Ripe

RuBP: Ribulose 1,5-Bisphosphate

RWC: Relative Water Content

Ser: Serine

sgRNA: Single Guide RNA

SHAM: Salicylhydroxamic Acid

SPS 1/2: Solanesyl Diphosphate Synthase 1 and 2

Succ: Succinate

$\tau_{a:}$ electron partitioning to the alternative oxidase pathway

T-DNA: Transfer DNA

Thr: Threonine

TP: Triose Phosphate

TCA Cycle: Tricarboxylic Acid Cycle

Tyr: Tyrosine

UCP: Uncoupling Protein

UCP1: Uncoupling Protein 1

UCPs: Uncoupling Proteins

UQ: Ubiquinone

Val: Valine

ν_{alt}: alternative oxidase pathway activity

V_{alt}: Capacity of the Alternative Pathway

ν_{cyt}: oxidase pathway activity

$V_{t:}$ Total respiration

WT: Wild-Type

Yang Cycle: Ethylene Biosynthesis Pathway

Summary

The research presented throughout this doctoral Thesis explores the roles of mitochondrial respiration and fibrillin proteins in plant metabolism, primarily using Arabidopsis (*Arabidopsis thaliana*) and tomato (*Solanum lycopersicum*) plants as model organisms. Previous studies have reported metabolic functions of fibrillin 6 (FBN6) and mitochondrial alternative oxidase (AOX) in plants, however, their roles during carotenoid biosynthesis and stress responses remain poorly understood. The objectives of the present Thesis were focused on (i) investigating the relevance of FBN6 for the production of carotenoids and subsequent responses to high light stress in Arabidopsis; (ii) studying the role of AOX respiration during the biosynthesis of stress-related primary metabolites in Arabidopsis; and (iii) analyze the contribution, *in vivo* regulation and (iv) different roles of mitochondrial respiration during carotenoid biosynthesis and ripening in tomato fruits. These objectives were addressed along four different chapters.

In chapter 1, the Arabidopsis FIBRILLIN6 (AtFBN6) protein is shown to be crucial for carotenoid biosynthesis, particularly under high light conditions. AtFBN6 promotes the activity of phytoene synthase (PSY), a key enzyme in the carotenoid biosynthetic pathway, highlighting its significant role in enhancing carotenoid levels. High light stress induces the expression of AtFBN6, which directly interacts with PSY to support increased carotenoid production. The absence of AtFBN6 results in decreased carotenoid levels, indicating its essential function in this biosynthetic process and its role in protecting plants from photooxidative damage under high light stress.

In chapter 2, the role of the AOX pathway in maintaining respiratory activity and redox balance during acute water and salt stress is unveiled by using Arabidopsis mutants lacking *AOX1a* gene (AtAOX1a). The *aox1a* mutants exhibit decreased photosynthetic performance and higher levels of oxidative stress-related metabolites, reinforcing the importance of AOX in cell redox balancing and preventing excessive reactive oxygen species (ROS) accumulation. Furthermore, the AOX pathway is shown to provide metabolic flexibility by enabling the synthesis of stress-related metabolites and supporting leaf osmoprotection.

In chapter 3, mitochondrial respiration and electron partitioning studies in tomato fruits of wild-type (WT) plants and chromorespiration-defective *ghost* mutants reveal that mitochondrial respiration is the primary energy and metabolite source during fruit ripening. The *in vivo* activity of the AOX pathway significantly increases at the breaker stage, becoming the main contributor to climacteric respiration. Such climacteric upregulation of the AOX pathway is mediated by a post-translational activation of the AOX protein, very likely through interactions with key organic acid activators. Overall, AOX respiration coincided with changes in primary metabolism suggesting its critical role in providing carbon precursors required for fruit ripening.

Finally in chapter 4, the generation of new *aox1a* mutants in tomato reveal the importance of AOX1a for normal growth and development of vegetative as well as fruit tissues in this species. Fruits from *aox1a* mutants exhibit altered respiration patterns and delayed ethylene-induced gene expression, which impacted ethylene and carotenoid metabolism during fruit ripening. Despite these early metabolic disruptions, *aox1a* mutants eventually compensate through the upregulation of AOX1b, partially restoring metabolic functions and carotenoid levels by the end of the ripening process.

Overall, these findings highlight the multifaceted roles of AOX and fibrillin proteins in plant metabolism, stress response, and development. They underscore the complexity of metabolic pathways involved in plant growth and adaptation, offering insights into how plants manage and respond to environmental stresses through intricate biochemical networks. These insights have potential applications in agricultural practices, particularly in developing crops with enhanced stress tolerance and optimized metabolic efficiency.

General Introduction

1. Plant carotenoids: biosynthesis and functions

Carotenoids are a diverse group of isoprenoid compounds naturally synthesized in all photosynthetic organisms, including plants, algae, and cyanobacteria, as well as in certain non-photosynthetic bacteria and fungi (Liang et al., 2018; Rodriguez-Concepcion et al., 2018). Most animals, except for a few such as pea aphids, spider mites, and gall midges, cannot produce carotenoids on their own but can accumulate them in specific body tissues. Like all plastidial isoprenoids, carotenoids are produced from precursors supplied by the methylerythritol 4- phosphate (MEP) pathway (Pokhilko et al., 2015). The first committed step of carotenoid biosynthesis is the condensation of two geranylgeranyl diphosphate (GGPP) molecules to produce phytoene (Rodriguez-Concepcion et al., 2018) (**Figure I-1**). This step, catalyzed by phytoene synthase (PSY), the main flux-controlling enzyme of the carotenoid pathway (Cao et al., 2019; Zhou et al., 2022) just the beginning of a complex and fascinating process. Several dehydrogenation and isomerization enzymatical steps convert uncolored phytoene into red lycopene (Rodriguez-Concepcion et al., 2018). Lycopene acts as a branching point for carotenoid production, depending on how the ends of its carbon chain are cyclized. The production of 2 β rings at the two ends of the chain produces β-carotene (β,β branch), while the output of 1 β ring and one ε ring produces α-carotene (β,ε branch). Oxygenation of the rings of carotenes produces xanthophylls such as violaxanthin and neoxanthin (β, β branch) or lutein (β,ε branch) (**Figure I-1**).

Carotenoids play indispensable roles in photosynthesis, aiding in assembling the photosynthetic machinery and in photoprotection by mitigating excess light energy through heat dissipation and free radical scavenging. They also contribute to the pigmentation of non-photosynthetic plant tissues, such as flower petals and fruits, facilitating animal attraction for pollination and seed dispersal. They accumulate in significant amounts within chloroplasts, closely associated with the photosynthetic apparatus, protecting it from photooxidative damage and aiding in light absorption. However, carotenoids reach their highest concentrations in chromoplasts, specialized plastids that store these highly lipophilic compounds in carotenoid-accumulating non-

photosynthetic tissues. For instance, tomatoes are known for their high lycopene content, while carrots are rich in beta-carotene, showcasing the diversity of carotenoid biosynthesis in different plants.

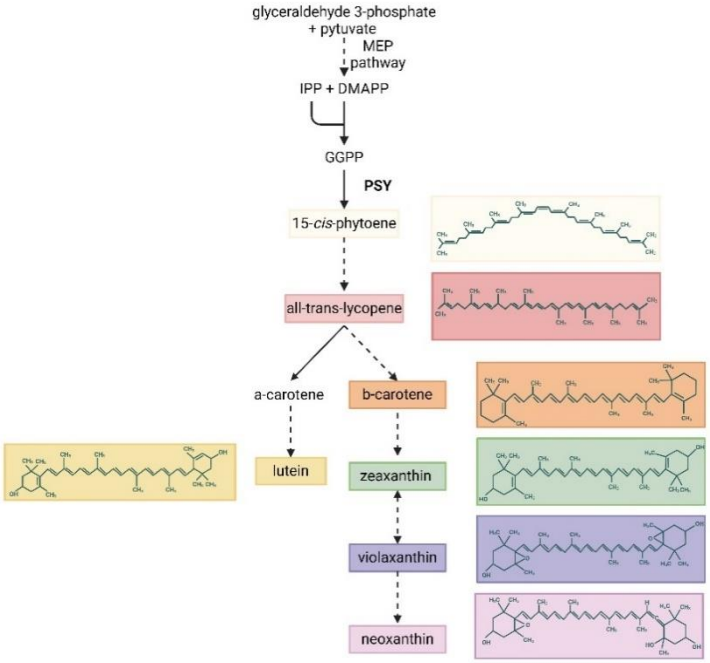


Figure I-1. Schematic representation of the carotenoid biosynthesis pathway.

Beyond their biological functions in plants, carotenoids have gained significant attention for their potential as natural pigments and nutritional supplements (Rodriguez-Concepcion et al., 2018). Their role as precursors of retinoids, including vitamin A, and their antioxidative properties make them crucial components of the human diet (Bolhassani et al., 2017; Meléndez-Martínez, 2019). Exploring these health-related attributes and the increasing demand for natural products has sparked intense interest in biotechnological strategies to enhance plant carotenoid production, opening up exciting possibilities for the future of nutrition and industry. However, despite notable progress in this area, significant gaps persist in our understanding of the regulatory mechanisms governing the carotenoid biosynthetic pathway across diverse plant organs and tissues as well as its interplay with other isoprenoid and primary metabolism pathways. Addressing

these knowledge deficits is essential for advancing our understanding of plant metabolism and harnessing the full potential of carotenoids for nutritional and industrial applications.

2. Plant plastoglobules and fibrillins: roles in carotenoid accumulation and stress

Chloroplasts are present in all green plant tissues, and they are characterized by an extensive thylakoid membrane system that facilitates photosynthesis (Jarvis and López-Juez, 2013). Plastoglobules (PGs) are lipid-containing structures that bud from the outer leaflet of the thylakoid membranes and remain associated with them (Bréhélin et al., 2007) (**Figure I-2**). First identified by Lichtenthaler in the early 1970s using transmission electron microscopy, these "osmophilic globuli" have been the subject of extensive research. Chloroplast PG act as a storage compartment containing tocopherols (vitamin E), phylloquinones (vitamin K1) and fatty acids, (Deruère et al., 1994). By contrast, PGs in chromoplasts contain several critical enzymes involved in the carotenoid biosynthetic pathway, highlighting their role in carotenoid synthesis and accumulation (Ytterberg et al., 2006).

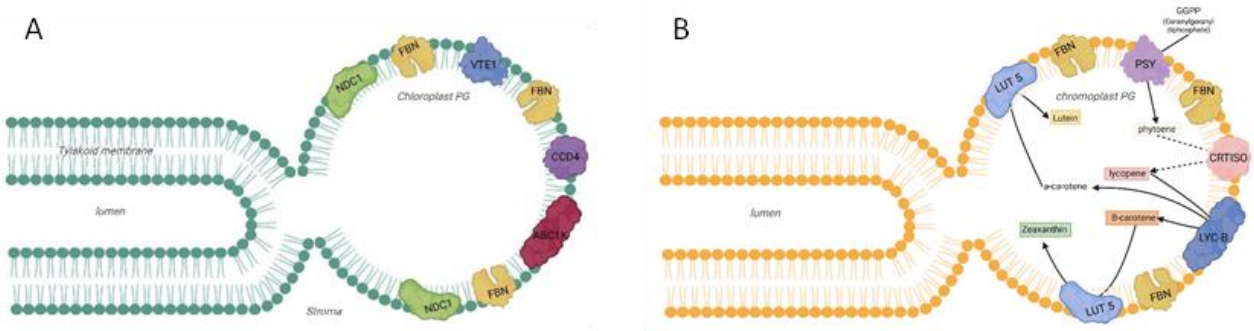


Figure I-2. Illustration of the physical link between the thylakoid membrane and the plastoglobule (PG). (A) Chloroplast PGs emerge from the outer leaflet of the thylakoid membrane at its curved regions. Key proteins include ABC1K (activity of bc1 complex-like kinases), CCD4 (carotenoid cleavage dioxygenase 4), FBNs (fibrillins), NDC1 (NAD(P)H dehydrogenase C1), and VTE1 (tocopherol cyclase). (B) Chromoplast PGs recruit the carotenoid biosynthetic pathway enzymes, including phytoene synthase (PSY). FBNs are also abundant. Adapted from Shanmugabalaji et al. (2022).

PGs contain a specialized proteome comprising around 30 proteins, categorized into structural proteins, regulatory kinases, and enzymes (Ytterberg et al., 2006). Among the structural proteins, plastid lipid-associated proteins, also known as fibrillins (FBNs) (Egea et al., 2010), have been identified in the PG proteomes of Arabidopsis (*Arabidopsis thaliana*) chloroplasts and bell pepper (*Capsicum annum*) chromoplasts (Ytterberg et al., 2006). FBNs are a family of nuclear-encoded proteins that contribute to PGs' structural organization and stability (Laizet et al., 2004). Gene families encoding FBNs in photosynthetic and non-photosynthetic organisms, are classified into 12 distinct clades with distinct molecular characteristics and functions (Laizet et al., 2004). This diversity reflects a broad range of biological roles beyond PGs, from maintaining plastid structural integrity to participating in metabolic processes essential for growth and adaptation from cyanobacteria to higher plants (Singh and McNellis, 2011).

In tomato (*Solanum lycopersicum*), FBN1, FBN2, and FBN4 accumulate significantly during fruit ripening (Winkenbach et al., 1976). This accumulation contributes to enhanced carotenoid production and storage in chromoplasts, which are responsible for the pigmentation and nutritional quality of the fruit. Similar functions have been observed in other plant species; for instance, homologs of FBN1 in rapeseed (*Brassica juncea*) and melon (*Cucumis melo*) also facilitate carotenoid accumulation in chromoplasts (Barsan et al., 2012; Suzuki et al., 2015; Zhou et al., 2023). In *Arabidopsis thaliana*, FBN isoforms such as FBN1a, FBN1b, and FBN2 are associated with PGs and are crucial for photoprotection and stress responses. These proteins help manage reactive oxygen species (ROS) and maintain the integrity of the photosynthetic apparatus under adverse conditions (Singh and McNellis, 2011). In this context, FBNs are upregulated in response to biotic and abiotic stresses, including pathogen attacks, drought, high light intensity, and temperature extremes. For example, in response to pathogen attacks, the accumulation of FBNs helps reinforce the structural integrity of plastids, which is essential for maintaining their function during infection (Leitner-Dagan et al., 2006; Margaria and Palmano, 2011). During drought conditions, FBNs aid in stabilizing the thylakoid membranes and PGs, preventing damage from desiccation and maintaining photosynthetic efficiency (Gillet et al., 1998). Under temperature stress, FBNs promote

stabilizing plastid membranes and associated structures, preventing protein denaturation and maintaining thylakoid membranes' fluidity to ensure photosynthetic activity (Singh and McNellis, 2011). Under cold stress, they assist in preserving the integrity of PGs and other plastid components, preventing freezing damage and supporting the plant's metabolic processes. Moreover, FBNs play a crucial role in photoprotection under high light stress by dissipating excess light energy and reducing the formation of ROS that can damage cellular components. By participating in ROS scavenging, FBN1a and FBN1b in *Arabidopsis thaliana* help maintain the redox balance within chloroplasts, thereby protecting the photosynthetic machinery from oxidative stress, i.e. stabilizing the photosystem II (PSII) (Yang et al., 2006). FBN6 also supports plant acclimation to light stress and contributes to scavenging ROS (Lee et al., 2020). These findings highlight the diverse roles of FBN isoforms in different plant species, underscoring the need for additional research.

Additionally, the expression of FBN genes is regulated by plant hormones such as abscisic acid (ABA), gibberellic acid (GA_3), and auxin (IAA). ABA, often called the stress hormone, increases during drought and high salinity conditions, leading to the upregulation of FBNs that enhance the plant's stress tolerance. In Arabidopsis, ABA treatment stimulates the accumulation of FBN1a, which in turn protects photosystem II (PSII) from photoinhibition (Yang et al., 2006). For instance, under drought stress, ABA-mediated upregulation of FBNs aids in stomatal closure, reducing water loss and maintaining cellular turgor. GA_3, known for its role in promoting growth and development, also influences FBN expression. During periods of rapid growth, GA_3 levels increase, coordinating the expression of FBNs to ensure that the expanding tissues have adequate protection against stress. GA_3 increases carotenoid accumulation in flower tissue of cucumber and activates the expression of the FBN1 gene (Leitner-Dagan et al., 2006). Auxin (IAA), essential for cell elongation and division, similarly regulates FBN-encoding genes to align plastid development with cellular growth, ensuring newly formed cells have the necessary plastid structures to perform their functions efficiently in bell peppers (Deruère et al., 1994).

Altogether, the evidence presented highlights the multifaceted roles of FBNs in plant development and stress responses by participating in ROS scavenging and maintaining

the stability of plastid structures (Kim et al., 2015; Lee et al., 2020). However, the function of most FBNs remains poorly understood and/or requires further research. Recently, the identification of FBN-interacting proteins has substantially improved our understanding of the function of different FBN family members, including those that are not found in PGs such as FBN5 and FBN6. Interestingly, Arabidopsis FBN6 was found to be among the proteins co-immunoprecipitated with a GFP-tagged version of PSY, the first and main rate-determining enzyme of the carotenoid pathway (Welsch et al., 2018). Furthermore, FBN6 is the only FBN enriched in purified envelope fractions where PSY is also localized (Ferro et al., 2010; Bouchnak et al., 2019). Therefore, it was tempting to speculate that this particular FBN isoform modulates PSY activity, thereby potentially impacting the metabolic flux of the carotenoid pathway in chloroplasts. **In Chapter 1 of this doctoral Thesis, the role of Arabidopsis FBN6 for carotenoid biosynthesis has been studied based on its interaction with PSY.**

3. Plant mitochondria and their energy-bypass systems

Besides plastids, mitochondria are another class of endosymbiotic organelles present in plant cells. Both organelles are central for plant metabolism under normal growth conditions and in response to stress. Chloroplasts are the site of photosynthesis and act as regulators of plant responses to abiotic and biotic stresses in part *via* the production of ROS as signaling molecules, which help initiate stress signaling responses through retrograde signaling, where stress signals are sent back to the nucleus to adjust gene expression and enhance stress tolerance (Welchen et al., 2021). When specialized in the biosynthesis and storage of particular metabolites, plastids might eventually lose their photosynthetic capacity and differentiate from chloroplasts into chromoplasts (carotenoids), amyloplasts (starch), or elaioplasts (fatty acids). Other specialized plastid types include those of etiolated seedlings (etioplasts) or senescent leaves (gerontoplasts), whereas leucoplasts are found in non-pigmented roots and shoot organs such as petals (Sadali et al., 2019). Mitochondria are not as diverse as plastids but they are essential in all tissues for plant respiration that uses photosynthetically produced carbohydrates to support growth and maintenance by providing carbon intermediates, reducing equivalents and ATP. Furthermore, plant mitochondria display a high degree of flexibility

by switching to alternative pathways to adjust their metabolic activities in response to changes in photosynthesis, photorespiration, stress and/or different developmental processes (O'Leary et al., 2019; Welchen et al., 2021).

The mitochondrial electron transport chain (mETC) is central for plant energy production through oxidative phosphorylation at the inner mitochondrial membrane (IMM), where a sequence of redox reactions drives ATP synthesis (**Figure I-3**). The oxidation of reducing equivalents by Complex I, known as NADH dehydrogenase, alongside various plant-specific alternative dehydrogenases facilitate the transfer of electrons from NAD(P)H to the ubiquinone pool. Complex II, or succinate dehydrogenase, part of the tricarboxylic acid (TCA) cycle, also contributes with electron transport to the ubiquinone pool. The electrons are then relayed from the ubiquinol pool to Complex III, and through cytochrome c, they reach Complex IV, also known as cytochrome c oxidase (COX). COX reduces molecular oxygen (O_2) to water (H_2O) through a four-electron transfer process. Complexes I, III, and IV are coupled with the translocation of protons from the mitochondrial matrix to the intermembrane space (IMS). The electrochemical gradient generates a proton motive force that is used by the ATP synthase (Complex V) to catalyze the conversion of ADP and inorganic phosphate (Pi) into ATP (Barreto et al., 2022) (**Figure I-3**).

While these complexes constitute the canonical ATP-producing pathway, plant mETC is characterized by containing alternative respiratory pathways involving the internal and external type II NAD(P)H dehydrogenases, uncoupling proteins (UCPs), and alternative oxidases (AOXs) (Barreto et al., 2022). The alternative oxidase (AOX) pathway directly couples the ubiquinol oxidation with the reduction of O_2 to H_2O without generating a proton gradient and thus bypassing the proton pumping at complexes III and IV. Some ATP is still produced through the AOX pathway if electrons arise from the NADH oxidation at the proton-pumping Complex I. However, if these electrons come from NAD(P)H oxidation by an alternative dehydrogenase or Complex II, the electron flow to AOX is entirely uncoupled from ATP production (Vanlerberghe, 2013). On the other hand, even if the COX pathway generates a proton gradient across the IMM, the uncoupling proteins (UCPs) can pump protons from the IMS back to the mitochondrial

matrix, thus uncoupling the electron transport from the ATP synthesis bypassing complex V. Therefore, both AOX and UCP systems can release energy as heat and uncouple respiration from ATP synthesis (Barreto et al., 2022) (**Figure I-3**).

Among the different alternative respiratory pathways, the AOX pathway has attracted most of the attention in the last decades, although some of its roles in plants (Del-Saz et al., 2018; McDonald, 2023) and other organisms (Li et al., 2024) are still a matter of debate. Despite its energy inefficiency, several studies have reported the crucial role of the AOX pathway in plants to produce heat, tolerate stress and maintain growth in balance with resource availability (Vanlerberghe, 2013; Del-Saz et al., 2018). By allowing ATP-uncoupled electron transport, the AOX pathway can reduce the excess of reducing power and prevent over-reduction of the mETC, which can otherwise come with increased ROS production and cellular damage (Del-Saz et al., 2018; Selinski et al., 2018b).

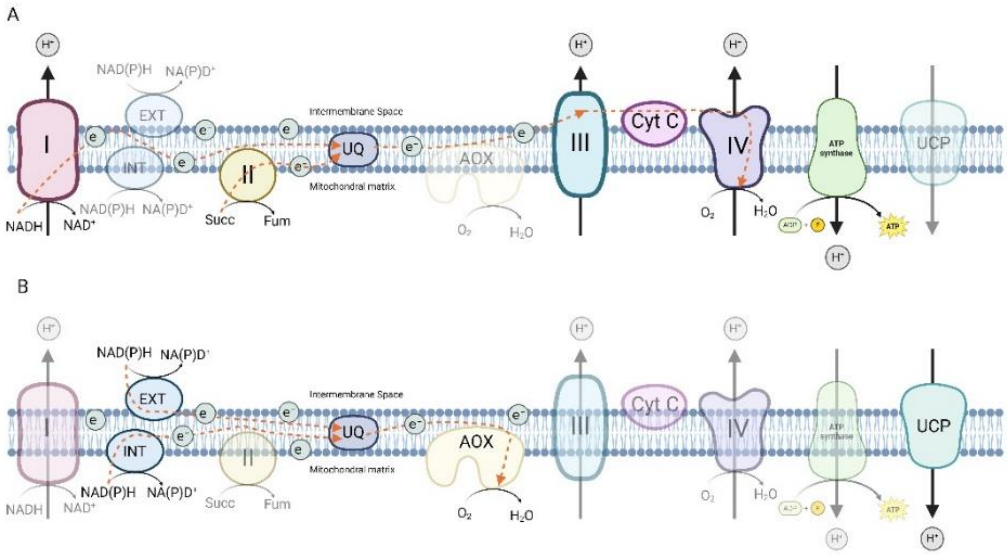


Figure I-3. Representation of the respiratory pathways in the mitochondrial electron transport chain (mETC) and ATP synthase in the inner membrane of plant mitochondria. **(**A) Cytochrome c oxidase (COX) pathway. (B) Alternative oxidase (AOX) pathway bypasses proton pumping complexes III and IV. ND_{ext} and ND_{int} represent the alternative non-proton pumping NAD(P)H dehydrogenases on the outer and inner surfaces of the mitochondrial inner membrane, respectively, which bypass proton pumping complexes I. Members of the mitochondrial uncoupling protein (UCP) family dissipate the proton gradient bypassing ATP synthase.

Beyond its metabolic roles, the AOX also influences mitochondrial retrograde signaling pathways that regulate nuclear gene expression, modulating signaling molecule levels such as superoxide, nitric oxide, and other redox couples. This signaling capacity allows AOX to play a general role in stress response mechanisms, by adjusting the expression of genes involved in stress tolerance and metabolic adjustments (Arnholdt-Schmitt et al., 2006; Vanlerberghe, 2013b). However, its function is not limited to the regulation of mitochondrial stress signaling but more generally for providing flexibility to primary metabolism (Del-Saz et al., 2018; Oh et al., 2023). **The role of AOX respiration during the biosynthesis of stress-related primary metabolites has been addressed in Chapter 2 of this doctoral Thesis.**

4. Plastid-mitochondria interactions

In green tissues, chloroplasts and mitochondria are tightly interconnected because they share crucial intermediates for cell carbon and energy metabolism (Kromer, 1995; Raghavendra and Padmasree, 2003; Watanabe et al., 2010; Vanlerberghe et al., 2020; Igamberdiev and Bykova, 2023). During photosynthesis, harvested light energy is converted to ATP and reducing equivalents which are then used for carbon and nitrogen assimilation in the chloroplasts. Photosynthetic CO_2 assimilation produces trioses phosphates (TPs) that can be exported to the cytosol and used for sucrose synthesis. The ATP needed for sucrose synthesis is thought to be supplied by the mitochondrial electron transport chain (Kromer et al., 1993) although some experimental evidence do not support this hypothesis (Carrari et al., 2003). Sucrose or TPs can enter the glycolytic pathway to produce substrates (i.e. pyruvate) for the TCA cycle (**Figure I-4**). Mitochondrial respiration in green tissues is not only related to sugars oxidation to generate ATP, but also generates carbon skeletons for amino acid synthesis and supports photorespiration (a process that helps recycle 2-phosphoglycolate into 3-phosphoglycerate, thus preventing the loss of carbon), nitrogen metabolism, and the export of redox equivalents from the chloroplast via the malate shuttle, which allows the transfer of NADPH from the chloroplast to the mitochondria, balancing cell redox state and enabling efficient metabolic regulation (**Figure I-4**).

The photorespiratory pathway represents a very important flux of leaf metabolites among chloroplast, peroxisome and mitochondria, where glycine is decarboxylated at the mitochondrial matrix generating CO_2, NH_4^+ and NADH. The vast amount of photorespiratory NADH produced at the mitochondria can be either exported to the cytosol through the malate–oxaloacetate shuttle, or reoxidized by the mitochondrial electron transport chain (mETC) (Igamberdiev and Bykova, 2023) (**Figure I-4**).

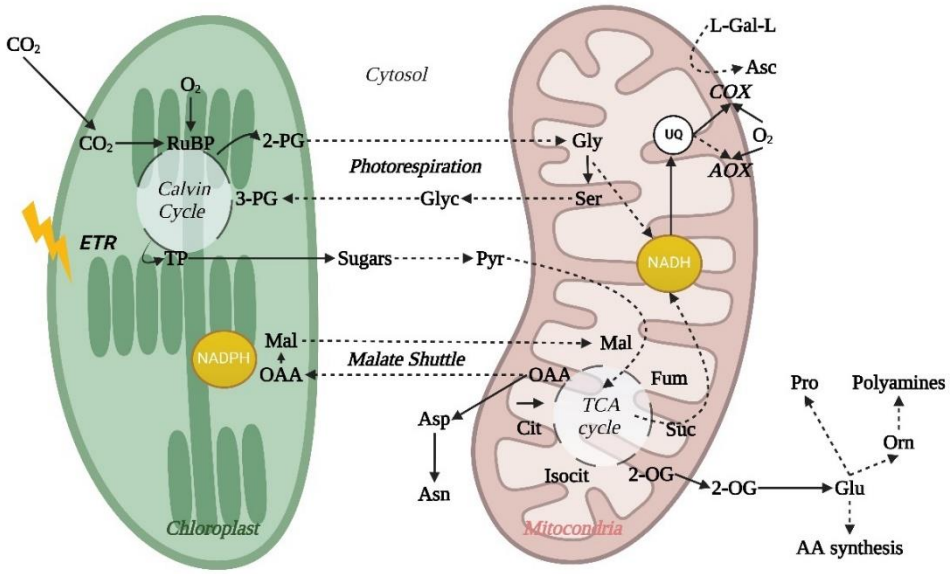


Figure I-4. Simplified metabolic interactions between chloroplasts and mitochondria in photosynthetic tissues. 2-OG, 2-Oxoglutarate; 2-PG, 2-Phosphoglycolate; 3-PG, 3-Phosphoglycerate; AA, Amino Acids; AOX, Alternative Oxidase; Asc, Ascorbic Acid; Asp, Aspartate; Asn, Asparagine; Cit, Citrate; COX, Cytochrome c Oxidase; ETR, Electron Transport Rate; Fum, Fumarate; Gly, Glycine; Glyc, Glycolate; Glu, Glutamate; Isocit, Isocitrate; L-Gal-L, L-Galactono-1,4-lactone; Mal, Malate; NADH, Nicotinamide Adenine Dinucleotide; NADPH, Nicotinamide Adenine Dinucleotide Phosphate;; OAA, Oxaloacetate; Orn, Ornithine; Pro, Proline; Pyr, Pyruvate; RuBP, Ribulose 1,5-Bisphosphate; Ser, Serine; Suc, Succinate; TP, Triose Phosphate; UQ, Ubiquinone.

Metabolic models predict that the alternative components of the mETC, such as the internal type II dehydrogenases and the alternative oxidase (AOX), become activated

under high photorespiratory conditions (Shameer et al., 2019; Igamberdiev and Bykova, 2023), however, direct *in vivo* evidence is still scarce. On the other hand, photosynthetic nitrogen assimilation and mitochondrial respiration are also linked through several metabolic reactions (Igamberdiev and Bykova, 2023) (**Figure 4**). Previous studies support the importance of the TCA cycle functioning in a non-cyclic mode for providing carbon precursors and reducing power needed for nitrogen assimilation and subsequent amino acid synthesis (Nunes-Nesi et al., 2007; Sweetlove et al., 2010; Igamberdiev and Bykova, 2023). Furthermore, the mETC plays an important role in photosynthetic performance by acting as a sink for the excess of reducing power from the chloroplast, i.e. under high light or ammonium stress (Noguchi and Yoshida, 2008; Podgórska et al., 2020).

Another important role of mitochondria in cell redox balance resides at the involvement of the mETC on the synthesis of ascorbate (Bartoli et al., 2000; Millar et al., 2003). Recently, an intriguing hypothesis has proposed that the AOX pathway can influence ascorbate synthesis by modulating the redox state of the mETC, particularly under stress, although *in vivo* evidence is lacking to support for this relationship (Matos et al., 2022). Environmental stresses impact the availability of light, CO_2, water, and nutrients, directly affecting photosynthetic processes. Under these conditions, the dynamic activation of the complex set of alternative proteins present in plant mETC provides metabolic flexibility to adjust carbon and energy supplies and demands (Del-Saz et al., 2018; O'Leary et al., 2019).

Mitochondria might also have a pivotal role to produce carotenoids in plastids of non-photosynthetic tissues. Among different non-photosynthetic plastids, relatively minor amounts of carotenoids are synthesized in etioplasts, amyloplasts and leucoplasts (Howitt and Pogson, 2006). However, chromoplasts are plastids highly specialized in the accumulation of carotenoids that are mainly present in flower and fruit tissues, serve as reservoirs for carotenoids, and provide attractive yellow to red hues that facilitate animal-mediated pollen and seed dispersal (Camara et al., 1995; Egea et al., 2010). During the ripening of many fruits, including tomato, the differentiation of chloroplasts into chromoplasts involves the complete degradation of chlorophylls, loss of the thylakoid

structures, and remodeling of the internal membrane system, in parallel to a massive accumulation of carotenoids in PGs and other storage structures such as fibrils, membranes and even crystals (Sadali et al., 2019). In contrast to leaf chloroplasts, the Calvin cycle is inactive in fruit chromoplasts and does not contribute to the MEP pathway (Lytovchenko et al., 2011; Garrido et al., 2023). Instead, the MEP pathway substrates, pyruvate and glyceraldehyde-3-phosphate (GAP), can be produced by glycolysis, whose flux tightly depends on respiratory metabolism during ripening of tomato fruits (Tucker, 1993). On the other hand, the provision of hexoses resulting from plastid starch breakdown and of metabolites imported from the cytosol are suggested to support the high demand of carbon precursors for the synthesis of carotenoids and other metabolites in tomato fruit chromoplasts (Bouvier and Camara, 2007).

As regard to energy production, climacteric fruits such as tomato show an increase in respiration in concert with the production of ethylene, the main hormone controlling fruit ripening, and both events precede carotenoid synthesis (Giovannoni, 2004). Respiratory pathways in the cytosol and mitochondria have been proposed as the main suppliers of ATP and metabolic precursors for ensuring the high activity of plastid MEP pathway in poplar leaves and thermogenic plants (Loreto et al., 2007; Terry et al., 2016). Furthermore, chromorespiration was shown to provide ATP in tomato fruit chromoplasts at late ripening stages (Renato et al., 2014) (**Figure I-5**). This respiratory process involves an electron transport chain at the thylakoidal membrane composed by a NAD(P)H dehydrogenase, cytochrome b6f complex and the plastid terminal oxidase (PTOX), which mediates the light-independent O_2 consumption coupled to the oxidation of the plastoquinone (PQ) pool (Renato et al., 2015) (**Figure I-5**). The electron transport through this chomorespiratory chain is coupled to proton translocation and ATP generation by a chromoplast ATP synthase (Renato et al., 2014) (**Figure I-5**), but the *in vivo* contribution of mito- *versus* chromo-respiratory pathways during fruit ripening remains to be determined. **In Chapter 3 and 4 of this doctoral Thesis, the contribution of mito- and chromorespiration and the role of the AOX pathway for carotenoid biosynthesis in tomato fruits have been investigated.**

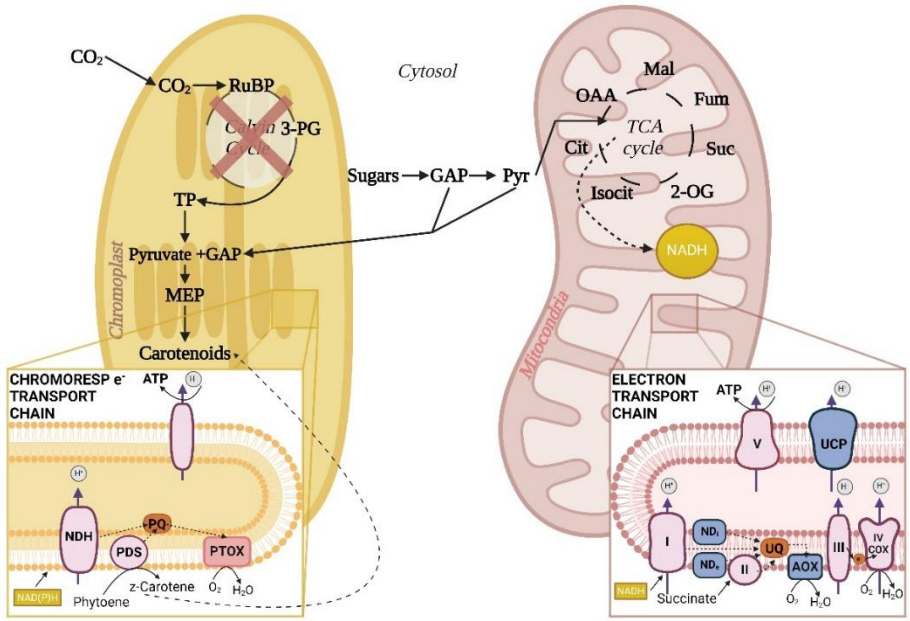


Figure I-5: Interactions between chromoplasts and mitochondria. The chromoplast electron transport chain involves NAD(P)H dehydrogenase (NDH), plastoquinone (PQ), phytoene desaturase (PDS), and plastid terminal oxidase (PTOX), which has a dual role in carotenoid synthesis and ATP generation. Pyruvate produced by glycolysis can be converted to acetyl-CoA at the mitochondrial matrix, entering the TCA cycle. The NADH produced by the TCA cycle can be oxidized by the mETC, which contains different complexes and alternative components (for details see **Figure 3**). 2-OG, 2-Oxoglutarate; 3-PG, 3-Phosphoglycerate; AA, Amino Acids; AOX, Alternative Oxidase; ATP, Adenosine Triphosphate; Cit, Citrate; CO_2, Carbon Dioxide; COX, Cytochrome c Oxidase; Fum, Fumarate; GAP, Glyceraldehyde-3-Phosphate; Glu, Glutamate; Isocit, Isocitrate; Mal, Malate; MEP, Methylerythritol Phosphate; NDH, NAD(P)H Dehydrogenase; O_2, Oxygen; OAA, Oxaloacetate; PQ, Plastoquinone; PDS, Phytoene Desaturase; Pro, Proline; PTOX, Plastid Terminal Oxidase; Pyr, Pyruvate; RuBP, Ribulose 1,5-Bisphosphate; Suc, Succinate; TP, Triose Phosphate; UCP, Uncoupling Protein; UQ, Ubiquinone.

Objectives

The research in this Thesis aims to investigate different mechanisms regulating the metabolic flux into the carotenoid pathway and their connection with mitochondria and responses to stress. For this, the following specific objectives were established:

1. Investigate the relevance of the interaction of PSY with FBN6 for the production of carotenoids and subsequent responses to high light stress in Arabidopsis.
2. Study the role of mitochondrial alternative oxidase (AOX) respiration during the biosynthesis of stress-related primary metabolites in Arabidopsis.
3. Analyze the contribution of mitochondrial respiration and chromorespiration to carotenoid biosynthesis in tomato fruits.
4. Clarify the role of the mitochondrial AOX for plant development and fruit metabolism (including carotenoid biosynthesis) in tomato.

Each of the four objectives were addressed in a corresponding chapter from 1 to 4.

Chapter 1: Arabidopsis FIBRILLIN6 influences carotenoid biosynthesis by directly promoting phytoene synthase activity

Introduction

Carotenoids are a family of plant isoprenoids with roles in photosynthesis and photoprotection in green tissues. They also function as pigments in non-photosynthetic tissues such as flower petals and ripe fruits to attract animals for pollination and seed dispersal. Carotenoids are also precursors of bioactive molecules in plants (including hormones such as abscisic acid and strigolactones) and animals (including retinoids such as vitamin A) (Rodriguez-Concepcion et al. 2018). Carotenoids accumulate at high levels in chloroplasts, where they are mostly associated with the photosynthetic apparatus. However, they are most abundant in chromoplasts, which are plastids specialized in the sequestration of these highly lipophilic compounds found in carotenoid-accumulating non-photosynthetic tissues (Rodriguez- Concepcion et al. 2018). Chromoplast ultrastructure changes depending on the species, organ, and carotenoid type they accumulate. For example, chromoplasts from carrot (*Daucus carota*) roots accumulate carotenoids as large crystals whereas those of red pepper (*Capsicum annuum*) contain a large number of plastoglobules (PG) with fibrillar extensions surrounded by an outer layer of proteins referred to as plastoglobulins or fibrillins (FBNs) (Egea et al. 2010).

FBNs are encoded by gene families in plants and algae that can be grouped into 12 clades (Singh and McNellis 2011; Kim and Kim 2022). They include members with diverse molecular masses, pI values, hydrophobicity profiles, and homology with lipocalins (small proteins involved in the binding and transport of small lipophilic compounds), suggesting that each FBN family member has specific biological function(s) (Singh and McNellis, 2011; Lundquist et al., 2012; Kim and Kim, 2022). In agreement, plastid types vary in their FBN composition, suggesting that specific FBNs might have specialized functions in different classes of plastids (Singh and McNellis 2011; Kim and Kim 2022). However, their mechanisms of action remain poorly understood in most cases. In tomato (*Solanum lycopersicum*), the PG-associated FBN1, FBN2, and FBN4 isoforms accumulate at high levels during fruit ripening, when carotenoids are actively produced and stored in chromoplasts (Barsan et al. 2012; Suzuki et al. 2015). FBN1 homologs from rapeseed (*Brassica juncea*) and melon (*Cucumis melo*) contribute to carotenoid accumulation in chromoplasts (Li et al. 2023; Zhou et al. 2023). By contrast, the Arabidopsis (*Arabidopsis thaliana*) homologs FBN1a, FBN1b, and FBN2 are involved

in photoprotection and stress responses (Torres-Romero et al. 2022) whereas FBN4 is likely involved in the partitioning of metabolites between the PG and thylakoid membranes of chloroplasts (Singh et al., 2012). Arabidopsis FBN1a, FBN1b, and FBN2 interact with each other around the PG surface, but FBN2 also plays FBN1-independent roles through interaction with other proteins (Torres-Romero et al. 2022). Arabidopsis FBN5 is a stromal protein involved not only in the acclimation to photooxidative stress but also in plastoquinone-9 biosynthesis by binding to solanesyl diphosphate synthases (Kim et al. 2015). FBN6 is needed for plants to acclimate to light stress, and it contributes to reactive oxygen species (ROS) scavenging (Lee et al. 2020). The role of other FBNs remains poorly studied (Singh and McNellis 2011; Kim and Kim 2022).

Arabidopsis FBN6 was found to be among the proteins co-immunoprecipitated with a GFP-tagged version of phytoene synthase (PSY), the first and main rate-determining enzyme of the carotenoid pathway (Welsch et al. 2018). Furthermore, FBN6 is the only FBN enriched in purified envelope fractions where PSY is also found (Ferro et al. 2010; Bouchnak et al. 2019). Therefore, we questioned whether this particular isoform modulates PSY activity, thereby potentially impacting the metabolic flux of the carotenoid pathway in chloroplasts. Besides confirming binding and co-localization of Arabidopsis FBN6 and PSY, we demonstrate the functional relevance of such an interaction.

Materials and methods

Plant material and growth conditions

N. benthamiana and Arabidopsis (*A. thaliana*) plants were grown as described (Morelli et al. 2023). The *fbn6-1* mutant (GABI_159E10) (Lee et al. 2020) was obtained from the Nottingham Arabidopsis Stock Centre (NASC). Homozygous lines were identified by genomic PCR with T-DNA and gene-specific primers (**Supplemental Table C1-1**). Transgenic lines overexpressing an RFP-tagged version of Arabidopsis FBN6 were generated in the Columbia-0 background using construct pGWB454-FBN6-RFP. Lines with a single T-DNA insertion were identified based on the Mendelian segregation of the kanamycin resistance marker gene, and transformants showing different levels of FBN6-RFP protein (as deduced from RFP fluorescence intensity) were selected for analysis. For

the de-etiolation experiments, seeds were surface-sterilized and sown on Petri dishes containing solid 0.5× MS medium without sucrose. After stratification for 3 d at 4°C in the dark, seeds were exposed to white light (50 μmol photons·m−2 s−1, referred to as normal light or NL) for 3 h at 22°C to stimulate synchronized germination. Then, plates were covered in aluminum foil and incubated at 22 °C in the dark for 3 d for seeds to germinate and produce etiolated seedlings. Such etiolated seedlings were either collected in the dark or exposed to NL to allow de-etiolation. For the intense light experiments, seedlings grown on plates for 9 d under NL were exposed for 24 h to 600 μmol photons·m−2 s−1 (referred to as high light or HL) or left under NL for the same time. *N. benthamiana* leaves were agroinfiltrated as described (Morelli et al. 2023). Some leaves were later treated with the commercial herbicide Zorial, containing 80% NFZ. The herbicide was diluted in a 0.05% (v/v) solution of Tween 20 in water to a final concentration of 2 μM NFZ. The solution was then infiltrated with a syringe on the leaf areas that has been agroinfiltrated with constructs of interest 24 h earlier (so the agroinfiltration halo was properly absorbed).

Gene constructs

The full coding region of the Arabidopsis FBN6 (AT5G19940) cDNA was PCR-amplified using primers AtFBN6-attB1-F and AtFBN6-attB2-R (**Supplemental Table C1-1**) and cloned into Gateway pDONR207 and subsequently pGWB420 (to create the FBN6-myc fusion) and pGWB454 (to create the FBN6-RFP fusion). Similarly, the FBN4-myc fusion was generated by PCR-mediated amplification of a cDNA sequence encoding full-length FBN4 (AT3G23400) with primers AtFBN4-attB1-F and AtFBN4-attB2-R (**Supplemental Table C1-1**) and cloned into Gateway pGWB420 via pDONR207. Constructs encoding PRK-myc (Barja et al. 2021) and PSY-GFP (Welsch et al. 2018) were previously available in the lab.

Microscopy

Fluorescent proteins transiently expressed in agroinfiltrated *N. benthamiana* leaves or stably produced in transgenic Arabidopsis lines were analyzed with a Leica TCS SP5 Confocal Laser Scanning Microscope using a 63× immersion objective. GFP fluorescence was detected using a PMT detector (gain 980) from 500 to 560 nm after

argon laser excitation at 488 nm (29%), while RFP was excited by a Diode laser 561 (20%) and, the signal was detected using a PMT detector (gain 76) from 570 to 630 nm. Chlorophyll autofluorescence was detected using a PMT detector (gain 41) from 650 to 750 nm after argon laser excitation at 488 nm (29%).

Co-immunoprecipitation and immunoblot assays

N. benthamiana leaves were agroinfiltrated with the appropriate constructs and samples were collected after 4 d for co-immunoprecipitation experiments performed as described (Barja et al. 2021). Immunoblot analysis of plant protein extracts was carried out as described (Paulišić et al., 2021). In the case of *E. coli*, extracts for immunoblot analysis were made by directly boiling pelleted cells in 12.5 mM Tris–HCl pH = 6.8, 4% (w/v) SDS. Blots were incubated with available antibodies against FBN1a and FBN2 (Morelli et al. 2023) diluted 1:5,000 or commercial antibodies against GFP (Invitrogen, 1:2,000) and Myc (Calbiochem, 1:5,000). Quantification of the signals was carried out as described (Morelli et al. 2023).

Gene expression and metabolite analysis

RNA isolation, cDNA synthesis, and reverse transcription quantitative PCR experiments were carried out as described (Barja et al. 2021) using the primers listed in **Supplemental Table C1-1**. Normalized transcript levels were calculated using Arabidopsis *UBC21* (At5g25760) as the reference gene. Carotenoids and chlorophylls were extracted from plant tissues, separated, identified, and quantified by HPLC-DAD (Barja et al. 2021).

Statistical analyses

One-way ANOVA followed by Tukey's multiple comparisons test and Student's *t*-test analyses were used to determine statistically significant differences.

Accession numbers

Sequence data from this article can be found under the following accession numbers: At5g17230 (PSY), At5g19940 (FBN6), At3g23400 (FBN4), Solyc09g090330 (SlFBN4), At1g32060 (PRK), At5g25760 (UBC21), and ADD79329 (crtB).

Results and discussion

Arabidopsis FBN6 and PSY physically interact in particular subplastidial locations

FBN6 was one of the proteins pulled down with a GFP antibody in Arabidopsis lines overexpressing the fusion protein PSY-GFP (Welsch et al. 2018), suggesting that FBN6 and PSY physically interact in vivo. To confirm this previously observed interaction and test its specificity, we performed co-immunoprecipitation experiments in *Nicotiana benthamiana* leaves. Constructs encoding C-terminal myc-tagged FBN6 and GFP-tagged PSY were co-agroinfiltrated in leaves, and 4 d later, protein extracts were used for immunoprecipitation using anti-myc antibodies (**Figure C1-1**). As a negative control, we used a myc-tagged version of Arabidopsis phosphoribulokinase (PRK), a stromal enzyme of the Calvin cycle (Barja et al. 2021). Immunoblot analysis of immunoprecipitated proteins with anti-GFP antibodies detected PSY-GFP in FBN6-myc but not in PRK-myc samples (**Figure C1-1A**). The specificity of the FBN6-PSY interaction was then tested by using a myc-tagged version of the FBN4 protein as a negative control (Torres-Romero et al. 2022). Results (**Figure C1-1B**) showed that Arabidopsis FBN4 does not interact with PSY, and this confirmed the specificity of FBN6 and PSY interaction.

When analyzing the co-immunoprecipitation assays, we noticed that the PSY-GFP protein concentrated in fluorescent dots within chloroplasts (**Figure C1-2A**). These dots are similar to those observed for PG-associated proteins (Lundquist et al., 2012; Gámez-Arjona et al., 2014; Morelli et al., 2023) and for PSY enzymes (Shumskaya et al. 2012) when fused to fluorescent protein tags. Interestingly, GFP-tagged Arabidopsis FBN6 shows a spotted distribution within chloroplasts despite the fact that the protein is not found in PG but localized in thylakoid and envelope membranes (Ferro et al. 2010; Lundquist et al. 2012; Bouchnak et al. 2019; Lee et al. 2020). To test whether the fluorescent dots observed in chloroplasts harboring FBN6-GFP and PSY-GFP proteins corresponded to the same or different subplastidial locations, we fused the red fluorescent protein (RFP) to FBN6 (FBN6-RFP construct) and co-agroinfiltrated it with the PSY-GFP construct. Confocal microscopy of the leaves 4 d after agroinfiltration showed a clear overlapping of RFP and GFP fluorescence signals (**Figure C1-2A**), indicating that FBN6 and PSY co-localize within chloroplasts, as expected for interacting proteins.

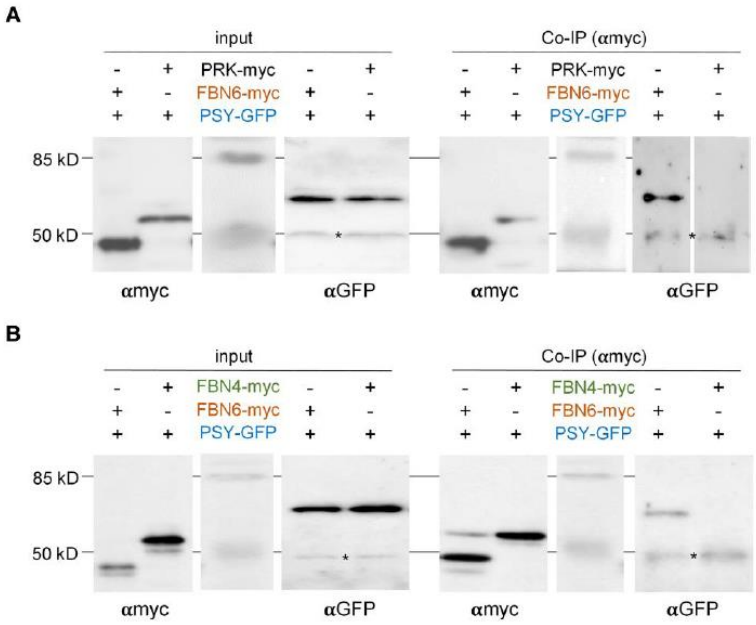


Figure C1-1. FBN6 and PSY can be immunoprecipitated together. N. benthamiana leaves were co-agroinfiltrated with the indicated combinations of proteins with C-terminal myc or GFP tags**.** Four days later, agroinfiltrated leaves were collected and used for protein extraction and analysis. Part of the protein extracts was used to test protein production (input) by immunoblot analyses with antibodies against myc (αmyc) or GFP (αGFP; asterisk marks the position of unspecific bands). The remaining protein extracts were used for co-immunoprecipitation (Co-IP) experiments using αmyc followed by immunoblot analyses with immunoblot analyses with αmyc (to confirm successful IP) and αGFP (to detect the presence of co-immunoprecipitated PSY-GFP protein). **A)** Experiment using the Calvin cycle enzyme PRK fused to the myc tag as a negative control. **B)** Experiment using the PG-ssociated FBN4 protein fused to the myc tag to test for the specificity of the FBN6-PSY interaction.

Despite the fact that FBN6-GFP has been previously found to co-localize with PG proteins fused to fluorescent tags in co-expression experiments similar to the results reported here, subsequent analysis of chloroplast membrane fractions argued against a localization of FBN6 in PG (Lee et al. 2020), a conclusion that is supported by proteomic data (Ferro et al. 2010; Lundquist et al. 2012; Bouchnak et al. 2019). While overexpression of FBNs and other PG-associated proteins typically results in PG

proliferation (Shanmugabalaji et al., 2013; Van Wijk and Kessler, 2017), overproduction of FBN6 or/and PSY proteins in agroinfiltrated leaf chloroplasts did not cause changes in PG core-associated proteins such as FBN1 or FBN2 homologs (**Figure C1-2B**). These results provide further indirect evidence that FBN6 and PSY are not PG-associated proteins. Together, we conclude that Arabidopsis FBN6 and PSY interact and preferentially co-localize in particular locations of the chloroplast such as envelope or thylakoid membrane domains different from PG.

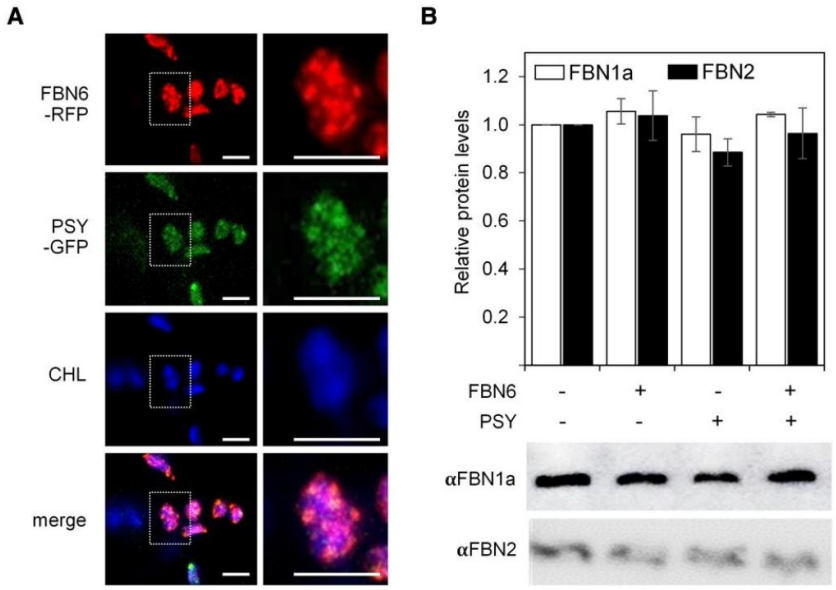


Figure C1-2. FBN6 and PSY co-localize in chloroplasts. *N. benthamiana* leaves were co-agroinfiltrated with constructs encoding FBN6-RFP and PSY-GFP, and 4 d later, samples were taken for confocal and immunoblot analyses. **A)** Representative confocal microscopy images of a leaf section transiently expressing the indicated fluorescent fusion proteins. All panels in the same column show the same field. RFP fluorescence is shown in the top panels, GFP fluorescence in the second row, and chlorophyll autofluorescence in the third row. Bottom panels show a merge of the 3 fluorescence channels. Right panels are a magnification of the area boxed in white in the left panels. Bars, 5 μm. **B)** Immunoblot analysis of the accumulation of FBNs identified using antibodies against Arabidopsis PG-associated FBN1a and FBN2 proteins in leaves expressing the indicated constructs or a GFP control (−/−). Quantification was made by relativizing each band intensity to the one obtained in the control. Representative results are shown in the lower panels. Barplot shows the mean ± SD values of quantitative data from n = 3 leaves.

FBN6 promotes PSY activity

To investigate whether FBN6 might influence PSY activity in the chloroplasts of plant cells, we analyzed the production of phytoene (the direct product of PSY activity) and downstream carotenoids in *N. benthamiana* leaves agroinfiltrated with constructs to transiently express the Arabidopsis genes encoding FBN6, PSY, or both (**Figure C1-3** and **Supplemental Tables C1-2** and **C1-3**). Control leaves were agroinfiltrated with a GFP construct. While phytoene was not detected in control or FBN6 samples, it was present in PSY samples, and it increased in samples agroinfiltrated with both FBN6 and PSY (**Figure C1-3A**). To investigate whether overexpression of FBN6 could also impact the endogenous PSY enzymes in *N. benthamiana* leaves, we used norflurazon (NFZ). This inhibitor prevents phytoene conversion into downstream carotenoids, thereby allowing indirect estimation of PSY activity through quantifying the amount of phytoene accumulation in NFZ-treated tissues. As expected, phytoene was detected in all the samples treated with NFZ. FBN6 samples showed a slight but statistically significant increase in phytoene compared with GFP controls, in agreement with the conclusion that FBN6 is a promoter of endogenous PSY activity. In *PSY*-overexpressing samples, the presence of FBN6 led to a much more obvious increase in phytoene content (**Figure C1-3A**). In the case of total carotenoids, FBN6 alone did not lead to increased levels but a combination of FBN6 and PSY resulted in more carotenoids than PSY alone (**Figure C1-3B**). FBN6 also promotes the activity of plant PSY (but not bacterial crtB) in *E.coli* cells, i.e., in the absence of other plastid proteins that might indirectly improve PSY activity (Iglesias-Sanchez et al., 2024; Annex 1). Consistent with the results in bacterial systems, the effect of FBN6 in enhancing PSY-promoted carotenoid accumulation in agroinfiltrated *N. benthamiana* leaf cells was not observed when crtB was used instead of the plant PSY enzyme (**Figure C1-3B**). Furthermore, PSY folding or degradation rate was not altered by the interaction with FBN6 (Iglesias-Sanchez et al., 2024; Annex 1). These results together support a positive and specific effect of FBN6 on PSY activity. Specifically, we can conclude that FBN6 interaction with PSY leads to a higher enzymatic activity.

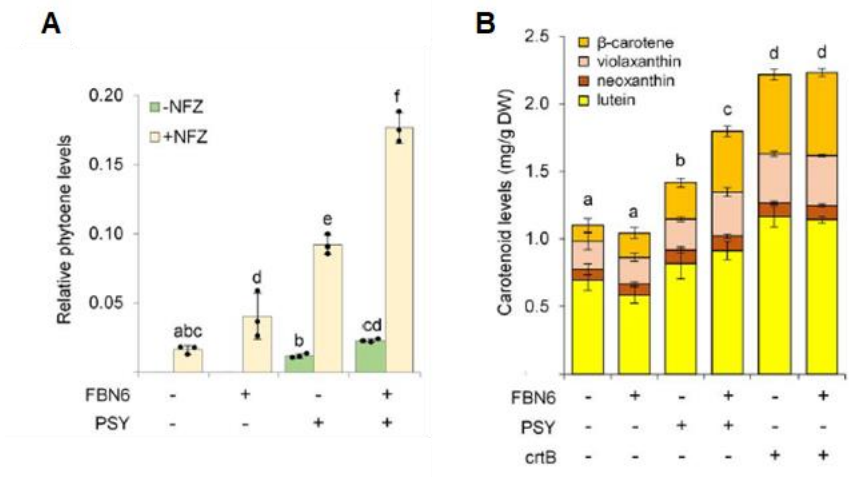


Figure C1-3. FBN6 promotes phytoene and downstream carotenoid production. *N. benthamiana* leaves were agroinfiltrated with the indicated constructs, and 4 d later, samples were taken for HPLC analysis of carotenoids. A GFP construct was used as a control. **A)** Phytoene levels in leaf samples either treated (+) or not (−) with NFZ 1 day after agroinfiltration with GFP, PSY, or/and FBN6 constructs. Values are represented relative to total carotenoid levels in untreated control leaves and they correspond to the mean ± SD of n = 3 leaf samples. **B)** Levels of downstream carotenoids in untreated samples. DW, dry weight. Values correspond to the mean ± SD of n = 3 leaf samples. In both plots, different letters represent statistically significant differences ($P < 0.05$) among means of total carotenoids according to one-way ANOVA followed by post hoc Tukey's tests. Supplemental Tables S2 and S3show absolute values of carotenoid and chlorophyll levels

Genetic evidence confirms the functional relevance of FBN6 for PSY activity

If FBN6 is a positive regulator of PSY activity, loss of FBN6 in mutants would be expected to prevent normal carotenoid synthesis. FBN6-defective Arabidopsis *fbn6-1* mutants were found to have reduced chlorophyll levels compared with wild-type (WT) controls, but no data on carotenoid levels were reported (Lee et al. 2020). In Arabidopsis, the most active production of carotenoids takes place during de-etiolation to protect the emerging photosynthetic apparatus against photooxidative damage caused by excess incoming light (Rodríguez-Villalón et al., 2009). The boost in carotenoid synthesis during de-etiolation is mediated in part by increased expression of the PSY-encoding gene in Arabidopsis (Rodríguez-Villalón et al., 2009; Toledo-Ortiz et al., 2010). Interestingly, the gene encoding FBN6 was also highly induced during this process

(**Figure C1-4A**). Because co-expression is only associative evidence of a possible common role, we next used genetics to test whether FBN6 activity was required for normal carotenoid production in etiolated and de-etiolating seedlings. Compared with the WT, the *fbn6-1* mutant contains similar levels of carotenoids in etiolated seedlings, but it shows a strongly attenuated production during de-etiolation (up to 24 h after illumination). As a result, greening (chlorophyll accumulation) was delayed (**Figure C1-4B** and **Supplemental Table C1-4**). After a few days under normal light (NL), the differences in carotenoid (and chlorophyll) levels between WT and *fbn6-1* plants were attenuated but still detectable (**Figure C1-4C** and **Supplemental Table C1-5**). To test the putative influence of increased FBN6 on carotenoid biosynthesis in etiolated and de-etiolating seedlings, we transformed Arabidopsis plants with a construct to overexpress an RFP-tagged FBN6 protein. Most transformants showed no RFP fluorescence, and the ones producing detectable levels of FBN6-RFP protein showed levels of total *FBN6* transcripts (endogenous and transgenic) that were similar or lower than those in untransformed controls (**Supplemental Figure C1-1**). These results suggest that accumulation of FBN6-encoding transcripts is tightly regulated, perhaps to maintain a balanced ratio with *PSY* transcripts (**Figure C1-4A**).

Carotenoid levels, but not *PSY* expression, increase when Arabidopsis plants are exposed to high light (HL), suggesting an up-regulation of PSY enzyme activity to increase the metabolic flux toward carotenoid synthesis (Kreslavski et al., 2021). Similar to *PSY*, transcripts encoding FBN6 also showed unchanged levels when 9-d-old Arabidopsis seedlings were exposed for 24 h to HL compared with controls left at NL for the same time (**Figure C1-4A**). Most interestingly, the HL-triggered increase in carotenoid levels was highly attenuated in FBN6-defective plants compared with the WT controls (**Figure C1-4C**). By contrast, the reduction in chlorophylls associated with HL exposure was similar in WT and *fbn6-1* seedlings in absolute terms but seemingly stronger in the mutant in relative terms (**Figure C1-4C**), likely because disrupted up-regulation of carotenoid contents in *fbn6-1* seedlings results in defective photoprotection and a higher chlorophyll degradation rate. We conclude that FBN6 is required to support the increase in carotenoid levels that takes place in response to HL, a role that is consistent with its proposed PSY-promoting activity.

An alternative connection between FBNs and carotenoids

FBN gene expression often parallels the carotenoid content of non-photosynthetic plant tissues, e.g. during fruit ripening, where their role is assumed to be mainly structural (Singh and McNellis 2011). Indeed, FBNs were initially identified as proteins specifically associated with carotenoid accumulation in fruit and petal chromoplasts, as components of "fibrils" and PG structures (Deruère et al., 1994; Vainstein et al., 1994). Similarly, green algae FBNs were also proposed to be involved in the formation and stabilization of the chloroplast eyespot, a carotenoid-rich light sensing system (Schmidt et al., 2006; Davidi et al., 2015). More recently, rapeseed and melon FBN1 homologs were shown to contribute to carotenoid accumulation by interacting with other proteins and promoting PG proliferation in flower and fruit chromoplasts (Li et al. 2023; Zhou et al. 2023). However, in plant chloroplasts, carotenoids are not normally concentrated in PG or any other lipid body but are distributed in thylakoids and, to a lower extent, envelope membranes (Morelli et al. 2023). Despite the fact that chloroplast FBNs are presumed to maintain photosynthetic function and are present in all the compartments where carotenoids are synthesized and accumulated, a direct functional association between FBNs and carotenoid biosynthesis has remained unexplored.

Studies on FBN-interacting proteins have substantially improved our understanding of the function of different FBN family members in chloroplasts. Arabidopsis FBN1a, FBN1b, and FBN2 interact with each other, presumably forming a network around the PG surface that might be important to recruit other FBN-interacting proteins to PG (Gámez- Arjona et al. 2014; Torres-Romero et al. 2022). For example, these FBNs interact with allene oxide synthase, which catalyzes one of the first steps of jasmonic acid (JA) biosynthesis. FBN2 also interacts with other proteins involved in different metabolic processes, including other enzymes of the JA pathway and the carotenoid cleavage dioxygenase CCD4, a PG-associated enzyme involved in carotenoid degradation (Torres-Romero et al., 2022). It was proposed that FBN2 might mediate the recruitment of JA biosynthetic enzymes to the PG under stress conditions, but the functional relevance of the interaction with CCD4 was not explored (Torres-Romero et al. 2022). FBN1a and FBN1b also interact with starch synthase isoform 4 (SS4), but the elimination of the

FBNs does not alter the initiation of starch granule formation (Gámez-Arjona et al. 2014). FBN4 interacts with the major ferredoxin protein in Arabidopsis (Fd2) and with harpin protein HrpN, an elicitor secreted by pathogenic bacteria that activates plant defense and resistance (Kim and Kim 2022). FBN5 participates in the production of the plastidial isoprenoid plastoquinone through interaction with solanesyl diphosphate synthase isoforms 1 and 2 (SPS1 and SPS2), which catalyze the first committed step in the production of the prenyl chain of the molecule (Kim et al. 2015).

The lipocalin motif of FBN4 likely contributes to the role of this isoform in the trafficking of plastoquinone and other small lipids between the thylakoids and the PG (Singh et al. 2012). Interestingly, FBN6 also contains a lipocalin motif (Singh and McNellis 2011). Based on that proposed for FBN5, a non-PG FBN protein, we speculate that direct interaction of FBN6 with PSY might result in improved activity of the enzyme by facilitating removal of the phytoene product from the active site. Regardless of the specific mechanism involved, our data support the conclusion that FBN6 plays a physiologically relevant role in carotenoid biosynthesis in Arabidopsis chloroplasts by physically binding to PSY to promote its enzymatic activity. Therefore, we demonstrate that FBNs promote not only the accumulation of carotenoids but also their biosynthesis. The unveiled role of FBN6 in carotenogenesis reported here can explain the phenotypes previously reported for the *fbn6-1* mutant, which were similar to those of mutants disrupted in ROS homeostasis (Lee et al. 2020). Because carotenoids are essential photoprotectants that dissipate excess light energy as heat and detoxify excess ROS in chloroplasts (Rodriguez-Concepcion et al. 2018), we conclude that the reduced acclimation to light stress and impaired ROS scavenging phenotypes observed in the *fbn6-1* mutant are likely a primary result of defective carotenoid biosynthesis. Lower growth, increased glutathione levels, or resistance to cadmium stress would be secondary effects of impaired ROS homeostasis.

Similar to the up-regulation of *PSY* and *FBN6* genes during Arabidopsis de-etiolation (**Figure C1-4A**), the burst in carotenoid synthesis that takes place during tomato fruit ripening is also associated with increased expression of genes encoding the corresponding PSY and FBN6 homologs (Barja et al., 2021; Sun et al., 2022). This

observation suggests that FBN6-dependent promotion of PSY activity and carotenoid biosynthesis might not be restricted to chloroplasts but can also occur in chromoplasts. Further experiments with FBN6-defective tomato plants should confirm this possibility and provide additional insights into the possible biotechnological use of this FBN isoform.

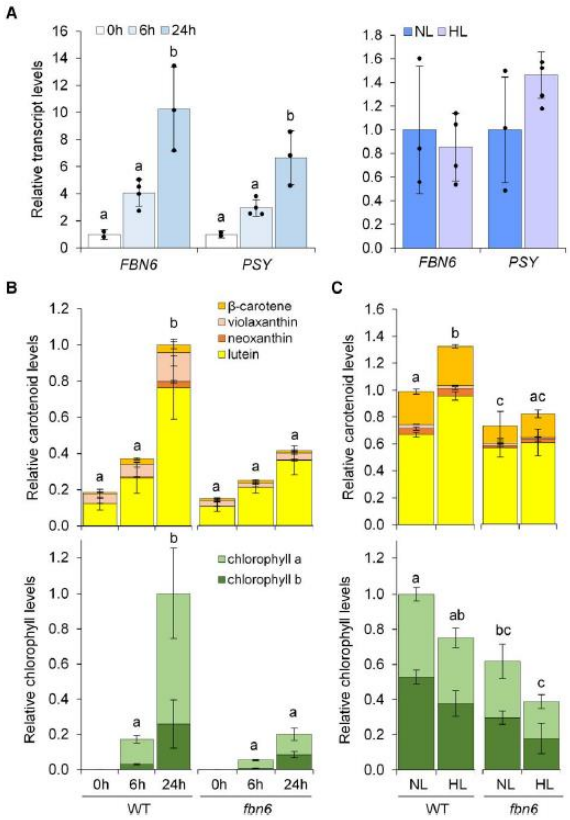


Figure C1-4. FBN6 is required for carotenoid production in Arabidopsis. De-etiolation experiments were carried out with Arabidopsis WT and FBN6-defective mutant seeds germinated in the dark for 3 d; the resulting etiolated seedlings were then exposed to white light for 6 and 24 h. For HL experiments, WT and *fbn6* seedlings germinated and grown under NL conditions for 9 d were exposed for 24 h to either NL (as a control) or HL. **A)** Expression profiles of genes encoding FBN6 and PSY during de-etiolation (left) or HL exposure (right) of WT seedlings. Transcript levels are normalized using the *UBC21* gene and shown relative to etiolated (0 h) or NL-exposed samples, respectively. **B)** Carotenoid and chlorophyll levels in de-etiolating WT and *fbn6* seedlings. Values are represented relative to total pigment levels in WT 24 h samples. **C)** Carotenoid and chlorophyll levels in HL-exposed WT and *fbn6* seedlings. Values are represented relative to total pigment levels in WT NL samples. In all plots, mean ± SD of $n \geq 3$ replicates are

represented. Letters represent statistically significant differences ($P < 0.05$) among means of total carotenoids and chlorophylls according to one-way ANOVA followed by post hoc Tukey's tests. Supplemental Tables S4 and S5 show absolute values of carotenoid and chlorophyll levels.

Supplemental Data

Primer Name	Use	Sequence (5'-3')
GK159E10-gF	Genotyping	TGGTCATAACGAGGAATCCAG
GK159E10-gR	Genotyping	ACGATATCAGGAGCATCGATG
AtFBN6-gF	Genotyping	CGCCATATGGTCAGTTCTGTTTCAGCTCC
AtFBN6-gR	Genotyping	GCGGAGCTCTTGACGCCTTCTAAAGACG
AtFBN4-attB1-F	Cloning	GGGGACAAGTTTGTACAAAAAAGCAGGCTGGATGGCGACTTCTTCTACTTTC
AtFBN4-attB2-R	Cloning	GGGGACCACTTTGTACAAGAAAGCTGGGTCAGCAATGACGAATACCCTAAG
cSlFBN4-Nde-F	Cloning	TACATATGCAGTCGGGTATTGATGAAGTC
cSlFBN4-Xho-R	Cloning	TGCTCGAGTGAGATAACGAAAACTCTAAG
AtFBN6-attB1-F	Cloning	GGGGACAAGTTTGTACAAAAAAGCAGGCTGGATGGCTGCGACTGCTTCTTCTC
AtFBN6-attB2-R	Cloning	GGGGACCACTTTGTACAAGAAAGCTGGGTCTTGACGCCTTCTAAAGACG
cAtFBN6-Nde-F	Cloning	CGCCATATGGTCAGTTCTGTTTCAGCTCC
cAtFBN6-Xho-R	Cloning	GCGCTCGAGTTGACGCCTTCTAAAGACG
AtPSY-attB1-F	Cloning	GGGGACAAGTTTGTACAAAAAAGCAGGCTGGATGTCTTCTTCTGTAGCAGTG
AtPSY-attB2-R	Cloning	GGGGACCACTTTGTACAAGAAAGCTGGGTCTATCGATAGTCTTGAACTTGAAG
cAtPSY-attB1-F	Cloning	GGGGACAAGTTTGTACAAAAAAGCAGGCTTCATGTCAAGCTTAGTAGCAAGTCC
cAtPSY-attB2-R	Cloning	GGGGACCACTTTGTACAAGAAAGCTGGGTTTCATATCGATAGTCTTGAACTTG
AtFBN6-qF	RT-qPCR	TGAAAGCGTTGGACAGTGAG
AtFBN6-qR	RT-qPCR	GAAGCTTCACTTCGCTTTCG
AtPSY-qF	RT-qPCR	GACACCCGAAAGGCGAAAGG
AtPSY-qR	RT-qPCR	CAGCGAGAGCAGCATCAAGC
AtUBC21-qF	RT-qPCR	TCAAATGGACCGCTCTTATC
AtUBC21-qR	RT-qPCR	CACAGACTGAAGCGTCCAAG

Supplemental Table C1-1. Primers used in this work.

Treatment	**Constructs**	**Phytoene** (µg/g DW)
Control (- NFZ)	GFP	0.0 ± 0.0
	FBN6	0.0 ± 0.0
	PSY	5.8 ± 0.8
	FBN6+PSY	11.2 ± 0.6
Treated (+NFZ)	GFP	7.9 ± 1.4
	FBN6	19.9 ± 8.2
	PSY	45.1 ± 3.5
	FBN6+PSY	86.6 ± 5.3

Supplemental Table C1-2. Phytoene levels in control and NFZ-treated N. benthamiana leaves agroinfiltrated with FBN6 and/or PSY constructs. Levels correspond to the mean ± SD of n=3 independent experiments.

Combination	β-carotene (µg/g DW)	Violaxanthin (µg/g DW)	Neoxanthin (µg/g DW)	Lutein (µg/g DW)	Total carotenoids (mg/g DW)	Total chlorophylls (mg/g DW)
GFP	118.2 ± 49.6	205.6 ± 62.8	79.5 ± 40.8	696.6 ± 77.4	1.1 ± 0.1	1.2 ± 0.1
FBN6	178.9 ± 41.9	195.9 ± 29.6	84.0 ± 14.9	583.7 ± 58.0	1.0 ± 0.1	1.1 ± 0.2
PSY	270.2 ± 32.3	227.0 ± 16.4	100.4 ± 25.3	818.3 ± 113.0	1.4 ± 0.2	1.3 ± 0.4
FBN6+PSY	446.9 ± 38.3	328.0 ± 34.4	106.8 ± 15.5	913.2 ± 67.0	1.8 ± 0.1	1.5 ± 0.2
crtB	585.4 ± 39.5	362.5 ± 18.3	102.5 ± 9.7	1165.3 ± 76.4	2.3 ± 0.1	1.1 ± 0.1
crtB+PSY	614.6 ± 30.6	368.0 ± 7.9	104.8 ± 11.1	1143.3 ± 23.5	2.4 ± 0.1	1.1 ± 0.1

Supplemental Table C1-3. Photosynthetic pigment levels in N. benthamiana leaves agroinfiltrated with FBN6, PSY and/or crtB constructs. Levels correspond to the mean ± SD of n=3 independent experiments.

Line	Time	β-carotene (µg/g DW)	Violaxanthin (µg/g DW)	Neoxanthin (µg/g DW)	Lutein (µg/g DW)	Chlorophyll *a* (µg/g DW)	Chlorophyll *b* (µg/g DW)
WT	0h	3.3 ± 1.1	19.1 ± 9.4	0.4 ± 0.3	46.0 ± 13.2	0.0 ± 0.0	0.0 ± 0.0
	6h	11.3 ± 2.2	25.6 ± 5.2	2.0 ± 0.4	98.1 ± 31.5	14.1 ± 2.0	2.9 ± 0.4
	24h	15.4 ± 7.6	59.4 ± 1.8	12.0 ± 2.0	283.2 ± 64.8	73.4 ± 25.1	25.5 ± 13.6
fbn6	0h	4.5 ± 1.2	11.6 ± 1.8	0.7 ± 0.2	38.5 ± 9.6	0.0 ± 0.0	0.0 ± 0.0
	6h	6.1 ± 1.9	7.4 ± 5.2	0.5 ± 0.1	77.4 ± 11.9	4.6 ± 0.3	0.7 ± 0.2
	24h	5.2 ± 1.6	14.0 ± 1.8	0.6 ± 0.1	132.1 ± 29.2	11.3 ± 3.5	8.4 ± 1.8

Supplemental Table C1-4. Photosynthetic pigment levels in etiolated and deetiolated WT and fbn6 Arabidopsis seedlings. Levels correspond to the mean ± SD of n=3 independent experiments.

Line	Light	β-carotene (mg/g DW)	Zeaxanthin (µg/g DW)	Violaxanthin (µg/g DW)	Neoxanthin (µg/g DW)	Lutein (mg/g DW)	Chlorophyll *a* (mg/g DW)	Chlorophyll *b* (mg/g DW)
WT	NL	0.33 ± 0.06	0.00 ± 0.00	43.73 ± 3.82	58.68 ± 10.25	0.90 ± 0.10	0.57 ± 0.16	0.62 ± 0.12
	HL	0.39 ± 0.06	0.87 ± 0.04	26.37 ± 2.35	76.05 ± 4.65	1.29 ± 0.10	0.44 ± 0.08	0.44 ± 0.10
fbn6	NL	0.17 ± 0.12	0.00 ± 0.00	23.65 ± 10.66	20.39 ± 16.95	0.78 ± 0.03	0.38 ± 0.06	0.36 ± 0.11
	HL	0.24 ± 0.02	0.29 ± 0.01	15.28 ± 1.47	36.38 ± 2.02	0.83 ± 0.06	0.25 ± 0.02	0.22 ± 0.12

Supplemental Table C1-5. Photosynthetic pigment levels in WT and fbn6 Arabidopsis seedlings exposed to high light. Levels correspond to the mean ± SD of n=3 independent experiments.

Chapter 2. The Lack of Alternative Oxidase 1a Restricts in vivo Respiratory Activity and Stress-Related Metabolism for Leaf Osmoprotection and Redox Balancing Under Sudden Acute Water and Salt Stress in *Arabidopsis thaliana*

Introduction

Plants display several mechanisms for drought and salinity tolerance, however, these come with high energy and carbon demands that plant metabolism meets by adjusting photosynthesis and respiration (Munns et al., 2020; Vanlerberghe et al., 2020). An important tolerance mechanism to drought and salinity resides in the accumulation of metabolites that play multiple protective roles, including primary metabolites such as organic acids, sugars and polyols (Sanchez et al., 2008; Fàbregas and Fernie, 2019), as well as polyamines (Alcázar et al., 2020). These stress-related metabolites (SRMs) from primary metabolism, protect against osmotic and oxidative stress, serve as energy sources and/or are involved in stress-signalling pathways (Slama et al., 2015; Pires et al., 2016; Fàbregas and Fernie, 2019). At the same time, the synthesis and degradation of several SRMs involve metabolic pathways that are tightly linked to respiratory metabolism (Pires et al., 2016; Batista-Silva et al., 2019; Bandehagh and Taylor, 2020)(. Thus, SRMs or their carbon precursors [i.e., glycolytic or tricarboxylic acid (TCA) cycle intermediates] are tightly associated to the generation of reducing equivalents (NADH and FADH2), from which oxidation is coupled to the mitochondrial electron transport chain (mETC). A distinctive feature of the plant mETC is the presence of two terminal oxidases. In addition to the cyanide sensitive cytochrome oxidase (COX), the presence of a cyanide-resistant alternative oxidase (AOX) that couples the oxidation of ubiquinol with the reduction of O2 to H2O, confers to mETC the capacity to sustain O2 consumption under COX restriction (Del-Saz et al., 2018; Vanlerberghe et al., 2020). Electron transport via the AOX pathway (AOP) is not coupled with energy conservation (Del-Saz et al., 2018; Vanlerberghe et al., 2020). Nonetheless, the AOP provides metabolic flexibility that helps plants acclimate to stress by allowing the oxidation of reducing equivalents coupled to TCA cycle and/or cytosolic reactions under conditions where the COX pathway (COP) is restricted (Del-Saz et al., 2018). In fact, the accumulation of SRMs has been reported to coincide with higher respiratory rates (Mattoo et al., 2006; Del-Saz et al., 2016; Pires et al., 2016; Bandehagh and Taylor, 2020), indicating an active mitochondrial metabolism under stress. Nevertheless, direct evidence about the influence of the AOP activity in modulating the synthesis of stress-related metabolites remains scarce.

The AOX protein is encoded by a multigene family which exhibits tissue-specific expression (Saisho et al., 1997; Clifton et al., 2006; Selinski et al., 2018a). AOX1 isoforms generally show the highest expression levels, being expressed in most tissues and induced by stress treatments in several species (Clifton et al., 2006; Vanlerberghe et al., 2020). Over the last two decades, reverse genetics has been used to decrease *AOX1* gene expression in order to test hypotheses regarding the role of the AOP. Following the suppression of *AOX1*, the amount of the AOX protein has been found to be markedly decreased concomitantly with a decrease in the AOP capacity (the maximum possible flux of electrons to AOX; (Guy and Vanlerberghe, 2005; Umbach et al., 2005; Watanabe et al., 2010; Florez-Sarasa et al., 2011; Xu et al., 2012; Vishwakarma et al., 2015; Zhang et al., 2016; Garmash et al., 2020). In parallel, many studies have observed an increase in AOX protein or capacity under stress in wild-type plants (reviewed in Vanlerberghe, 2013; and in Vanlerberghe et al., 2020). In fact, a regulated overcapacity of AOP is thought to be required for ensuring an adequate activity under conditions inducing metabolic fluctuations(Rasmusson et al., 2009; Florez-Sarasa et al., 2011). By contrast to AOP capacity, *in vivo* AOP activity can be directly determined in the absence of added inhibitors by measuring the differential oxygen isotope discrimination during respiration (Day et al., 1996; Del- Saz et al., 2017). While there is substantial evidence on the molecular mechanisms regulating the AOX gene expression in response to drought and salinity stresses (Vanlerberghe, 2013; Dahal and Vanlerberghe, 2017; Zhu et al., 2018; Gong et al., 2020), only some studies have addressed when and to which extent the *in vivo* AOP activity is effectively responding. The *in vivo* AOP activity was reported to increase in response to severe drought and salt stress (Ribas-Carbo et al., 2005; Del-Saz et al., 2016), while unaltered activities were reported under milder or longer drought/salinity periods (Galle et al., 2010; Martí et al., 2011). These different responses denote, as previously highlighted (Munns et al., 2020), that *in vivo* AOP activity determinations in combination with detailed metabolic and molecular analyses remain crucial for understanding the key changes in energy and carbon metabolism conferring drought (Vanlerberghe et al., 2020) and salt (Munns et al., 2020) tolerance.

In order to gain insight into the role of the AOP during stress-related metabolism, wild-type *Arabidopsis thaliana* plants and *aox1a* T-DNA insertional mutants, were treated

with high concentrations (1 day, 300 mM) of mannitol and salt (NaCl), known to greatly induce the accumulation of several SRMs (Del-Saz et al., 2016; Darko et al., 2019). The AOX capacity in leaves was measured using the liquid-phase Clark-type oxygen electrode technique and in parallel, leaf levels of primary metabolites and respiratory-related transcripts were also determined. In addition, leaf relative water content as well as photosynthetic performance, determined by chlorophyll fluorescence analysis in the dark and in the light, was also studied. We hypothesized that the lack of *AOX1a* will be associated with lower leaf rates of AOP respiration and less accumulation of SRMs under severe water and salt stress, with consequences for plant performance under stress.

Materials and methods

Plant Material and Growth Conditions

Seeds of wild-type (WT) *A. thaliana* Columbia 0 (Col 0) and *aox1a* T-DNA insertion line (SALK_084897) were sown in pre-wetted pots with a mixture of peat-perlite (3:1). The T-DNA insertion within the *Arabidopsis AOX1a* gene was confirmed by genomic PCR with T-DNA-specific primers and seeds from a homozygous line were used for the experiments. Pots were placed in plastic trays used for sub-irrigation. Plants were grown in a growth chamber for 32–35 days at 12 h/12 h photoperiod, 150 µmol quanta m^{-2} s^{-1} light intensity, 25 ºC/ 20 ºC day/night temperature and relative humidity above 50%. Plants were watered twice a week with half-strength Hoagland's solution (Epstein et al., 1972). On days 32–35, plants were divided in three groups, one was watered normally (control plants) while the other two were irrigated with watering solution containing 300mM of sodium chloride (NaCl-treated plants) or 300 mM mannitol (Mannitol-treated plants). The analyses of control and treated plants were performed one day after the irrigation. All the experiments were repeated at least twice, and data is presented as a pool of at least two individual experiments (i.e., each consisting of two to four biological replicates/plants per genotype and treatment), since similar results were obtained in each individual experiment.

Leaf Water Status

Leaf relative water content (RWC) was determined as follows:

$$RWC\ (\%) = (FW - DW)/(TW - DW) \times 100$$

where fresh (FW), turgid (TW) and dry (DW) weight of leaves were measured. FW was determined immediately after sampling; TW was obtained after incubating leaf discs in distilled water for 48 h in the dark at 4 ºC (to minimize respiration losses) and DW was determined after drying for at least 2 days in an oven at 60-70 ºC.

Respiration Measurements

Leaves were placed in the dark for 30 min to avoid light- enhanced dark respiration. The capacity of the alternative pathway (V_{alt}) was determined with an oxygen electrode as previously described (Del-Saz et al., 2016), and results were expressed in nmol O2 g^{-1} dry weight s^{-1} as the mean ± SE of five or six biological replicates. Dry weights were obtained after drying leaves for 2 days at 60-70 ºC.

Photosynthetic Measurements

Chlorophyll fluorescence measurements were carried out on rosette leaves using a MAXI-PAM fluorometer (Heinz Walz GmbH) as previously described (Morelli et al., 2021; Annex 2). Briefly, for every measurement six rosette leaves from each plant were considered. The actual quantum efficiency of the photosystem II (PSII)-driven electron transport (ΦPSII) was determined under different light intensities (in µmol photons $m^{-2}s^{-1}$ of photon flux density, PPFD): 800, 700, 600, 500, 400, 300, 200, 150, 100, 75, 50, 25 and 0. The chloroplast electron transport rate (ETR) was calculated as the product of ΦPSII x PPFD x 0.84 x 0.5, where 0.84 and 0.5 were assumed values for the leaf light absorptance and the fraction of absorbed quanta available for PSII. From the light response curves, the associated parameters ETR_{max} (maximum electron transport rate) and alpha (photosynthetic rate in light limited region of the light curve) were characterized by fitting iteratively the model of the rETR versus E curves using MS Excel Solver (Platt and Gallegos, 1980). The fit was very good in all the cases ($r > 0.98$). After the light curves, the maximum quantum efficiency of PSII, F_v/F_m, was calculated as $(F_m - F_o)/F_m$, where F_m and F_o are the maximum and the minimum fluorescence of dark-adapted samples, respectively. For dark acclimation, plants were incubated for at

least 30 min in darkness to allow the full relaxation of photosystems.

Metabolite Profiling

Metabolite extractions were performed as described previously (Lisec et al., 2006) using approximately 50 mg of leaf tissue, previously frozen-powdered. Derivatization and GC–TOF–MS analyses were carried out as described previously (Lisec et al., 2006). Metabolites were identified manually by TagFinder software (Luedemann et al., 2012) using the reference library mass spectra and retention indices housed in the Golm Metabolome Database;(http://gmd.mpimp-golm.mpg.de/) (Kopka et al., 2005). The parameters used for the peak annotation of the 46 metabolites can be found in **Supplementary Table C2- 1**, which follows previously reported recommendations (Fernie et al., 2011).

To process the GC-TOF-MS results, the intensity of a selected unique ion shown in **Supplementary Table C2-1** was normalized to that of ribitol which was added to each sample as an internal standard, as well as to the fresh weight of the materials used for metabolite extraction. Fresh weight was then corrected by dry weight/fresh weight ratios used to determine the leaf RWC (see Section "Leaf Water Staus"). Thereafter, data were normalized to the mean value of Col-0 wild-type (WT) plants under control conditions (i.e., the value of all metabolites for WT at control conditions was set to 1). This normalization allowed the comparison of the relative metabolite levels among genotypes and treatments (**Supplementary Table C2-2**). In addition, leaf absolute metabolite levels (μmol gDW^{-1}) were also determined for all the metabolites detected and present in the authentic standards mixture (**Supplementary Table C2-3**). The experimental samples and standards mixtures containing 0, 100, 200, 500, and 1,000 ng of each compound were analysed in the same GC-MS runs, and the absolute metabolite amounts in the samples were calculated by extrapolation from standard curves using the peak intensity of a representative mass fragment. Values presented for both relative and absolute levels are means SE of four to six replicates corresponding to several fully expanded rosette leaves.

Western Blot Analysis

Protein extraction and western blot analysis was performed as previously described (Florez-Sarasa et al., 2016) with some modifications. Total plant protein extracts were obtained from 20 mg of frozen leaf powder resuspended in 100 µl SDS sample buffer [2% (w/v) SDS, 62.5mM Tris–HCl (pH 6.8), 10% (v/v) glycerol and 0.007% (w/v) bromophenol blue], 50 mM DTT and protease inhibitor cocktail (Roche Basel, Switzerland). Samples were incubated 30 min at 4◦C to allow full reduction of the AOX protein and then boiled (95◦C) for 5 min. The resuspended sample was centrifuged at 14,000 rpm for 10 min. After loading 25 µl on a 12% SDS-PAGE gel, proteins were transferred to a 0.45 µm Nitrocellulose membrane (Armersham Protan) using a semi-dry Trans-Blot® Turbo™ Transfer System of Bio-Rad. Membranes were incubated overnight at 4◦C with diluted 1:500 polyclonal anti-AOX, AOX1 and 2 (AS04054, Agrisera, Sweden) or diluted 1:5,000 anti-Porin, voltage-dependent anion-selective channel protein 1–5 (AS07212, Agrisera, Sweden). Incubation with 1:20,000 horseradish peroxidase secondary antibodies (Cytiva) during 1h at room temperature. The detection of immunoreactive bands was performed using ECL SuperSignal™ West Femto Maximum Sensitivity Substrate (Thermo Fisher). Chemiluminescent signals were collected by IQ 800 Armersham (Cytiva). The protein band quantifications were performed with ImageJ analysis software according to the manufacturer's instructions. The obtained band intensities for AOX were corrected for their corresponding porin band intensities and then normalized to the levels of the WT plants under control conditions (i.e., WT levels were set to 1). Three different immunoblot experiments per protein were performed and the image shown in **Figure C2-1B** belong to one of the three membranes obtained. Samples used in each of the three western blot experiments were a mixture of aliquots belonging to two biological replicates from the same six biological replicates used for the gene expression analysis. The relative values presented in **Figure C2-1B** are means of the three western blot experiments.

Gene Expression Analysis

RNA was isolated from lyophilized leaves by using Maxwell ® RSC Instrument (Promega Biotech Ibérica, Madrid, Spain) according to the manufacturer's instructions, and was quantified using a NanoDrop 1000 spectrophotometer (Thermo Scientific,2).

Afterward cDNA synthesis was performed following the recommendations of the Transcriptor First Strand cDNA Synthesis Kit (Roche Basel, Switzerland). Relative mRNA abundance was evaluated by quantitative PCR using LightCycler 480 SYBR Green I Master Mix (Roche Basel, Switzerland) on a LightCycler 480 real- time PCR system (Roche Basel, Switzerland). Primers used and the related information are detailed in the **Supplementary Table C2-4**. Two technical replicates of each biological replicate were performed, and the mean values were used for further calculations. *Arabidopsis thaliana* AtUbqC (At5g25760) was used as a reference gene to correct for differences in the total amount of transcripts and the $2-\Delta\Delta Ct$ method (Livak and Schmittgen, 2001) was used to calculate the fold-change of gene expression. Finally, data were normalized to the mean value of plants under control conditions in each genotype (i.e., the level of all transcripts for WT and *aox1a* mutants at control was set to 1).

Statistical Analyses

For the statistical analyses in **Figures C2-1–4 and C2-6**, a one- way ANOVA with a level of significance of $P < 0.05$ was performed with SPSS statistical software package, version 25 (IBM Corp., 2016, Armonk, New York, NY, USA), and Duncan's posthoc test was used to determine statistically significant differences. In addition, Student's t tests were used for the statistical analyses in **Figures C2-1B, C2-5, C2-6, Supplementary Figure C2-1**, **Supplementary Tables C2-2, C2-3** in order to determine significant ($P < 0.05$) differences between genotypes under each experimental condition **(Figure C2-5, Supplementary Figure C2-1, Supplementary Tables C2-2, C2-3)**, or to determine significant ($P < 0.05$) differences between control and stress treatments in each genotype **(Figures C2-1B, C2-6, Supplementary Tables C2-2, C2-3)**.

Results

The Alternative Oxidase Capacity and Expression in aox1a and Wild-Type Plants Under Control and Stress Conditions

The capacity of the alternative oxidase pathway (V_{alt}), measured as the KCN-resistant respiration, was determined in both genotypes under control and stress treatments (**Figure C2-1**). As expected, V_{alt} was significantly ($P < 0.05$) lower in *aox1a* mutants than in WT plants (5.9 and 19.1 nmol O_2 g^{-1} DW s^{-1}, respectively) under control

conditions.

Under stress, V_{alt} increased in WT plants after salt treatment, while mannitol-treated plants displayed an intermediate V_{alt} increased in WT plants after salt treatment, while mannitol-treated plants displayed an intermediate V_{alt} (**Figure C2-1A**). On the other hand, V_{alt} remained similar in *aox1a* mutants under control and stress conditions, and it was much lower as compared to WT plants under stress conditions. Then, the AOX protein levels were determined in leaf crude extracts after immunoblotting analyses and quantified after normalization to mitochondrial porin levels (**Figure C2-1B**). In the line with respiratory capacity, the AOX protein levels were similarly increased after both stress treatments in WT plants. We did not detect any signal of AOX protein in the *aox1a* mutants as previously reported (Giraud et al., 2008; Strodtkötter et al., 2009). Thereafter, the expression profiles of the five genes encoding the AOX protein in Arabidopsis were determined by qPCR analyses in both genotypes under control and stress conditions (**Figure C2-1C**). Transcript levels of the *AOX1a* gene were not detected in the *aox1a* mutant, thus confirming the expected effect of the *aox1a* mutation, while the expression of this gene was induced in WT plants under both stress conditions (**Figure C2-1C**), particularly under salinity (7.2-fold increase). The transcript levels of *AOX1b* and *AOX2* were below the level of detection in all control and most of the stress-treated samples. The transcript levels of *AOX1c* were generally not responsive to stress, except for the slight significant ($P < 0.05$) increase in WT plants after mannitol treatment. On the other hand, the levels of *AOX1d* transcripts were highly responsive to both stress conditions, particularly in the *aox1a* mutants, which display a much higher response than in WT plants.

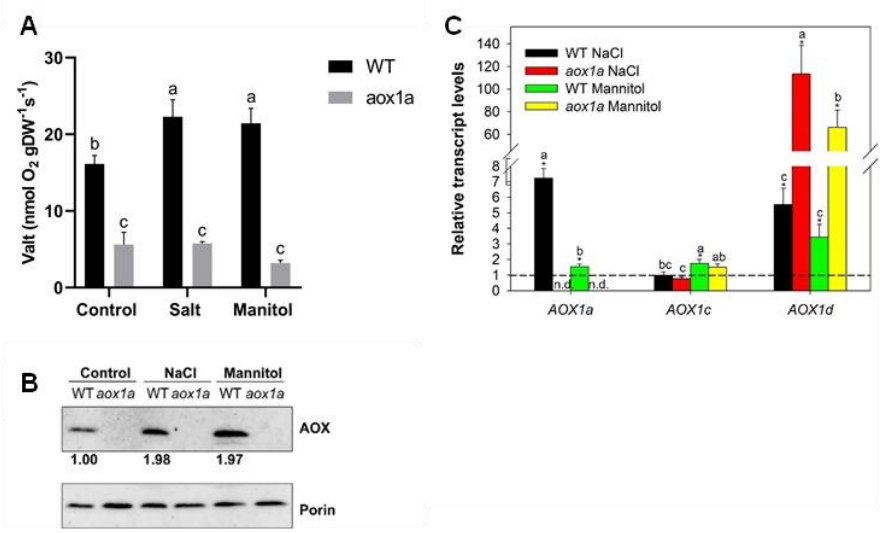


Figure C2-1. Alternative oxidase (AOX) pathway capacity (Valt) and expression analysis. **A)** V_{alt} determined (see section "Materials and Methods") in leaves of wild-type Col 0 (WT) and *aox1a* *Arabidopsis thaliana* plants untreated with NaCl or Mannitol (Control), and after 1 day of severe NaCl or Mannitol treatments (300 mM). Values are means ± SE of 5–6 biological replicates. Significant differences ($P < 0.05$) are denoted by different letters. **B)** Western blot analysis of AOX and porin (VDAC) protein levels from total leaf protein extracts (see section "Material and Methods" for details). The intensities of the signals from AOX were normalized to those from porin (VDAC) and are expressed relative to WT levels under control conditions. The normalized intensity values shown are averages of three independent blots. **C)** Transcript levels of genes encoding AOX isoforms determined by qPCR analyses (see Materials and Methods for details) under control and stress conditions. Data are shown as fold-changes relative to control conditions (i.e., all control values were set to 1, which is denoted by the dashed line). Primers used and gene information can be found in Supplementary Table 4. Values are means ± SE of 5–6 replicates and asterisks denote significant differences ($P < 0.05$) to the control condition for each gene expression analysis. Letters denote significant differences ($P < 0.05$) among genotypes and stress conditions for each gene expression analysis. n.d. (not detected).

Leaf Phenotype and Water Status in*aox1a* and Wild-Type Plants Under Control and Stress Conditions

Wild-type (WT) and *aox1a* mutant plants did not show visual differences under control conditions, as previously observed in several other studies (**Figure C2-2A**). Acute salt and mannitol treatments caused minor leaf wilting in both WT and *aox1a* mutant plants

after one day of stress (**Figure C2-2A**). Leaf relative water content (RWC) was determined as an indicator of water status in both genotypes after salt and mannitol treatments (**Figure C2-2B**). Salinity provoked a reduction of leaf RWC in both genotypes, while a significant ($P < 0.05$) reduction of leaf RWC after mannitol treatment was only observed in the *aox1a* mutants. Under both stress conditions, the leaf RWC was significantly ($P < 0.05$) lower in the *aox1a* mutants as compared to WT plants.

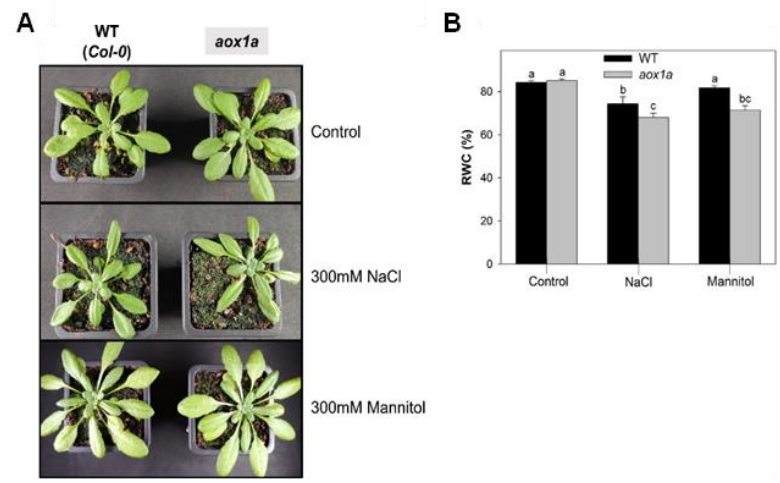


Figure C2-2. Visual phenotype and relative water content**. A)** Photographs representative of WT and *aox1a* plants untreated with NaCl or Mannitol (Control), and after 1 day of severe NaCl or Mannitol treatments (300 mM). **B)** Leaf relative water content (RWC) in leaves of WT and *aox1a* plants under control and stress conditions. Values are means ± SE of 10–12 biological replicates. Significant differences ($P < 0.05$) are denoted by different letters.

Photosynthetic Parameters in *aox1a* andWild-Type Plants Under Control and Stress Conditions

The chloroplast electron transport rate (ETR) was determined at different light intensities in *aox1a* and WT plants under control and stress conditions (**Figure C2-3A**). While similar light-response curves were obtained in both genotypes under control conditions, some differences were observed under stress (**Figure C2-3A**). Light curves were modelled to obtain photosynthetic parameters (see section "Materials and Methods" for details) such as alpha, which indicates the photosynthetic rate in the light-limited region of the light curve, and the maximum electron transport rate (ETR_{max}; **Figure C2-3B**). Both parameters were similar among genotypes under control conditions. Regarding

alpha, only *aox1a* mutants displayed a significant ($P < 0.05$) reduction after salt treatment as compared to control conditions, and this parameter became significantly ($P < 0.05$) lower in *aox1a* as compared to WT under salinity. On the other hand, the ETR_{max} was clearly reduced under both stress conditions and in both genotypes but notably, this parameter was significantly lower in the *aox1a* mutants as compared to WT plants under mannitol stress. In addition, the maximum efficiency of PSII (F_v/F_m) was determined by measuring chlorophyll fluorescence after dark adaptation, in order to evaluate the level of photoinhibitory stress after salt and mannitol treatments (**Figure C2-3B**). The F_v/F_m was also reduced in both genotypes under both stress conditions, and salinity was the condition inducing higher photoinhibition in both genotypes (**Figure C2-3B**). Notably, the *aox1a* mutants displayed significantly lower F_v/F_m after both stress treatments as compared to WT plants (**Figure C2-3B**). Overall, these results indicate a similar photosynthetic performance among genotypes under control conditions, however, the *aox1a* mutants displayed higher photoinhibition and lower photosynthetic activity under stress conditions.

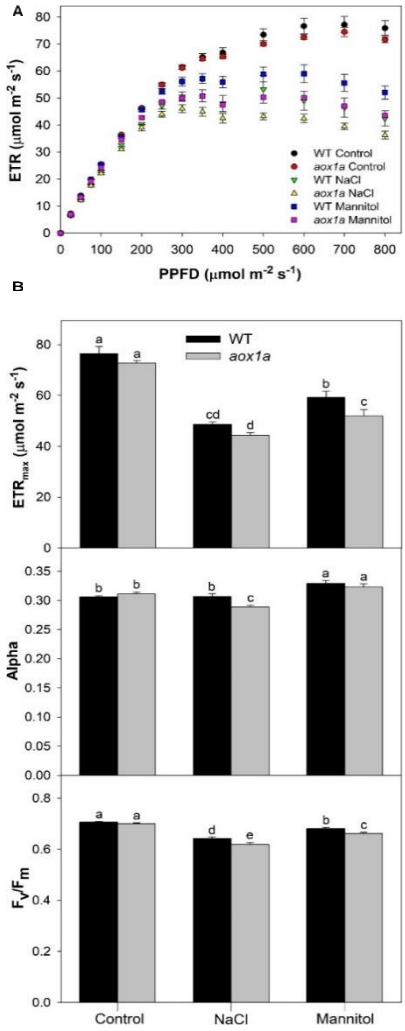


Figure C2-3. Photosynthetic activity and capacity under different light intensities. **A)** Light curves showing light dependent response (see Materials and Methods for details) of the chloroplast electron transport rate (ETR) in leaves of wild-type Col 0 (WT) and *aox1a A. thaliana* plants untreated with NaCl or Mannitol (Control), and after 1 day of severe NaCl or Mannitol treatments (300 mM). Values are means ± SE of 5–6 biological replicates. **B)** Maximum electron transport rate (ETR_{max}) and photosynthetic rate in light limited region (alpha) were derived from light curves (see Materials and Methods for details) performed under control and stress conditions. The maximum quantum efficiency of PSII (F_v/F_m) was determined after 30 min in darkness (see Materials and Methods for details) under control and stress conditions. Values are means ± SE of 5–6 biological replicates. Significant differences ($P < 0.05$) are denoted by different letters.

Metabolite Profiling in *aox1a* and Wild-Type Plants Under Control andStress Conditions

In order to further investigate the metabolic changes underlying the different physiological responses observed in the *aox1a* mutants, gas chromatography-time of flight-mass spectrometry (GC–TOF–MS) metabolite profiling analysis was performed on rosette leaves from plants grown under control and stress conditions (**Figure C2-4** and **Supplementary Table C2-2**). A total of 45 metabolites were identified using gas chromatography-mass spectrometry (GC-MS), including several amino acids, organic acids, sugars and sugar alcohols (**Supplementary Tables C2-1, C2-2; Figure C2-4**). Relative metabolite levels were normalized to the mean levels of WT plants under control conditions (**Supplementary Table C2-1** and **Figure C2-4**). Under control conditions, the *aox1a* mutants displayed higher levels of putrescine (2.31-fold), glycine (1.37-fold), erythritol (2.59-fold) and maltose (1.69-fold) as well as of the TCA cycle intermediates, citrate (1.62-fold), fumarate (1.30-fold) and malate (1.55-fold). Under stress, leaves of WT plants displayed significant increases in 31 metabolites after salt and mannitol treatments (**Figure C2-4** and **Supplementary Table C2-2**). While many of the metabolites increasing after mannitol treatment were the same as those increasing under salinity, there were several exceptions: alanine, glutamate, ornithine, citrate, glycerol and urea, which did not significantly ($P < 0.05$) increase after mannitol treatment; and glutamine, fumarate, erythritol, galactinol, xylose and trehalose, which increased only after mannitol treatment (**Figure C2-4** and **Supplementary Table C2-2**). On the other hand, only glycerate and pyruvate displayed decreased levels after both stress treatments, and dehydroascorbate was reduced only after salt treatment (**Figure C2-4** and **Supplementary Table C2-2**).

Metabolite levels in the *aox1a* mutants displayed similar patterns after both stress treatments as compared with WT plants (**4**). Nevertheless, the levels of asparagine, glycine, proline, malate and spermidine, although following similar stress-induced patterns in both genotypes, were significantly ($P < 0.05$) higher in *aox1a* mutants than in WT plants under salinity (**Figure C2-4**). On the other hand, aspartate, dehydroascorbate and fructose were significantly ($P < 0.05$) lower in *aox1a* mutants than in WT plants after salt treatment. Regarding mannitol stress, only aspartate and glycerate levels were

significantly ($P < 0.05$) higher in *aox1a* mutants than in WT plants. On the other hand, fumarate, citrate, fructose and glucose were significantly ($P < 0.05$) lower in *aox1a* mutants than in WT plants after mannitol treatment.

Additionally, absolute levels of metabolites were determined to evaluate the physiological relevance for the accumulation of the stress-related metabolites with protective functions.

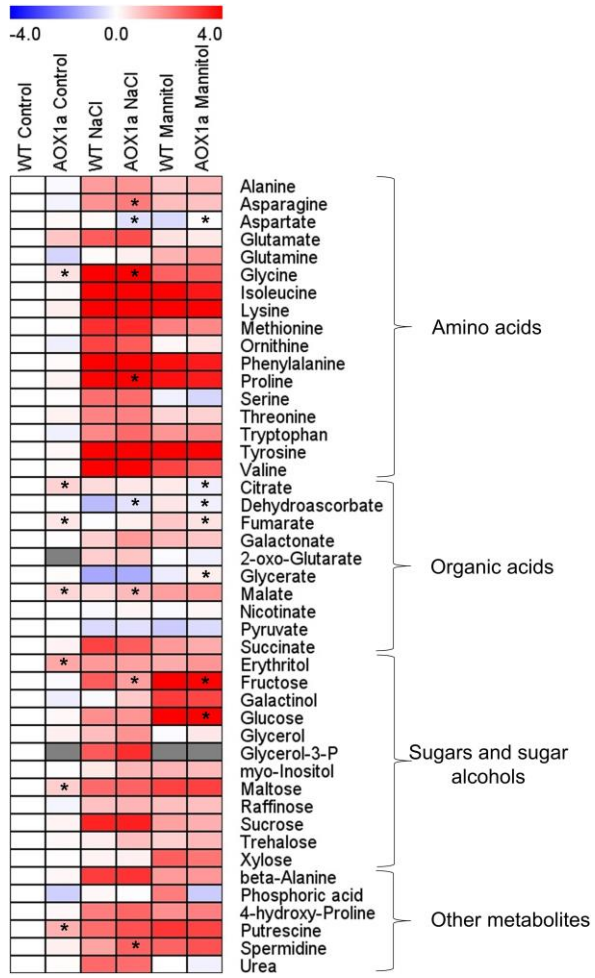


Figure C2-4. Metabolite profiles showing relative changes in primary metabolism. Heat map showing the relative levels of the GC-MS-analysed metabolites in leaves of wild-type Col 0 (WT) and *aox1a A. thaliana* plants untreated with NaCl or Mannitol (Control), and after 1 day of severe NaCl or Mannitol treatments (300 mM). Metabolites were clustered per class into amino acids,

organic acids, sugars and sugar alcohols, and other metabolites. Relative metabolite levels were normalized to the mean level of the WT plants under control conditions and fold-change values were log2 transformed (i.e., the level of all metabolites of WT plants under control conditions is 0). In this heat map, red and blue colours represent log2 fold-increased and -decreased metabolites, respectively. Gray colours indicate the metabolites not detected in some experimental conditions. Values are means ± SE of 4–6 replicates and asterisks denote significant differences ($P < 0.05$) to the WT plants in each experimental condition. The statistical differences between control and stress treatments in each genotype are presented in **Supplementary Table C2-2**.

The absolute levels of 37 metabolites, present in our standard mixture, were determined for all conditions in both genotypes (**Supplementary Figure C2-2** and **Supplementary Table C2-3**). Metabolites in order of absolute abundance under salinity conditions are shown in **Supplementary Figure C2-3.** Among the metabolites observed as significantly different between WT or *aox1a* mutants under salinity (**Figure C2-4** and **Supplementary Table 2**), glycine and proline were above 2 µmol gDW^{-1} in either WT or *aox1a* mutants, while malate, fructose and asparagine displayed lower amounts in the range of 0.3–0.8 µmol gDW^{-1} (**Supplementary Figure C2-2** and **Supplementary Table C2-3**). With respect to mannitol treatment, glucose was by far the most abundant metabolite (56.5 and 34.1 µmol gDW^{-1} in WT and *aox1a* mutant, respectively) that was significantly lower in the *aox1a* mutants, followed by fumarate (10.4 and 7.6 µmol gDW^{-1}) and fructose (4.1 and 2.0 µmol gDW^{-1}; **Supplementary Figure C2-2** and **Supplementary Table C2-3**).

Gene Expression of Other Alternative Respiratory Components in *aox1a* and Wild-Type Plants Under Control and Stress Conditions

The relative levels of transcripts encoding mitochondrial proteins of the alternative respiratory pathways, other than AOX, were determined by qPCR in both WT and *aox1a* mutants (**Supplementary Figure C2-1** and **Figure C2-5**). The aim of these gene expression analysis was to evaluate possible compensations from other alternative respiratory pathways for the lack of the *AOX1a* gene expression as well as the degree of mitochondrial stress perturbation. Regarding genes encoding alternative NAD(P)H dehydrogenases, transcript levels of *NDB3* were under the limit of detection while *NDB2*

expression displayed a higher stress-response in the *aox1a* mutants as compared to WT (**Figure C2-5**), a similar trend as the observed for the AOX1d (**Figure C2-1C**). On the other hand, genes encoding NDA1 and NDA2 proteins were not responsive to stress conditions. Finally, the transcript levels of genes encoding uncoupling proteins (UCPs) were also evaluated (**Supplementary Figure C2-1** and **Figure C2-5**); *UCP2* transcript levels were under the limit of detection while *UCP1* transcripts did not display any significant change under stress in both genotypes (**Figure** C2-**5**).

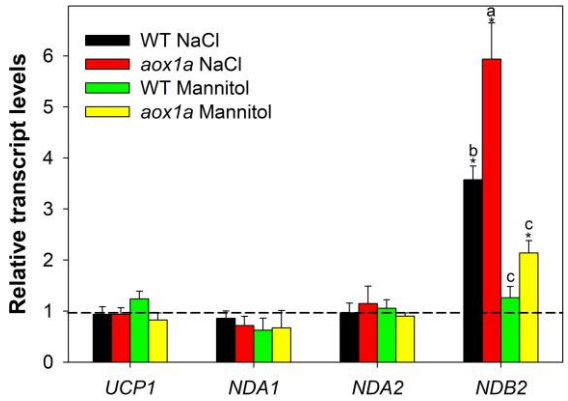


Figure C2-5. Gene expression analyses of alternative respiratory components**.** Transcript levels of genes encoding uncoupling proteins and alternative NAD(P)H dehydrogenases were determined by qPCR analyses (see Materials and Methods for details) in leaves of wild-type Col 0 (WT) and *aox1a A. thaliana* plants untreated with NaCl or Mannitol (Control), and after 1 day of severe NaCl or Mannitol treatments (300 mM). Data is shown as fold-changes relative to control conditions (i.e., all control values were set to 1, which is denoted by the dashed line). Primers used and gene information can be found in **Supplementary Table C2-4**. Values are means ± SE of 5–6 replicates and asterisks denote significant differences ($P < 0.05$) to the control condition for each gene expression analysis. Letters denote significant differences ($P < 0.05$) among genotypes and stress conditions for each gene expression analysis.

Discussion

Responses of plant respiration to abiotic stresses are largely variable (Lambers and Oliveira, 2019; O'Leary et al., 2019). This variability can be partly explained by plants' ability to adjust respiratory energy and carbon demands through changes in the partitioning of electrons between the cytochrome and alternative oxidase pathways (COP

and AOP; Del-Saz et al., 2018; Lambers and Oliveira, 2019; O'Leary et al., 2019), without necessarily involve a major change in total respiration rate. In particular, the responses of the *in vivo* AOP and COP activities to salt (Martí et al., 2011; Del-Saz et al., 2016; Sánchez-Guerrero et al., 2019) and water stress (Guy and Vanlerberghe, 2005; Ribas-Carbo et al., 2005; Galle et al., 2010; Sanhueza et al., 2013) are variable, however, a common pattern emerge with the electron partitioning to AOX usually increasing, either by a decrease in COP activity, increase in AOP activity or both (Del-Saz et al., 2018). Notably, a specific increase in the *in vivo* AOP activity (i.e., in the absence of COP changes), was observed in leaves of *Medicago truncatula* genotypes after a sudden severe salt stress (Del-Saz et al., 2016). Such a particular AOP activation *in vivo* is in line with its proposed role in providing metabolic flexibility to carbon and energy metabolism under short-term environmental perturbations (Del-Saz et al., 2018), as well as its role as a first line of defense against oxidative stress (Moller, 2001). Following previous evidence, we have here investigated the role of the AOP under sudden acute salt stress in more detail. Our hypothesis was that AOP response in *aox1a* mutants will be curtailed under acute stress, which would impair stress-related metabolism as compared to WT plants. In addition, we also applied a high mannitol concentration to both genotypes for exploring whether similar effects on the respiration and stress-related metabolism were observed after an acute osmotic stress in the absence of ionic toxicity. We are aware that osmotic stress conditions applied here were not fully controlled by our experimental approach with plants grown in soil, however, our previous observations (Del-Saz et al., 2016) and those presented here show and track typical physiological (**Figures C2-2, C2-3**) and molecular (**Figure C2-4**) responses to salt and water stress, thus allowing the establishment of relationships between the degree of water and (photo)oxidative stress with the metabolic changes studied.

The Lack of *AOX1a* Does Not Impair Alternative Oxidase Pathway *in vivo* Activity Under Control Conditions but Restricted Its Response to Stress

As expected, the capacity of the AOP was significantly lower in the *aox1a* mutant than in WT plants (**Figure C2-1A**), although it was not completely abolished in agreement with previous observations (Watanabe et al., 2010; Vishwakarma et al., 2015; Zhang et al., 2016). Oxygen isotope discrimination in the presence of KCN (of approx. 31‰) has

provided additional evidence supporting that remaining O_2 consumption after KCN treatment was mainly due to leaf AOX (maximum) activity (Del-Saz et al., 2022; Annex 3). Indeed, *aox1a* mutants displayed similar total respiration, electron partitioning and *in vivo* AOP activity as WT plants under control conditions (Del-Saz et al., 2022; Annex 3). These results are very similar to those reported in *AtAOX1a* anti-sense plants, previously obtained at the laboratory of the honourable Prof. James Siedow, grown under different light intensities (Florez-Sarasa et al., 2011). Our previous (Florez-Sarasa et al., 2011; Del-Saz et al., 2022; Annex 3) and current data (**Figure 1A**) show that AOX is almost fully engaged in *aox1a* impaired plants. Altogether, these results confirm that *AOX1a* isoform is not essential for maintaining leaf *in vivo* AOX activity under non-stress conditions. On the other hand, AOX protein signal could not be detected in the *aox1a* mutants under control conditions (**Figure C2-1B**) as in previous reports (Giraud et al., 2008; Strodtkötter et al., 2009; Oh et al., 2022). However, it is likely that samples after mitochondrial isolation or enrichment in mitochondrial membranes are required for the detection of low abundance AOX proteins (Oh et al., 2022). Indeed, AOX1D protein was detected in enriched mitochondrial membrane samples from *aox1a* mutants after proline incubation (Oh et al., 2022). Furthermore, evidence for the involvement in AOX capacity of isoforms other than AOX1a has recently been provided (Oh et al., 2022). To this respect, while single *aox1a* and *aox1d* mutants displayed lower AOX capacity as compared to WT plants, the reduction in AOX capacity was clearly more pronounced in double mutants *aox1a-aox1d* (Oh et al., 2022). While the relationship between protein levels and cyanide-resistant respiration may not be linear (Gonzalez- Meler et al., 1999) our and previous results (Oh et al., 2022) suggest that both AOX1a and AOX1d proteins can be responsible for AOX capacity in Arabidopsis plants. Notably, transcript levels of other AOX isoforms or alternative components of the mitochondrial respiratory chain in *aox1a* mutants were not higher than in WT plants (**Supplementary Figure C2-1**). Therefore, our and previous results in transcript and protein amounts suggest that *in vivo* AOP activity under non-stress conditions could be achieved without any additional induction of other AOX isoforms (i.e., AOX1c or AOX1d proteins). However, post-translational activation of the remaining AOX isoforms in *aox1a* mutants could also contribute to the previously observed *in vivo* AOP activity (Del-Saz et al., 2022; Annex 3). To this respect, while moderate increases in the

levels of some TCA cycle intermediates (citrate, malate and fumarate) were observed in *aox1a* mutants under control conditions (**Figure C2-4**), none of them have been shown to act as allosteric activators of any AOX isoform (Selinski et al., 2018a). However, analysis of AOX allosteric activators at the subcellular (mitochondrial) level would be required to attribute their effects on AOX activation *in vivo*.

Both stress treatments, significantly increased transcript levels of *AOX1a* and *AOX1d* in WT plants (**Figure C2-1B**), thus both isoforms could potentially contribute to the observed increase in AOP capacity (**Figure C2-1A**) and *in vivo* activity (Del-Saz et al., 2022; Annex 3). On the other hand, the absence of *AOX1a* expression in the *aox1a* mutants coincided with a much higher induction of the *AOX1d* transcript levels (approx. 20 times higher) under both stress conditions, as compared to WT plants (**Figure C2-1B**). However, this response was not coupled to a significant ($P < 0.05$) increase in the AOX capacity or protein level under our experimental conditions (**Figure C2-1**). Moreover, the lack of *in vivo* AOP activity response previously observed in *aox1a* mutant leaves (Del-Saz et al., 2022; Annex 3) clearly suggests that the absence of *AOX1a* was not compensated by other AOX isoforms (i.e., AOX1d) under stress conditions. These results are in line with previous observations suggesting no functional compensation for the lack of *AOX1a* under stress via high induction of AOX1d after respiratory inhibitor (Strodtkötter et al., 2009) and metal stress treatments (Keunen et al., 2015). The *aox1a* mutants did not show respiratory response to acute salt and water stress, since AOP was the main contributor to this respiratory response in our experimental conditions (Del-Saz et al., 2022; Annex 3). This AOP-specific response to acute salt stress was previously observed in a *Medicago truncatula* sensitive genotype (Del-Saz et al., 2016), which fits with the *Arabidopsis thaliana* behaviour, as a salt-sensitive species (Kazachkova et al., 2018). In addition, mannitol treatment induced a similar *in vivo* respiratory response as salt stress treatment (Del-Saz et al., 2022; Annex 3), which suggests that the osmotic stress generated after both treatments is likely the main responsible for the observed *in vivo* AOP specific response. In fact, the lack of *in vivo* AOP response in *aox1a* mutants coincided with a more pronounced reduction in leaf RWC under both stress conditions, as compared to WT plants (**Figure C2-2**), which could be related to a reduced osmotic adjustment. Osmotic adjustment is an essential trait that plants use to maintain turgor by balancing the osmotic pressure imposed during salt or water stresses (Munns and

Gilliham, 2015). While osmotic adjustment using inorganic ions is energetically "cheaper" than using organic solutes, salt-sensitive species usually rely on ion exclusion (particularly in leaves) and accumulation of organic solutes (Munns and Gilliham, 2015). In the present study, salt and mannitol treatments induced a large accumulation of several stress-related metabolites (SRMs; **Figure C2-4**), many of them being well-known for their roles in osmoregulation and osmoprotection (Slama et al., 2015).

The Lack *in vivo* Alternative Oxidase Pathway Response Under Stress Altered the Accumulation of Stress-Related Metabolites Involved in Leaf Osmoregulation and Redox Balance

Osmotic stress has immediate effects on plant growth, and the accumulation of osmolytes is part of the typical plant responses involved in osmotic adjustment (Munns and Gilliham, 2015). The accumulation of osmolytes is favoured under conditions when plant growth declines before photosynthesis, which can result in a relatively favourable carbon status allowing the use of photosynthates for osmolyte production at low cost (Hummel et al., 2010). In our short-term stress study, photosynthesis was not strongly affected, particularly at growth light intensity (**Figure C2-3**), which suggests minor limitations on C availability. In agreement, a large accumulation of sugars, sugar alcohols and amino acids was observed in both genotypes after stress treatments (**Figure C2-4**). Previous reports suggest that accumulation of sugars in leaves of Arabidopsis and other species after mannitol and salt treatments have a prominent role on osmotic adjustment (Thalmann and Santelia, 2017; Gurrieri et al., 2020). On the other hand, the accumulation of amino acids (i.e., proline) is a well-known mechanism contributing to osmoprotection and osmoregulation in different species (Slama et al., 2015). The relatively low concentrations of amino acids as typically observed in Arabidopsis leaves suggest their roles as osmoprotectants of subcellular structures in scavenging reactive oxygen species or counteracting redox imbalances, rather than contributing to osmotic adjustment (Shabala and Shabala, 2011; Slama et al., 2015; Gurrieri et al., 2020). Our results are in line with these observations since the levels of sucrose, glucose and fructose were not only highly accumulated, but also reached the highest absolute amounts, as compared to highly accumulated amino acids such as proline and glycine (**Supplementary Figure C2-2**). Importantly, the accumulation of glucose and fructose in the *aox1a* mutants was lower as compared with WT plants (**Figure C2-4**), and together with their lower relative

water content (RWC), suggests a decreased osmotic adjustment in the *aox1a* mutants (**Figure C2-6**). In this line, the *aox1a* mutants after mannitol treatment also displayed lower levels of fumarate, which was among the top three most abundant metabolites under stress (**Supplementary Figure C2-2**), and this metabolite was previously suggested to have a high contribution to osmotic adjustment in Arabidopsis under severe drought (Hummel et al., 2010). The lower photosynthetic performance of *aox1a* mutants could partly explain their lower sugar levels, which in turn could slow down the carbon flow through glycolysis and consequently the TCA cycle activity for the fumarate production (**Figure C2-6**). Nevertheless, fumarate can also be produced from malate which levels could be altered by the redox imbalances in *aox1a* plants. Furthermore, the accumulation of osmolytes is thought to be the result of the coordinated regulation of biosynthetic and catabolic pathways (Slama et al., 2015), many of which are tightly linked to respiratory pathways (Bandehagh and Taylor, 2020). Therefore, we cannot discard that the lower accumulation of fumarate and citrate observed in *aox1a* mutants after mannitol treatment could be partly due to a reduced TCA cycle activity as a direct consequence of a reduction in matrix NADH reoxidation by the AOP. Future experiments determining carbon fluxes (i.e., with ^{13}C labelled substrates under control and osmotic stress conditions) could unveil the precise nature of the observed altered accumulation of TCA cycle intermediates.

Impairment of photosynthetic performance and higher photoinhibition have been observed in other *aox1a* suppressed plants under drought (Giraud et al., 2008; Dahal et al., 2014, 2017; Dahal and Vanlerberghe, 2017, 2018) high light (Florez- Sarasa et al., 2011) and temperature (Watanabe et al., 2010; Li et al., 2020) stress, which have been attributed to the role of the AOP in providing flexibility to carbon and energy metabolism in photosynthetic tissues, particularly under stress (Del-Saz et al., 2018; Vanlerberghe et al., 2020). In our study, while both stress conditions induced photoinhibition in both genotypes (**Figure C2-3**), the decrease in F_v/F_m was higher under salinity as compared to mannitol stress (**Figure C2-3**), thus suggesting that ion toxicity probably led to higher oxidative stress at the chloroplast level. In line with a higher oxidative stress after salt treatment, as compared to mannitol treatment, both genotypes displayed higher levels of different metabolites with known functions on protecting against oxidative stress

themselves (i.e., dehydroascorbate, proline, asparagine; **Figure C2-4** and **Supplementary Table C2-2**) or as precursors of oxidative stress- related specialized metabolites (i.e., phenylalanine and tyrosine for phenylpropanoids synthesis; **Figure C2-4** and **Supplementary Table C2-2**), as well as higher levels of transcripts encoding oxidative stress-responsive genes (*AOX1a* and *NDB2*; **Figure C2-5**). The AOP activity in WT plants was significantly higher after salt than after mannitol stress (Del-Saz et al., 2022; Annex 3). Importantly, the *aox1a* mutants, lacking stress response of the *in vivo* AOP activity, displayed higher levels of proline, asparagine, spermidine, and dehydroascorbate when compared to WT plants (**Figure C2-4, C2-6**). Increased levels of all these metabolites indicate a higher induction of metabolic pathways involved in redox balancing and avoidance of excessive ROS accumulation under stress (Szabados and Savouré, 2010; Maaroufi-Dguimi et al., 2011; Alcázar et al., 2020; Foyer et al., 2020). Moreover, higher glycine levels in *aox1a* mutants under salinity denotes a restriction in photorespiration due to reduction of glycine decarboxylation (**Figure 6**), as has been previously reported in *aox1a* mutants (Strodtkötter et al., 2009; Zhang et al., 2017; Li et al., 2020). Finally, higher malate levels in *aox1a* mutants could indicate an impairment in the reductant export from the chloroplast via the malate valve (**Figure 6**), as previously suggested (Yoshida et al., 2007; Dinakar et al., 2010; Vishwakarma et al., 2015).

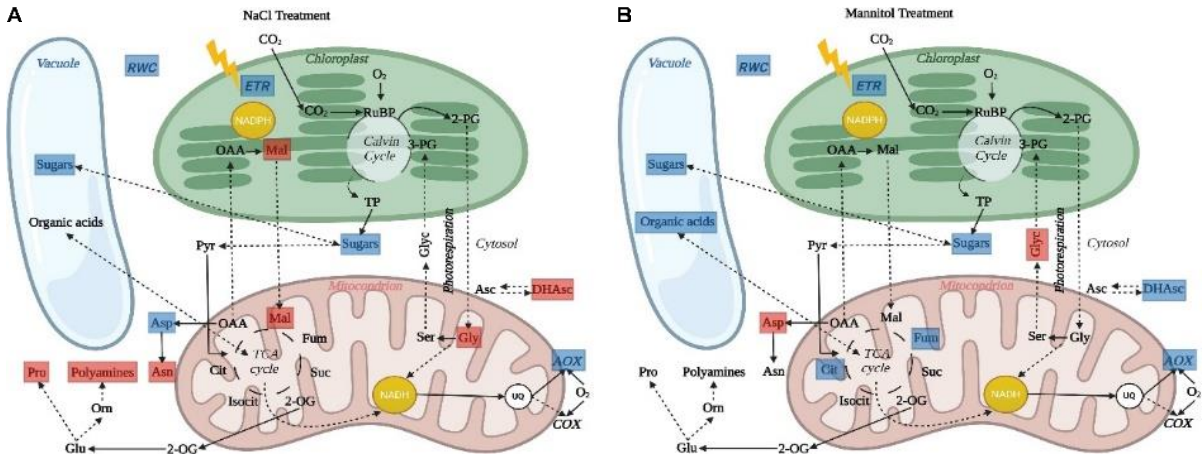


Figure C2-6. Schematic overview illustrating the impact of in vivo AOP restriction on leaf cell physiology and metabolism in aox1a plants after **A)** salt and **B)** mannitol treatments. Blue and red

boxes indicate significant ($P < 0.05$) reductions and increases, respectively, in physiological indicators and metabolite levels in *aox1a* mutants as compared to WT plants. After both stress treatments, the lack of *in vivo* AOP response was associated to reduced sugars (glucose, fructose or both) accumulation in *aox1a* mutants, which can be partially explained by their lower photosynthetic activity. Reduced accumulation of sugars in *aox1a* mutants could affect their osmotic adjustment as reflected by their lower relative water content (RWC). The reduction of fumarate and citrate accumulation in *aox1a* plants, the former likely contributing the decreased osmotic adjustment, may be explained by a TCA activity impairment triggered by the lack of response on the *in vivo* AOP activity, which allows matrix NADH re-oxidation without energy demand (i.e., ATP for growth) constrains. This limitation in NADH reoxidation can also explain the accumulation of photorespiratory cycle intermediates glycine (**A**) and glycerate (**B**). In addition, ion toxicity effects imposed by salinity could be aggravated by the lack of AOP response and, according to its role in avoiding ROS formation, thus trigger additional oxidative stress that was reflected in the alteration of other metabolic pathways involved in redox balancing and ROS detoxification (A), as denoted by the accumulation of malate, dehydroascorbate, proline, polyamines (spermidine) and asparagine. Image created with BioRender (https://biorender.com)

Conclusion

Mitochondrial function has been suggested to be essential for drought and salinity tolerance in plants as it can have roles in signal transduction, ion exclusion and homeostasis, ROS detoxification, the generation of ATP, and carbon balance (Bandehagh and Taylor, 2020; Munns et al., 2020; Vanlerberghe et al., 2020). However, information about the *in vivo* AOP and COP activity and their metabolic roles under water and salt stress remain scarce. The different metabolic responses in *aox1a* mutants lacking *in vivo* AOP response under stress (**Figure 6**) reinforce the relevant roles of the AOX previously suggested in redox balancing, avoidance of excessive ROS accumulation and photosynthetic performance. Furthermore, we here provide new evidence on the *in vivo* regulation and metabolic role of the AOP in the accumulation of stress-related metabolites associated to osmoregulation. While further experiments would be required to unravel the precise direction of subcellular carbon fluxes and its direct relationship with the *in vivo* AOP response, our results provide evidence on the contribution of the AOP in providing flexibility to carbon metabolism for biosynthesis, in addition to its role in cell redox balancing and preventing mitochondrial ROS formation (Smith et al., 2009; Vanlerberghe et al., 2020). Metabolites including TCA cycle intermediates (malate, citrate and fumarate), proline and hexoses, which were altered by the absence of *in vivo* AOP activity in this study, are similar to those typically altered when comparing salt-sensitive species *A. thaliana* with its relatives exhibiting salt-tolerance (Kazachkova et al., 2018). Therefore, our results provide important additional evidence reinforcing previous suggestions for AOX manipulation as a reasonable strategy for improving salt-tolerance in salt-sensitive crops (Smith et al., 2009), notwithstanding other important strategies involving salt-tolerant crops (Ventura et al., 2015; Fernie and Yan, 2019). Whether a higher AOP capacity or activity is primed for a better performance in case of salinity exposure remains to be investigated in a wider range of salt-tolerant crops. In addition, the relevance of AOP and its coordinated regulation with other alternative respiratory pathways under longer exposure to salt and/or water stress remains to be investigated in depth.

Supplemental Data

	A	B	C	D	E	F	G	H	I	J	K	L
1	Experiment title:	Metabolite profiles of *eca1a* mutants after salt and mannitol stress				Peak/compound no.- number referenced back to the main text			Mass to charge ratio (m/z)			
2	Organism/Plant age:	*Arabidopsis thaliana*				Ref.- Time- Time expected; Tag Time Index and Time deviation			(S)- identification confirmed by a standard compound			
3	Organ/tissue:	Leaves				Putative Name- putative identification of the metabolite/derivative			I, II, III- different isomers			
4	Analytical tool:	GC-TOF-MS				Corresponding metabolite name in literature			Identification level (A,B, C, D-) (A) standard or NMR, (B) MS/MS, (C) MS*, (D) MS only			
5	Peak/ Compound no.	Time Expected	Tag Time Index	Time Deviation	Putative metabolite name (Derivative)	Corresponding Metabolite in Literature	Metabolite Class	Mol formula	Mass to charge ratio (m/z)	Species detected before	Ref	Identification level (A-D)
6	1	222548	-9,15		M000071_A104002-101_METB_222650_TOF_Pyruvic acid (1ME)O(3)(1TMS)	Pyruvate	Acid (Oxo)	C3H4O3	174	Tomato, Arabidopsis, potato, grapevine and others		A
7	2	271580	-0,1		M000050_A122001-101_METB_271580_TOF_Alanine, DL- (2TMS)	Valine	Acid (Amino)	C5H11NO2	144	Tomato, Arabidopsis, potato, grapevine and others		A
8	3	287278	-0,03		M000053_A123001-101_METB_287278_TOF_Leucine, DL- (2TMS)	Alanine	Acid (Amino)	C3H7NO2	116	Tomato, Arabidopsis, potato, grapevine and others		A
9	4	319193	-0,03		M000017_A132002-101_METB_319193_TOF_Isoleucine, L- (2TMS)	Isoleucine	Acid (Amino)	C6H13NO2	158	Tomato, Arabidopsis, potato, grapevine and others		A
10	5	332443	-0,37		M000075_A129001-101_METB_333520_TOF_Phosphoric acid (3TMS)	Phosphoric acid	Phosphate	H3O4P	299	Tomato, Arabidopsis, potato, grapevine and others		A
11	6	340357	338818	-0,2	M000084_A127002-101_METB_340357_TOF_Urea (2TMS)	Urea	Amide	C4H8N2O	189	Tomato, Arabidopsis, potato, grapevine and others		A
12	7	345050	344295	-0,23	M000079_A135003-101_METB_345050_TOF_Glycerol, DL- (3TMS)	Glycerol	Acid	C3H8O3	292	Tomato, Arabidopsis, potato, grapevine and others		A
13	8	364565	364241	-0,06	M000078_A136001-101_METB_364565_TOF_Alanine, beta- (2TMS)	Beta-Alanine	Acid (Amino)	C3H7NO2	189	Tomato, Arabidopsis, potato, grapevine and others		A
14	9	365427	364803	-0,13	M000074_A134001-101_METB_365427_TOF_Succinic acid (2TMS)	Succinate	Acid	C4H6O4	247	Tomato, Arabidopsis, potato, grapevine and others		A
15	10	368395	367319	-0,3	M000018_A140001-101_METB_368395_TOF_Threonine, DL- (3TMS)	Threonine	Acid (Amino)	C4H9NO3	117	Tomato, Arabidopsis, potato, grapevine and others		A
16	11	388210	385684	-0,14	M000457_A133004-101_METB_388210_TOF_Nicotinic acid (1TMS)	Nicotinate	Acid	C6H5NO2	180	Tomato, Arabidopsis, potato, grapevine and others		A
17	12	394455	393912	-0,06	M000027_A146001-101_METB_394455_TOF_Serine, beta- (3TMS)	beta-Alanine	Acid (Amino)	C3H7NO2	248	Tomato, Arabidopsis, potato, grapevine and others		A
18	13	404455	403772	-0,06	M000054_A144001-101_METB_404455_TOF_Fumaric acid (2TMS)	Fumarate	Acid	C4H4O4	245	Tomato, Arabidopsis, potato, grapevine and others		A
19	14	440985	440474	-0,11	M000065_A149001-101_METB_440985_TOF_Malic acid, DL- (3TMS)	Malate	Acid	C4H6O5	233	Tomato, Arabidopsis, potato, grapevine and others		A
20	15	448453	448074	-0,03	M000073_A153003-101_METB_448453_TOF_Proline, 4-hydroxy-, DL-, trans- (3TM	4-hydroxy-Proline	Acid (Amino)	C5H9NO3	140	Tomato, Arabidopsis, potato, grapevine and others		A
21	16	457283	456775	-0,03	M000033_A152002-101_METB_457283_TOF_Aspartic acid, L- (3TMS)	Aspartate	Acid (Amino)	C4H7NO4	232	Tomato, Arabidopsis, potato, grapevine and others		A
22	17	462462	462289	-0,01	M000035_A154001-101_METB_462462_TOF_Methionine, DL- (2TMS)	Methionine	Acid (Amino)	C5H11NO2S	176	Tomato, Arabidopsis, potato, grapevine and others		A
23	18	475425	474922	-0,08	M000043_A156001-101_METB_475425_TOF_Glutamic acid, DL- (3TMS)	Glutamate	Acid (Amino)	C5H9NO4	246	Tomato, Arabidopsis, potato, grapevine and others		A
24	19	498150	497775	-0,04	M000579_A160001-101_METB_498150_TOF_Xylose, D- (1ME)O(4TMS)	Xylose	Sugar (Pentose, aldose	C5H10O5	160	Tomato, Arabidopsis, potato, grapevine and others		A
25	20	507780	507375	-0,09	M000096_A163001-101_METB_507780_TOF_Glutamic acid, DL- (3TMS)	Glutamate	Acid (Amino)	C5H9NO4	246	Tomato, Arabidopsis, potato, grapevine and others		A
26	21	517180	517066	-0,1	M000188_A175002-101_METB_517180_TOF_Putrescine (4TMS)	Putrescine	Amine	C4H12N2	174	Tomato, Arabidopsis, potato, grapevine and others		A
27	22	527047	526747	-0,09	M000272_A165004-101_METB_527047_TOF_Gluconic acid-1,5-lactone (4TM	Gluconic acid-1,5-lactone	Acid (Oxo)	C6H10O6	292	Tomato, Arabidopsis, potato, grapevine and others		A
28	23	531145	530588	-0,11	M000111_A164001-101_METB_531145_TOF_Phenylalanine, DL- (2TMS)	Phenylalanine	Acid (Amino)	C9H11NO2	218	Tomato, Arabidopsis, potato, grapevine and others		A
29	24	559100	548548	-0,1	M000013_A168001-101_METB_559100_TOF_Asparagine, DL- (2TMS)	Asparagine	Acid (Amino)	C4H8N2O3	116	Tomato, Arabidopsis, potato, grapevine and others		A
30	25	557320	555955	-0,22	000245_A172001-101_METB_557320_TOF_Glucose, 1,6-anhydro, beta-D- (3TM	Glucose, 1,6-anhydro, beta-D-	Sugar (anhydride)	C6H10O5	204	Tomato, Arabidopsis, potato, grapevine and others		A
31	26	570427	570449	0,03	M000028_A183002-101_METB_570427_TOF_Ornithine, DL- (4TMS)	Ornithine	Acid (Amino)	C5H12N2O2	142	Tomato, Arabidopsis, potato, grapevine and others		A
32	27	574222	573776	-0,14	M000238_A182001-101_METB_574222_TOF_Glucose-6-phosphate, beta-D- (4TS	Glucose-6-phosphate	Aldehyde (Polyol)	C6H13O9P	318	Tomato, Arabidopsis, potato, grapevine and others		A
33	28	624222	623722	-0,08	M000252_A185002-101_METB_624222_TOF_Dehydroascorbic acid, dimer (T	Dehydroascorbate	Acid (Heterocyclic)	C6H6O6	348	Tomato, Arabidopsis, potato, grapevine and others		A
34	29	626880	625822	-0,17	M000586_A189002-101_METB_626880_TOF_Galactonic acid (6TMS)	Galactonate	Acid (Heterocyclic	C6H12O7	292	Tomato, Arabidopsis, potato, grapevine and others		A
35	30	653910	653994	0,04	M000060_A209002-101_METB_653910_TOF_Inositol, myo- (6TMS)	myo-Inositol	Polyol	C6H12O6	305	Tomato, Arabidopsis, potato, grapevine and others		A
36	31	658237	657681	-0,09	M000035_A194002-101_METB_658237_TOF_Tyrosine, DL- (3TMS)	Tyrosine	Acid (Amino)	C9H11NO3	218	Tomato, Arabidopsis, potato, grapevine and others		A
37	32	673265	672907	-0,07	M000040_A196002-101_METB_673265_TOF_Serine (3TMS)	Serine	Acid (Amino)	C3H7NO3	204	Tomato, Arabidopsis, potato, grapevine and others		A
38	33	815200	813920	-0,16	M000012_A219008-101_METB_815200_TOF_Tryptophan, L- (2TMS)	Tryptophan	Acid (Amino)	C11H12N2O2	218	Tomato, Arabidopsis, potato, grapevine and others		A
39	34	870355	868838	-0,2	M000048_A214001-101_METB_870355_TOF_Maltose, D- (1ME)O(8TMS)	Maltose	Sugar (Disaccharide)	C12H22O11	204	Tomato, Arabidopsis, potato, grapevine and others		A
40	35	876240	874646	-0,17	M000071_A214002-101_METB_876240_TOF_Trehalose, alpha, alpha-, D- (8TMS	Trehalose	Sugar (Disaccharide)	C12H22O11	191	Tomato, Arabidopsis, potato, grapevine and others		A
41	36	934280	933415	-0,19	M000073_A296002-101_METB_940280_TOF_Galactinol (9TMS)	Galactinol	Sugar (Trisaccharide)	C12H22O11	204	Tomato, Arabidopsis, potato, grapevine and others		A
42	37	1003120	1001119	-0,2	M000077_A298002-101_METB_1003120_TOF_Raffinose (8TMS)	Raffinose	Sugar (Trisaccharide)	C18H32O16	361	Tomato, Arabidopsis, potato, grapevine and others		A
43	38	325180	324404	-0,23	M000031_A133001-101_METB_325180_TOF_Glycine (2TMS)	Glycine	Acid (Amino)	C2H5NO2	174	Tomato, Arabidopsis, potato, grapevine and others		A
44	39	338893	337655	-0,29	M000029_A132003-101_METB_338893_TOF_Proline, L- (2TMS)	Proline	Acid (Amino)	C5H9NO2	142	Tomato, Arabidopsis, potato, grapevine and others		A
45	40	357523	356608	-0,24	M000015_A138001-101_METB_357523_TOF_Serine, DL- (3TMS)	Serine	Acid (Amino)	C3H7NO3	204	Tomato, Arabidopsis, potato, grapevine and others		A
46	41	371255	370549	-0,19	M000064_A137001-101_METB_371255_TOF_Sumarate acid (2TMS)	Fumarate	Acid	C4H4O4	245	Tomato, Arabidopsis, potato, grapevine and others		A
47	42	378278	377722	-0,23	M000044_A139001-101_METB_378278_TOF_Threonic acid (4TMS)	Threonic acid	Sugar (Tetraacid)	C4H8O5	292	Tomato, Arabidopsis, potato, grapevine and others		A
48	43	578380	576444	-0,5	M000582_A187002-101_METB_578380_TOF_Fructose, D- (1ME)O(4TMS)	Fructose	Sugar (Hexose, ketose	C6H12O6	217	Tomato, Arabidopsis, potato, grapevine and others		A
49	44	580450	579560	-0,44	M000049_A188002-101_METB_580450_TOF_Glucose, D- (1ME)O(4TMS)	Glucose	Sugar (Hexose, aldose	C6H12O6	160	Tomato, Arabidopsis, potato, grapevine and others		A
50	45	582883	582883	0	M000069_A192004-101_METB_582883_TOF_Citric acid (4TMS)	Citrate	Acid	C6H8O7	273	Tomato, Arabidopsis, potato, grapevine and others		A
51	46	615467	615467	0,02	M000014_A192003-10*_METB_615467_TOF_Lysine, L- (4TMS)	Lysine	Acid (Amino)	C6H14N2O2	156	Tomato, Arabidopsis, potato, grapevine and others		A

Supplemental Table C2-1. Overview of the metabolite reporting list.

	Control		NaCl		Mannitol	
Metabolite	*WT*	*AOX1a*	*WT*	*AOX1a*	*WT*	*AOX1a*
Amino acids						
Alanine	1±0.29	0.94±0.23	**1.47±0.13**	1.71±0.27	1.80±0.43	**2.17±0.30**
Asparagine	1±0.15	0.90±0.06	**3.24±0.25**	**4.18±0.25***	**2.07±0.35**	1.97±0.47
Aspartate	1±0.14	1.07±0.18	1.05±0.04	0.73±0.09*	0.68±0.08	0.98±0.05*
Glutamate	1±0.25	1.86±0.39	**5.85±0.45**	**6.87±1.46**	1.38±0.30	1.27±0.29
Glutamine	1±0.28	0.64±0.30	1.05±0.19	1.18±0.42	**2.27±0.29**	**3.22±0.56**
Glycine	1±0.07	1.37±0.05*	**56.51±4.62**	**79.66±9.89***	**8.05±0.88**	**8.34±2.09**
Isoleucine	1±0.05	1.07±0.04	**64.58±2.20**	**58.38±7.21**	**16.24±1.87**	12.69±6.28
Lysine	1±0.09	1.21±0.11	**81.72±4.81**	**67.33±10.05**	**23.07±2.32**	18.14±7.94
Methionine	1±0.12	1.02±0.04	**9.61±0.75**	**10.24±2.19**	**3.94±0.57**	3.61±1.28
Ornithine	1±0.18	0.84±0.06	**7.71±0.71**	**5.94±0.99**	1.10±0.12	1.36±0.23
Phenylalanine	1±0.12	1.05±0.07	**61.98±3.71**	**51.78±7.20**	**14.07±1.85**	11.96±6.22
Proline	1±0.15	1.13±0.13	**15.64±1.25**	**22.99±1.78***	**13.70±3.89**	**11.95±2.88**
Serine	1±0.08	1.02±0.04	**23.75±1.96**	**24.11±3.48**	**4.24±1.38**	**3.16±0.51**
Threonine	1±0.06	1.16±0.07	**3.88±0.19**	**3.94±0.59**	**1.60±0.06**	1.63±0.21
Tryptophan	1±0.08	0.86±0.09	**3.66±0.75**	5.07±1.71	**3.19±0.77**	3.69±1.93
Tyrosine	1±0.13	1.08±0.11	**67.80±6.57**	**51.06±11.72**	**27.17±3.85**	24.75±12.79
Valine	1±0.03	1.04±0.03	**24.39±0.71**	**21.64±2.16**	**7.80±0.69**	5.83±2.46
Organic acids						
Citrate	1±0.13	1.62±0.19*	**1.47±0.12**	1.31±0.10	1.26±0.08	**0.84±0.13***
Dehydroascorbate	1±0.17	1.02±0.16	**0.48±0.03**	0.74±0.12*	1.33±0.15	0.86±0.06*
Fumarate	1±0.05	1.30±0.09*	0.98±0.06	1.20±0.19	**1.85±0.11**	1.35±0.12*
Galactonate	1±0.10	1.02±0.08	**1.67±0.23**	3.03±0.75	**2.14±0.14**	**1.82±0.19**
2-oxo-Glutarate	1†*	n.d.	1.72±0.15	1.89±0.35	0.98±0.14	0.85±0.15
Glycerate	1±0.04	1.04±0.06	**0.39±0.03**	**0.41±0.09**	**0.83±0.03**	1.19±0.10*
Malate	1±0.12	1.55±0.16*	**1.48±0.10**	2.11±0.29*	**2.81±0.25**	**3.04±0.33**
Nicotinate	1±0.11	1.01±0.08	0.95±0.14	1.11±0.18	0.94±0.14	1.10±0.17
Pyruvate	1±0.08	1.01±0.07	**0.68±0.09**	**0.72±0.07**	**0.58±0.03**	**0.69±0.05**
Succinate	1±0.11	1.14±0.09	**7.76±0.36**	**5.77±0.89**	**3.06±0.32**	2.47±0.74
Sugar and sugars alcohols						
Erythritol	1±0.11	2.59±0.27*	3.04±1.08	2.78±0.40	**2.51±0.26**	3.16±0.66
Fructose	1±0.07	0.95±0.12	**5.88±0.47**	**2.83±0.96***	**31.96±2.48**	**15.72±3.04***
Galactinol	1±0.17	0.84±0.23	0.96±0.10	1.79±0.37	**8.44±0.10**	**7.58±0.37**
Glucose	1±0.17	1.09±0.17	**3.40±0.21**	**3.14±0.62**	**168.6±8.62**	**101.92±20.9***
Glycerol	1±0.10	1.19±0.13	**2.05±0.15**	3.26±0.84	0.98±0.11	1.31±0.28
Glycerol-3-P	1†	n.d.	6.10±0.82	9.71±2.99	n.d.	n.d.
myo-Inositol	1±0.05	1.03±0.14	**1.28±0.08**	2.19±0.40	**2.25±0.08**	**2.11±0.11**
Maltose	1±0.13	1.69±0.32*	**5.10±0.76**	**5.49±1.11**	**7.83±2.05**	7.91±3.10
Raffinose	1±0.15	0.90±0.19	**1.98±0.17**	**2.24±0.41**	**2.03±0.38**	**2.00±0.34**
Sucrose	1±0.05	1.14±0.08	**10.99±0.33**	**11.44±1.90**	**2.77±0.63**	2.40±0.62
Trehalose	1±0.11	1.09±0.14	1.21±0.09	2.01±0.49	**1.68±0.18**	2.18±0.69
Xylose	1±0.08	1.03±0.08	1.13±0.07	1.17±0.14	**5.72±0.63**	4.44±1.59
Others metabolites						
beta-Alanine	1±0.10	1.09±0.05	**8.27±0.50**	**9.24±1.15**	**2.98±0.28**	3.07±0.86
Phosphoric acid	1±0.49	0.60±0.09	1.08±0.23	0.98±0.21	4.14±3.50	0.58±0.08
4-hydroxy-Proline	1±0.08	1.09±0.06	**4.15±0.25**	**5.30±0.94**	**3.36±0.27**	**4.01±0.56**
Putrescine	1±0.15	2.31±0.48*	**4.94±0.62**	**6.70±0.97**	**8.94±1.27**	**7.64±1.85**
Spermidine	1±0.12	1.19±0.44	**2.72±0.51**	**5.49±1.05***	**5.43±0.84**	6.52±1.63
Urea	1±0.30	1.04±0.12	**5.14±1.09**	**4.84±0.99**	1.01±0.14	0.87±0.44

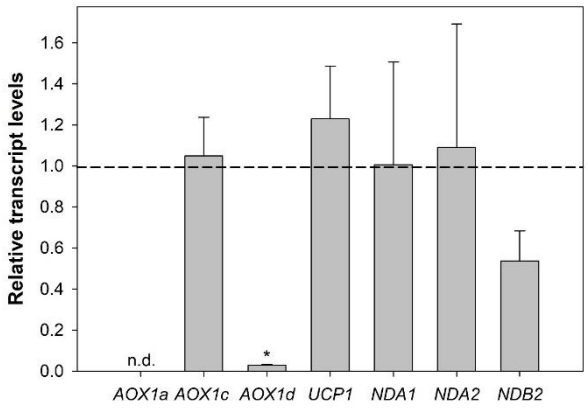
Supplemental Table C2-2. Relative metabolite levels in leaves of WT and aox1a plants under control conditions and after 1 day of severe (300 mM) NaCl and Mannitol treatments as measured by GC-MS (see material and methods for details). Data is presented as means ± SE for 4 to 6 biological replicates normalized to the mean level of the WT plants under control conditions. Bold numbers denote significant differences ($P < 0.05$) to the control condition in each genotype separately. Asterisks denote significant differences ($P < 0.05$) between WT and *aox1a* plants in each experimental condition. †Denotes metabolites detected only in one replicate in WT at control conditions. 'n.d.' denotes cases for not detected metabolites.

	Control		NaCl		Mannitol	
Metabolite	*WT*	*AOX1a*	*WT*	*AOX1a*	*WT*	*AOX1a*
Amino acids						
Alanine	0.509±0.146	0.479±0.120	**1.51±0.305**	1.64±0.410	0.919±0.222	**1.10±0.150**
Asparagine	0.145±0.022	0.130±0.009	**0.469±0.037**	**0.604±0.037***	**0.299±0.051**	0.285±0.068
Aspartate	0.082±0.011	0.088±0.015	0.087±0.004	0.060±0.007*	0.056±0.006	0.081±0.004*
Glutamate	0.316±0.079	0.588±0.122	**1.85±0.141**	**2.17±0.461**	0.437±0.095	0.402±0.093
Glutamine	0.364±0.102	0.233±0.108	0.381±0.070	0.429±0.153	**0.826±0.105**	**1.17±0.203**
Glycine	0.183±0.012	0.252±0.009*	**7.14±0.580**	**10.01±1.24***	**1.01±0.111**	**1.05±0.263**
Isoleucine	0.022±0.001	0.023±0.001	**1.41±0.048**	**1.28±0.158**	**0.355±0.041**	0.278±0.137
Lysine	0.013±0.001	0.015±0.001	**1.03±0.061**	**0.852±0.127**	**0.292±0.029**	0.229±0.100
Methionine	0.010±0.001	0.010±0.000	**0.092±0.007**	**0.099±0.021**	**0.038±0.005**	0.035±0.012
Ornithine	0.008±0.001	0.006±0.000	**0.059±0.005**	**0.045±0.008**	0.008±0.001	0.010±0.002
Phenylalanine	0.018±0.002	0.019±0.001	**1.12±0.067**	**0.933±0.130**	**0.254±0.033**	0.216±0.112
Proline	0.150±0.022	0.170±0.020	**2.34±0.188**	**3.44±0.266***	**2.05±0.582**	**1.79±0.431**
Serine	0.875±0.067	0.892±0.036	**4.22±0.348**	**4.28±0.618**	**0.752±0.245**	**0.561±0.091**
Tryptophan	0.008±0.001	0.007±0.001	**0.029±0.006**	0.040±0.013	**0.025±0.006**	0.029±0.015
Tyrosine	0.004±0.001	0.004±0.000	**0.271±0.026**	**0.204±0.047**	**0.109±0.015**	0.099±0.051
Valine	0.082±0.002	0.086±0.002	**2.01±0.0.059**	**1.78±0.178**	**0.643±0.057**	0.480±0.203
Organic acids						
Citrate	0.022±0.003	0.035±0.004*	**0.032±0.003**	0.028±0.002	0.027±0.002	**0.018±0.003***
Fumarate	4.68±0.269	4.95±0.180*	5.52±0.364	6.77±1.06	**10.41±0.619**	7.59±0.649*
2-oxo-Glutarate	0.024†*	n.d.	0.040±0.004	0.044±0.008	0.023±0.003	0.020±0.004
Glycerate	1.49±0.062	1.55±0.083	**0.584±0.050**	**0.607±0.131**	**1.23±0.040**	1.77±0.145*
Malate	0.365±0.044	0.567±0.058*	**0.540±0.038**	0.772±0.105*	**1.03±0.092**	**1.11±0.121**
Pyruvate	1.23±0.096	1.24±0.090	**0.840±0.112**	**0.890±0.092**	**0.710±0.041**	**0.845±0.061**
Succinate	0.033±0.004	0.037±0.003	**0.254±0.012**	**0.189±0.029**	**0.100±0.011**	0.081±0.024
Sugar and sugars alcohols						
Erythritol	0.014±0.001	0.035±0.004*	0.041±0.015	0.038±0.005	**0.034±0.003**	0.043±0.009
Fructose	0.129±0.009	0.123±0.015	**0.759±0.060**	**0.365±0.123***	**4.12±0.320**	**2.03±0.393***
Galactinol	0.039±0.007	0.033±0.009	0.038±0.004	0.070±0.015	**0.330±0.039**	**0.296±0.041**
Glucose	0.335±0.059	0.364±0.056	**1.14±0.071**	**1.05±0.207**	**56.49±2.89**	**34.15±7.00***
Glycerol	0.101±0.010	0.120±0.013	**0.206±0.015**	0.329±0.085	0.099±0.011	0.132±0.028
Glyerol-3-P	0.014†	n.d.	0.088±0.012	0.140±0.043	n.d.	n.d.
myo-Inositol	0.634±0.035	0.653±0.087	**0.811±0.049**	1.39±0.256	**1.43±0.053**	**1.34±0.067**
Raffinose	0.337±0.051	0.303±0.064	**0.666±0.058**	**0.754±0.139**	**0.682±0.129**	**0.674±0.113**
Sucrose	1.74±0.084	1.98±0.140	**19.11±0.580**	**19.90±3.30**	**4.82±1.103**	4.17±1.08
Trehalose	0.011±0.001	0.012±0.001	0.013±0.001	0.022±0.005	**0.018±0.002**	0.024±0.007
Xylose	0.040±0.003	0.041±0.003	0.046±0.003	0.047±0.006	**0.230±0.025**	0.178±0.064
Others metabolites						
beta-Alanine	0.015±0.002	0.016±0.001	**0.122±0.007**	**0.136±0.017**	**0.044±0.004**	0.045±0.013
Phosphoric acid	0.011±0.005	0.007±0.001	0.012±0.003	0.011±0.002	0.046±0.039	0.006±0.001
Putrescine	0.029±0.004	0.068±0.014*	**0.145±0.018**	**0.197±0.029**	**0.263±0.038**	**0.225±0.055**

Supplemental Table C2-3. Absolute metabolite levels in leaves of WT and AOX1a plants under control conditions and after 1 day of severe (300 mM) NaCl and Mannitol treatments as measured by GC-MS (see material and methods for details). Data is presented as means ± SE for 4 to 6 biological replicates. Bold numbers denote significant differences ($P < 0.05$) to the control condition in each genotype separately. Asterisks denote significant differences ($P < 0.05$) between WT and *aox1a* plants in each experimental condition. †Denotes metabolites detected only in one replicate in WT at control conditions. 'n.d.' denotes cases for not detected metabolites.

Target	Gene name	Locus	Forward primer	Reverse Primer
AtUbqC	Ubiquitine C	AT5G25760	TCAAATGGACCGCTCTTATC	CACAGACTGAAGCGTCCAAG
AtUCP1	Uncoupling Mitochondrial Protein 1	AT3G54110	TCTGCTCTTGCTGGTGATGT	TACCCAGTGCACCTGTTGTC
At UCP2	Uncoupling Mitochondrial Protein 2	AT5G58970	GGATTTCAAACCAAGGATCG	AGCGCACTAACTCCTTCCAG
AtNDA1	Alternative NAD(P)H Dehydrogenase A1	AT1G07180	CTCCGTGAGAGCAAGGAAGG	GGCGAAGTGGAGGGGATATG
AtNDA2	Alternative NAD(P)H Dehydrogenase A2	AT2G29990	CGAGAGCAAGGACGCAAAAG	CAGTAGGCCGAGATTGAGAC
AtNDB2	Alternative NAD(P)H Dehydrogenase B2	AT4G05020	ACTGACTCTCAAAGAGTTCC	CCGATTTGAACTCTTCGATC
AtNDB3	Alternative NAD(P)H Dehydrogenase B3	AT4G21490	GGTGAGTAGCCAAAGACGTG	GAAGATCGGTAATGCCATGC
AOX1a	Alternative oxidase 1a	AT3G22370	CCGATTTGTTCTTCCAGAGG	GCGCTCTCTCGTACCATTTC
AOX1b	Alternative oxidase 1b	AT3G22360	CTTTTCTTCCAGAGGCGGTA	TTAGGTTTCGCGACTTCCAT
AOX1c	Alternative oxidase 1c	AT3G27620	CCGATCTTTTCTTCCAGAGG	TGGGAGAGATTATGTATCCGATT
AOX1d	Alternative oxidase 1d	AT1G32350	GCCATGGGATTCATACAAAC	CACATGTGCTTCCTCTGAAAA
AOX2	Alternative oxidase 2	AT5G64210	TGGGAAGATCGAGAATGTTG	TCCTTGATTGCGAATGTCAG

Supplemental Table C2-4. Primers used in the qPCR analyses performed in this study.



Supplementary Figure C2-1. Gene expression analyses of alternative respiratory components under control conditions**.** Transcript levels of genes encoding alternative oxidases, uncoupling proteins and alternative NAD(P)H dehydrogenases were determined by qPCR analyses (see Materials and Methods for details) in leaves of wild-type Col 0 (WT) and aox1a A. thaliana plants as described in Figure 5A, 6. Data is shown as fold-changes relative to WT (i.e., all WT values were set to 1, which is denoted by the dashed line). Primers used and gene information can be found in Supplementary Table 4. Values are means ± SE of 5–6 replicates and asterisks denote significant differences ($P < 0.05$) to the WT for each gene expression analysis. n.d. (not detected).

	WT Control	*aox1a* Control	WT NaCl	*aox1a* NaCl	WT Mannitol	*aox1a* Mannitol
Sucrose	1739	1984	19114	19903	4821	4171
Glycine	183	252	7098	10005	1011	1048
Fumarate	5626	7328	5522	6766	10410	7586
Serine	875	892	4219	4282	752	561
Proline	150	170	2343	3444	2052	1790
Valine	82	86	2010	1784	643	480
Glutamate	316	588	1848	2169	437	402
Alanine	509	479	1511	1635	919	1104
Isoleucine	22	23	1412	1277	355	278
Glucose	335	364	1139	1053	56494	34149
Phenylalanine	18	19	1117	933	254	216
Lysine	13	15	1034	852	292	229
Pyruvate	1232	1240	840	890	710	845
myo-Inositol	634	653	811	1387	1425	1337
Fructose	129	123	759	365	4123	2028
Raffinose	337	303	666	754	682	674
Glycerate	1489	1545	584	607	1232	1774
Malate	365	567	540	772	1027	1111
Asparagine	145	130	469	604	299	285
Glutamine	364	233	381	429	826	1174
Tyrosine	4	4	271	204	109	99
Succinate	33	37	254	189	100	81
Glycerol	101	120	206	329	99	132
Putrescine	29	68	145	197	263	225
beta-Alanine	15	16	122	136	44	45
Methionine	10	10	92	99	38	35
Aspartate	82	88	87	60	56	81
Ornithine	8	6	59	45	8	10
Xylose	40	41	46	47	230	178
Erythritol	14	35	41	38	34	43
2-oxo-Glutarate	24		40	44	23	20
Galactinol	39	33	38	70	330	296
Citrate	22	35	32	28	27	18
Tryptophan	8	7	29	40	25	29
Trehalose	11	12	13	22	18	24
Phosphoric acid	11	7	12	11	46	6

Supplementary Figure C2-2. Metabolite profiles showing absolute changes in primary metabolism. Coloured table showing the absolute levels (µmol gDW–1) of the GC-MS-analysed metabolites in leaves of wild-type Col 0 (WT) and *aox1a A. thaliana* plants untreated with NaCl or Mannitol (Control), and after 1 day of severe NaCl or Mannitol treatments (300 mM). Metabolites are shown in order of absolute abundance under 300 mM NaCl conditions. In this table, the intensity of the red colour indicates the absolute level of the metabolite as well as the green bars inside the cells. Values are means of 4–6 replicates and the statistical differences to the WT plants in each experimental condition as well as between control and stress treatments in each genotype are presented in **Supplemental Table C2-2**.

Chapter 3: The in vivo post-translational activation of alternative oxidase triggers climacteric respiration in tomato

Introduction

Tomato (*Solanum lycopersicum*) is the main model system for fleshy fruit ripening studies at biochemical, genetic and molecular levels (Giovannoni et al., 2017; Zhu et al., 2018; Li et al., 2019; Kaur et al., 2023). In this economically relevant fruit, a sudden increase in respiration occurs at the onset of ripening, usually in concert with increased ethylene production that eventually impacts fruit color, firmness, taste, and flavor (Klee and Giovannoni, 2011). In plants, respiration involves three main steps: glycolysis in the cytosol, the tricarboxylic acid (TCA) cycle in the mitochondrial matrix, and the electron transport chain in the inner mitochondrial membrane (Fernie et al., 2004). The last step includes alternative respiratory pathways involving internal and external type II NAD(P)H dehydrogenases, uncoupling proteins (UCPs) and alternative oxidases (AOXs) (Moller et al., 2021). AOX constitutes the cyanide-insensitive pathway that forks away from the cytochrome c oxidase (COX) pathway at the level of ubiquinone (UQ) bypassing proton pumping through complexes III and IV (Del-Saz et al., 2018; Moller et al., 2021), whereas UCPs uncouple the proton gradient (Vercesi et al., 2006; Barreto et al., 2020). Both the redox (AOX) and the proton electrochemical gradient (UCP) energy-dissipating pathways lead to a decrease in ATP synthesis. However, AOX and UCP activities are beneficial for plant performance under different physiological conditions mainly due to their roles in providing metabolic flexibility and in lowering the level of mitochondrial reactive oxygen species (ROS) (Del-Saz et al., 2018; Barreto et al., 2020). Several AOX and UCP homologs have been reported in tomato (Holtzapffel et al., 2003; Vercesi et al., 2006; Xu et al., 2012) and some of them have been proposed to participate in tomato fruit ripening (Almeida et al., 1999; Holtzapffel et al., 2003; Xu et al., 2012). However, the precise contribution and metabolic role of AOX during climacteric respiration and fruit ripening remains unclear (Xu et al., 2012; Neelwarne, 2015b; Hewitt and Dhingra, 2020). Notably, we still lack fundamental information about the *in* vivo electron partitioning between the AOX and the COX pathways during fruit ripening.

Early studies assessed tomato fruit respiration by using specific respiratory inhibitors (Theologis and Laties, 1978; Xu et al., 2012), which are not adequate for measuring *in vivo* respiratory activities (Day et al., 1996; Del-Saz et al., 2018). Alternatively, *in vivo* electron partitioning between the AOX and the COX pathways can be determined using the O_2 isotope (^{18}O) discrimination technique (Del-Saz et al., 2017, 2018a), which allows

for precise estimations of the energy-efficiency of respiration. The ^{18}O discrimination technique has been applied to study respiration in different species and tissues exposed to many different conditions (Del-Saz et al., 2017, 2018). However, the application of this technique in fruit tissues has been limited due to (i) the limitation of O_2 diffusion due to pericarp thickness (Del-Saz et al., 2017) and (ii) the interference of non-mitochondrial O_2 consumption, mainly due to wounding respiration (Theologis and Laties, 1978; Moller et al., 1988) and chromorespiration, i.e., a respiratory process located in plastids which involves the NAD(P)H dehydrogenase complex and the plastid terminal oxidase (PTOX) (Renato et al., 2014). These and other technical difficulties in measuring fruit respiration have been recognized and bypassed by using a stoichiometric model, which predicted a peak of respiratory flux (CO_2 released) and energy dissipation just before ripening and coinciding with the climacteric peak of respiration (Colombié et al., 2017). While this model has been used to calculate theoretical AOX- and UCP-associated respiratory fluxes during fruit ripening in different conditions (Colombié et al., 2017), experimental confirmation is missing.

Tomato ripening also involves the differentiation of chloroplasts into chromoplasts, specialized plastids that accumulate high levels of carotenoid pigments (Giovannoni et al., 2017). Carotenoid overaccumulation, together with chlorophyll degradation, change the fruit color from green to red during ripening. The supply of energy (ATP) and carbon precursors for the synthesis of carotenoids and other health-promoting metabolites during fruit ripening is assumed to rely on sugar import from source tissues. Chromorespiration was shown to provide ATP in tomato fruits at late ripening stages (Renato et al., 2014), but other respiratory pathways acting in the cytosol and mitochondria are proposed to be the main suppliers of ATP and metabolic precursors for chromoplast metabolism (Bouvier and Camera, 2007; Beauvoit et al., 2018; Pott et al., 2019). In the present study, we have used wild-type tomato plants (cv. Ailsa Craig) as well as PTOX-defective *ghost* mutants (Barr et al., 2004) to experimentally determine the *in vivo* activities of the AOX and COX pathways during tomato fruit ripening. These data in combination with transcript and metabolite profiling analyses revealed key regulations of the *in vivo* AOX activity as well as metabolic connections to ethylene and carotenoid synthesis.

Material and Methods

Plant material and growth conditions

Seeds from tomato (*Solanum lycopersicum* cv. Ailsa Craig) wild-type (WT) plants were sown in small pots and grown under controlled walk-in-growth chamber conditions: 16h/8h light/dark photoperiod, day/night temperature 24°C /22°C; photosynthetic photon flux density (PPFD) of 400 μmol m^{-2} s^{-1}. After two weeks, plants were transplanted into 2 L pots containing a mixture of substrate:vermiculite:perlite (3:1:1) and kept under similar growing conditions for at least 2 months. Tomato *ghost* seeds were kindly provided by Dr. Marcel Kuntz and grown under similar conditions for 6-7 months, except for a lower light intensity (approx. PPFD of 100 μmol m^{-2} s^{-1}) supplied in a separated zone of the same walk-in-growth chamber.

Flowers were labeled at anthesis, and the date was recorded to register the number of days in fruit development (i.e. days post-anthesis, DPA). Fruits from WT and *ghost* plants (Figure 1) were harvested at the following ripening stages based on fruit size and color: mature green (MG, when reached full size but remained green, ~30 to 35 DPA), breaker (BR, ~when color change started), orange (OR) and red (R) in WT fruits; mature white (MW, ~40 DPA), breaker (BR), yellow (Y) in *ghost* fruits. Each harvested fruit was cut into pericarp slices and divided into subsamples (approx. 0.3g each) that were used for respiration analysis (fresh tissue) or immediately frozen in liquid nitrogen and stored at -80ºC for subsequent RNA and metabolite analysis.

Respiration and oxygen isotope discrimination analysis

Initially, respiration analyses were performed by using liquid-phase Clark-type oxygen electrodes (Rank Brothers LTD Dual Digital Model 20). Fruit pericarp samples were cut into slices, weighed and incubated for 5, 20, and 40 min with the respiration buffer (30 mM MES, 0.2 mM $CaCl_2$ pH 6.2) (**Figure C3-2**). Thereafter, pericarp slices were placed into the oxygen electrode cuvettes containing respiration buffer and the oxygen uptake rate was measured in complete darkness at a constant temperature of 25 °C. Oxygen consumption rates were also performed after incubations with respiration buffer containing 5 mM potassium cyanide (KCN) or 1 mM octyl-gallate (OGAL). In addition, OGAL and salicylhydroxamic acid (SHAM) were subsequently added into the cuvette at

1mM and 20mM concentrations during measurements of KCN-inhibited tissues to compare their inhibitory effect on the AOX pathway (**Figure C3-2C**). All these measurements were performed before oxygen concentration reached half-air saturation levels to avoid oxygen-limiting conditions inside the cuvette (particularly important when AOX-dependent oxygen consumption is measured).

Thereafter, ^{18}O discrimination analyses during respiration were performed by using a dual-inlet isotope ratio mass spectrometer (DI-IRMS) system as previously described (Del-Saz et al., 2017) with the following modifications for fruit tissues. After the information obtained with the oxygen electrode measurements, the sliced pericarp tissues were incubated with or without inhibitors for approx. 20 min before placing the samples in a 3 ml cuvette connected to the DI-IRMS system and an air-tight syringe containing 2 ml of air. Initially, different sizes of the sliced pericarp tissue were tested (**Supplemental Figure C3-1**) and only those pericarp pieces of approx. or less than 2 mm thick and 1 cm length displayed no artefactual ^{18}O discrimination by diffusion (see Del-Saz et al., 2017 for technical details related to O_2 diffusion problems). To calculate the partitioning of electrons to the alternative pathway (τ_a), the end-point discrimination values corresponding to the AOX and COX pathways were determined in WT fruits at all developmental stages as well as in *ghost* fruits at the MW and Y stages (**Table C3-1**). The ^{18}O discrimination by the AOX pathway (Δ_a) was determined in the presence of 5 mM KCN in all cases. In WT fruits at the MG stage, the ^{18}O discrimination by COX was determined in the presence of 20 mM SHAM ($\Delta_{c\text{-}SHAM}$) and it was not significantly different from the ^{18}O discrimination in the presence of 1 mM OGAL ($\Delta_{c\text{-}OGAL}$). Moreover, $\Delta_{c\text{-}OGAL}$ values were similar at all developmental stages tested in both WT and *ghost* fruits and therefore, they were used as the end-point discrimination values corresponding to the COX pathway for each developmental stage. Thereafter, the ^{18}O discrimination in the absence of inhibitors (Δ_n) was determined in both WT and *ghost* fruits at all the mentioned developmental stages (**Table C3-1**). Finally, the individual activities of the COX (v_{cyt}) and AOX (v_{alt}) pathways were obtained as previously described (Del-Saz et al., 2017), by multiplying the total oxygen uptake rate (V_t) and the τ_a (**Figure C3-2C**).

After both electrode and DI-IRMS measurements, samples were oven-dried at 60 °C for at least 48 h to determine dry weights (DWs). All respiration and ^{18}O discrimination data are means ± SE of 3-6 biological replicates corresponding to different fruits.

Gene Expression analysis

RNA was isolated from lyophilized (previously frozen) pericarp tissue by using Maxwell® RSC Plant RNA Kit (Promega Biotech Ibérica, Madrid, Spain) and an automated system Maxwell® RSC Instrument (Promega Biotech Ibérica, Madrid, Spain) according to the manufacturer's instructions, and was quantified using a NanoDrop 1000 spectrophotometer (Thermo Scientific, http://www.nanodrop.com/). Afterwards cDNA synthesis was performed following the recommendations of the Transcriptor First Strand cDNA Synthesis Kit (Roche Basel, Switzerland). Relative mRNA abundance was evaluated by quantitative PCR using LightCycler 480 SYBR Green I Master Mix (Roche Basel, Switzerland) on a LightCycler 480 real-time PCR system (Roche Basel, Switzerland). Primers used and the related information are detailed in **Supplemental Table C3-1**. Two technical replicates of each biological replicate were performed, and the mean values were used for further calculations. Tomato ACT4 (Solyc04g011500) was used as a reference gene to correct for differences in the total amount of transcripts and the 2-ΔΔCt method (Livak and Schmittgen, 2001) was used to calculate the fold-change of gene expression. Finally, data were normalized to the mean value of MG and MW fruits for WT and *ghost* mutants, respectively (i.e. the level of all transcripts for WT fruits at MG and *ghost* mutants fruits at MW was set to 1). Values presented in Figure 3 are means ± SE of 3-6 biological replicates corresponding to different fruits.

Primary metabolite and carotenoids profiling

Primary metabolite extractions were performed as described previously (Lisec et al., 2006) using approximately 10 mg of lyophilized pericarp tissue, previously frozen. Derivatization and GC–TOF–MS analyses were carried out as described previously (Lisec et al., 2006). Metabolites were identified manually by TagFinder software (Luedemann et al., 2012) using the reference library mass spectra and retention indices housed in the Golm Metabolome Database (http://gmd.mpimpgolm.mpg.de) (Kopka et al., 2005). The parameters used for the peak annotation of all detected metabolites can be found in **Supplemental Table C3-2**, which follows previously reported

recommendations (Fernie et al., 2011). Data were normalized to the mean value of MG and MW fruits for WT and *ghost* mutants, respectively (i.e., the value of all metabolites for MG or MW was set to 1). Values presented in **Supplemental Tables C3-3** and **C3-4**, **Figure C3-4** and **Supplemental Figure C3-2** are means ± SE of 4-6 biological replicates corresponding to different fruits.

Carotenoids and chlorophylls were determined as previously described (Fernández-Cancelo et al., 2022; Annex 4) by the Agilent 1200 series HPLC system (Agilent Technologies).

Statistical Analyses

For the statistical analyses in **Table C3-1, Figures C3-2, C3-3** and **C3-5**, a one-way ANOVA with a level of significance of $P < 0.05$ was performed with the SPSS statistical software package, version 25 (IBM Corp., 2016, Armonk, New York, NY, USA), and Duncan's posthoc test was used to determine statistically significant differences. Student's t-tests were used for the statistical analyses in **Figure C3-6**, **Supplemental Figure C3-1**, **Supplemental Tables C3-3** and **C3-4** to determine significant ($P < 0.05$) differences between MG and other ripening stages.

Results

Measurements of oxygen consumption in tomato fruit tissues

Respiration under our experimental plant growth conditions was initially assessed with an oxygen electrode in sliced pericarp tissues from wild-type (WT) tomato fruits at four different stages of development selected based on color: mature green (MG), breaker (BR), orange (OR) and red (R) (**Figure C3-1**). O_2 consumption was determined after different times of incubation with the respiration buffer containing $CaCl_2$ to avoid and wash out the so called 'wounding' or 'residual respiration' (Theologis and Laties, 1978; Moller et al., 1988). Respiration rates among different time incubation points were not statistically different ($P<0.05$) at any developmental stage (**Figure C3-2A**). An incubation time of 20 min prior to the measurement of respiration was chosen for all subsequent respiration analyses, because it is adequate for comparing uninhibited and inhibitor-treated samples, thus avoiding side effects arising from long incubation periods

(Moller et al., 1988). We next tested the effects of respiratory inhibitors on oxygen consumption rates (**Figure C3-2B**). Octyl-gallate (OGAL) at 1 mM concentration was reported to inhibit O_2 consumption in tomato fruit pericarp only at late stages of ripening (OR and R), when plastid terminal oxidase (PTOX) is highly expressed (Renato et al., 2014). Based on these and other results, it was assumed that OGAL (at approx. 1 mM) could be used to specifically inhibit PTOX (and not AOX) in fruit pericarp tissues (Renato et al., 2014). However, our experiments using 1 mM OGAL in the presence of the COX inhibitor potassium cyanide (KCN) do not support this conclusion (**Figure C3-2B**). Specifically, if OGAL was only inhibiting PTOX, no effect should be observed on MG and BR fruit (which lack PTOX activity). However, the KCN-resistant respiration at MG and BR stages was substantially reduced after OGAL treatment, thus suggesting a strong inhibitory effect of OGAL over the AOX (**Figure C3-2B**). Consistent with this conclusion, adding the AOX inhibitor SHAM did not alter the effect of KCN plus OGAL treatments in MG and BR fruit samples (**Figure 2B**).

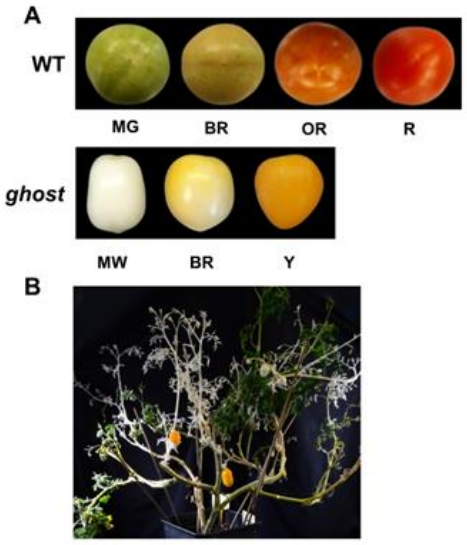


Figure C3-1. Wild-type (WT) and ghost mutant visual phenotypes**. A)** WT and *ghost* tomato fruits at different ripening stages: MG, mature green; BR, breaker; OR, orange; R, red; MW, mature white; Y, yellow. **B)** Representative image of a *ghost* mutant plant with albino and yellow tomato fruits after 7 months of growth.

Measurements of oxygen isotope discrimination in tomato fruit tissues

To measure ^{18}O discrimination in fruit pericarp tissue, we initially optimized sample preparation in the absence (Δ_n) and presence of the respiratory inhibitors KCN (Δ_a, ^{18}O discrimination of AOX) and SHAM ($\Delta_{c\text{-}SHAM}$, ^{18}O discrimination of COX). When pericarp samples were sliced into pieces of different thickness, results were variable and values were lower than those previously published for several tissues and species, i.e. Δ_c and Δ_n between 18 and 20 ‰ and Δ_a between 26 and 30 ‰ (Ribas-Carbo et al., 2005) (**Supplemental Figure C3-1**). This was very likely due to the effect of ^{18}O discrimination by diffusion through dense or thick tissues (Del-Saz et al., 2017). Following previous procedures with thick tissues from *Opuntia ficus indica* (i.e. cladode pieces of 2 mm thickness (Gomez-Casanovas et al., 2007), we sliced the fruit pericarp samples in approx. 2 mm thick and 1 cm length pieces (**Supplemental Figure C3-1**). This resulted in ^{18}O discrimination values that were less variable and, most importantly, within the expected range (**Supplemental Figure C3-1**).

Based on the described results, we next carried out the assessment of ^{18}O discrimination in the absence and presence of respiratory inhibitors at different fruit ripening stages (**Table C3-1**). As indicated above, measurements of oxygen consumption rates suggested that OGAL inhibits AOX in addition to PTOX. Consistently, ^{18}O discrimination in the presence of OGAL ($\Delta_{c\text{-}OGAL}$) at the MG stage was lower than in the absence of inhibitors (Δ_n) but similar to that SHAM-treated ($\Delta_{c\text{-}SHAM}$) samples (**Table C3-1**), thus demonstrating that both SHAM and OGAL had a similar inhibitory effect on AOX. Furthermore, $\Delta_{c\text{-}OGAL}$ values in the range of those typically reported as end-point COX values (i.e. 18-20 ‰) were found at all ripening stages. Together with our previous results (**Figure C3-2B**), these data confirm that OGAL inhibits *in vivo* AOX activity and cannot be used to specifically inhibit only PTOX. As an alternative strategy, we used the tomato PTOX-defective *ghost* mutant (Barr et al., 2004) (**Figure C3-1C**) to evaluate the contribution of chromorespiration to the total respiration of the tomato fruit pericarp at different ripening stages (**Table C3-1**). Because of the absence of chlorophylls and carotenoid pigments in *ghost* tomato fruits prevent using the same color-based classification of ripening stages used with WT fruits, we refer to their fruit development stages as mature white (MW, when reached full size), breaker (BR, when yellow flavonoid pigments start to accumulate) and yellow (Y, when fruit becomes fully colored)

(**Figure C3-1B**). $\Delta_{c\text{-}OGAL}$ was very similar in WT and *ghost* tomatoes at all ripening stages, thus reinforcing our previous conclusion on the inhibitory effect of OGAL on AOX. Notably, Δ_a was also similar in WT and *ghost* fruits at both non-ripe (MG and MW) and ripe (R and Y) stages (**Table C3-1**). Therefore, these results suggest that the contribution of PTOX-based chromorespiration to O_2 consumption in the pericarp of ripening fruit is minor compared to that of mitochondrial respiration.

	MG	BR	OR	R	MW	Y
Δ_a (‰)	31.2 ± 0.4c	31.3 ± 0.4c	30.8 ± 0.6bc	29.6 ± 0.2ab	30.6 ± 0.3abc	29.4 ± 0.7a
Δ_n (‰)	21.5 ± 0.1ab	22.1 ± 0.4bc	21.0 ± 0.3a	21.1 ± 0.3ab	22.4 ± 0.4c	21.4 ± 0.3ab
$\Delta_{c\text{-}OGAL}$ (‰)	18.8 ± 0.5	18.0 ± 0.2	18.5 ± 0.4	18.2 ± 0.7	18.1 ± 0.4	18.4 ± 0.5
$\Delta_{c\text{-}SHAM}$ (‰)	18.1 ± 0.5	-	-	-	-	-

Table C3-1. Oxygen isotope discrimination (‰) in the absence of inhibitors (Δ_n), in the presence of 20 mM SHAM ($\Delta_{c\text{-}SHAM}$), 5 mM KCN (Δ_a) and 1 mM OGAL ($\Delta_{c\text{-}OGAL}$) in mature green (MG), breaker (BR), orange (OR) and red (R) fruits from wild-type tomato plants as well as in mature white (MW) and yellow ripened (Y) fruits from ghost plants**.** Values are mean ± SE of three to six replicates. Significant ($p < 0.05$) differences between species are denoted by different letters.

Respiration and electron partitioning between AOX and COX during ripening

^{18}O discrimination data (**Table C3-1**) were used to determine the electron partitioning to AOX (τ_a) at each fruit ripening stage (**Figure C3-2C**). There was a significant ($p<0.05$) increase in τ_a at the BR stage as compared to the MG stage (**Figure C3-2C**). Total respiration rate (V_t) also increased at BR stage but it significantly ($P<0.05$) decreased towards R stage, similar to that previously reported in tomato cv. Ailsa Craig fruits (Renato et al., 2014). Parameters V_t and τ_a were then used to determine the *in vivo* activities of COX and AOX pathways (Del-Saz et al., 2017). The *in vivo* COX pathway activity (v_{cyt}) remained unchanged from MG to BR stage and later decreased, being significantly lower in R tomato fruits (**Figure C3-2C**). On the other hand, the *in vivo* AOX pathway activity (v_{alt}) significantly ($P<0.05$) increased at the BR stage becoming the main contributor to climacteric respiration. Notably, the AOX capacity, determined as KCN-resistant respiration, was not significantly increased at the BR stage (**Figure C3-**

2B). These results underline the critical importance of assessing *in vivo* AOX activity, as determined by ^{18}O discrimination analysis.

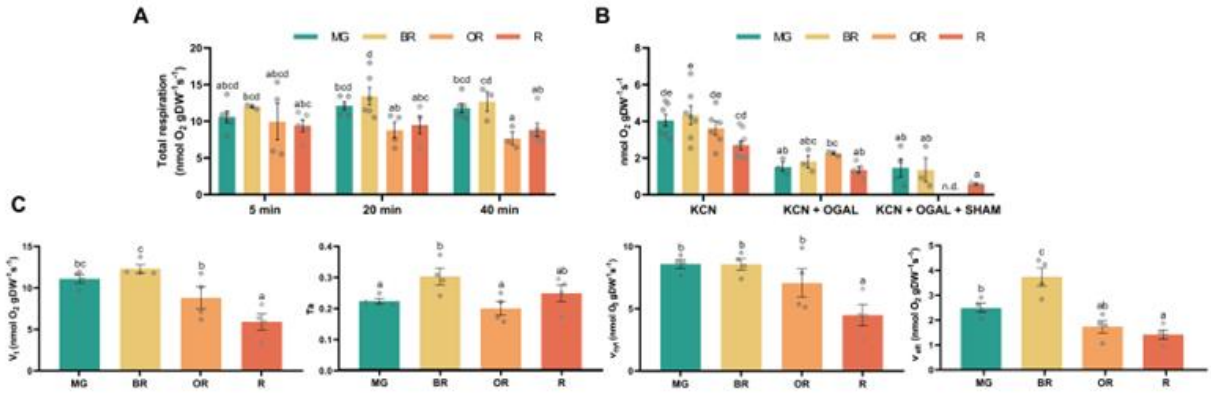


Figure C3-2. Respiratory pathways in wild-type (WT) fruits at different ripening stages. **A)** Total respiration rates after 5, 20, and 40 minutes of incubation with respiration buffer. **B)** Respiration rates after sequential additions of 5 mM potassium cyanide (KCN), 1 mM octyl gallate (OGAL) and 20 mM salicylhydroxamic acid (SHAM). **C)** Total respiration (V_t), electron partitioning to the alternative oxidase pathway (τ_a), cytochrome oxidase pathway activity (ν_{cyt}), and alternative oxidase pathway activity (ν_{alt}). Values represent means ± SE of 3-6 biological replicates. Significant differences ($P < 0.05$) are indicated by different letters.

Transcript levels of AOX and ripening-related genes during tomato fruit ripening

To confirm that the color-based classification of WT and *ghost* fruits actually corresponded with similar ripening stages, transcript levels of ripening marker genes such as *E8* (encoding 2-oxoglutalate-dependent dioxygenase), *ACS2* (aminocyclopropane-1-carboxylate synthase 2), and *PG2a* (polygalacturonase 2a) were quantified by qRT-PCR (**Figure C3-3**). As expected, all three ripening-related genes displayed low or undetectable expression at the MG (WT) or MW (*ghost*) stages, and a prominent increase was observed at the BR stage, when climacteric ethylene and respiration responses are induced (**Figure C3-3**). While *ACS2* transcript levels kept increasing at later stages of ripening, the expression of *PG2a* and, to a lower extent, *E8*, decreased in ripe fruit at the R (WT) or Y (*ghost*) stage (**Figure C3-3**). These patterns resemble those previously reported in tomato fruits and thus validate the adequate sampling and selection of the different ripening stages in both WT and *ghost* fruits. The same RNA samples were next

used to check the expression of AOX-encoding genes expressed in tomato fruits (AOX1a and AOX1b). Transcript levels of *AOX1a* steadily increased during fruit ripening and peaked at the R / Y stage, while the levels of *AOX1b* did not significantly change even though they showed a tendency to decrease during ripening (**Figure C3-3**).

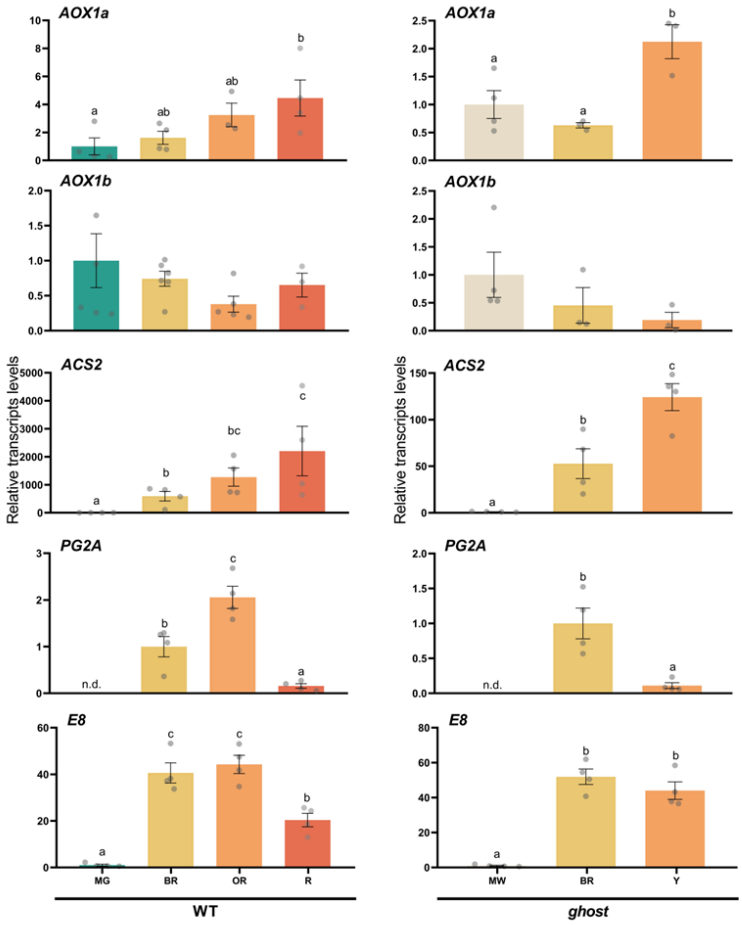


Figure C3-3. Relative transcript levels of AOX- and ripening-related genes in WT and ghost mutant fruits at different ripening stages. AOX1a: alternative oxidase 1a; AOX1b: alternative oxidase 1b; E8: 2-oxoglutarate-dependent dioxygenase ethylene-responsive protein; ACS2: aminocyclopropane-1-carboxylate synthase 2; PG2a: polygalacturonase 2a. Data are presented as fold-changes relative to the mature green (MG) stage, with control values set to 1. Values are means ± SE of three to six replicates. Significant differences ($P < 0.05$) are indicated by different letters. "n.d." denotes "not detected."

Metabolite profiles in WT and *ghost* fruits during ripening

Fruit samples like those used for qRT-PCR analysis of gene expression were used to compare the metabolic profiles of WT and *ghost* lines during ripening. A total of 48 and 47 primary metabolites were annotated after GC-TOF-MS analyses in fruit pericarp tissues from WT and *ghost* plants, respectively (**Supplemental Tables C3-2, C3-3** and **C3-4, Figure C3-4**). Relative metabolite levels were determined after normalization by the mean levels of WT and *ghost* pericarp samples at MG and MW stages, respectively (**Supplemental Tables C3-3, C3-4, Figure C3-4**). The levels of most of the detected metabolites significantly changed ($P<0.05$) at the onset of ripening (BR stage) (**Figure C3-4, Supplemental Tables C3-3** and **C3-4**), typically showing similar levels or trends along fruit ripening (**Figure C3-4**). Considering the observed increase in AOX climacteric respiration at the BR stage (**Figure C3-3**), we focused our analysis on the significant changes observed at the BR stage (**Figure C3-6**). The complete metabolite profiling data set and statistical analyses are shown in Supplemental Tables 3 and 4. Most of the metabolites displaying significantly lower levels at BR stage in WT fruit were amino acids including valine (Val; 0.22-fold), isoleucine (Ile, 0.50), glycine (Gly; 0.35), proline (Pro; 0.49), alanine (Ala; 0.41), threonine (Thr; 0.66), tyrosine (Tyr; 0.40) and tryptophan (Trp; 0.48), but also glycerate (0.65), beta-alanine (0.41) and raffinose (0.46) (**Figure C3-5, Supplemental Table C3-3**). On the other hand, the only two amino acids displaying significantly higher levels at the BR stage were aspartate (Asp; 1.79-fold) and methionine (Met; 1.75-fold). Other metabolites significantly ($P<0.05$) increased at the BR stage in WT fruits were dehydroascorbate (Dhasc; 2.29-fold), galacturonate (3.26), xylose (1.45), pyruvate (Pry; 1.87), citrate (Cit; 1.74), 2-oxoglutarate (2-OG; 3.35), succinate (Succ; 2.37) and adenosine-5-monophosphate (2.29). Similarly, organic acids including Cit (2.36), 2-OG (2.49), Succ (2.70), Dhasc (1.34), galacturonate (not detected at MW) as well as xylose (3.13) and adenosine-5-monophosphate (not detected at MW) were increased in *ghost* fruits at the BR stage. Also as in WT fruits, amino acids Met (3.83) and Asp (2.70) were increased, while valine (0.64-fold) and alanine (0.36) were decreased. However, other aspartate family amino acids were only increased in *ghost* fruits, including threonine (2.70), homoserine (2.18) and asparagine (3.77) as well as glutamate (8.74), lysine (2.15), Trp (6.64), ornithine (2.19) and serine (Ser; 3.34). In

addition, malate (0.60), *myo*-inositol (0.52), and GABA (0.63) displayed substantially lower levels in *ghost* BR fruits (**Figure C3-4**).

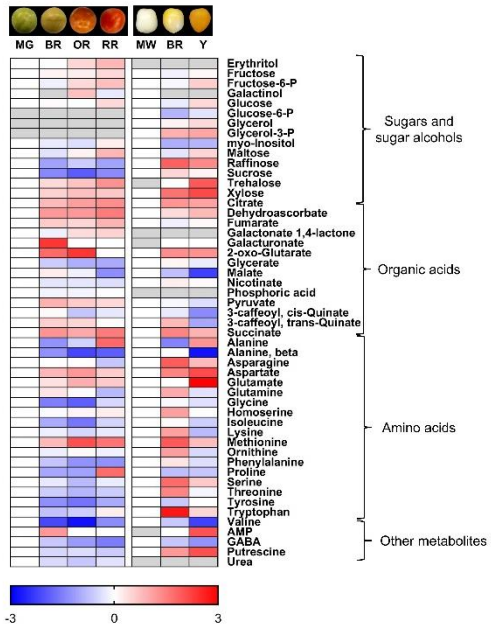


Figure C3-4. Metabolite profiles showing relative changes in primary metabolism in WT and ghost fruits at different ripening stages. The heatmap displays the relative levels of metabolites analyzed by GC-MS in WT and *ghost* mutant fruits. Relative metabolite levels were normalized to the mean level of the MG (WT) or MW (*ghost*) stage and log2-transformed (i.e., levels at MG and MW stages are set to 0). Red and blue colors represent log2 fold-increases and decreases in metabolite levels, respectively. Gray indicates metabolites not detected under certain experimental conditions. Values are means ± SE of 4–6 replicates. Statistical differences between MG or MW and other ripening stages are shown in **Supplemental Tables C3-3** and **C3-4**.

The metabolic profiling of WT and *ghost* fruit was complemented with the HPLC-DAD analyses of carotenoids, probably the most conspicuous group of metabolites associated to tomato ripening (**Figure C3-5**) (Klee and Giovannoni, 2011; Llorente et al., 2016). The biosynthesis of carotenoids, which is strongly activated in WT fruit from the BR stage, starts with the production of phytoene. Then, desaturation reactions that require PTOX activity in ripening fruit (Shahbazi et al., 2007) convert non-colored phytoene into red-colored lycopene. Further downstream reactions produce β-carotene (the main pro-vitamin A carotenoid) and lutein (the most abundant carotenoid in the chloroplasts of green tissues) (Rodriguez-Concepcion et al., 2018). An increase in the levels of phytoene,

lycopene and β-carotene in concert with a decrease of lutein was observed during ripening of WT fruits. Also expectedly, lycopene became the most abundant carotenoid in R fruit (**Figure C3-5**). By contrast, phytoene was virtually the only carotenoid found in *ghost* fruit, reaching levels that were significantly ($P<0.05$) higher than those of lycopene and total carotenoids in WT fruits when ripe (Y vs. R). Overall, the total carotenoid content was not significantly ($P<0.05$) different among genotypes at non-ripened stages (MG vs MW).

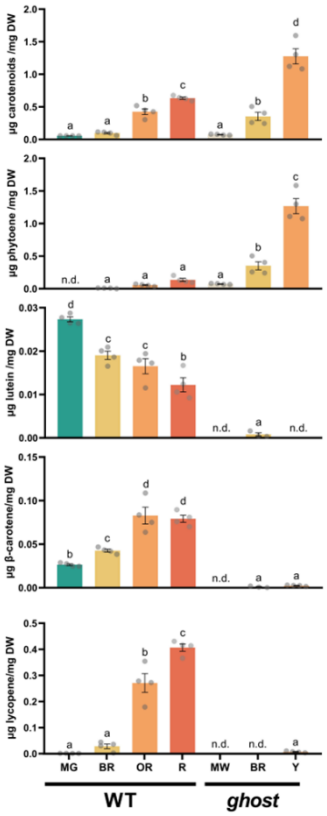


Figure C3-5. Levels of individual carotenoids (phytoene, lycopene, lutein and b-carotene) as well as total carotenoids and chlorophylls in fruits of WT and ghost mutant at different ripening stages. Values are means ± SE of 4 replicates and different letters represent statistically significant differences (one-way ANOVA followed by Duncan's multiple comparisons test, $P < 0.05$).

Discussion

^{18}O discrimination analyses in WT and *ghost* mutants: new opportunities and future perspectives

It is well established that COX ^{18}O discrimination (Δ_c) is 18-20 ‰ while AOX ^{18}O discrimination (Δ_a) is around 30 ‰ in green tissues and 26 ‰ in non-green tissues due to different AOX isoforms (Del-Saz et al., 2017). Then, the ^{18}O discrimination of a given tissue in the absence of inhibitors (Δ_n) falls in between Δ_c and Δ_a depending on the partitioning of electrons between COX and AOX (τ_a) (Ribas-Carbo et al., 1995). Our first trials in pericarp tissue slices yielded Δ values below those typically observed (Supplemental Figure 1), most likely because of the O_2 diffusion limitation that occurs in thick tissues (Del-Saz et al., 2017). In case there is a diffusion limitation during respiration measurements, the Δ due to diffusion (Δ_d) is then measured together with Δ due to the enzymatic reactions (i.e. due to terminal oxidases). Since Δ_d is much lower than enzymatic Δ (around 6-8 ‰, Ribas-Carbo M personal communication), the measured Δ during respiration would be lower than expected. The limitation of O_2 diffusion across most plant tissues is usually low enough not to affect enzymatic Δ measurements (Ribas-Carbo et al., 1997). For example, values of Δ_c, Δ_a, and Δ_n in soybean roots and cotyledons were very similar to those obtained from liquid-phase measurements in mitochondrial isolations from the same tissues, the last obviously lacking any limitation in O_2 diffusion (Ribas-Carbo et al., 1997). However, O_2 diffusion limitation in dense tissues such as seeds or fruits is much higher. Therefore, care must be taken when fruit tissues are measured, particularly with a gas-phase ^{18}O discrimination technique. Our strategy was to cut the tomato pericarp into thin slices to remove the O_2 diffusion limitation, similarly, as previously performed in *Opuntia ficus-indica* cladodes (Gomez-Casanovas et al., 2007).

Even when careful tissue preparation is followed, tomato fruit O_2 consumption could potentially be influenced by chromorespiration, since PTOX has been described to play an important role during fruit chromoplast metabolism (Renato et al., 2014). We performed oxygen consumption and discrimination experiments by using OGAL because it was previously reported as a specific inhibitor for PTOX. However, our results clearly show a strong inhibitory effect of OGAL over AOX in tomato fruit pericarp (**Figure C3-**

2B, Table C3-1). In agreement, previous *in vitro* data obtained in isolated mitochondria showed that OGAL is a potent inhibitor of AOX (I50 ≈ 0.07-0.3uM; (Hoefnagel et al., 1995), similarly as of PTOX (I50 ≈ 0.4uM, Josse et al., 2003). Furthermore, recent studies in cells and purified proteins (Barsottini et al., 2020; Romero-Aguilar et al., 2020) have also reported the strong inhibitor effect of OGAL over the AOX.

To bypass these limitations, Δ_a was determined in WT and *ghost* mutant fruits lacking PTOX to determine the contribution of chromorespiration to the O_2 consumption in tomato fruits (**Table C3-1**). Chromorespiration is the light-independent O_2 consumption involving an electron transport chain at the thylakoidal membrane composed by the NAD(P)H dehydrogenases, cytochrome b6f complex and PTOX, as well as the ATP synthase (Renato et al., 2015). The similar Δ_a values observed in WT and *ghost* mutant fruits suggest a minor contribution of PTOX respiration to pericarp O_2 consumption. While we cannot discard that ^{18}O discrimination of PTOX (not directly determined here) and AOX could be similar, previous evidence (Renato et al., 2014) and the results presented here suggest that chromorespiration could become of some relevance for ATP synthesis only at the end of ripening, when the *in vivo* COX respiration decreases.

In summary, the values of Δ_a and Δ_c in pericarp tissue from fruits at all ripening stages, obtained after careful considerations taken for tissue incubations and inhibitor treatments, were very similar to those obtained in other tissues (Del-Saz et al., 2017). Moreover, the discrimination values in the absence of inhibitors (Δ_n) fell in between Δ_a and Δ_c. We, therefore, conclude that our methodology adaptations to measure mitochondrial electron partitioning in tomato pericarp tissue resulted in no apparent technical or biological artifacts derived from discrimination by diffusion, wound respiration, or the activity of the PTOX. The application of this technique in future studies involving fruits of different species (climacteric and non-climacteric) and/or (ripening-related) mutants opens a great window of opportunities for a better understanding of energy metabolism during fruit development and ripening.

***In vivo* regulation of fruit respiration and consequences for energy metabolism during tomato fruit ripening.**

Respiration in fruits is essential to provide carbon skeletons and energy for the synthesis of nucleic acids and proteins as well as new pigments and flavor compounds, all being highly demanded during ripening (Tucker, 1993; Pott et al., 2019). In this context, the observed constant *in vivo* COP activity (v_{cyt}) during the climacteric peak of respiration at the BR stage could supply the ATP required for these high energy-demanding processes at the onset of ripening. On the other hand, the observed decrease of v_{cyt} at R stage agrees with previous observations showing a decreased number of energized (ATP-producing) mitochondria in ripe fruits (Renato et al., 2014). In addition, the lower mitochondrial ATP production in ripe fruits has been suggested to be influenced by increased AOX and uncoupling protein expression (Holtzapffel et al., 2002; Renato et al., 2014). However, our data suggest that decreased mitochondrial ATP production in ripe fruits is mainly a consequence of decreased v_{cyt}, rather than increased *in vivo* AOX activity (v_{alt}).

Importantly, v_{alt} significantly ($P<0.05$) increased at the BR stage becoming the main contributor to the climacteric respiration. These results agree with previous evidence suggesting that the AOX pathway is highly relevant during climacteric respiration in tomato (Xu et al., 2012; Colombié et al., 2017). Delayed ripening and reduced total respiration have been reported in tomato fruits of AOX-silenced plants (Xu et al., 2012). In addition, the fluxes through AOX and UCP respiration were predicted to increase at the climacteric peak by using a constraint-based metabolic modeling approach (Colombié et al., 2017). Our experimental data not only support previous simulations predicting the AOX increase at BR stage, but also provide quantitative *in vivo* fluxes through AOX and COX pathways during fruit ripening. In addition, the fact that v_{cyt} was not increased during the climacteric peak could also reflect a minor role of the UCPs at this stage. Changes on UCP activity should impact the activity of the ATP-coupled COX pathway, as previously discussed in thermogenic tissues of the sacred lotus (Watling et al., 2006). Since direct measurements of the *in vivo* UCP activity are not currently plausible, further experiments involving UCP activity alterations (i.e. by inhibitor treatment or genetic manipulation) would be required to clarify the precise roles of the UCPs during fruit ripening.

Regarding AOX regulation, the expression of *AOX1a* and *AOX1b* genes, which encode the main isoforms expressed in tomato fruits, did not correlate with v_{alt} (**Figures C3-2C** and **C3-3**). The lack of correlation between the expression of AOX-encoding genes and *in vivo* activity is frequently observed and can be explained by the important contribution of AOX post-translational regulation (Del-Saz et al., 2018; Selinski et al., 2018a). AOX is usually found in its reduced state *in vivo* (Florez-Sarasa et al., 2019), which is a prerequisite for its allosteric activation by α-ketoacids through the formation of a thiohemiacetal bond occurring at conserved Cys residues. *In vitro* studies have shown that the activation of AOX by different organic acids from the TCA cycle is isoform-specific (Selinski et al., 2018a). When the regulatory Cys position is substituted by a Ser residue (Ser) by site-directed mutagenesis, the Ser-type AOX isoform becomes insensitive to 2-oxo acids (i.e. pyruvate) but is activated by succinate (Selinski et al., 2018a). This Ser-type AOXs occur naturally in some species (Grant et al., 2009) including the tomato isoform AOX1b (Holtzapffel et al., 2003). In the present study, an increase in the key allosteric regulators of the Cys-type AOX1a (pyruvate and 2-oxoglutarate) and of the Ser-type AOX1b (succinate) were observed at the BR stage in concert with the increase of v_{alt} (**Figures C3-2C** and **C3-6**). Together, these results strongly suggest a posttranslational activation of AOX at the BR stage. Notably, the fact that Ser-type AOX1b cannot be inactivated by Cys-oxidation suggests that this isoform can be highly active, if expressed, when succinate levels accumulate. While the basal level of expression of AOX1b is lower than AOX1a, its special regulatory feature together with its relatively high expression at non-ripened stages (**Figure C3-3**), makes this isoform a possible candidate for regulating climacteric respiration. However, the relative contribution of each isoform to climacteric respiration *in vivo* and its organic acid regulation will require further experimentation, for instance by studying the respiratory metabolism responses of isoform-specific mutants.

Coordinated changes in primary metabolism and electron partitioning to AOX allows for the accumulation of key ripening-related metabolic precursors

In addition to the changes in TCA cycle intermediates, the coordinated increase of v_{alt} with other changes in key primary metabolites at the climacteric peak also suggests relevant metabolic roles of AOX (**Figure C3-6**). Among all amino acids, the only two

displaying high levels at the climacteric peak were aspartate (Asp) and methionine (Met), which are precursors for the synthesis of ethylene (**Figure C3-6**), the most important hormone triggering fruit ripening. Respiration is thought to provide the ATP required for the Yang cycle, thus allowing the recycling of methionine for the biosynthesis of ethylene (**Figure C3-5**; Yang and Hoffman, 1984). In this line, an increase in COX-dependent respiration would be expected at the climacteric peak given its ATP-coupled nature. However, our results clearly show that climacteric peak is mainly driven by the non-phosphorylating AOX pathway. Previous studies in leaf and root tissues suggest different roles of the AOX in providing metabolic flexibility under high cell energy (ATP) charge, and when there is a high carbon skeletons demand (Del-Saz et al., 2018). In this line, a high respiratory flux at the climacteric peak would be required to provide the carbon precursors (oxalacetate and aspartate) needed for 'de novo' Met synthesis. Despite the Yang cycle allows for the synthesis of ethylene precursors while recycling Met, there is evidence indicating that 'de novo' synthesis of Met becomes relevant when high rates of ethylene production occur in tomato fruits (Katz et al., 2006). Therefore, a high carbon flux towards Met synthesis should be expected during the climacteric peak of ethylene production and could presumably be fulfilled from respiratory pathways (**Figure C3-6**). In line with this, the combined decrease in sucrose and increase in pyruvate levels suggest a high glycolytic flux at the BR stage (**Figure C3-6**). Increased levels of pyruvate and other glycolytic intermediates can also serve as precursors for the synthesis of secondary metabolites such as flavonoids and carotenoids (Aharoni and Galili, 2011; Rodríguez-Concepción and Boronat, 2015; Zhang et al., 2015; Enfissi et al., 2017). Incremented levels of pyruvate and aspartate were consistently observed in ripened fruits of geranylgeranyl diphosphate synthase (GGPPS) mutants, which displayed an important restriction in carotenoid synthesis (Barja et al., 2021). In the present study, we also determined the carotenoids and primary metabolite profiles in *ghost* mutant fruits at three maturation stages (**Supplemental Figures C3-2, C3-3** and **C3-4**). The *ghost* mutants were previously characterized by displaying profound changes in their carotenoid profiles at ripened stages compared to WT fruits (Barr et al., 2004; Shahbazi et al., 2007). An almost complete restriction of the carotenoid pathway at the phytoene desaturase reaction was also observed here, since carotenoid accumulation along *ghost* fruit ripening was mainly due to increasing phytoene levels (**Figure C3-5**). Moreover, total carotenoid

accumulation was higher at *ghost* mutant, thus suggesting a higher flux through the MEP pathway as compared to WT fruits (**Figure C3-5**). The high demand for pyruvate in *ghost* fruits could explain its lack of accumulation at BR stage as compared to WT fruits. Primary metabolites related to TCA cycle, ethylene synthesis, and cell wall increased over ripening in the *ghost* mutant similarly to WT, indicating a similar climacteric response (**Figure C3-4** and **Supplemental Figure C3-2**). However, increased levels of some metabolites over ripening may denote changes in carbon flow from the TCA cycle to stress-related amino acids (Glu, GABA, Orn, Lys and Asn). On the other hand, differences on the ripening patterns of shikimate derived amino acids (Trp and Tyr) are likely linked to different flavonoid accumulation. Overall, responses of primary metabolism in *ghost* tomato fruits indicate a similar climacteric response in the absence of chromorespiration as compared to wild-type fruits, although with some re-arrangements in stress-related amino acid and shikimate derived amino acids.

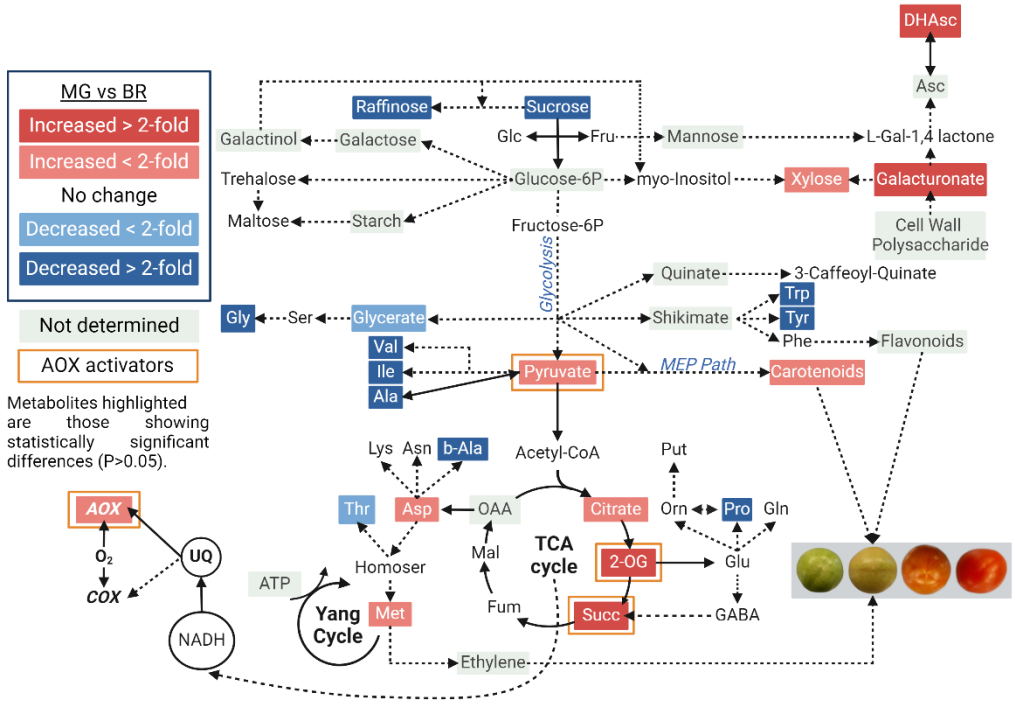


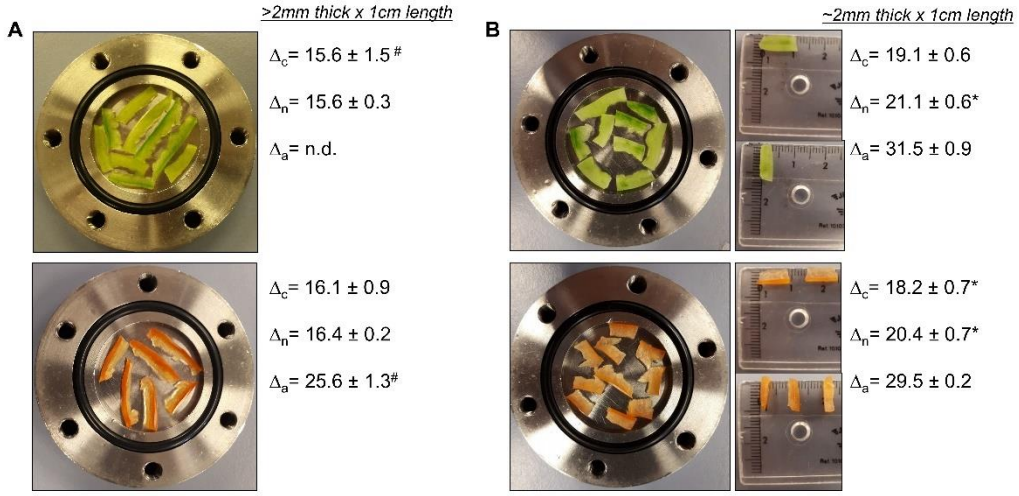
Figure C3-6. Metabolic model showing changes in respiratory and associated metabolism at the climacteric peak of WT tomato fruit ripening (BR stage). Blue and red boxes indicate significantly ($P < 0.05$) decreased or increased metabolites and respiratory activities, respectively, in BR as compared to MG stage. Activators of the AOX1a (Pyruvate and 2-oxoglutarate) and AOX1b

(succinate) isoforms are highlighted with orange boxes. Image created with BioRender. (https://biorender.com).

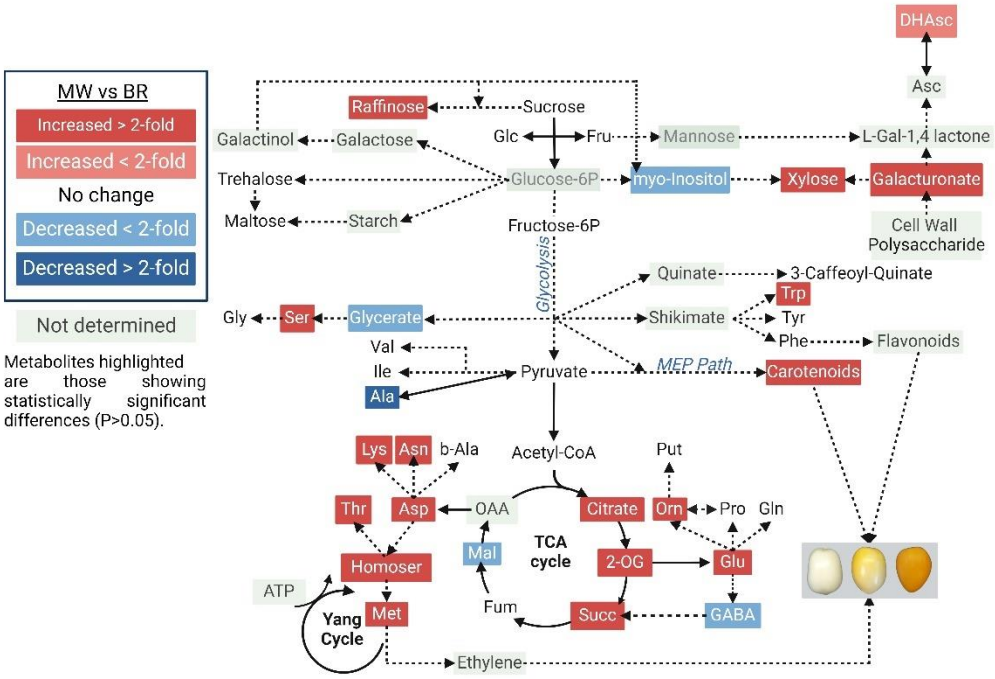
Conclusion

In summary, we propose a positive feedback regulation by which increased pyruvate and succinate levels produced from sucrose oxidation at BR stage can allosterically activate the AOX1a and AOX1b isoforms, which allows the reoxidation of NAD(P)H escaping the ATP respiratory control (**Figure C3-6**). Such a climacteric burst of the non-phosphorylating AOX pathway respiration could allow for a high rate of glycolytic and TCA cycle flux to provide carbon precursors for ethylene (Methionine) and carotenoid biosynthesis (pyruvate and trioses phosphates) (**Figure C3-6**). New opportunities are now open for measuring *in vivo* respiratory activities in climacteric and non-climacteric fruits as well as in ripening mutants, which will be key to better understand fruit ripening and disentangle the precise hierarchy of the metabolic processes involved.

Supplemental Data



Supplemental Figure C3-1. Photographs of the sliced pericarp tissue at MG and R stages of different sizes placed at the DI-IRMS cuvette, and effects on the 18O discrimination**.** Pericarp slices of more than 2 mm thick and 1 cm length **A)**, and of approx. 2 mm thick and 1 cm length **B)** are shown together with their corresponding values of ^{18}O discrimination by the AOX pathway (Δ_a, after 10mM KCN treatment), by COX (Δ_c, after 20mM SHAM treatment), and in the absence of inhibitors (Δ_n). The ^{18}O discrimination data are means ± SE of 3-5 biological replicates corresponding to different fruits. Asterisks denotes significant differences ($P < 0.05$). n.d., 'not determined'; #only 2 replicates available.



Supplementary Figure C3-2. Changes in respiratory and associated metabolism at the climacteric peak of ghost tomato fruit ripening (BR stage). Blue and red boxes indicate significantly ($P < 0.05$) decreased or increased metabolites and respiratory activities, respectively, in BR as compared to MW stage. Image created with BioRender. (https://biorender.com).

Sl-AOX1a	Solyc08g075540	SlAOX1a-qPCR-Fv SlAOX1a-qPCR-Rv	TTGTTTTAGGCCATGGGAGACTT CAGTGGGGAAACGAAGGATCT
Sl-AOX1b	Solyc08g075550	SlAOX1b-qPCR-Fw SlAOX1b-qPCR-Rv	CACACTGATGCAACCAACGC TACGTCTCCCATGGCCTGAA
Sl-ACS2	Solyc01g095080	SlACS2-Fw SlACS2-Rv	CGTTTGAATGTCAAGAGCCAGG TCGCGAGCGCAATATCAAC
Sl-PG2a	Solyc10g080210	SlPGA-qPCR-Fw SlPGA-qPCR-Rv	ATGGCAATGGACAAGTATGGTG TTAAGGCCGTTGGTGCATC
Sl-E8	Solyc09g089580	SlE8-qPCR-Fw SlE8-qPCR-Rv	AGCTGCAAGTTGGAGAGACACG CCGCATGGAGTTGGAAATTC
Sl-ACT4	Solyc04g011500	Sl ACT4-qPCR-Fw Sl ACT4-qPCR-Rv	CCTTCCACATGCCATTCTCC CCACGCTCGGTCAGGATCT

Supplemental Table C3-1. Primers used in qPCR studies performed in this work.

	A	B	C	D	E	F	G	H	I	J	K	L
1	**Experiment title:**	Metabolite profiles of tomato wild-type and ghost mutants during ripening				Peak/compound no.- number referenced back to the main text			Mol. Formula- molecular formula of the metabolite or its FA adduct;			
2	**Organism/Plant sp.**	Solanum lycopersicum				Ret. Time- Time expected, Tag Time Index and Time deviation			Mass to charge ratio (m/z)			
3	**Organ/tissue:**	Fruit Pericarp				Putative Name- putative identification of the metabolite/derivative			(S)- identification confirmed by a standard compound			
4	**Analytical tool:**	GC-TOF-MS				Corresponding metabolite name in literature			I, II, III- different isomers			
5									Identification level (A; B; C; D)- (A) standard or NMR; (B) MS/MS; (C) MS^{E}; (D) MS or			
6	**Peak/Compound no.**	**Time Expected**	**Tag Time Index**	**Time Deviation**	**Putative metabolite name (Derivative)**	**Corresponding Metabolite in Literature**	**Metabolite Class**	**Mol formula**	**Mass to charge ratio (m/z)**	**Species detected before**	**Ref.**	**Id. level (A-D)**
7	1	222650	222348	-0,15	M000071_A1040002-101_METB_222650_TOF_Pyruvic acid (1MEOX) (1TMS)	Pyruvate	Acid (Oxo)	C3H4O3	174	Tomato, Arabidopsis, potato, grapevine and others		A
8	2	271580	271806	0,1	M000030_A1220001-101_METB_271580_TOF_Valine, DL- (2TMS)	Valine	Acid (Amino)	C5H11NO2	144	Tomato, Arabidopsis, potato, grapevine and others		A
9	3	291783	291776	-0,03	M000053_A1290003-101_METB_291783_TOF_Glycerol (3TMS)	Glycerol	Polyol	C3H8O3	205	Tomato, Arabidopsis, potato, grapevine and others		A
10	4	319193	319036	-0,03	M000017_A1320002-101_METB_319193_TOF_Isoleucine, L- (2TMS)	Isoleucine	Acid (Amino)	C6H13NO2	158	Tomato, Arabidopsis, potato, grapevine and others		A
11	5	325180	324856	-0,1	M000031_A1330001-101_METB_325180_TOF_Glycine (3TMS)	Glycine	Acid (Amino)	C2H5NO2	174	Tomato, Arabidopsis, potato, grapevine and others		A
12	6	333520	332443	-0,37	M000075_A1290001-101_METB_333520_TOF_Phosphoric acid (3TMS)	Phosphorate	Phosphate	H3O4P	299	Tomato, Arabidopsis, potato, grapevine and others		A
13	7	338693	338620	-0,04	M000029_A1320003-101_METB_338693_TOF_Proline, L- (2TMS)	Proline	Amide	C5H9NO	142	Tomato, Arabidopsis, potato, grapevine and others		A
14	8	340357	339818	-0,2	M000364_A1270002-101_METB_340357_TOF_Urea (2TMS)	Urea	Amide	CH4N2O	189	Tomato, Arabidopsis, potato, grapevine and others		A
15	9	342530	342246	-0,07	M000114_A1330002-101_METB_342530_TOF_Butyric acid, 4-amino- (2TMS)	4-Aminobutanoic Acid	Acid (Amino)	C4H9NO2	103	Tomato, Arabidopsis, potato, grapevine and others		A
16	10	345050	344205	-0,23	M000073_A1350003-101_METB_345050_TOF_Glyceric acid, DL- (3TMS)	Glycerate	Acid	C3H6O4	292	Tomato, Arabidopsis, potato, grapevine and others		A
17	11	354060	353867	-0,06	M000026_A1360002-101_METB_354060_TOF_Alanine, DL- (3TMS)	Alanine	Acid (Amino)	C3H7NO2	188	Tomato, Arabidopsis, potato, grapevine and others		A
18	12	357523	357021	-0,13	M000015_A1380001-101_METB_357523_TOF_Serine, DL- (3TMS)	Serine	Acid (Amino)	C3H7NO3	204	Tomato, Arabidopsis, potato, grapevine and others		A
19	13	365427	364803	-0,13	M000074_A1340001-101_METB_365427_TOF_Succinic acid (2TMS)	Succinate	Acid	C4H6O4	247	Tomato, Arabidopsis, potato, grapevine and others		A
20	14	368365	367319	-0,3	M000016_A1400001-101_METB_368365_TOF_Threonine, DL- (3TMS)	Threonine	Acid (Amino)	C4H9NO3	117	Tomato, Arabidopsis, potato, grapevine and others		A
21	15	371255	370722	-0,15	M000067_A1370001-101_METB_371255_TOF_Fumaric acid (2TMS)	Fumarate	Acid (Dicarboxylic)	C4H4O4	245	Tomato, Arabidopsis, potato, grapevine and others		A
22	16	386210	385694	-0,14	M000457_A1330004-101_METB_386210_TOF_Nicotinic acid (1TMS)	Nicotinate	Acid	C6H5NO2	180	Tomato, Arabidopsis, potato, grapevine and others		A
23	17	394250	393982	-0,06	M000027_A1440001-101_METB_394250_TOF_Alanine, beta- (3TMS)	beta-Alanine	Acid (Amino)	C3H7NO2	248	Tomato, Arabidopsis, potato, grapevine and others		A
24	18	404940	405841	0,21	M000019_A1460001-101_METB_404940_TOF_Homoserine, DL- (3TMS)	Homoserine	Acid (Amino)	C4H9NO3	119	Tomato, Arabidopsis, potato, grapevine and others		A
25	19	408455	408118	-0,06	M000054_A1500002-101_METB_408455_TOF_Erythritol (4TMS)	Erythritol	Polyol	C4H10O4	205	Tomato, Arabidopsis, potato, grapevine and others		A
26	20	440995	440474	-0,11	M000065_A1490001-101_METB_440995_TOF_Malic acid, DL- (3TMS)	Malate	Acid	C4H6O5	233	Tomato, Arabidopsis, potato, grapevine and others		A
27	21	457283	456775	-0,03	M000033_A1520002-101_METB_457283_TOF_Aspartic acid, L- (3TMS)	Aspartate	Acid (Amino)	C4H7NO4	232	Tomato, Arabidopsis, potato, grapevine and others		A
28	22	474325	473799	-0,11	M000018_A1520001-101_METB_474325_TOF_Methionine, DL- (2TMS)	Methionine	Acid (Amino)	C5H11NO2S	176	Tomato, Arabidopsis, potato, grapevine and others		A
29	23	492650	492221	-0,08	M000032_A1740008-101_MST_492650_TOF_Glutamine, DL- (4TMS)	Glutamine	Acid (Amino)	C5H10N2O3	227	Tomato, Arabidopsis, potato, grapevine and others		A
30	24	498150	497775	-0,04	M000579_A1660001-101_METB_498150_TOF_Xylose, D- (1MEOX) (4TMS)	Xylose	Sugar (Pentose, aldose	C5H10O5	160	Tomato, Arabidopsis, potato, grapevine and others		A
31	25	507780	507375	-0,09	M000036_A1630001-101_METB_507780_TOF_Glutamic acid, DL- (3TMS)	Glutamate	Acid (Amino)	C5H9NO4	246	Tomato, Arabidopsis, potato, grapevine and others		A
32	26	517180	517566	0,1	M000186_A1750002-101_METB-METB_517180_TOF_Putrescine (4TMS)	Putrescine	Amine	C4H12N2	174	Tomato, Arabidopsis, potato, grapevine and others		A
33	27	523947	522791	-0,19	M000571_A1580004-101_METB_523947_TOF_Glutaric acid, 2-oxo- (1MEOX) (2TMS)	2-oxo-Glutarate	Acid (Oxo)	C5H6O5	198	Tomato, Arabidopsis, potato, grapevine and others		A
34	28	531145	530508	-0,11	M000011_A1040001-101_METB_531145_TOF_Phenylalanine, DL- (2TMS)	Phenylalanine	Acid (Amino)	C9H11NO2	218	Tomato, Arabidopsis, potato, grapevine and others		A
35	29	550100	549546	-0,1	M000013_A1680001-101_METB_550100_TOF_Asparagine, DL- (3TMS)	Asparagine	Acid (Amino)	C4H8N2O3	116	Tomato, Arabidopsis, potato, grapevine and others		A
36	30	570427	570449	0,03	M000028_A1620002-101_METB-METB_570427_TOF_Ornithine, DL- (4TMS)	Ornithine	Acid (Amino)	C5H12N2O2	142	Tomato, Arabidopsis, potato, grapevine and others		A
37	31	574230	573233	-0,18	M000328_A1770002-101_METB_574230_TOF_Glycerol-3-phosphate, DL- (4TMS)	Glycerol-3-P	Alcohol (Phosphate)	C3H9O6P	299	Tomato, Arabidopsis, potato, grapevine and others		A
38	32	579380	576444	-0,5	M000606_A1870002-101_METB_579380_TOF_Fructose, D- (1MEOX) (5TMS)	Fructose	Sugar (Hexose, ketose)	C6H12O6	217	Tomato, Arabidopsis, potato, grapevine and others		A
39	33	590400	587560	-0,44	M000040_A1890002-101_METB_590400_TOF_Glucose, D- (1MEOX) (5TMS)	Glucose	Sugar (Hexose, aldose)	C6H12O6	160	Tomato, Arabidopsis, potato, grapevine and others		A
40	34	592883	592883	0	M000069_A1820004-101_METB-METB_592883_TOF_Citric acid (4TMS)	Citrate	Acid	C6H8O7	273	Tomato, Arabidopsis, potato, grapevine and others		A
41	35	615467	616388	0,13	M000014_A1920003-101_METB_615467_TOF_Lysine, L- (4TMS)	Lysine	Acid (Amino)	C6H14N2O2	156	Tomato, Arabidopsis, potato, grapevine and others		A
42	36	618870	618615	-0,13	M000639_A1890003-101_METB_618870_TOF_Galactonic acid-1,4-lactone, D(-)- (4TMS)	D-Galacto-1,4-lactone	Acid (Hexonic)	C6H12O7	178	Tomato, Arabidopsis, potato, grapevine and others		A
43	37	624990	624222	-0,06	M000082_A1850002-101_METB-METB_624990_TOF_Dehydroascorbic acid dimer (TMS)	Dehydroascorbate	Acid	C6H6O6	316	Tomato, Arabidopsis, potato, grapevine and others		A
44	38	632880	632250	-0,08	M000690_A1960003-101_METB_632880_TOF_Galacturonic acid, D- (1MEOX) (5TMS)	Galacturonate	Acid (Hexuronic)	C6H10O7	194	Tomato, Arabidopsis, potato, grapevine and others		A
45	39	653910	653994	0,04	M000060_A2090002-101_METB_653910_TOF_Inositol, myo- (6TMS)	myo-Inositol	Polyol	C6H12O6	305	Tomato, Arabidopsis, potato, grapevine and others		A
46	40	658337	657691	-0,09	M000035_A1940002-101_METB_658337_TOF_Tyrosine, DL- (3TMS)	Tyrosine	Acid (Amino)	C9H11NO3	218	Tomato, Arabidopsis, potato, grapevine and others		A
47	41	767060	765960	-0,15	M000510_A2320002-101_METB_767060_TOF_Fructose-6-phosphate (1MEOX) (6TMS)	Fructose-6-phosphate	Sugar (Phosphate)	C6H13O9P	260	Tomato, Arabidopsis, potato, grapevine and others		A
48	42	781350	778808	-0,35	M000513_A2350002-101_METB-METB_781350_TOF_Glucose-6-phosphate (1MEOX) (6TMS)	Glucose-6-phosphate	Sugar (Phosphate)	C6H13O9P	260	Tomato, Arabidopsis, potato, grapevine and others		A
49	43	790560	790597	0	M000012_A2230001-101_METB_790560_TOF_Tryptophan, L- (3TMS)	Tryptophan	Acid (Amino)	C11H12N2O2	204	Tomato, Arabidopsis, potato, grapevine and others		A
50	44	840783	837519	-0,37	M000044_A2640001-101_METB_840783_TOF_Sucrose, D- (8TMS)	Sucrose	Sugar (Disaccharide)	C12H22O11	361	Tomato, Arabidopsis, potato, grapevine and others		A
51	45	870355	868638	-0,2	M000048_A2740001-101_METB_870355_TOF_Maltose, D- (1MEOX) (8TMS)	Maltose	Sugar (Disaccharide)	C12H22O11	204	Tomato, Arabidopsis, potato, grapevine and others		A
52	46	876240	874646	-0,17	M000671_A2740002-101_METB_876240_TOF_Trehalose, alpha,alpha'- D- (8TMS)	Trehalose	Sugar (Disaccharide)	C12H22O11	191	Tomato, Arabidopsis, potato, grapevine and others		A
53	47	940280	938445	-0,19	M000673_A2990002-101_METB_940280_EIROE_Galactinol (9TMS)	Galactinol	Polyol	C12H22O11	204	Tomato, Arabidopsis, potato, grapevine and others		A
54	48	996820	995772	-0,11	M000644_A2990001-101_METB_996820_TOF_Quinic acid, 3-caffeoyl-, cis- (6TMS)	Quinic acid, 3-caffeoyl-, cis-	ate (Phenylpropanoyl,	C16H18O9	787	Tomato, Arabidopsis, potato, grapevine and others		A
55	49	1025600	1024785	-0,08	M000003_A3110001-101_METB_1025600_TOF_Quinic acid, 3-caffeoyl-, trans- (6TMS)	Quinic acid, 3-caffeoyl-, trans-	ate (Phenylpropanoyl,	C16H18O9	787	Tomato, Arabidopsis, potato, grapevine and others		A
56	50	1033367	1031719	-0,16	M000049_A3370002-101_METB_1033367_TOF_Raffinose (11TMS)	Raffinose	Sugar (Trisaccharide)	C18H32O16	361	Tomato, Arabidopsis, potato, grapevine and others		A
57	51	1054900	1054424	-0,05	M000284_A3070003-101_METB_1054900_TOF_Adenosine-5-monophosphate (5TMS)	Adenosine-5-monophosphate	cleotide (Monophospha	C10H14N5O7P	347	Tomato, Arabidopsis, potato, grapevine and others		A

Supplemental Table C3-2. Parameters used for peak annotation of all detected metabolites.

Metabolite	MG	BR	OR	RR
Pyruvate	1 ± 0,13	1,87 ± 0,2*	1,52 ± 0,12*	1,36 ± 0,14
Valine	1 ± 0,12	0,22 ± 0,03*	0,14 ± 0,06*	0,39 ± 0,11*
Isoleucine	1 ± 0,08	0,5 ± 0,07*	0,32 ± 0,1*	0,7 ± 0,18
Glycine	1 ± 0,25	0,35 ± 0,05*	0,27 ± 0,08*	0,73 ± 0,22
Phosphoric acid	1 ± 0,08	0,91 ± 0,04	0,92 ± 0,04	0,99 ± 0,07
Proline	1 ± 0,18	0,49 ± 0,11*	0,47 ± 0,11*	3,3 ± 1,09
Urea	1 ± 0,1	0,74 ± 0,14	0,64 ± 0,12*	0,8 ± 0,27
GABA	1 ± 0,16	0,64 ± 0,14	0,44 ± 0,12*	0,34 ± 0,12*
Glycerate	1 ± 0,06	0,65 ± 0,08*	0,52 ± 0,14*	0,5 ± 0,09*
Alanine	1 ± 0,14	0,41 ± 0,04*	0,7 ± 0,2	3,38 ± 1,34
Serine	1 ± 0,11	0,83 ± 0,21	0,57 ± 0,13*	0,85 ± 0,17
Succinante	1 ± 0,06	2,37 ± 0,18*	1,98 ± 0,34*	2,92 ± 0,59*
Threonine	1 ± 0,09	0,66 ± 0,11*	0,55 ± 0,17*	0,66 ± 0,16
Fumarate	1 ± 0,11	1,51 ± 0,27	1,4 ± 0,12*	1,84 ± 0,31*
Nicotinate	1 ± 0,15	0,81 ± 0,08	0,82 ± 0,12	0,76 ± 0,08
Alanine, beta	1 ± 0,18	0,41 ± 0,09*	0,22 ± 0,06*	0,27 ± 0,1*
Homoserine	1 ± 0,15	0,97 ± 0,1	1,08 ± 0,2	1,15 ± 0,26
Erythritol	1 ± 0,1	1,01 ± 0,09	1,38 ± 0,15	1,78 ± 0,32*
Methionine	1 ± 0,19	1,75 ± 0,21*	4,11 ± 0,55*	3,08 ± 0,59*
Glutamine	1 ± 0,17	1,22 ± 0,23	0,97 ± 0,33	0,56 ± 0,22
Xylose	1 ± 0,07	1,45 ± 0,1*	1,66 ± 0,17*	1,56 ± 0,07*
Putrescine	1 ± 0,17	0,73 ± 0,21	0,75 ± 0,26	0,65 ± 0,17
2-oxo-Glutarate	1 ± 0,1	3,35 ± 0,11*	5,14 ± 0,53*	9,6 ± 2,07*
Phenylalanine	1 ± 0,1	0,63 ± 0,2	0,41 ± 0,15*	0,41 ± 0,09*
Asparagine	1 ± 0,26	0,99 ± 0,18	1,01 ± 0,35	0,63 ± 0,18
Ornithine	1 ± 0,14	0,88 ± 0,2	1,04 ± 0,29	0,89 ± 0,21
Lysine	1 ± 0,11	0,88 ± 0,14	0,73 ± 0,21	0,83 ± 0,17
Galactonate 1,4-lactone	1 ± 0,12	0,89 ± 0,08	1,31 ± 0,17	1,43 ± 0,2
Dehydroascorbate	1 ± 0,15	2,29 ± 0,08*	2,3 ± 0,1*	2,91 ± 0,37*
Galacturonate	1 ± 0,06	3,26 ± 0,35*	45,69 ± 12,35*	46,49 ± 8,01*
myo-Inositol	1 ± 0,08	0,85 ± 0,1	0,77 ± 0,07	1,14 ± 0,05
Tyrosine	1 ± 0,2	0,4 ± 0,1*	0,32 ± 0,11*	0,5 ± 0,21
Fructose-6-P	1 ± 0,12	0,88 ± 0,06	1,35 ± 0,14	1,67 ± 0,12*
Tryptophan	1 ± 0,15	0,48 ± 0,09*	0,67 ± 0,25	1,14 ± 0,19
Maltose	1 ± 0,15	0,79 ± 0,08	1,11 ± 0,17	1,79 ± 0,25*
Trehalose	1 ± 0,18	1,34 ± 0,07	1,6 ± 0,27	2,43 ± 0,19*
Galactinol	1 ± 0,39	n.d.	1,65 ± 1,19	0,84 ± 0,1
3-caffeoyl, cis-Quinate	1 ± 0,23	1,04 ± 0,26	0,62 ± 0,11	0,83 ± 0,21
3-caffeoyl, trans-Quinate	1 ± 0,28	1,47 ± 0,24	1,4 ± 0,62	1,02 ± 0,35

Supplemental Table C3-3. Relative metabolite levels detected by GC-MS in WT tomato fruits**.** Values were determined after normalization by the mean levels of WT pericarp samples at mature green (MG) stage. Levels correspond to the mean ± SE of n=4-6 independent replicates. Asterisks denote significant differences ($P < 0.05$) between MG and other ripening stages (BR, OR, R). 'n.d.' denotes 'not detected'.

Metabolite	MW	BR	Y
Alanine	1 ± 0,16	0,36 ± 0,06*	2,37 ± 0,37*
Pyruvate	1 ± 0,2	0,94 ± 0,13	0,76 ± 0,06
Valine	1 ± 0,19	0,64 ± 0,09*	0,21 ± 0,03*
Glycerol	1 ± 0,23	1,1 ± 0,18	1,35 ± 0,28
Isoleucine	1 ± 0,2	1,03 ± 0,13	0,67 ± 0,22
Glycine	1 ± 0,15	0,95 ± 0,19	0,78 ± 0,15
Proline	1 ± 0,16	0,59 ± 0,13	0,63 ± 0,38
GABA	1 ± 0,08	0,63 ± 0,13*	0,42 ± 0,11*
Glycerate	1 ± 0,09	1,07 ± 0,27	0,85 ± 0,1
Serine	1 ± 0,18	3,34 ± 0,95*	1,55 ± 0,46
Succinate	1 ± 0,23	2,7 ± 0,55*	1,83 ± 0,41
Threonine	1 ± 0,21	2,7 ± 0,51*	0,93 ± 0,24
Fumarate	1 ± 0,12	0,88 ± 0,11	1,05 ± 0,2
Nicotinate	1 ± 0,14	1,13 ± 0,16	1,03 ± 0,18
beta-Alanine	1 ± 0,16	0,99 ± 0,13	0,14 ± 0,05*
Homoserine	1 ± 0,13	2,18 ± 0,28*	0,99 ± 0,22
Methionine	1 ± 0,23	3,83 ± 0,43*	1,7 ± 0,49
Glutamine	1 ± 0,3	1,98 ± 0,46	0,78 ± 0,34
Xylose	1 ± 0,06	3,13 ± 0,68*	4,38 ± 0,78*
Putrescine	1 ± 0,16	2,3 ± 0,66	4,15 ± 0,94*
2-oxo-Glutarate	1 ± 0,1	2,49 ± 0,47*	2,43 ± 0,34*
Phenylalanine	1 ± 0,27	1,22 ± 0,39	0,77 ± 0,24
Asparagine	1 ± 0,32	3,77 ± 0,16*	1,75 ± 0,54
Ornithine	1 ± 0,23	2,19 ± 0,32*	0,74 ± 0,29
Glycerol-3-P	1†	1,89 ± 0,24	2,07 ± 0,27
Lysine	1 ± 0,31	2,15 ± 0,35*	0,57 ± 0,18
Galacturonate	n.d.	1 ± 0,28	12,33 ± 1,32*
Dehydroascorbate	1 ± 0,07	1,34 ± 0,05*	1,76 ± 0,14*
myo-Inositol	1 ± 0,08	0,52 ± 0,08*	0,55 ± 0,18*
Tyrosine	1 ± 0,27	0,65 ± 0,24	0,12 ± 0,03*
Fructose-6-P	1 ± 0,16	0,94 ± 0,15	1,47 ± 0,13*
Glucose-6-P	1 ± 0,15	0,54 ± 0,08	0,8 ± 0,05
Tryptophan	1 ± 0,23	6,64 ± 2,38*	1,39 ± 0,81
Maltose	1 ± 0,2	0,81 ± 0,19	1,4 ± 0,13
Trehalose	n.d.	1 ± 0,31	3,87 ± 0,74*
Galactinol	1 ± 0,62	n.d.	n.d.
3-caffeoyl, cis-Quinate	1 ± 0,15	0,84 ± 0,17	0,39†
3-caffeoyl, trans-Quinate	1 ± 0,13	1,77 ± 0,74	0,49†
Raffinose	1 ± 0,06	3,64 ± 0,6*	2,58 ± 0,51

Supplemental Table C3-4. Relative metabolite levels detected by GC-MS in ghost tomato fruit**s**. Values were determined after normalization by the mean levels of WT pericarp samples at mature white (MW) stage. Levels correspond to the mean ± SE of n=4 independent replicates. Asterisks denote significant differences ($P < 0.05$) between MG and other ripening stages (BR and Y). 'n.d.' denotes 'not detected'. †Denotes metabolites detected only in one replicate in MW at control conditions.

Chapter 4: Lack of alternative oxidase 1a restricts carbon supply for carotenoid and ethylene biosynthesis during tomato fruit ripening

Introduction

Tomato (*Solanum lycopersicum*) is one of the most cultivated fruits worldwide and its production has increased more than five times in the last 50 years (FAOSTATS, 2023). Tomato is used as a model for crop species and fleshy fruits because of advantageous features such as a short life cycle, easy growth in greenhouses and open fields, availability of genetic resources, and easy genetic transformation (Just et al., 2013). Moreover, tomato has been the main model plant for studying fruit ripening (Klee and Giovannoni, 2011; Neelwarne, 2015a). As opposed to non-climacteric fruits (i.e. grape, strawberry, cherry, citrus, etc.), the ripening of climacteric fruits (i.e. tomato, apple, banana, mango, avocado, etc.) is characterized by a rise in respiration and ethylene production around the ripening on-set (Fukano and Tachiki, 2021). As ethylene levels rise, they trigger various metabolic pathways that lead to the production of carotenoids, including lycopene, which is responsible for the red color of ripe tomatoes. The increase in carotenoids not only contributes to the fruit pigmentation but also enhances its nutritional value, providing important antioxidants and vitamin A precursors (Klee and Giovannoni, 2011; Rodríguez-Concepción and Boronat, 2015).

Tomato carotenoids are isoprenoids synthesized via the plastidial methylerythritol 4-phosphate (MEP) pathway from pyruvate and glyceraldehyde 3-phosphate (GAP). The photosynthesis-fueled Calvin cycle feeds the MEP pathway for carotenoid biosynthesis in chloroplasts. In ripe tomato fruits, however, carotenoids are produced and accumulated in chromoplasts, photosynthetically inactive plastids differentiated from chloroplasts (Rodríguez-Concepción and Boronat, 2015). The origin of the carbon precursors and energy for carotenoid biosynthesis in chromoplasts is still unclear. Both pyruvate and GAP are produced in the cytosol as intermediates from glycolysis, whose flux tightly depends on respiratory metabolism during tomato fruit ripening (Tucker, 1993). Cytosolic glycolysis, together with the tricarboxylic acid (TCA) cycle in the mitochondrial matrix, and the electron transport chain (mETC) in the inner mitochondrial membrane are the three processes involved in respiration (Fernie et al., 2004). Glycolysis plays a pivotal role by breaking down carbohydrates to pyruvate, yielding ATP and NADH, thus serving as an energy source without photosynthesis. Pyruvate is then imported and metabolized at the mitochondrial matrix through the TCA cycle to generate

a vast amount of reducing power (as NADH and FADH), which can then be oxidized by the mETC and couple respiratory flux to ATP synthesis. However, plant mETC is characterized by containing alternative respiratory pathways which are not coupled to ATP production, and involve the internal and external type II NAD(P)H dehydrogenases, uncoupling proteins (UCPs), and alternative oxidases (AOXs) (Moller et al., 2021).

The AOX pathway has been proposed to play different roles in fruit ripening (Hewitt and Dhingra, 2020). Tomato AOX-silenced plants, with RNAi targeted to all AOX isoforms, displayed a delayed ripening that was attributed to the impairment of ethylene-induced climacteric respiration (Xu et al., 2012). However, the precise contribution of the different AOX isoforms during climacteric respiration as well as their role in fruit primary and carotenoid metabolism remains poorly understood. In tomato, there are four genes encoding the AOX, one AOX2 and three AOX1 types (*AOX1a*, *AOX1b*, and *AOX1c*). Among them, the *AOX1a* displays the highest levels of expression in all tissues, showing increasing levels as tomato fruits develop, mature and ripen (**Supplemental Figure C4-1**). The *AOX1b* gene shows its higher expression levels in roots and fruits at the mature green stage, while *AOX1c* is mainly expressed in roots (**Supplemental Figure C4-1**). Although the selective expression of AOX isoforms can influence its overall activity, a crucial layer of AOX regulation involves posttranslational modifications which mainly involve changes in redox status and allosteric interactions with organic acids (Selinski et al., 2018a; Florez-Sarasa et al., 2019). Our results from Chapter 3 strongly suggest that AOX is activated through posttranslational mechanisms during climacteric respiration. Notably, *in vitro* studies have shown that the activation of AOX by different organic acids from the TCA cycle, i.e. as those induced in parallel to *in vivo* AOX activity (Chapter 3), is isoform-specific (Selinski et al., 2018a), which could be relevant for the case of the isoforms expressed in tomato fruits (AOX1a and AOX1b).

Here we explored a possible link between respiratory metabolism and carotenoid biosynthesis through the AOX-mediated provision of carbon skeletons (pyruvate and GAP) for the MEP pathway in tomato fruit ripening using newly generated *aox1a* knockout mutants, and also treatments with the AOX inhibitor octyl-gallate (OGAL). Since AOX respiration is intrinsically less efficient in ATP production, we have also studied different plant growth and development parameters in the *aox1a* mutants.

Material and methods

Plant material and growth conditions

Three different lines of tomato (*Solanum lycopersicum* cv. MicroTom) plants were used in this work: one wild type (WT) and two CRISPR Cas9 mutant lines (*a1.1* and *a2.3*). Seeds from all plant lines were sown in small pots and grown under controlled growth chamber conditions: 16h/8h of light/dark photoperiod, 24°C/22ºC day/night temperature, and a light intensity of 350 µmol/m^2/s. After 14 days of growth, plants were transferred to 0.5 L pots containing a mixture of substrate:vermiculite:perlite (3:1:1). Pericarp samples were harvested at different maturity stages: Mature Green (MG), MG+1, MG+2, MG+3, MG+5, MG+7, MG+9, MG+11 and MG+13. These stages were accurately tracked by labelling flowers on anthesis day and counting the days post-anthesis. By using this method, we accurately determined the MG stage and subsequently calculated the number of days required to reach the Breaker (BR) stage. Additionally, the transitional periods between fruit stages were visually assessed starting from the BR stage, characterized by the onset of yellow coloring on the fruit.

For the experiments of tomato fruit injections, three to four WT fruits per treatment were injected on-vine at the MG stage, following a similar protocol as previously described for *Agrobacterium* infiltrations (Fernandez-Moreno et al., 2013). In a preliminary experiment, we adapted this method to Micro-Tom tomato fruits and tested the effect of 1mL injections of MG fruits with 700 µM norflurazon (NFZ, stock in DMSO), which is a specific inhibitor of carotenoid synthesis (**Supplemental Figure C4-2**). Our preliminary results suggest that our injections, as performed, can have effects on the whole fruit. Thereafter, three to four fruits per treatment were injected on-vine at the MG stage with the following solutions: two water solutions containing 1 mM and 2 mM Octyl-gallate (OGAL) prepared from stock solutions in DMSO; and a water with DMSO as a control solution. Four fruits were then collected for AOX capacity and carotenoid accumulation analysis at the following stages: MG+3, MG+4, MG+5, MG+7, MG+9, MG+11 and MG+13.

Constructs and tomato transformation

For the generation of the *aox1a* mutant plants, two single guide RNAs (sgRNA) sequences were designed to create short deletions using the CRISPRP 2.0 online tool (http://crispr.hzau.edu.cn/CRISPR2/; (Liu et al., 2017)) shown in **Figure C4-1A**. A pair of primers for each guide was designed, denaturalized, and assembled into a pENC1.1 (pENTRY) vector previously digested with BbsI restriction enzyme. The entry vectors contained the corresponding sgRNA expression cassette flanked by Bsu36I and MluI restriction sites, and by Gateway recombinant sites to allow both types of interchange with a pDE-Cas9 plasmid (pDESTINY) providing kanamycin resistance. *Agrobacterium tumefaciens* GV3101 strain was used to stably transform tomato MicroTom cotyledons with plasmids harboring two sgRNAs to disrupt *AOX1a* genomic sequences as described previously (Fernandez et al., 2009). Primers are detailed in **Supplemental Table C4-1**. *In vitro* regenerated T1 lines were identified based on kanamycin resistance (100μgml^{-1}) and confirmed by PCR genotyping analyses. Homozygous T2 lines lacking Cas9 were obtained after segregation. Two (*a1.1*) and (*a2.3*) stable T3 lines were used for further experiments with two different truncated AOX1a proteins (**Figure C4-1A**).

Plant growth and development characterization

Plants were monitored throughout their development and first flower buds; first anthesis flower; first fruit with a diameter of 0.3 cm; first fruit in breaker, orange, and red dates were determined. In addition, the number of flowers that are open or in a later stage was counted at 34 and 50 days after transfer (DAT) to bigger pots. Pictures of the front- and top view of the plants were taken at 15, 30, 50, 65, and 80 DAT. The height of the plant was measured at 20, 30, 50, and 90 DAT. Also, fruit weight, diameter, and volume were determined in red ripe (RR) fruits. Finally, the total number of fruits per plant and the total biomass of the shoot and roots were determined.

Respiration analysis

Respiration analyses were performed using a liquid-phase Clark-type oxygen electrode (Rank Brothers LTD Dual Digital Model 20). Fruits from each line were harvested at different stages: mature green (MG, considered at 35 days after anthesis), MG+1, MG+2,

MG+3, MG+5, MG+7, MG+9, MG+11 and MG+13. Fruits were cut into slices, weighed, and incubated for approx. 10 min in respiration buffer (30 mM MES, 0.2 mM $CaCl_2$ pH 6.2). Thereafter fruit slices were placed into the electrode cuvette containing respiration buffer and oxygen uptake rate was measured in complete darkness and at a constant temperature of 24 °C. After approx. 6 min (always above 50 % of the total oxygen consumed at the cuvette) potassium cyanide (KCN) was added to a final concentration of 1 mM to inhibit the COX pathway and measure the AOX capacity as KCN-resistant respiration for another 25-30 min. After the measurements, samples were dried in an oven for at least 48 h at 60 °C to determine dry weights (DW).

Gene expression analysis

Total RNA was isolated from tomato freeze-dried tissue using the Maxwell® RSC Plant RNA Kit with the Maxwell® RSC Instruments (Promega) following the manufacturer's instructions. RNA was quantified using a NanoDropTM 8000 spectrophotometer (Thermo Fischer Scientific) and integrity was assessed by agarose gel electrophoresis. The Prime-Script RT reagent Kit (Takara) was used to reverse transcribe 0.5 µg of extracted RNA into 20 µL of cDNA, which was subsequently diluted ten-fold and stored at -20 °C for further analysis. Relative mRNA abundance was evaluated via real-time quantitative Polymerase Chain Reaction (RT-qPCR) in a reaction volume of 10 µL containing 5 µL of the LightCycler 480 SYBR Green I Master Mix (Roche), 0.3 µM of each specific forward and reverse primer and 2 µL of cDNA. The RT-qPCR was carried out on a LightCycler 480 Real-Time PCR System (Roche). The primers used and the related information is detailed in **Supplemental Table C4-1**. Three independent biological replicates of each condition/genotype and at least two technical replicates of each biological replicate were performed. The *Solanum lycopersicum* ACT4 (Solyc04g011500) was used as a reference gene to correct for differences in the total amount of transcripts and the $2^{-\Delta\Delta Ct}$ method (Livak and Schmittgen, 2001) was used to calculate the fold-changes in gene expression. Finally, data were normalized to the mean value of WT tomato fruit at MG stage.

Primary metabolite profiling

Metabolite extractions were performed as described previously (Lisec et al., 2006) using approximately 10 mg of lyophilized and powdered tomato pericarp tissue. The GC-MS analyses were carried out with a 5977C GC/MSD (Agilent) following parameters described previously (Lisec et al., 2006) with modifications on the MS scan rate. Metabolites were identified manually by TagFinder software (Luedemann et al., 2012) using the reference library mass spectra and retention indices housed in the Golm Metabolome Database (http://gmd.mpimpgolm.mpg.de; (Kopka et al., 2005). The parameters used for the peak annotation of the 59 metabolites can be found in **Supplemental Table C4-2**, which follows previously reported recommendations (Fernie et al., 2011).

To quantify the GC-MS mass chromatogram results, the intensity of a selected unique ion shown in **Supplemental Table C4-2** was normalized to that of ribitol which was added to each sample as an internal standard, as well as to the lyophilized weight of the material used for metabolite extraction. Thereafter, data was normalized to the mean value of WT fruits at the MG stage (i.e., the value of all metabolites for MG-WT was set to 1). This normalization allowed the comparison of the relative metabolite levels among genotypes and ripening stages (**Supplemental Table C4-3 and C4-4, Figure C4-8, C4-9 and C4-10**).

Carotenoids and chlorophylls analysis

Carotenoids and chlorophylls were extracted in 2 mL Eppendorf tubes from 15 mg of freeze-dried pericarp tissues from tomato fruits, using 1 mL of hexane:acetone:methanol (2:1:1) as the extraction solvent and 15 µg of canthaxanthin (Sigma) as an internal control. After vortexing for 10 s and lysing the tissue with 4 mm glass beads for 1 min at 30 Hz in a TissueLyser II (QIAGEN), 100 µL of water was added. Then, 1 min of TissueLyser was carried out again and samples were centrifuged for 3 min at 3,000 rpm and 4 °C. Organic phase (upper) was kept in a new tube and the rest was re-extracted with 1 mL hexane:acetone:methanol (2:1:1, 1) min of TissueLyser and centrifuging for 5 min at maximum speed and 4 °C. The new organic phase was mixed with that previously extracted and evaporated for 1 h using a SpeedVac system (Eppendorf

Concentrator Plus). Extracted metabolites were then completely re-dissolved in 150 µL of acetone and filtered with 0.2 µm filters into amber-colored 2 mL glass vials. Separation and detection of isolated compounds was performed using an Agilent 1200 series HPLC system (Agilent Technologies) from 33 µL of prepared samples as described previously (Fraser et al., 2000). The HPLC equipment was coupled to a Photometric Diode Array (PDA) detector, allowing the detection of the full UV-visible absorption spectra of carotenoids and chlorophylls.

Statistical and data analyses

For the statistical analyses a one-way ANOVA with a level of significance of $P < 0.05$ was performed with Q19 SPSS statistical software package, version 25 (IBM Corp., 2016, Armonk, New York, NY, USA), and Duncan's posthoc test was used to determine statistically significant differences. Student's t-test with a level of significance of $P < 0.05$ were also applied in **Figure C4-4** and **C4-6** to compare the *aox1a* mutant lines against WT plants at each ripening stage. The heatmap was created using the R software (v4.2.3) (Rstudio Team, 2020 and the R Package "ComplexHeatmap" (Gu, 2022). Detailed R script for **Figure C4-8** can be found in **Supplemental Figure C4-3**.

Results and discussion

Generation of *AOX1a* knock-out lines

AOX1a-defective tomato mutants were generated by using the CRISPR-Cas9 system. Two single guides (sgRNA) were designed using CRISPR-P2.0 web-based software (Liu et al., 2017) to generate deletions in the *AOX1a* gene sequence (**Figure C4-1A**, **Supplemental Table C4-1** for primers details). Wild-type (WT) plants of the MicroTom cultivar were transformed and two independent, Cas9 negative, homozygous *aox1a* mutant lines were selected and named *a1.1* and *a2.3* (**Figure C4-1B**). The nucleotide deletions in both lines generated premature translation STOP codons (**Figure C4-1A**), thus resulting in mutant proteins that were shorter (62 aa for *a1.1*, and 48 aa for *a2.3*) than the WT (358 aa). Therefore, we considered these two alleles as knockout mutants and selected them for the rest of the experiments. Next, the AOX capacity was measured

in leaves from WT and mutant plants to confirm the effects of the *AOX1a* mutation (**Figure C4-1C**). Both mutant lines displayed very similar AOX capacity, which was strongly reduced as compared to WT plants (**Figure C4-1C**).

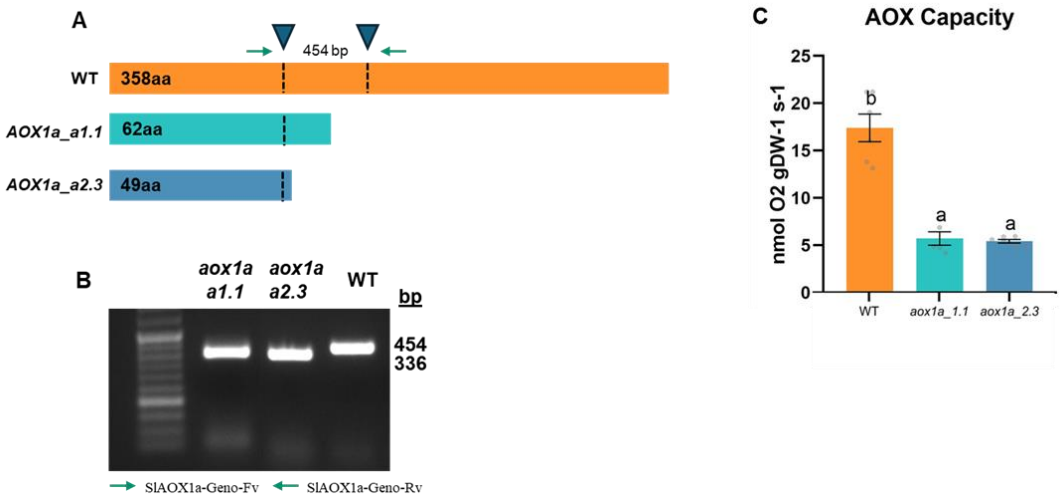


Figure C4-1. Tomato *aox1a* mutants**. A)** Scheme representing the wild-type *AOX1a* protein, and the mutant versions generated by CRISPR-Cas9. The region targeted by the designed sgRNAs is indicated with an arrowhead and a dotted line. Green arrows represent the position of primers for PCR-based genotyping (**Supplemental Figure C4-2** for primers details). **B)** Agarose gel showing the PCR genotyping results with AOX1a genotyping primers. **C)** AOX capacity in leaves of WT and *aox1a* mutant lines measured as KCN-resistant respiration.

Mutant *aox1a* lines show alterations in growth and development

Similar reductions on AOX capacity to those observed in our tomato CRISPR-edited lines have been reported in different studies using *aox1a* KO mutants in *Arabidopsis thaliana*, which showed no phenotypic difference with WT controls under non-stressed conditions (Del-Saz et al., 2022; Annex 3); Giraud et al., 2008; Vishwakarma et al., 2015; Watanabe et al., 2010; Zhang et al., 2016). To test whether tomato plant growth was impacted by the drop in AOX capacity, the two *aox1a* mutant lines (*a1.1* and *a2.3*) were germinated and grown together with WT plants in small pots, and subsequently transferred to larger containers after 14 days. Front and top-view images were taken at different days after transfer (DAT, 15, 30, 50, 65, and 80, **Supplemental Figure C4-4**). Visual differences between WT and edited lines were minor, consistent with that previously described for Arabidopsis *aox1a* KO mutants and *AOX1a* down-regulated

tobacco and tomato plants (reviewed in Vanlerberghe et al., 2020; Xu et al., 2012; Zhu et al., 2018). However, our two *aox1a* mutant lines showed reduced height at DAT30, 50 and 90 (**Figure C4-2A**). This observation aligns with findings from Zhu et al. (2018), who reported changes in lateral shoot growth in cv. MicroTom tomato plants following AOX downregulation. In addition, our *aox1a* mutants displayed lower biomass accumulation compared to WT plants, in both shoots and roots (**Figure C4-2B**), which was not previously reported in *aox1a* mutants or transgenic plants in Arabidopsis or tomato. Nonetheless, shoot to root ratios were maintained as in WT plants (**Figure C4-2C**).

Regarding transition events from vegetative to reproductive stages, both *aox1a* mutant lines displayed a delay on the first fruit appearance as compared to WT plants (**Figure C4-2D**, P=0.049 for *a1.1* and P=0.051 for *a2.3*). Despite the slight delay on fruit set in the mutant lines, their ability to reproduce and generate fruits was not impaired. Nevertheless, the total number of fruits produced per plant was significantly lower in both the *aox1a* mutant lines (**Figure C4-2E**), and their fruits displayed significantly lower weight, height, and diameter (**Figure C4-2F-H**). These findings contrast with those reported by Xu et al. (2012), who observed increased fruit weight and size in AOX-downregulated lines. It is important to note that our gene editing approach ensured a complete knock-out of the *AOX1a* gene, while previous studies used RNAi-based knock down approaches, which were not restricted to the *AOX1a* gene and were performed in another cultivar. Milder effects of the AOX down-regulated plants at the vegetative stages and fruit development, as compared to those observed here in our *aox1a*-KO mutants, might be the reason for this discrepancy. Overall, the observed consistent reductions in plant growth and productivity on both *aox1a* mutant lines highlights the AOX pathway is also fundamental under non-stress conditions, as previously suggested (Del-Saz et al., 2018). Studies on AOX-suppressed plants have overlooked the effects on growth, particularly under non-stress conditions, and are limited to very few plant species (reviewed in Vanlerberghe et al., 2020). Given the AOX pathway limited efficiency for ATP synthesis, a reduction on the activity of this pathway has been proposed as a strategy to enhance crop productivity (Garcia et al., 2023). However, our results are in line with another study reporting reductions in plant vegetative growth in AOX2 knockdown soybean plants under non-stress conditions (Chai et al., 2012). Future studies involving

non-model species with different AOX isoforms remain necessary for a better understanding of the intricate relationship between the AOX pathway and plant growth.

Inhibition of fruit AOX *in vivo* delays the onset of ripening

Recent studies have demonstrated that octyl-gallate (OGAL) is a very effective inhibitor of AOX enzymes *in vitro* (Xu et al., 2021). Moreover, our results from Chapter 3 clearly show that 1 mM OGAL effectively inhibits the AOX pathway *in vivo*. To confirm whether AOX inhibition had a negative effect on fruit ripening, as observed in tomato

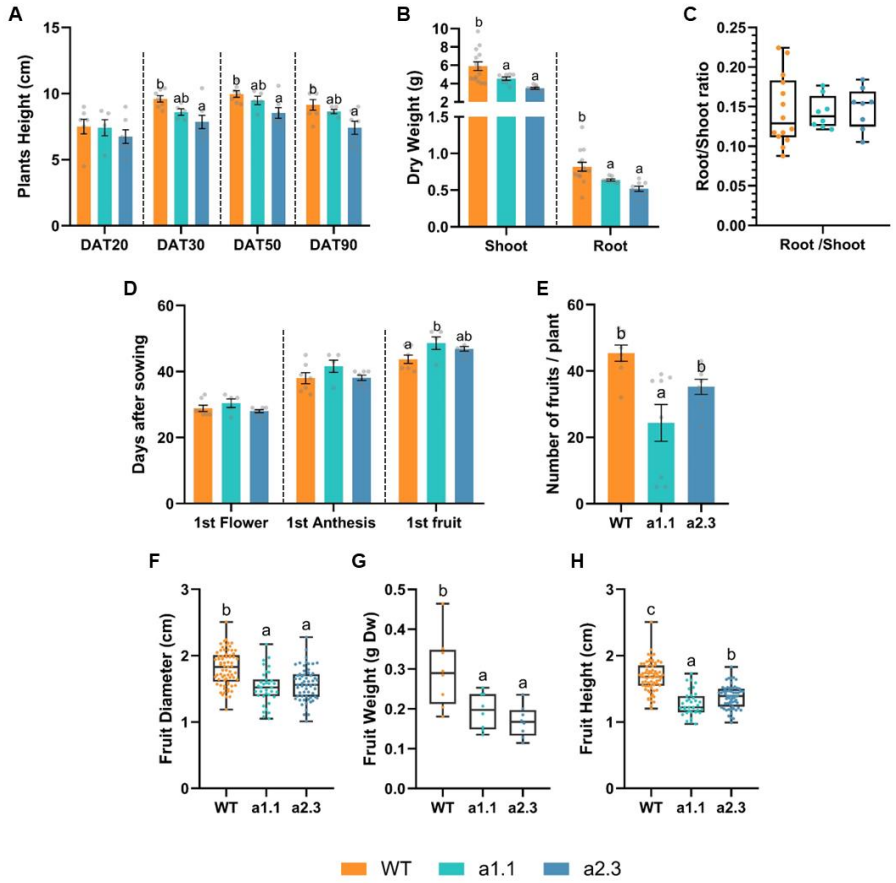


Figure C4-2. Wild-type and *aox1a* mutant lines (*a1.1* and *a2.3*) at different growth and developmental stages. (a) Plant height at 20, 30, 50, and 90 days after transfer to bigger pots. (b) Root and shoot biomass (dry weight) accumulated at the end of the experiment (approx. 100DAT). (c) Root-to-shoot ratio. (d) Number of days to reach different developmental stages. (e) Total number of fruits per plant. Fruit (f) diameter, (g) dry weight, and (h) height. Data corresponds to the mean ±SE of n=8 independent plants. Letters denotes statistical differences ($P<0.05$).

AOX-silenced plants (Xu et al., 2012), WT fruits were infiltrated *on-vine* at MG stage with 1 mM OGAL, 2 mM OGAL or water (with DMSO) as a negative control (**Figure C4-3A**). The AOX capacity (V_{alt}) increased at MG+4 stage in water-treated fruits, while this response was absent in OGAL-treated ones (**Figure C4-3B**). Notably, the breaker (BR) stage in water-treated fruits was visually observed on the following day, at MG+5 stage, while OGAL treated fruits remained greener (**Figure C4-3B**). Changes in V_{alt} from MG+4 onwards were not different in OGAL treated as compared to water-treated fruits (**Figure C4-3B**). With respect to carotenoid levels, OGAL treated fruits showed slightly lower carotenoid contents at MG+9 and MG+11, although differences were not statistically significant ($P<0.05$). It is likely that the observed consistent effects of OGAL treatments at early stages of ripening were diluted with time, whereas accumulated AOX-independent (side) effects of OGAL cannot be discarded. Indeed, AOX-independent effects of OGAL and SHAM were observed particularly during long-time incubation periods (Romero-Aguilar et al., 2020). In this context, AOX-interfering genetic approaches should avoid possible side effects of pharmacological treatments on other oxidases (Romero-Aguilar et al., 2020; Oh et al., 2022).

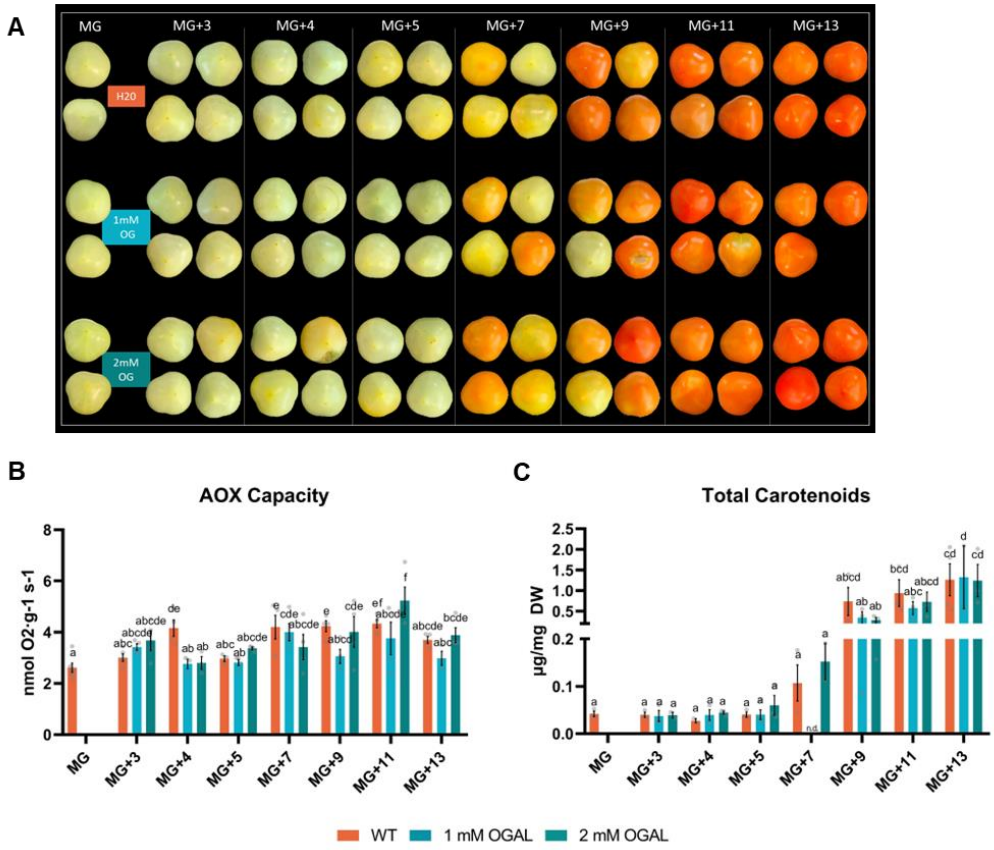


Figure C4-3. A) Representative images of WT tomato fruits infiltrated *on-vine* with H_2O, 1mM or 2mM of Octyl-gallate (OGAL) at MG stage. Tomato fruits were collected at different time points: MG, MG+3, MG+4, MG+5, MG+7, MG+9, MG+11, MG+13. **B)** AOX capacity ($V_{alt,}$ nmol $O_2 \cdot g^{-1} \cdot s^{-1}$) measured at different maturity stages on fruits treated with 1 mM and 2 mM OGAL on-vine was determined as KCN-resistant respiration. **C)** Total carotenoids levels were determined by HPLC analysis in pericarps from tomato fruits infiltrated *on-vine* with water (control) and 1 mM and 2 mM OGAL. Data are means ± SE of 3-4 replicates and letters denote significant differences ($P<0.05$).

Next, *on-vine* ripening was evaluated in the newly generated *aox1a* CRISPR-Cas9 mutants (**Figure C4-4**). Transition times from MG to BR and from BR to Orange (OR) stages were significantly longer in both *aox1a* mutants compared to WT fruits (**Figure C4-4B-C**). However, the subsequent transitions from OR to Red (R) and from R to Red Ripe (RR) stages were similar in all lines (**Figure C4-4D-E**). Previously reported results in tomato fruits from AOX knock-down plants were mainly focused on *off-vine*

(postharvest) ripening (Xu et al., 2012). Important differences in primary metabolite patterns were observed between *on-vine* and *off-vine* ripening in tomato fruits (Osorio et al., 2020), some of those involving AOX expression regulators (i.e. citrate (Cit)). In our current *on-vine* ripening study, the *aox1a* fruits displayed a delay on the onset of ripening, as can be visually observed at MG+5, MG+7 and MG+9 stages when compared to WT fruits (**Figure C4-4A**). Remarkably, these stages are on time frame with the BR stage, when the typical climacteric respiratory burst and ethylene peak production has been reported (Xu et al., 2012; Renato et al., 2014). In agreement with these effects around BR stage, the typical increase in transcript levels from ethylene-induced genes (*E8* and *PG2a*) was also delayed and/or attenuated in both *aox1a* mutants as compared to WT fruits (**Figure C4-5**). Therefore, our results strongly suggest that *AOX1a* is important for triggering the ethylene-induced responses in fruits during *on-vine* ripening. Moreover, these observations perfectly fit with the peak of AOX *in vivo* activity (v_{alt}) at BR stage found in **Chapter 3**.

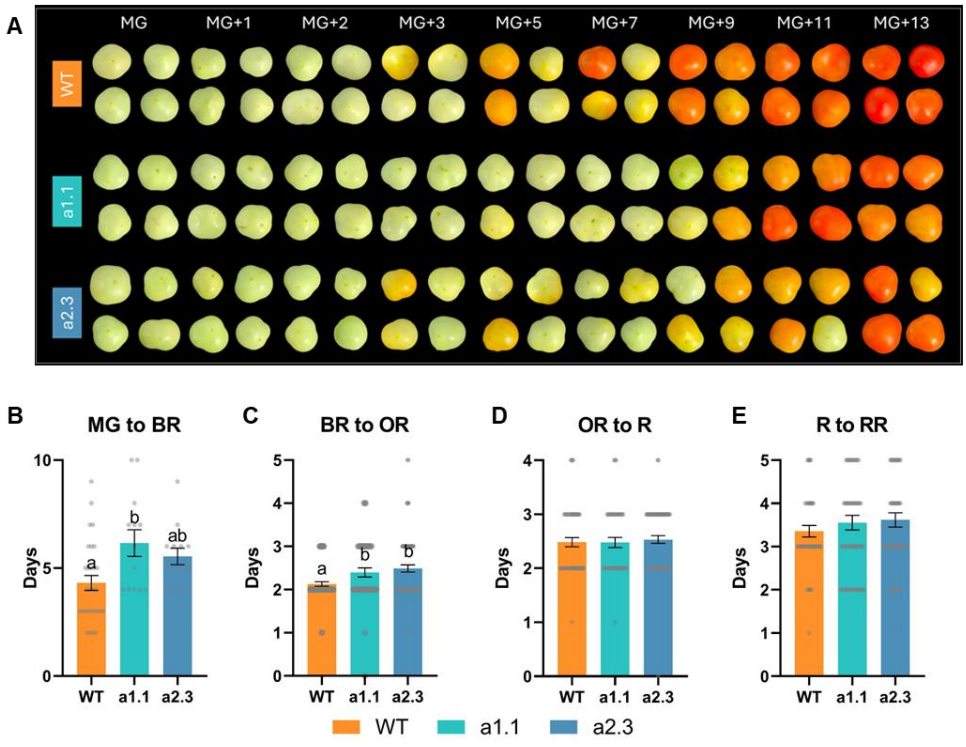


Figure C4-4. Visual phenotypes and ripening stages of tomato fruits from wild-type (WT) and *aox1a* mutant (a1.1 and a2.3) lines. **A)** Pictures of harvested tomato fruits at mature green (MG),

MG+1, MG+2, MG+3, MG+5, MG+7, MG+9, MG+11, MG+13 stages. **B)** Number of days from the MG to the breaker (BR) stage, **C)** BR to the orange stage (OR), **D)** OR to the red (R) stage, and R to the red ripe (RR) stage. Data corresponds to the mean ±SE of n=13-90 independent fruits. Letters denotes statistical differences ($P<0.05$).

Lack of AOX1a disturbs the peak of climacteric respiration and carotenoid accumulation

In parallel to the observed shifts on ethylene-induced responses in *aox1a* mutants, the rates of total respiration and AOX capacity were markedly altered in fruits of both *aox1a* mutant lines (**Figure C4-6**). Total respiration at MG stage was generally high in all three lines probably driven by the energy demand for growth still present at our experimental conditions (**Figure C4-6A**). Our intensive respiration measurements throughout several ripening stages revealed two respiratory peaks in WT fruits at the MG+2 (pre-BR) and MG+5 (BR) stages (**Figure C4-6A**). After MG+5 stage, respiration rates steadily declined until R stages. Similar patterns of O_2 consumption-based respiration rates were previously reported in tomato fruits (Xu et al., 2012; Renato et al., 2014), although only a single peak was reported. Both respiration peaks in fruits of the *a1.1* line were observed later (at MG+3 and MG+9 stages) compared to WT fruits, and only a single peak of respiration was evident (at the MG+5 stage) in fruits of the *a2.3* line. These shifts or absence of respiration peaks observed in fruits of both mutants (**Figure C4-6A**) are in line with, and could explain, the observed delay of the onset of ethylene-induced ripening (**Figure 4 and 5**). Whether altered patterns in total respiration were due to adjustments on AOX or COX *in vivo* activities can be determined by using the O_2 isotope discrimination technique, which allows for precise measurements of electron partitioning between the two respiratory pathways (Del-Saz et al., 2018). Our results from Chapter 3 show that the increase in tomato fruit total respiration at BR stage is entirely due to an increase in AOX *in vivo* activity (ν_{alt}). Therefore, altered respiratory responses in *aox1a* mutants are very likely due to changes in ν_{alt}. The ν_{alt} response to high light (Florez-Sarasa et al., 2011) and salinity stress (Del-Saz et al., 2022; Annex 3; Chapter 2) in Arabidopsis *aox1a* suppressed plants was shown to be curtailed by their limitation in AOX capacity (V_{alt}) (Del-Saz et al., 2022; Annex 3; Florez-Sarasa et al., 2011). In other words, when V_{alt} is genetically reduced and cannot respond to a given stimulus, an induction of ν_{alt} is not possible. To seek for this possible AOX limitations in our mutants, V_{alt} was

determined in all three lines at all fruit ripening stages (**Figure C4-6B**). V_{alt} was consistently and markedly lower in fruits of both *aox1a* mutants at all ripening stages as compared to WT fruits (**Figure C4-6B**). Therefore, it is very likely that reduced V_{alt} in the *aox1a* mutants was limiting their v_{alt} response at the time when WT fruits typically display their respiration peaks (MG+2 and MG+5). Indeed, V_{alt} in WT fruits steadily increased from MG+3 until MG+5 and remained high until the end of ripening, thus denoting no limitation was present in WT fruits to induce v_{alt}. Only the expression of *AOX1a* gene followed a similar pattern to V_{alt} in WT fruits (**Figure C4-6**), which suggests the main role of the AOX1a isoform to determine the V_{alt} in tomato fruits. Good correlations between AOX capacity and expression have been reported in several studies (reviewed in McDdonald et al., 2002 and in Del-Saz et al., 2018). However, total respiration patterns (i.e. increased until MG+5 and then decreased) are not correlated with V_{alt} (i.e. steadily increased until the end of ripening). Post-translational regulation mechanisms (i.e. allosteric activation of AOX by organic acids) are frequently reported to be the most important factors regulating respiration (Del-Saz et al., 2018). As discussed in **Chapter 3**, post-translational activation of the AOX is very likely regulating respiration in climacteric fruits. Despite their low rates, *a1.1* and *a2.3* lines displayed significant increases in V_{alt} at later stages than WT, MG+9 and MG+5, respectively (**Figure C4-6A**), which matched their highest respiration peaks (**Figure C4-6B**). Therefore, the shifted increments on total respiration and V_{alt} in *aox1a* mutants suggest for possible compensations from other respiratory components.

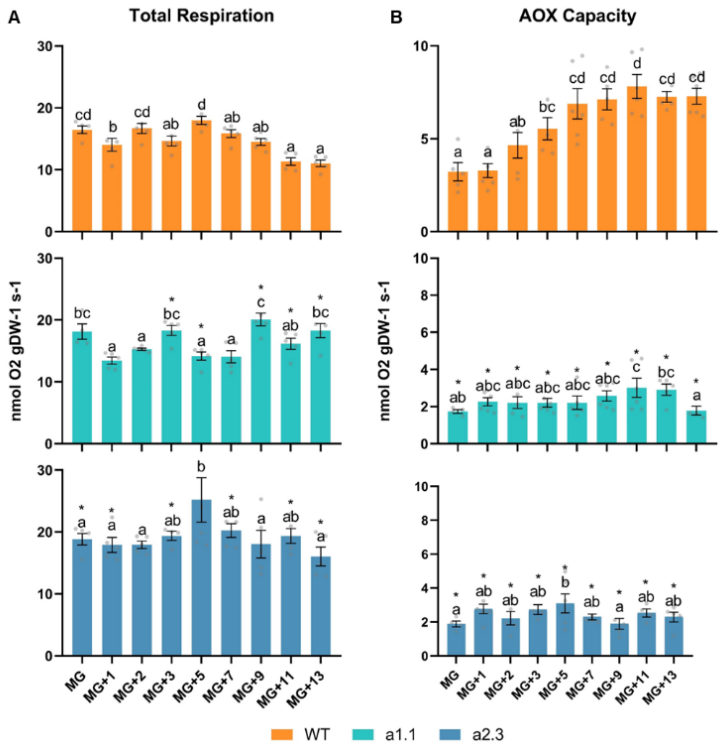


Figure C4-5. Respiration analyses on fruits of WT and *aox1a* mutant lines harvested at MG, MG+1, MG+2, MG+3, MG+5, MG+7, MG+9, MG+11, and MG+13 ripening stages. **A)** Total respiration and **B)** AOX capacity. Data correspond to the mean ±SE of n=4-6 independent fruits. Letters denote statistically significant differences (P<0.05) between ripening stages in each line, and asterisks denote statistically significant differences (P<0.05) to WT samples at ripening stage.

The levels of expression of *AOX2* and *UCP1* genes were generally lower in both *aox1a* mutants than in WT and followed the same attenuated pattern observed in ethylene-induced genes (**Figure C4-5**). However, this was not the case for *AOX1b* expression (**Figure C4-5**), which displayed disturbed patterns that, in some cases, were higher in *aox1a* mutants than in WT, i.e. at MG+9 and MG+5 in *a1.1* and *a2.3*, respectively, matching with their highest V_{alt} and total respiration rates (**Figure C4-6**). It is important to highlight that while transcript levels of *AOX1b* are much lower than of *AOX1a*, the encoded protein has Serine (Ser) substitutions at the highly conserved cysteine regulatory residues (Holtzapffel et al., 2003). The Ser-type AOX1b protein cannot be inactivated by Cys-oxidation which suggests that this isoform would be highly active, if expressed,

when succinate levels accumulate and regardless of the oxidative (stress) conditions. Therefore, changes on *AOX1b* expression together with its special regulatory features makes this isoform a crucial candidate for regulating climacteric respiration and possibly allowing *aox1a* mutants to re-establish climacteric respiration. Further experiments involving plants with altered AOX1b, AOX1a, and double mutants will be required to shed more light in the relative contribution of each AOX isoform to climacteric respiration *in vivo* and its organic acid regulation.

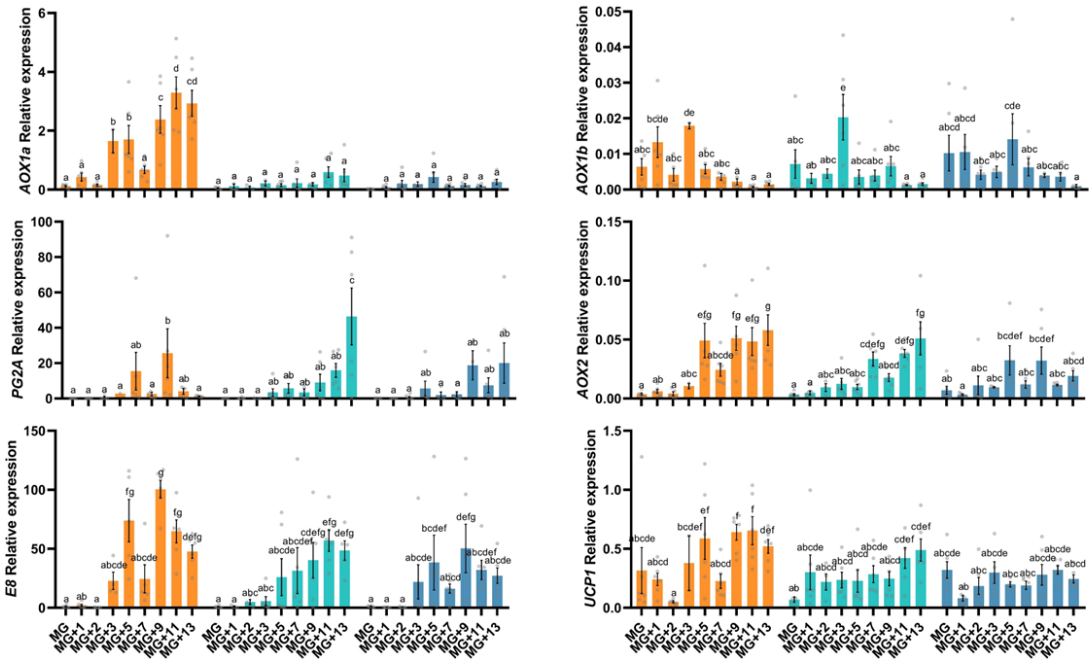


Figure C4-6. Relative transcript levels of AOX- and ripening-related genes in WT and *aox1a* mutant fruits at different ripening stages. AOX1a: alternative oxidase 1a; AOX1b: alternative oxidase 1b; AOX2: alternative oxidase 2; E8: 2-oxoglutarate-dependent dioxygenase ethylene-responsive protein; PG2a: polygalacturonase 2a; UCP1: uncoupling protein 1. Values are means ± SE of three to six replicates. Significant differences ($P < 0.05$) are indicated by different letters.

In line with disturbed respiratory responses, the reduction of chlorophyll levels occurred more rapidly in WT compared to the mutant lines, suggesting a difference in the degradation processes (**Figure C4-7**). Chlorophyll reduction is a reverse process to total carotenoid accumulation typically observed during fruit ripening (Trudel and Ozbun, 1970). In WT fruits, phytoene and lycopene were detected at MG+5 and MG+7 whereas

they were minor or undetectable in *aox1a* mutant fruits. Thereafter, phytoene and particularly lycopene were boosted at MG+9 in WT fruits while they remained very low in both mutants. These results could denote a limitation of carbon skeletons for the MEP pathway with the consequent restriction on the biosynthesis of carotenoids in *aox1a* mutants. In this context, altered patterns of pyruvate accumulation were observed between WT and *aox1a* mutants, the last displaying higher levels at MG+2 (P=0.14 for *a1.1* and P=0.20 for *a2.3*), and MG+13 (P=0.05 for *a1.1* and P=0.0008 for *a2.3*) (**Figure 10, Supplemental Tables C4-3 and C4-4**). On the other hand, altered patterns in glucose and glycerate levels could also be observed in both mutants (**Figure C4-10, Supplemental Table C4-4**). These metabolic differences together with altered respiration rates could denote restrictions on the glycolytic pathway in *aox1a* mutants. Nevertheless, phytoene and lycopene concentrations exhibited a significant increase in *aox1a* mutant lines at MG+11 and MG+13 stages, ultimately achieving WT carotenoid levels by MG+13 (**Figure C4-7**). As commented above, *aox1a* mutants also displayed increased respiration rates, albeit displaced to later developmental stages, probably due to an activation of the AOX1b. This compensation may have allowed the *aox1a* mutants to re-establish carotenoid accumulation (**Figure C4-7**) and reach similar color (**Figure C4-4A**) as WT fruits by the MG+13 stage.

Lack of AOX1a strongly restricts the synthesis of primary metabolite precursors for ethylene biosynthesis

Profiles of primary metabolites were characterized throughout ripening in fruits of both *aox1a* lines (*a1.1* and *a2.3*) alongside with WT (**Figure C4-8**). A clustered heatmap analysis clearly showed two groups containing samples at early and at late ripened stages (**Figure C4-8**). This cluster separation supports previous results showing that the most profound changes in primary metabolite profiles during tomato fruit ripening occur from BR stage onwards (Osorio et al., 2011). In this line, the pre-BR (non-ripened) cluster included samples at MG, MG+1, MG+2, and MG+3 stages from all three lines, except for the case of MG+3 stage in the *a2.3* line (**Figure C4-8**). The subclades in this non-ripened cluster did not group the different lines, thus generally denoting metabolic consequences of the *AOX1a* mutation at early ripening stages were still not profound. In contrast, the subclades of the ripening cluster (i.e. BR to RR) clearly separated WT from

both mutant lines. The first subclade contained both mutant lines at the MG+13 stage, highlighting that the effects of *AOX1a* mutation on primary metabolism were accumulated consistently at the end of the ripening process. The second clade was further divided into three distinct subclades, two of them containing only mutant samples (except for WT at MG+7) and a third one separating WT samples (except for *a1.1* at MG+11). Primary metabolites displaying statistically significant changes ($P<0.05$) that are consistent in both mutants compared to WT are shown separately for the ripened and non-ripened clusters at **Supplemental Figure C4-5 and C4-6**, respectively. In general, this clustering pattern is in line with the delay on the transition around BR stage (**Figure C4-4A**) and denote the important metabolic role of the AOX around BR stage, which greatly impact primary metabolism at later stages.

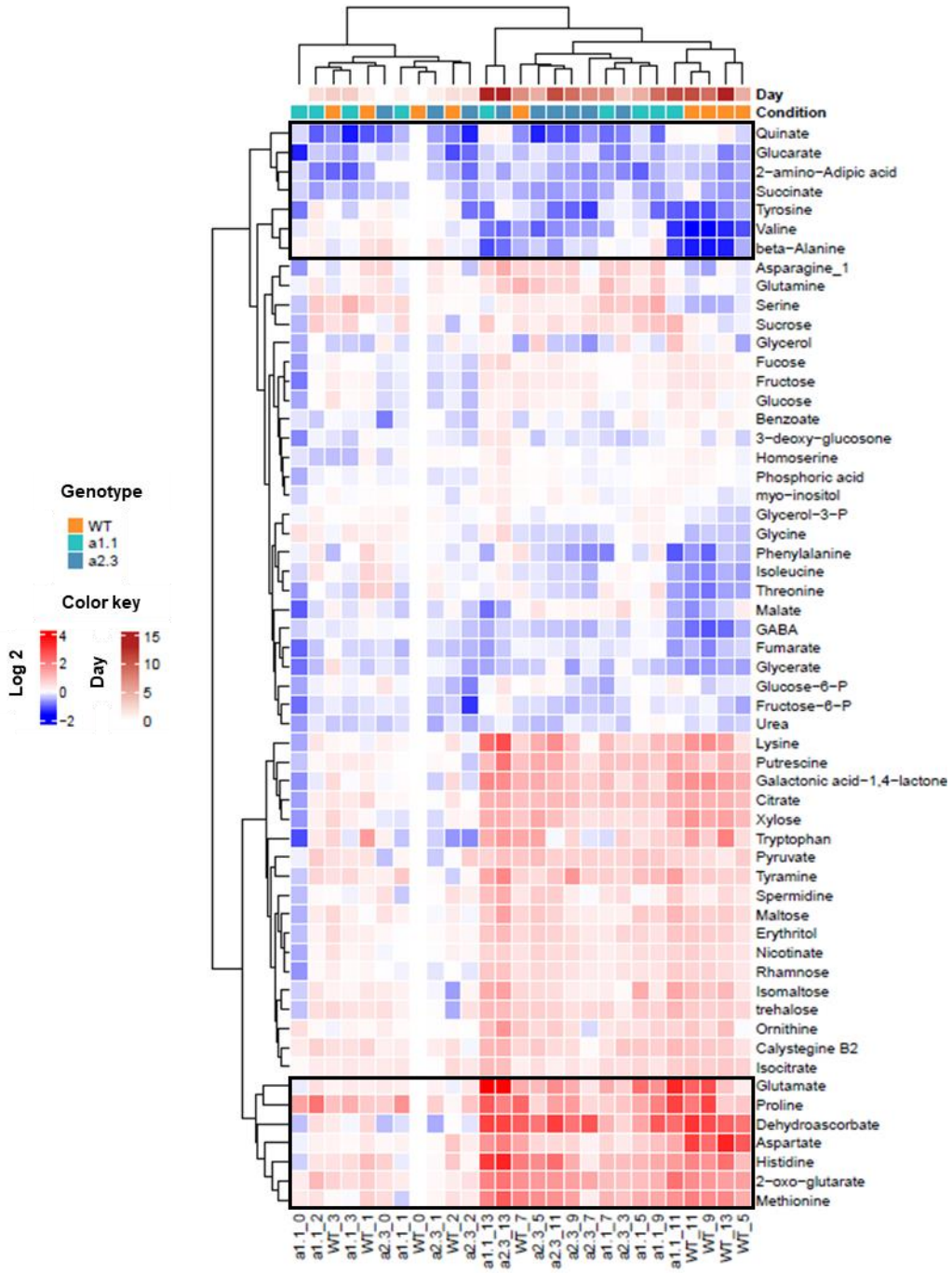


Figure C4-7. Heatmap showing relative changes in primary metabolism in WT and *aox1a* mutant fruits at different ripening stages. Relative metabolite levels were normalized to the mean level of WT at the MG stage, and log2-transformed (i.e., levels at WT-MG are set to 0). Red and blue colors represent log2 fold-increases and decreases in metabolite levels, respectively. Cluster

analysis was performed following by 'ComplexHeatmap' package in R. Dendrogram reveals correlation between tomato fruit lines, ripening stages and metabolites. Black boxes delimited the cases for which metabolites displayed the more pronounced responses (decreases at the top and increases at the bottom) during ripening. Values are means ± SE of 4–6 replicates. Statistical differences between MG and *aox1a* mutant lines ripening stages are shown in **Supplemental Table C4-3** and **C4-4**.

Regarding metabolite groups, two major clusters separated the metabolites displaying increases along ripening (at the bottom of **Figure C4-8**) from those displaying decreases and/or minor changes (**Figure C4-8**). The two clades at the top of the cluster grouped seven metabolites with the more pronounced decreases along fruit ripening including 2-amino-adipic acid, beta-alanine, glucarate, quinate, succinate, tyrosine, and valine (**Figure C4- C4-8**).

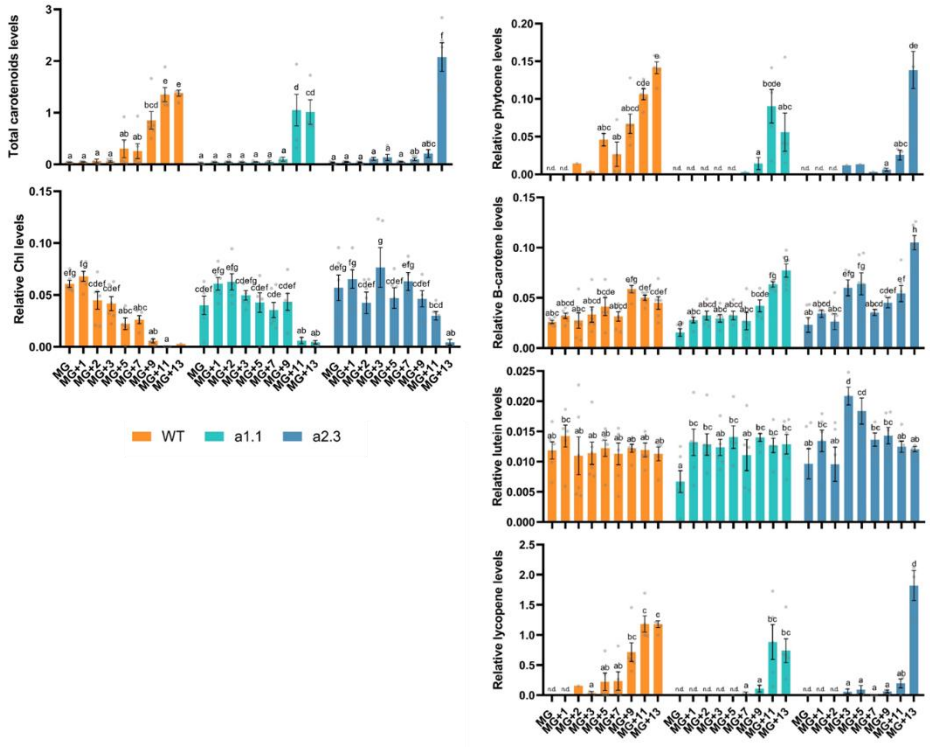


Figure C4-8. Levels of individual carotenoids (phytoene, lutein, lycopene, and b-carotene) as well as total carotenoids and chlorophylls in fruits of WT and *aox1a* mutant lines at different ripening stages. Values are means ± SE of four to six replicates and different letters represent statistically significant differences ($P < 0.05$).

Most of these metabolites were reported to decrease during fruit ripening in previous studies (Carrari and Fernie, 2006; Osorio et al., 2011; Quinet et al., 2019), and also in our results from **Chapter 3** (except succinate). However, we could not detect any consistent and statistically significant ($P<0.05$) difference when both mutants were compared to WT at each developmental stage, except for quinate (**Figure C4-9, Supplemental Table C4-3 and C4-4**). On the other hand, the cluster at the bottom of the heatmap included 2-oxo-glutarate (2-OG), aspartate (Asp), dehydroascorbate (DHasc), glutamate (Glu), histidine (His), methionine (Met), and proline (Pro) (**Figure C4-8**), which displayed the most pronounced increases at ripened stages (**Figure C4-9, Supplemental Figure C4-5**), also in concordance with our results in **Chapter 3** (except for Pro). Statistically significant ($P<0.05$) differences in the patterns of all these metabolites were observed between WT and *aox1a* mutant fruits at ripened stages with the exception of DHasc (**Figure C4-9, Supplemental Figure C4-5**). Strikingly, Glu was very highly accumulated (>50-fold change, **Supplemental Figure C4-5**) at the end of ripening in both mutant lines, while this behaviour was absent in WT fruits. Notably, both mutant lines also showed altered patterns in the levels of 2-OG, which is a key carbon precursor that links TCA cycle with amino acid metabolism through Glu metabolism (Forde and Lea, 2007). Given that respiration and V_{alt} was restricted in the *aox1a* mutants around BR stage (**Figure C4-5**), limited mitochondrial NADH reoxidation probably hindered the activity of TCA cycle dehydrogenases such as 2-OG dehydrogenase, thus promoting 2-OG accumulation. Under high NADH matrix concentrations, the conversion of 2-OG to Glu would be favored in the *aox1a* mutants either via Glu: 2-oxoglutarate aminotransferase (GOGAT) or glutamate dehydrogenase (GDH) (Forde and Lea, 2007), and against the generation of downstream TCA cycle intermediates. Pro can be synthesized from Glu (Kavi Kishor et al., 2022) and both metabolites displayed mirrored changes in WT (around MG+7 and MG+9) and in both mutants, although at later ripening stages (**Figure C4-9 and Supplemental Figure C4-5**). Together with Glu levels, the most remarkable difference observed was the almost complete abolished accumulation of Asp in both mutant lines, while this metabolite displayed >10-fold increase at MG+5 in WT fruits, i.e. around BR stage, and reached even higher levels at the end of ripening (**Figure C4-9 and Supplemental Figure C4-5**). Asp is required for the generation of Met which in turn is the main precursor for ethylene biosynthesis through the Yang cycle (Yang and Hoffman,

1984). Even if this cycle allows for the synthesis of ethylene precursors while recycling Met, 'de novo' synthesis of Met is also relevant for ethylene production during tomato fruit ripening (Katz et al., 2006). Noticeably, about 50-80% of the Met produced in plants is used for the synthesis of ethylene (Ranocha et al., 2001; Hesse et al., 2004). Therefore, a high carbon demand for Met synthesis should be expected during the climacteric peak of ethylene production, and presumably fulfilled from Asp and TCA cycle intermediates. Our results then denote that restricted AOX respiration in *aox1a* mutants greatly affected Asp accumulation at ripened stages, thus limiting Met synthesis which in turn could curtail ethylene synthesis.

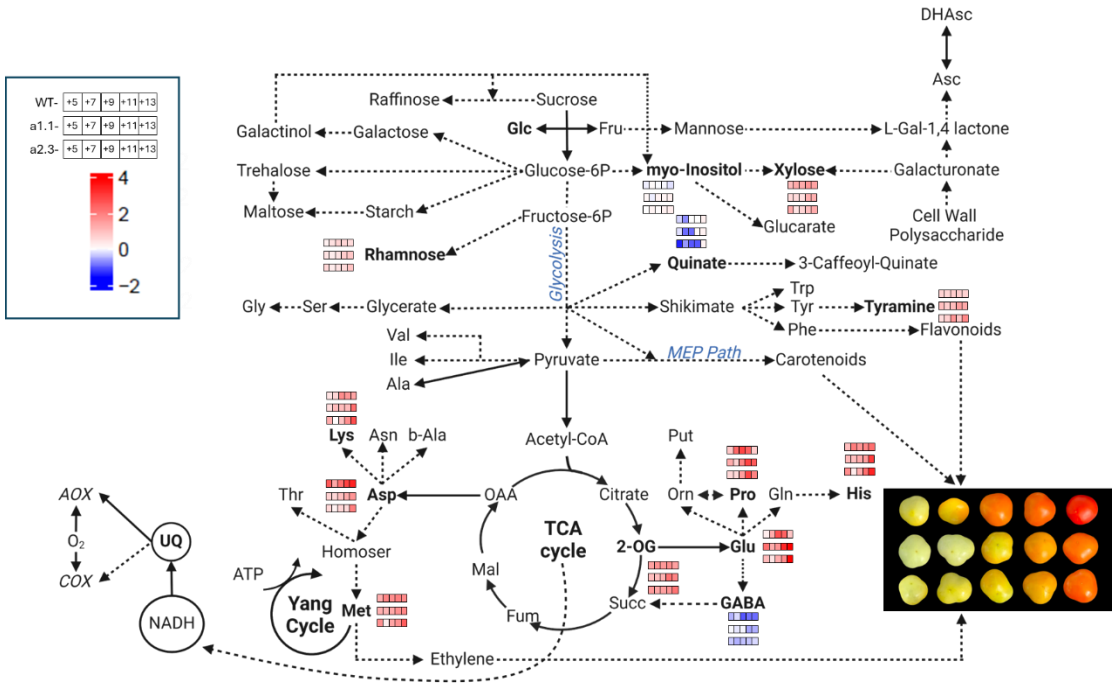


Figure C4-9. Metabolite profiles showing relative changes in primary metabolism in WT and *aox1a* mutant fruits during ripened stages (MG +5, MG+7, MG+9, MG+11 , and MG+13). The heatmap displays the relative levels of metabolites analyzed by GC-MS in WT and *aox1a* mutant fruits. Relative metabolite levels were normalized to the mean level of the WT at MG stage and log2-transformed (i.e., levels at WT at MG stages are set to 0). Red and blue colors represent log2 fold-increases and decreases in metabolite levels, respectively. Values are means ± SE of 4–6 replicates. Statistical differences between MG or MW and other ripening stages are shown in **Supplemental Tables C4-3**.

In addition to changes in ripening stages, important physiological, molecular and metabolic responses have been characterized at pre-BR stages in this study thanks to our intensive sampling during this timeframe (**Figure C4-5, C4-6, C4-10 and Supplemental Figure C4-6**). First increases of respiration (MG+2, **Figure C4-6**), V_{alt} (MG+3, **Figure 6**) and *AOX1a* expression (MG+3, **Figure C4-5**) in WT fruits were detected during pre-BR stages and preceded the notable increases in ethylene responsive genes (MG+3 and MG+5, **Figure C4-5**). Furthermore, all these responses were clearly attenuated and/or shifted in the *aox1a* mutants (**Figure C4-5** and **C4-6**). In line with this, significant metabolic differences were detected in WT fruits during pre-BR (non-ripened) stages **(**MG+1 and MG+2) as compared to MG, including increases in Cit, His, isoleucine (Ile), threonine (Thr), tryptophan (Trp), Met and Asp (**Figure C4-10** and **Supplemental Figure C4-6**), while these responses were absent (or delayed in the case of Cit) in fruits of both *aox1a* mutants. Overall, respiration, metabolic profiling and expression analysis in the *aox1a* mutans and WT lines reveal the key role of the AOX pathway for the synthesis of aspartate family amino acids including Asp and Met, which are required for ethylene synthesis during climacteric ripening (**Figure C4-9 and C4-10**).

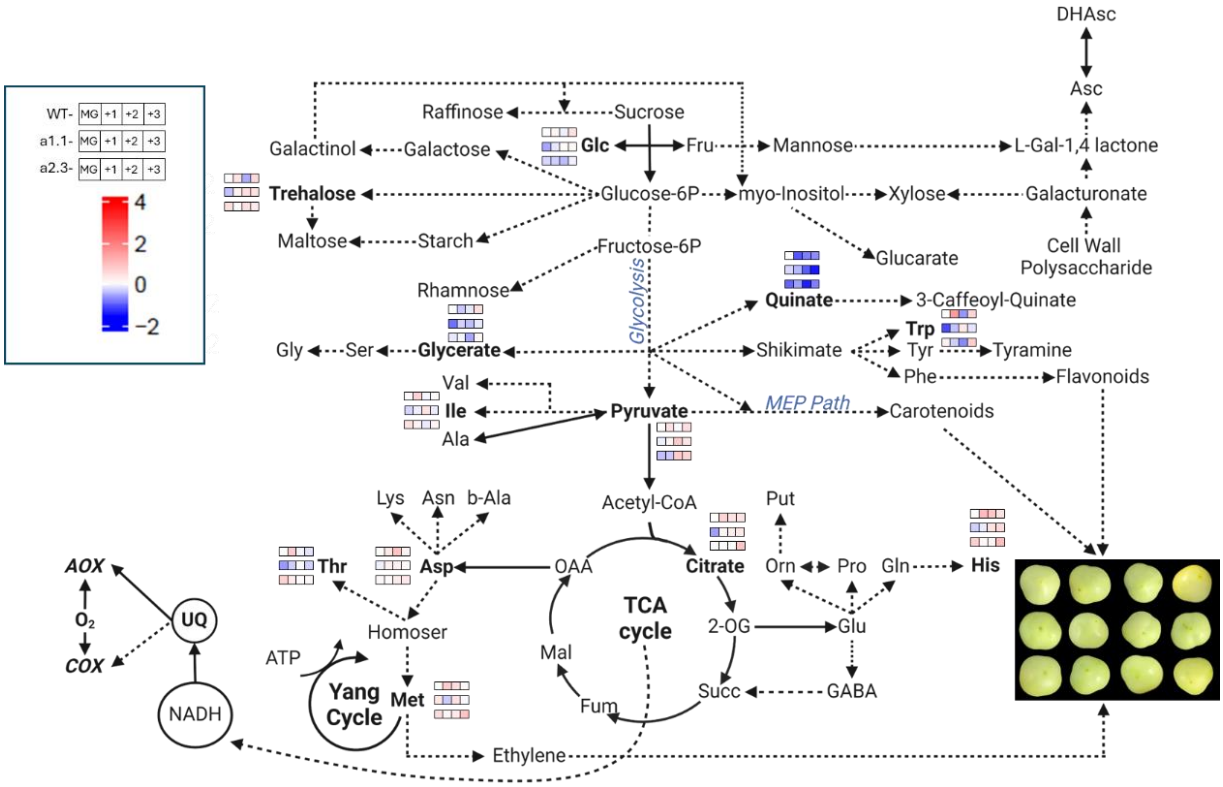


Figure C4-10. Metabolite profiling showing relative changes in primary metabolism in WT and *aox1a* mutant fruits during non-ripened stages (MG, MG+1, MG+2, and MG+3). The heatmap displays the relative levels of metabolites analyzed by GC-MS in WT and *aox1a* mutant fruits. Relative metabolite levels were normalized to the mean level of the WT at MG stage and log2-transformed (i.e., levels at WT at MG stages are set to 0). Red and blue colors represent log2 fold-increases and decreases in metabolite levels, respectively. Values are means ± SE of 4–6 replicates. Statistical differences between MG or MW and other ripening stages are shown in **Supplemental Tables S4**.

Conclusions

Moderate reductions in plant height, biomass, fruit size and number in *aox1a* mutants denotes an important role of AOX1a for normal growth and development in tomato plants under non-stress conditions. The absence of AOX1a leads to disrupted patterns in fruit respiration (delayed or absent respiration peaks), delayed ethylene-induced gene expression and carotenoid synthesis. While ripening-related metabolism (i.e. carotenoid synthesis) was mainly re-established by the end of ripening probably through altered

AOX1b expression, pronounced alterations of the TCA cycle and related metabolism remained. These metabolic restrictions strongly suggest the crucial role of the AOX pathway in supplying of aspartate and methionine for the climacteric biosynthesis of ethylene.

Supplemental data

Gene	AGI code	Primer	Sequence
RNA-guide 1	Solyc08g075540	RNA guide 1-Fw	ATTGCGTTACTTTTCAACTACAGT
		RNA guide 1-Rv	AAACACTGTAGTTGAAAAGTAACG
RNA-guide 2	Solyc08g075540	RNA guide 2-Fw	ATTGGGAGAAAGTGGCAGTAACGT
		RNA guide 2-Rv	AAACACGTTACTGCCACTTTCTCC
Cas9		Cas 9-Fw	TCCCTCATCAGATCCACCTC
		Cas 9-Rv	CTGAAACCTGAGCCTTCTGG
Sl-AOX1a	Solyc08g075540	SlAOX1a-Geno-Fv	CCTTCTTCCTCAAGTTTCTTTC
		SlAOX1a-Geno-Rv	CAGTACCATCTGGTTTAGTAG
Sl-AOX1a	Solyc08g075540	SlAOX1a-qPCR-Fv	TTGTTTTAGGCCATGGGAGACTT
		SlAOX1a-qPCR-Rv	CAGTGGGGAAACGAAGGATCT
Sl-AOX1b	Solyc08g075550	SlAOX1b-qPCR-Fw	CACACTGATGCAACCAACGC
		SlAOX1b-qPCR-Rv	TACGTCTCCCATGGCCTGAA
Sl-AOX1c	Solyc08g005550	SlAOX1c-qPCR-Fw	CCACTTTGCATCGGATATTTATTAC
		SlAOX1c-qPCR-Rv	AGTGATACCCAAGTGGAGCTG
Sl-AOX2	Solyc01g105220	SlAOX2-qPCR-Fw	CGCAAGTTCGAGCACAGT
		SlAOX2-qPCR-Rv	TAGGCAGTCTCCAGTAGTCAAT
Sl-PGA	Solyc10g080210	SlPGA-qPCR-Fw	ATGGCAATGGACAAGTATGGTG
		SlPGA-qPCR-Rv	TTAAGGCCGTTGGTGCATC
Sl-E8	Solyc09g089580	SlE8-qPCR-Fw	AGCTGCAAGTTGGAGAGACACG
		SlE8-qPCR-Rv	CCGCATGGAGTTGGAAATTC
Sl-ACT4	Solyc04g011500	Sl ACT4-qPCR-Fw	CCTTCCACATGCCATTCTCC
		Sl ACT4-qPCR-Rv	CCACGCTCGGTCAGGATCT

Supplemental Table C4-1. Primers used in this work

Supplemental Table C4-2. Parameters used for peak annotation of all detected metabolites.

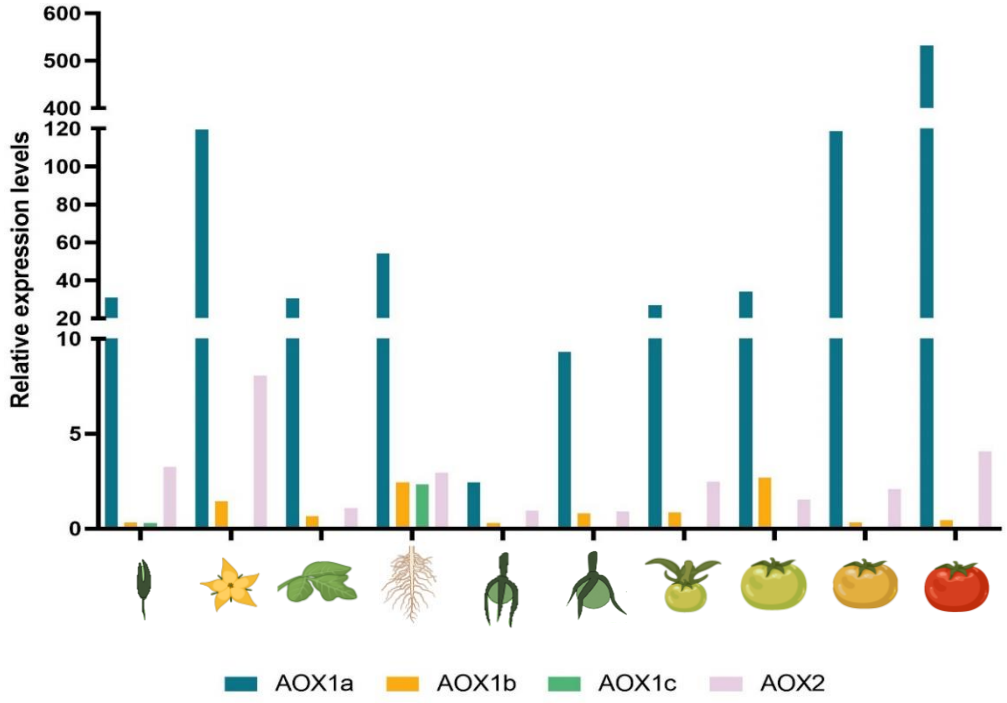
	A	B	C	D	E	F	G	H	I	J	K	L
1	**Experiment title:**			Metabolite profiles of tomato wild-type and ghost mutants during ripening		Peak/compound no.- number referenced back to the main text			Mass to charge ratio (m/z)			
2	**Organism/Plant species:**			Solanum lycopersicum		Ret . Time- Time expected, Tag Time Index and Time deviation			(S)- identification confirmed by a standard compound			
3	**Organ/tissue:**			Fruit Pericarp		Putative Name- putative identification of the metabolite/derivative			I, II, III- different isomers			
4	**Analytical tool:**			GC-TOF-MS		Corresponding metabolite name in literature			Identification level (A; B; C; D)- (A) standard or NMR; (B) MS/MS; (C) MS^E; (D) MS only			
5						Mol. Formula- molecular formula of the metabolite or its FA adduct;						
6	**Peak/Compound no.**	**Time Expected**	**Tag Time Index**	**Time Deviation**	**Putative metabolite name (Derivative)**	**Corresponding Metabolite in Literature**	**Metabolite Class**	**Mol formula**	**Mass to charge ratio (m/z)**	**Species detected before**	**Ref**	**Identification level (A-D)**
7	1	222650	222201	-0.23	M000071_A104002-101_METB_222650_TOF_Pyruvic acid (1MEOX) (1TMS)	Pyruvate	Acid (Oxo)	C3H4O3	174	Tomato, Arabidopsis, potato, grapevine and others		A
8	2	271580	272223	0.23	M000030_A122001-101_METB_271580_TOF_Valine, DL- (2TMS)	Valine	Acid (Amino)	C5H11NO2	144	Tomato, Arabidopsis, potato, grapevine and others		A
9	3	291783	292902	0.39	M000053_A129003-101_METB_291783_TOF_Glycerol (3TMS)	Glycerol	Polyol	C3H8O3	205	Tomato, Arabidopsis, potato, grapevine and others		A
10	4	319193	319548	0.10	M000017_A132002-101_METB_319193_TOF_Isoleucine, L- (2TMS)	Isoleucine	Acid (Amino)	C6H13NO2	158	Tomato, Arabidopsis, potato, grapevine and others		A
11	5	325180	325258	0.01	M000031_A133001-101_METB_325180_TOF_Glycine (3TMS)	Glycine	Acid (Amino)	C2H5NO2	174	Tomato, Arabidopsis, potato, grapevine and others		A
12	6	333520	334028	0.11	M000075_A129001-101_METB_333520_TOF_Phosphoric acid (3TMS)	Phosphorate	Phosphate	H3O4P	225	Tomato, Arabidopsis, potato, grapevine and others		A
13	7	338693	338884	0.04	M000029_A132003-101_METB_338693_TOF_Proline, L- (2TMS)	Proline	Amide	CH4N2O	142	Tomato, Arabidopsis, potato, grapevine and others		A
14	8	340357	341228	0.25	M000364_A127002-101_METB_340357_TOF_Urea (2TMS)	Urea	Amide	CH4N2O	171	Tomato, Arabidopsis, potato, grapevine and others		A
15	9	345050	345469	0.13	M000073_A135003-101_METB_345050_TOF_Glyceric acid, DL- (3TMS)	Glycerate	Acid	C3H6O4	189	Tomato, Arabidopsis, potato, grapevine and others		A
16	10	357523	358140	0.17	M000015_A138001-101_METB_357523_TOF_Serine, DL- (3TMS)	Serine	Acid (Amino)	C3H7NO3	204	Tomato, Arabidopsis, potato, grapevine and others		A
17	11	365427	365737	0.06	M000074_A134001-101_METB_365427_TOF_Succinic acid (2TMS)	Succinate	Acid	C4H6O4	247	Tomato, Arabidopsis, potato, grapevine and others		A
18	12	368365	368096	-0.08	M000016_A140001-101_METB_368365_TOF_Threonine, DL- (3TMS)	Threonine	Acid (Amino)	C4H9NO3	219	Tomato, Arabidopsis, potato, grapevine and others		A
19	13	371255	371604	0.07	M000067_A137001-101_METB_371255_TOF_Fumaric acid (2TMS)	Fumarate	Acid (Dicarboxylic)	C4H4O4	245	Tomato, Arabidopsis, potato, grapevine and others		A
20	14	386210	385657	-0.16	M000457_A133004-101_METB_386210_TOF_Nicotinic acid (1TMS)	Nicotinate	Acid	C6H5NO2	180	Tomato, Arabidopsis, potato, grapevine and others		A
21	15	394250	394463	0.06	M000027_A144001-101_METB_394250_TOF_Alanine, beta- (3TMS)	beta-Alanine	Acid (Amino)	C3H7NO2	174	Tomato, Arabidopsis, potato, grapevine and others		A
22	16	404940	405068	0.05	M000019_A146001-101_METB_404940_TOF_Homoserine, DL- (3TMS)	Homoserine	Acid (Amino)	C4H9NO3	128	Tomato, Arabidopsis, potato, grapevine and others		A
23	17	408455	409793	0.38	M000054_A150002-101_METB_408455_TOF_Erythritol (4TMS)	Erythritol	Polyol	C4H10O4	217	Tomato, Arabidopsis, potato, grapevine and others		A
24	18	440995	440995	-0.01	M000065_A149001-101_METB_440995_TOF_Malic acid, DL- (3TMS)	Malate	Acid	C4H6O5	233	Tomato, Arabidopsis, potato, grapevine and others		A
25	19	452200	453962	0.36	M000114_A133002-101_METB_342530_TOF_Butyric acid, 4-amino- (2TMS)	4-Aminobutanoic Acid	Acid (Amino)	C4H9NO2	246	Tomato, Arabidopsis, potato, grapevine and others		A
26	20	457283	457317	0.01	M000033_A152002-101_METB_457283_TOF_Aspartic acid, L- (3TMS)	Aspartate	Acid (Amino)	C4H7NO4	232	Tomato, Arabidopsis, potato, grapevine and others		A
27	21	474325	474607	0.04	M000018_A152001-101_METB_474325_TOF_Methionine, DL- (2TMS)	Methionine	Acid (Amino)	C5H11NO2S	176	Tomato, Arabidopsis, potato, grapevine and others		A
28	22	479050	480130	0.20	M000013_A168001-101_METB_550100_TOF_Asparagine, DL- (3TMS)	Asparagine	Acid (Amino)	C4H8N2O3	188	Tomato, Arabidopsis, potato, grapevine and others		A
29	23	490485	491216	0.13	M000028_A182002-101_METB-METB_570427_TOF_Ornithine, DL- (4TMS)	Ornithine	Acid (Amino)	C5H12N2O2	142	Tomato, Arabidopsis, potato, grapevine and others		A
30	24	492650	493027	0.06	M000032_A174008-101_MST_492650_TOF_Glutamine, DL- (4TMS)	Glutamine	Acid (Amino)	C5H10N2O3	227	Tomato, Arabidopsis, potato, grapevine and others		A
31	25	493370	494158	0.16	M000579_A166001-101_METB_498150_TOF_Xylose, D- (1MEOX) (4TMS)	Xylose	Sugar (Pentose, aldose	C5H10O5	217	Tomato, Arabidopsis, potato, grapevine and others		A
32	26	507780	508445	0.12	M000036_A163001-101_METB_507780_TOF_Glutamic acid, DL- (3TMS)	Glutamate	Acid (Amino)	C5H9NO4	246	Tomato, Arabidopsis, potato, grapevine and others		A
33	27	515530	516255	0.06	M000590_A172002-101_METB_515530_TOF_Rhamnose, DL- (1MEOX) (4TMS)	Rhamnose	Sugar (Hexose, deoxy)	C6H12O5	117	Tomato, Arabidopsis, potato, grapevine and others		A
34	28	517180	517600	0.09	M000186_A175002-101_METB-METB_517180_TOF_Putrescine (4TMS)	Putrescine	Amine	C4H12N2	174	Tomato, Arabidopsis, potato, grapevine and others		A
35	29	522140	522910	0.25	M000591_A173002-101_METB_522140_TOF_Fucose, DL- (1MEOX) (4TMS)	Fucose	Sugar (Hexose, deoxy)	C6H12O5	117	Tomato, Arabidopsis, potato, grapevine and others		A
36	30	523847	524080	-0.08	M000571_A158004-101_METB_523847_TOF_Glutaric acid, 2-oxo- (1MEOX) (2TMS)	2-oxo-Glutarate	Acid (Oxo)	C5H6O5	198	Tomato, Arabidopsis, potato, grapevine and others		A
37	31	531145	531005	-0.01	M000011_A164001-101_METB_531145_TOF_Phenylalanine, DL- (2TMS)	Phenylalanine	Acid (Amino)	C9H11NO2	192	Tomato, Arabidopsis, potato, grapevine and others		A
38	32	553540	553524	0.01	M000592_A172006-101_METB_553540_TOF_Adipic acid, 2-amino-, DL- (3TMS)	2-amino-Adipic acid	Acid (Amino)	C6H11NO4	217	Tomato, Arabidopsis, potato, grapevine and others		A
39	33	563070	563132	0.08	M000360_A181006-101_METB_563070_TOF_Calystegine B2 (1MEOX) (4TMS)	Calystegine B2	Calystegine	C7H13NO4	257	Tomato, Arabidopsis, potato, grapevine and others		A
40	34	574230	575683	0.22	M000328_A177002-101_METB_574230_TOF_Glycerol-3-phosphate, DL- (4TMS)	Glycerol-3-P	Alcohol (Phosphate)	C3H9O6P	299	Tomato, Arabidopsis, potato, grapevine and others		A
41	35	577930	578699	0.16	M000007_A185001-101_METB_577930_TOF_Quinic acid, D(-)- (5TMS)	Quinate	Acid	C7H12O6	255	Tomato, Arabidopsis, potato, grapevine and others		A
42	36	579380	579200	-0.06	M000606_A187002-101_METB_579380_TOF_Fructose, D- (1MEOX) (5TMS)	Fructose	Sugar (Hexose, ketose)	C6H12O6	307	Tomato, Arabidopsis, potato, grapevine and others		A
43	37	592883	592510	-0.08	M000069_A182004-101_METB-METB_592883_TOF_Citric acid (4TMS)	Citrate	Acid	C6H8O7	273	Tomato, Arabidopsis, potato, grapevine and others		A
44	38	597845	596608	-0.06	M000608_A182003-101_METB-METB_597845_TOF_Isocitric acid, DL- (4TMS)	Isocitrate	Acid	C6H8O7	465	Tomato, Arabidopsis, potato, grapevine and others		A
45	39	598880	598392	-0.11	M000040_A189002-101_METB_590400_TOF_Glucose, D- (1MEOX) (5TMS)	Glucose	Sugar (Hexose, aldose)	C6H12O6	160	Tomato, Arabidopsis, potato, grapevine and others		A
46	40	618870	619772	0.18	M000639_A189003-101_METB_618870_TOF_Galactonic acid-1,4-lactone, D(-)- (4TMS)	D-Galactono-1,4-lactone	Acid (Hexonic)	C6H12O7	217	Tomato, Arabidopsis, potato, grapevine and others		A
47	41	618870	618271	-0.08	M000014_A192003-101_METB_615467_TOF_Lysine, L- (4TMS)	Lysine	Acid (Amino)	C6H14N2O2	305	Tomato, Arabidopsis, potato, grapevine and others		A
48	42	624990	626455	0.20	M000639_A189003-101_METB_618870_TOF_Galactonic acid-1,4-lactone, D(-)- (4TMS)	Galactonic acid-1,4-lactone	Acid (polyhydroxy)	C6H10O6	173	Tomato, Arabidopsis, potato, grapevine and others		A
49	43	632880	629990	-0.35	M000082_A185002-101_METB-METB_624990_TOF_Dehydroascorbic acid dimer (TMS)	Dehydroascorbate	Acid	C6H6O6	316	Tomato, Arabidopsis, potato, grapevine and others		A
50	44	638360	639396	0.15	M000081_A191004-101_METB_638360_TOF_Tyramine (3TMS)	Tyramine	Amine	C8H11NO	174	Tomato, Arabidopsis, potato, grapevine and others		A
51	45	653910	653335	-0.08	M000060_A209002-101_METB_653910_TOF_Inositol, myo- (6TMS)	myo-Inositol	Polyol	C6H12O6	191	Tomato, Arabidopsis, potato, grapevine and others		A
52	46	658337	658604	0.04	M000035_A194002-101_METB_658337_TOF_Tyrosine, DL- (3TMS)	Tyrosine	Acid (Amino)	C9H11NO3	218	Tomato, Arabidopsis, potato, grapevine and others		A
53	47	660120	660791	0.10	M000643_A194009-101_METB_660120_TOF_Glucaric acid-1,4-lactone (4TMS)	Glucarate	Acid (polyhydroxy)	C6H8O7	217	Tomato, Arabidopsis, potato, grapevine and others		A
54	48	679450	678244	-0.16	M000039_A192006-101_METB_679450_TOF_Histidine, L- (3TMS)	Histidine	Acid (Amino)	C6H9N3O2	154	Tomato, Arabidopsis, potato, grapevine and others		A
55	49	723585	723727	-0.01	M000106_A220002-101_METB_728760_TOF_Spermidine (4TMS)	Spermidine	Amine	C7H19N3	144	Tomato, Arabidopsis, potato, grapevine and others		A
56	50	767060	767200	0.06	M000510_A232002-101_METB_767060_TOF_Fructose-6-phosphate (1MEOX) (6TMS)	Fructose-6-phosphate	Sugar (Phosphate)	C6H13O9P	315	Tomato, Arabidopsis, potato, grapevine and others		A
57	51	776505	773544	-0.38	M000513_A235002-101_METB-METB_781350_TOF_Glucose-6-phosphate (1MEOX) (6TMS)	Glucose-6-phosphate	Sugar (Phosphate)	C6H13O9P	87	Tomato, Arabidopsis, potato, grapevine and others		A
58	52	790560	790205	-0.06	M000012_A223001-101_METB_790560_TOF_Tryptophan, L- (3TMS)	Tryptophan	Acid (Amino)	C11H12N2O2	202	Tomato, Arabidopsis, potato, grapevine and others		A
59	53	840783	840783	0.00	M000044_A264001-101_METB_840783_TOF_Sucrose, D- (8TMS)	Sucrose	Sugar (Disaccharide)	C12H22O11	361	Tomato, Arabidopsis, potato, grapevine and others		A
60	54	876240	877488	0.17	M000671_A274002-101_METB_876240_TOF_Trehalose, alpha,alpha'-, D- (8TMS)	Trehalose	Sugar (Disaccharide)	C12H22O11	191	Tomato, Arabidopsis, potato, grapevine and others		A
61	55	887905	890392	0.29	M000048_A274001-101_METB_870355_TOF_Maltose, D- (1MEOX) (8TMS)	Maltose	Sugar (Disaccharide)	C12H22O11	361	Tomato, Arabidopsis, potato, grapevine and others		A
62	56	909948	909559	-0.10	M000107_A287001-101_METB_909948_TOF_Isomaltose (1MEOX) (8TMS)	Isomaltose	Sugar (Disaccharide)	C12H22O11	204	Tomato, Arabidopsis, potato, grapevine and others		A

Metabolite	WT_MG+5	WT_MG+7	WT_MG+9	WT_MG+11	WT_MG+13	a1_MG+5	a1_MG+7	a1_MG+9	a1_MG+11	a1_MG+13	a2_MG+5	a2_MG+7	a2_MG+9	a2_MG+11	a2_MG+13
2-amino-Adipic acid	0.62 ± 0.1ab	0.82 ± 0.14b	0.64 ± 0.07ab	0.69 ± 0.09ab	0.48 ± 0.1ab	0.37 ± 0.04a	0.58 ± 0.12ab	0.63 ± 0.11ab	0.78 ± 0.18b	0.8 ± 0.12b	0.77 ± 0.06b	0.49 ± 0.09ab	0.56 ± 0.13ab	0.6 ± 0.11ab	0.57 ± 0.04ab
2-oxo-glutarate	4.3 ± 1.1abc	5.52 ± 1.02abc	4.9 ± 0.18abc	5.81 ± 0.62bc	4.32 ± 0.37abc	2.73 ± 0.53a	2.71 ± 0.4a	3.24 ± 0.45ab	8.89 ± 0.68d	6.76 ± 0.73cd	4.75 ± 0.87abc	3.83 ± 0.74ab	4.26 ± 0.79ab	4.97 ± 1.17abc	8.6 ± 1.52d
3-deoxy-glucosone	0.75 ± 0.17ab	1.13 ± 0.12ab	0.79 ± 0.12a	1.14 ± 0.19ab	1.16 ± 0.11ab	0.79 ± 0.12a	0.78 ± 0.1a	0.9 ± 0.2a	1.04 ± 0.39ab	1.47 ± 0.15b	0.7 ± 0.13a	0.88 ± 0.16a	0.82 ± 0.2a	0.93 ± 0.13a	1.52 ± 0.26b
Asparagine	0.85 ± 0.23a	1.93 ± 0.59ab	0.55 ± 0.24a	0.67 ± 0.12a	1.14 ± 0.33a	1.44 ± 0.39a	2.08 ± 0.78ab	2.37 ± 0.74ab	0.96 ± 0.2a	2.1 ± 0.78ab	1.87 ± 0.6ab	0.96 ± 0.42a	2.1 ± 0.82ab	1.86 ± 0.36ab	3.53 ± 0.94b
Aspartate	13.11 ± 3.83bc	3.92 ± 1.31a	9.44 ± 1.91bc	19.36 ± 6.39b	30.29 ± 9.33c	2.04 ± 0.57a	1.86 ± 0.35a	2.59 ± 0.71a	3.67 ± 0.65a	5.15 ± 1.18a	1.83 ± 0.63a	1.21 ± 0.15a	1.88 ± 0.17a	1.76 ± 0.44a	7.32 ± 1.2a
Benzoate	1.09 ± 0.16a	0.75 ± 0.12a	1.08 ± 0.15a	1.33 ± 0.3a	1.31 ± 0.42a	1.39 ± 0.39a	0.76 ± 0.11a	0.94 ± 0.23a	1.17 ± 0.23a	1.16 ± 0.2a	1.1 ± 0.12a	0.81 ± 0.12a	1.11 ± 0.29a	0.91 ± 0.07a	1.4 ± 0.49a
beta-Alanine	0.6 ± 0.23abc	0.62 ± 0.17abc	0.22 ± 0.02a	0.23 ± 0.03a	0.24 ± 0.07a	0.97 ± 0.16bc	1.06 ± 0.22cd	1.57 ± 0.47d	0.3 ± 0.02a	0.32 ± 0.04a	0.74 ± 0.16abc	0.77 ± 0.23abc	0.83 ± 0.27abc	0.53 ± 0.11abc	0.4 ± 0.09ab
Citrate	2.74 ± 0.45abcd	2.55 ± 0.39abcd	3.3 ± 0.15bcd	3.6 ± 0.09d	3.34 ± 0.2cd	2.24 ± 0.33ab	2.39 ± 0.4abc	2.53 ± 0.36abcd	3.27 ± 0.03bcd	3.29 ± 0.36bcd	2.73 ± 0.22abcd	2.02 ± 0.31a	2.75 ± 0.39abcd	2.96 ± 0.51abcd	3.54 ± 0.27d
Dehydroascorbate	8.32 ± 5.1abc	11.84 ± 2.53abcd	16.12 ± 5.14abcd	23.32 ± 2.79d	11.48 ± 5.49abcd	3.97 ± 1.04ab	3.32 ± 1.65a	12.98 ± 1.2abcd	9.43 ± 3.42abcd	18.66 ± 2cd	8.37 ± 2.56abc	14.02 ± 3.77abcd	8.47 ± 1.44abc	19.99 ± 2.91cd	18.26 ± 2.1bcd
Erythritol	1.52 ± 0.25ab	1.77 ± 0.13abcd	2.08 ± 0.13bcd	2.31 ± 0.12cde	2.02 ± 0.17abcd	1.89 ± 0.3abcd	1.42 ± 0.22a	1.54 ± 0.22ab	2.39 ± 0.34de	2.37 ± 0.23de	2.15 ± 0.22bcd	1.39 ± 0.12a	1.67 ± 0.15abcd	1.96 ± 0.13abcd	2.85 ± 0.19e
Fructose	1.22 ± 0.19ab	1.45 ± 0.07ab	1.5 ± 0.09b	1.49 ± 0.07b	1.27 ± 0.06ab	1.23 ± 0.09ab	1.04 ± 0.17a	1.18 ± 0.14ab	1.48 ± 0.07b	1.47 ± 0.1b	1.35 ± 0.11ab	1.32 ± 0.13ab	1.3 ± 0.18ab	1.36 ± 0.1ab	1.3 ± 0.2ab
Fructose-6-P	0.57 ± 0.15a	0.81 ± 0.24a	0.94 ± 0.38a	0.84 ± 0.23a	0.71 ± 0.18a	1.03 ± 0.31a	0.68 ± 0.2a	0.84 ± 0.27a	0.9 ± 0.16a	1 ± 0.22a	0.82 ± 0.21a	0.74 ± 0.25a	0.65 ± 0.19a	0.71 ± 0.2a	1.21 ± 0.29a
Fucose	1.06 ± 0.14ab	1.16 ± 0.08abc	1.34 ± 0.04abcd	1.48 ± 0.05cd	1.32 ± 0.14abcd	1.24 ± 0.13abc	1 ± 0.4a	1.16 ± 0.06abc	1.44 ± 0.06bcd	1.66 ± 0.18de	1.24 ± 0.08abc	1.07 ± 0.04ab	1.18 ± 0.07abc	1.39 ± 0.09abcd	1.88 ± 0.29e
Fumarate	0.78 ± 0.17abc	0.94 ± 0.11bc	0.46 ± 0.08a	0.67 ± 0.05abc	0.7 ± 0.08abc	0.96 ± 0.21bc	0.82 ± 0.18abc	0.99 ± 0.17c	0.53 ± 0.04ab	0.54 ± 0.09abc	0.91 ± 0.18c	0.93 ± 0.09bc	0.81 ± 0.11abc	0.89 ± 0.18bc	0.72 ± 0.06abc
GABA	0.62 ± 0.16abc	0.8 ± 0.1bc	0.34 ± 0.06a	0.41 ± 0.07a	0.4 ± 0.12a	0.96 ± 0.09c	0.85 ± 0.06bc	0.93 ± 0.12bc	0.57 ± 0.12ab	0.61 ± 0.15abc	0.71 ± 0.09abc	0.61 ± 0.11abc	0.68 ± 0.15abc	0.7 ± 0.13abc	0.78 ± 0.08bc
Galactonic acid-1,4-lactone	3.45 ± 1.34abc	3.17 ± 0.95abc	5.57 ± 1.52abc	5.51 ± 1.25abc	4.39 ± 1.38bc	2.32 ± 1.04abc	2.82 ± 1.12abc	1.75 ± 0.27a	4.3 ± 1.38abcd	6.09 ± 1.91c	3.58 ± 0.77abc	2.02 ± 0.42ab	2.48 ± 0.48abc	2.9 ± 0.37abc	5.78 ± 1.55bc
Glucarate	0.57 ± 0.15a	0.66 ± 0.1a	0.81 ± 0.17a	0.76 ± 0.11a	0.45 ± 0.08a	0.8 ± 0.21a	0.47 ± 0.1a	0.59 ± 0.09a	0.76 ± 0.1a	0.74 ± 0.13a	0.86 ± 0.13a	0.9 ± 0.24a	0.68 ± 0.24a	0.7 ± 0.1a	0.87 ± 0.24a
Glucose	1.17 ± 0.21a	1.42 ± 0.16a	1.41 ± 0.05a	1.22 ± 0.09a	0.95 ± 0.1a	1.14 ± 0.07a	0.96 ± 0.19a	0.98 ± 0.12a	1.46 ± 0.25a	1.28 ± 0.17a	1.23 ± 0.11a	1.38 ± 0.17a	1.17 ± 0.23a	1.18 ± 0.11a	1.22 ± 0.37a
Glucose-6-P	0.89 ± 0.3a	1 ± 0.33a	0.72 ± 0.22a	1.02 ± 0.4a	0.86 ± 0.29a	1.01 ± 0.33a	0.57 ± 0.24a	0.95 ± 0.37a	1.3 ± 0.45a	0.95 ± 0.21a	1.21 ± 0.42a	0.68 ± 0.2a	0.83 ± 0.29a	1.07 ± 0.4a	1.51 ± 0.54a
Glutamate	1.32 ± 0.2a	3.53 ± 1.49a	15.51 ± 9.12a	11.36 ± 6.55a	2.46 ± 0.51a	9.12 ± 6.75a	3.61 ± 2.08a	5.34 ± 2.56a	28.82 ± 7ab	52.6 ± 13.24b	2.86 ± 1.6a	1.48 ± 0.37a	3.49 ± 0.97a	5.79 ± 2.88a	50.75 ± 21.55b
Glutamine	0.87 ± 0.2a	3.21 ± 1.5b	1.03 ± 0.22a	0.83 ± 0.2a	0.97 ± 0.21a	1.28 ± 0.28ab	2.88 ± 0.73ab	2.3 ± 0.72ab	1.21 ± 0.37ab	1.47 ± 0.35ab	2.35 ± 0.9ab	1.17 ± 0.33ab	1.95 ± 0.43ab	1.87 ± 0.37ab	2.19 ± 0.43ab
Glycerate	0.56 ± 0.11a	0.71 ± 0.1ab	0.53 ± 0.05a	0.51 ± 0.04a	0.59 ± 0.08ab	0.8 ± 0.11ab	0.62 ± 0.06ab	0.69 ± 0.1ab	0.63 ± 0.07ab	0.57 ± 0.04a	0.74 ± 0.06ab	0.89 ± 0.16bc	0.54 ± 0.05a	1.11 ± 0.1c	0.69 ± 0.08ab
Glycerol	0.57 ± 0.14a	0.58 ± 0.06a	0.92 ± 0.19ab	1.27 ± 0.26ab	1.15 ± 0.45ab	0.94 ± 0.38ab	0.8 ± 0.32a	0.8 ± 0.28a	2.48 ± 0.63c	1.22 ± 0.15ab	2.05 ± 0.83bc	0.51 ± 0.1a	0.69 ± 0.25a	0.71 ± 0.15a	1.17 ± 0.17ab
Glycerol-3-P	0.73 ± 0.08a	0.98 ± 0.1abc	0.86 ± 0.11a	0.9 ± 0.08ab	0.75 ± 0.06a	1.25 ± 0.12cd	1.01 ± 0.07abc	1.2 ± 0.08bcd	0.99 ± 0.09abc	1.02 ± 0.08abc	0.87 ± 0.07ab	0.99 ± 0.12abc	0.97 ± 0.09abc	1.04 ± 0.07abc	1.43 ± 0.2d
Glycine	0.69 ± 0.14a	0.82 ± 0.18a	0.73 ± 0.15a	0.65 ± 0.04a	0.72 ± 0.11a	1.18 ± 0.15a	0.86 ± 0.22a	1.17 ± 0.24a	1.05 ± 0.17a	1.27 ± 0.37ab	0.76 ± 0.16a	0.71 ± 0.21a	0.74 ± 0.13a	0.79 ± 0.19a	1.82 ± 0.34b
Histidine	2.79 ± 0.86a	7.42 ± 3.45a	5.14 ± 1.99a	6.46 ± 1.44a	9.16 ± 2.65a	2.99 ± 0.88a	2.72 ± 0.5a	3.66 ± 0.65a	4.52 ± 0.61a	21.12 ± 4.61b	5.86 ± 1.05a	1.36 ± 0.33a	3.53 ± 0.57a	9.51 ± 2.64a	30.09 ± 6.2c
Homoserine	0.93 ± 0.09a	1.04 ± 0.12ab	1.19 ± 0.18ab	1.24 ± 0.22ab	1.03 ± 0.14ab	1.04 ± 0.22ab	1.05 ± 0.06ab	1.07 ± 0.08ab	1.11 ± 0.07ab	1.2 ± 0.2ab	1.01 ± 0.11ab	0.91 ± 0.09a	1 ± 0.08a	1.1 ± 0.14ab	1.51 ± 0.24b
Isocitrate	2.03 ± 0.08abcd	1.25 ± 0.14a	2.1 ± 0.01bcd	2.26 ± 0.04cd	2.29 ± 0.01cd	1.87 ± 0.28abc	1.79 ± 0.23abc	1.48 ± 0.24abc	2.11 ± 0.06bcd	2.84 ± 0.17d	1.66 ± 0.02abc	1.28 ± 0.21a	1.56 ± 0.07abc	1.09 ± 0.25abcd	2.74 ± 0.07d
Isoleucine	0.54 ± 0.13a	0.83 ± 0.31ab	0.48 ± 0.1a	0.51 ± 0.06a	0.62 ± 0.13a	1.03 ± 0.18ab	0.98 ± 0.28ab	0.97 ± 0.24ab	0.6 ± 0.11a	0.98 ± 0.35ab	0.87 ± 0.15ab	0.61 ± 0.15a	0.78 ± 0.2ab	0.76 ± 0.1ab	1.31 ± 0.19b
Isomaltose	1.49 ± 0.15a	1.84 ± 0.25ab	2.3 ± 0.32abc	2.78 ± 0.26abc	2.93 ± 0.31abc	3.62 ± 1.12bc	1.32 ± 0.35a	1.38 ± 0.16a	3.81 ± 0.63c	3.53 ± 0.95bc	1.79 ± 0.26ab	1.23 ± 0.19a	1.3 ± 0.07a	1.67 ± 0.1ab	4.2 ± 0.38c
Lysine	1.53 ± 0.23ab	1.91 ± 0.52ab	5.79 ± 1.93bc	5.07 ± 1.22abc	4.1 ± 1.24ab	1.71 ± 0.13ab	2.82 ± 0.42ab	2.83 ± 0.59ab	2.86 ± 0.67ab	9.24 ± 2.08c	3.54 ± 0.52ab	1.07 ± 0.18a	2.5 ± 0.32ab	5.78 ± 1.19bc	15.76 ± 1.96d
Malate	1.29 ± 0.4cd	1.07 ± 0.21abcd	0.6 ± 0.18abc	0.49 ± 0.05ab	0.76 ± 0.26abc	1.05 ± 0.18abcd	1.21 ± 0.22cd	1.29 ± 0.2cd	0.61 ± 0.14abc	0.41 ± 0.07a	1.51 ± 0.19d	1.16 ± 0.12bcd	1.18 ± 0.17bcd	1.09 ± 0.25abcd	0.59 ± 0.26abc
Maltose	1.7 ± 0.23a	1.88 ± 0.34a	2.01 ± 0.31a	2.18 ± 0.4ab	2.2 ± 0.46ab	2.27 ± 0.37ab	1.24 ± 0.38a	1.93 ± 0.62a	3.04 ± 0.67ab	2.2 ± 0.23ab	2.33 ± 0.43ab	1.33 ± 0.23a	1.39 ± 0.26a	1.95 ± 0.42a	4.22 ± 1.48b
Methionine	3.56 ± 0.74ab	6.61 ± 2.36b	5.72 ± 0.76b	7.18 ± 0.85b	6.24 ± 1.42b	3.44 ± 1.33ab	3.15 ± 0.71ab	3.77 ± 0.59ab	5.37 ± 0.55ab	6.5 ± 0.97b	5.62 ± 1.46b	1.3 ± 0.09a	4.1 ± 0.64ab	5.51 ± 1.72ab	12.62 ± 1.74c
myo-Inositol	0.91 ± 0.1abc	1.06 ± 0.14abcde	0.98 ± 0.1abcd	0.96 ± 0.08abcd	0.88 ± 0.07a	1.11 ± 0.06abcde	0.9 ± 0.11ab	1.19 ± 0.12bcde	1.15 ± 0.06bcde	1.24 ± 0.11de	1.01 ± 0.1abcde	1.17 ± 0.1bcde	1.05 ± 0.07abcde	1.23 ± 0.06cde	1.31 ± 0.12e
Nicotinate	1.51 ± 0.25abc	1.54 ± 0.03abc	1.77 ± 0.12abc	2.09 ± 0.11c	1.67 ± 0.16abc	1.7 ± 0.16abc	1.28 ± 0.16a	1.64 ± 0.22abc	1.91 ± 0.18bcd	1.91 ± 0.14bc	1.97 ± 0.39bc	1.46 ± 0.11ab	1.75 ± 0.13abc	1.71 ± 0.15abc	2.04 ± 0.19bc
Ornithine	0.98 ± 0.12ab	2.4 ± 0.69bc	1.74 ± 0.4abc	2.41 ± 0.37abc	2.67 ± 0.51c	1.57 ± 0.23abc	1.47 ± 0.24abc	1.96 ± 0.39abc	1.89 ± 0.17abc	2.68 ± 0.43abc	1.77 ± 0.25abc	0.79 ± 0.11a	1.59 ± 0.18abc	2.19 ± 0.46abc	5.1 ± 0.64c
Phenylalanine	0.65 ± 0.22ab	1.59 ± 0.86ab	0.38 ± 0.05b	0.53 ± 0.1a	0.71 ± 0.13ab	0.8 ± 0.12ab	0.45 ± 0.04ab	1.37 ± 0.74ab	0.35 ± 0.04a	0.6 ± 0.17ab	0.79 ± 0.2ab	0.48 ± 0.16ab	0.57 ± 0.12ab	0.7 ± 0.18ab	1.17 ± 0.31ab
Phosphoric acid	0.96 ± 0.08ab	1.06 ± 0.05abc	1.09 ± 0.07abc	1.2 ± 0.05cd	1.03 ± 0.03abc	1.02 ± 0.07abc	0.96 ± 0.04ab	1.03 ± 0.07abc	1.16 ± 0.04bcd	1.2 ± 0.1cd	1.04 ± 0.06abc	0.91 ± 0.04a	0.98 ± 0.04ab	1.11 ± 0.07abcd	1.29 ± 0.05d
Proline	2.34 ± 0.63a	10.55 ± 4.05abc	18.04 ± 7.68c	7.86 ± 3.07ab	2.13 ± 0.55a	3.64 ± 0.62a	1.99 ± 0.28a	6.92 ± 1.28ab	18.78 ± 3.1c	13.04 ± 1.48cd	1.84 ± 0.36a	1.79 ± 0.29a	4.53 ± 0.95ab	4.27 ± 1.06ab	6.96 ± 1.52ab
Putrescine	2.36 ± 0.83ab	2.57 ± 0.63ab	1.95 ± 0.12ab	3.03 ± 0.26ab	3.34 ± 0.5ab	2.43 ± 0.45ab	2.62 ± 0.5ab	2.23 ± 0.38ab	3.75 ± 0.45b	2.77 ± 0.42ab	3.58 ± 0.36ab	1.56 ± 0.2a	2.3 ± 0.19ab	3.54 ± 0.29ab	8.48 ± 2.24c
Pyruvate	2.17 ± 0.22ab	2.33 ± 0.32ab	1.66 ± 0.21ab	1.86 ± 0.26ab	1.41 ± 0.08a	2.38 ± 0.46ab	1.87 ± 0.15ab	2.3 ± 0.31ab	1.93 ± 0.35ab	1.94 ± 0.23ab	2.78 ± 0.3b	2.02 ± 0.18ab	2.02 ± 0.38ab	2.01 ± 0.33ab	2.62 ± 0.81ab
Quinate	0.76 ± 0.02bcd	0.49 ± 0.08abc	1 ± 0.05def	1.03 ± 0def	1.26 ± 0.05f	0.82 ± 0.02cde	0.4 ± 0.01abc	0.39 ± 0.04abc	1.07 ± 0.13def	1.22 ± 0.16ef	0.24 ± 0a	0.52 ± 0.11abc	0.35 ± 0.03ab	0.34 ± 0.02ab	1.2 ± 0.11ef
Rhamnose	1.44 ± 0.23ab	1.57 ± 0.14abc	1.96 ± 0.14bcde	1.9 ± 0.07abcd	1.73 ± 0.14abc	1.5 ± 0.23ab	1.32 ± 0.18a	1.51 ± 0.14ab	2.15 ± 0.17cde	2.35 ± 0.33de	1.86 ± 0.19abcd	1.35 ± 0.11ab	1.55 ± 0.11abc	1.73 ± 0.16abc	2.48 ± 0.24e
Serine	0.87 ± 0.25a	1.39 ± 0.45ab	0.6 ± 0.1a	0.64 ± 0.13a	0.62 ± 0.12a	2.51 ± 0.4b	2.49 ± 0.5b	3.66 ± 1.01c	0.86 ± 0.06a	0.89 ± 0.11a	1.36 ± 0.13ab	1.64 ± 0.37ab	1.26 ± 0.4a	1.27 ± 0.32a	1.25 ± 0.17a
Spermidine	1.44 ± 0.11ab	1.44 ± 0.28ab	1.23 ± 0.08ab	1.42 ± 0.22ab	1.79 ± 0.13ab	0.98 ± 0.15a	1.51 ± 0.16ab	1.19 ± 0.19a	2.26 ± 0.33abc	2.64 ± 0.92bc	2.24 ± 0.29abc	0.97 ± 0.15a	1.31 ± 0.2ab	2.14 ± 0.34ab	3.54 ± 0.43c
Succinicate	0.55 ± 0.11a	0.61 ± 0.06ab	0.59 ± 0.02ab	1.14 ± 0.4b	0.52 ± 0.06a	0.63 ± 0.09ab	0.61 ± 0.12ab	0.53 ± 0.04a	0.74 ± 0.09ab	0.74 ± 0.08ab	0.53 ± 0.06a	0.53 ± 0.06a	0.53 ± 0.05ab	0.53 ± 0.1a	0.86 ± 0.17ab
Sucrose	0.92 ± 0.14ab	1.53 ± 0.28abcd	1.11 ± 0.3abc	1.23 ± 0.42abc	0.81 ± 0.18a	2.09 ± 0.2bcde	1.66 ± 0.36abcd	2.46 ± 0.83de	3.04 ± 0.56e	2.23 ± 0.51cde	1.27 ± 0.15abcd	1.71 ± 0.17abcd	1.29 ± 0.22abcd	1.65 ± 0.22abcd	1.08 ± 0.15abc
Threonine	0.57 ± 0.14ab	1.27 ± 0.53abc	0.41 ± 0.08a	0.49 ± 0.06ab	0.55 ± 0.1ab	0.97 ± 0.15abc	1.34 ± 0.51bc	1.65 ± 0.49c	0.56 ± 0.07ab	0.89 ± 0.22abc	0.86 ± 0.15abc	0.66 ± 0.18ab	0.76 ± 0.2ab	0.78 ± 0.08ab	1.2 ± 0.16abc
Trehalose	1.89 ± 0.14ab	2.06 ± 0.2abc	2.05 ± 0.13abc	2.21 ± 0.16abcd	2.19 ± 0.12abcd	2.14 ± 0.33abcd	1.93 ± 0.05ab	1.92 ± 0.25ab	3.04 ± 0.1d	2.87 ± 0.46cd	2.11 ± 0.16abc	1.76 ± 0.28a	1.61 ± 0.11a	1.92 ± 0.11ab	2.82 ± 0.34bcd
Tryptophan	1.69 ± 0.36abcd	3.7 ± 1.35abcd	2.15 ± 0.47abcd	4.08 ± 0.71cd	7.07 ± 0.81e	1.54 ± 0.52abc	0.8 ± 0.15a	1.97 ± 0.69abcd	2.23 ± 0.44abcd	3.45 ± 1.64abcd	4.02 ± 0.68bcd	0.85 ± 0.24ab	1.9 ± 0.41abcd	0.96 ± 0.1abc	4.79 ± 0.67de
Tyramine	2 ± 0.44a	1.93 ± 0.49a	2.18 ± 0.37a	2.14 ± 0.42a	2 ± 0.29a	2.69 ± 0.45ab	2.13 ± 0.44a	2.81 ± 0.41ab	4.42 ± 0.47c	3.78 ± 0.35bc	1.69 ± 0.32a	2.04 ± 0.31a	5.18 ± 0.9cd	2.41 ± 0.18ab	6.28 ± 0.97d
Tyrosine	0.61 ± 0.24ab	0.87 ± 0.46ab	0.32 ± 0.05a	0.32 ± 0.03a	0.46 ± 0.09ab	0.79 ± 0.12ab	0.88 ± 0.27ab	0.39 ± 0.08ab	0.36 ± 0.04ab	0.41 ± 0.07ab	0.69 ± 0.21ab	0.29 ± 0.02a	0.38 ± 0.09ab	0.41 ± 0.04ab	1.08 ± 0.21b
Urea	0.76 ± 0.11a	0.74 ± 0.1a	0.9 ± 0.07a	0.8 ± 0.09a	0.7 ± 0.11a	1 ± 0.08a	0.85 ± 0.22a	1.1 ± 0.1a	1 ± 0.11a	0.78 ± 0.15a	0.66 ± 0.07a	0.92 ± 0.08a	0.66 ± 0.11a	0.93 ± 0.05a	0.38 ± 0.09ab
Valine	0.33 ± 0.12ab	0.57 ± 0.37ab	0.2 ± 0.04a	0.2 ± 0.02a	0.25 ± 0.05a	0.87 ± 0.2bc	0.6 ± 0.09ab	1.17 ± 0.39c	0.27 ± 0.04ab	0.45 ± 0.15ab	0.37 ± 0.05ab	0.55 ± 0.16ab	0.56 ± 0.2ab	0.49 ± 0.18ab	0.38 ± 0.06ab
Xylose	2.86 ± 0.31abcd	2.33 ± 0.35ab	3.63 ± 0.21bcd	5.19 ± 0.1e	4.18 ± 0.32de	1.76 ± 0.1a	1.73 ± 0.46a	1.64 ± 0.49a	3.42 ± 0.27bcd	3.44 ± 0.34bcd	3.8 ± 0.45cd	1.54 ± 0.2a	1.93 ± 0.23a	2.7 ± 0.57abc	3.6 ± 0.4bcd

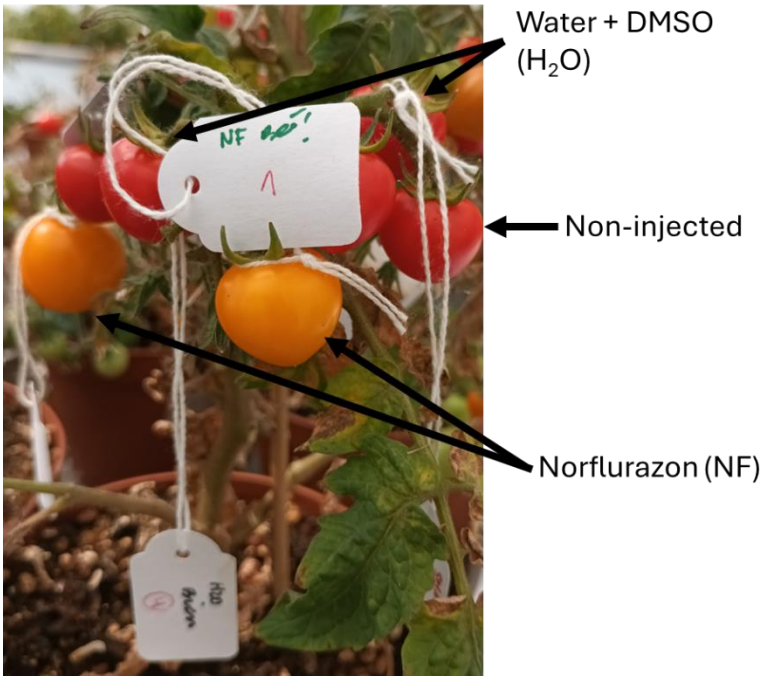
Supplemental Table C4-3. Relative metabolite levels from MG+5 to MG+13 stages detected by GC-MS in tomato WT and *aox1a* mutant fruits. Values were determined after normalization by the mean levels of WT pericarp samples at mature green (MG) stage. Levels correspond to the mean ± SE of n=4-6 independent replicates. Letters denote significant differences ($P < 0.05$) among genotypes at all ripening stages 'n.d.' denotes 'not detected'.

Metabolite	WT_MG	WT_MG+1	WT_MG+2	WT_MG+3	a1_MG	a1_MG+1	a1_MG+2	a1_MG+3	a2_MG	a2_MG+1	a2_MG+2	a2_MG+3
2-amino-Adipic acid	1 ± 0.17b	0.62 ± 0.13ab	0.63 ± 0.26ab	0.38 ± 0.07a	0.79 ± 0.22ab	1 ± 0.19b	0.44 ± 0.11a	0.34 ± 0.07a	1.03 ± 0.21b	0.72 ± 0.13ab	0.4 ± 0.08a	0.47 ± 0.07a
2-oxo-glutarate	1 ± 0.16a	2.09 ± 0.35ab	1.3 ± 0.15ab	1.98 ± 0.37ab	1.34 ± 0.2ab	1.33 ± 0.19ab	2.96 ± 1.11b	1.65 ± 0.3ab	1.56 ± 0.45ab	1.1 ± 0.17a	1.61 ± 0.38ab	2.55 ± 0.62ab
3-deoxy-glucosone	1 ± 0.14b	1.08 ± 0.18b	0.87 ± 0.2ab	0.85 ± 0.08ab	0.47 ± 0.14ab	0.95 ± 0.11ab	0.93 ± 0.12ab	0.72 ± 0.07ab	0.96 ± 0.21ab	0.92 ± 0.13ab	0.75 ± 0.23ab	0.7 ± 0.09ab
Asparagine	1 ± 0.15abc	1.83 ± 0.48abc	1.16 ± 0.26abc	0.81 ± 0.16ab	0.51 ± 0.14ab	0.93 ± 0.12abc	1.09 ± 0.07abc	1.1 ± 0.18abc	1.91 ± 0.7bc	1.49 ± 0.45abc	0.68 ± 0.21abc	2.23 ± 0.89c
Aspartate	1 ± 0.14a	1.42 ± 0.25ab	2.38 ± 1.02b	1.18 ± 0.2a	0.92 ± 0.15a	1.21 ± 0.19a	1.21 ± 0.16a	1.07 ± 0.12a	1.1 ± 0.2a	1.05 ± 0.19a	1.32 ± 0.09ab	1.4 ± 0.31ab
Benzoate	1 ± 0.15b	0.92 ± 0.09ab	0.77 ± 0.14ab	0.97 ± 0.15b	0.85 ± 0.06ab	0.88 ± 0.14ab	0.73 ± 0.15ab	0.92 ± 0.12ab	0.44 ± 0.06a	1.01 ± 0.16b	0.66 ± 0.13ab	1.06 ± 0.35b
beta-Alanine	1 ± 0.15a	1.63 ± 0.35ab	0.92 ± 0.21a	0.84 ± 0.22a	1.18 ± 0.36ab	1.18 ± 0.11ab	1.25 ± 0.22ab	0.94 ± 0.11a	1.82 ± 0.37b	1.43 ± 0.23ab	0.87 ± 0.25a	0.94 ± 0.2a
Citrate	1 ± 0.13abc	1.86 ± 0.22cd	1.5 ± 0.38bc	1.5 ± 0.12bc	0.55 ± 0.17a	1.11 ± 0.1ab	1.28 ± 0.17abc	1.4 ± 0.19bc	1.1 ± 0.22ab	0.99 ± 0.14ab	1.02 ± 0.4ab	2.42 ± 0.2d
Dehydroascorbate	1 ± 0.31a	1.84 ± 0.65a	1 ± 0.39a	1.35 ± 0.22a	0.67 ± 0.05a	0.82 ± 0.09a	1.65 ± 0.48a	0.95 ± 0.17a	0.66 ± 0.12a	0.59 ± 0.13a	0.84 ± 0.24a	1.88 ± 0.72a
Erythritol	1 ± 0.06ab	1.27 ± 0.14abc	1.21 ± 0.29abc	1.71 ± 0.27cd	0.67 ± 0.05a	0.99 ± 0.08ab	1.19 ± 0.15abc	1.3 ± 0.16bc	1.11 ± 0.19ab	1.05 ± 0.12ab	1.12 ± 0.28ab	1.87 ± 0.15d
Fructose	1 ± 0.09bcd	1.17 ± 0.13cd	0.87 ± 0.2ab	1.34 ± 0.11d	0.43 ± 0.12a	0.89 ± 0.07bc	1.03 ± 0.11bcd	1.14 ± 0.11cd	0.8 ± 0.15abc	0.74 ± 0.1abc	0.66 ± 0.18ab	1.01 ± 0.17bcd
Fructose-6-P	1 ± 0.32a	0.84 ± 0.24a	0.75 ± 0.29a	0.9 ± 0.25a	0.4 ± 0.2a	0.84 ± 0.26a	0.78 ± 0.19a	0.78 ± 0.21a	0.9 ± 0.26a	0.68 ± 0.17a	0.28 ± 0.08a	0.79 ± 0.22a
Fucose	1 ± 0.09bc	1.01 ± 0.07bc	0.9 ± 0.15abc	1.21 ± 0.14c	0.54 ± 0.13a	0.94 ± 0.02bc	0.96 ± 0.07bc	1.01 ± 0.1bc	0.87 ± 0.15abc	0.86 ± 0.07abc	0.74 ± 0.19ab	1.02 ± 0.06bc
Fumarate	1 ± 0.12b	0.77 ± 0.1ab	0.69 ± 0.16ab	1.06 ± 0.2b	0.38 ± 0.12a	0.63 ± 0.05ab	0.7 ± 0.08ab	0.77 ± 0.1ab	0.83 ± 0.19ab	0.75 ± 0.06ab	0.64 ± 0.19ab	0.89 ± 0.12b
GABA	1 ± 0.09ab	1.07 ± 0.07b	0.86 ± 0.15ab	0.85 ± 0.12ab	0.73 ± 0.16ab	1 ± 0.03ab	0.94 ± 0.06ab	0.9 ± 0.05ab	0.96 ± 0.12ab	0.93 ± 0.07ab	0.69 ± 0.16a	0.74 ± 0.08ab
Galactonic acid-1,4-lactone	1 ± 0.18ab	1.29 ± 0.21ab	1.75 ± 0.68b	1.75 ± 0.47b	0.5 ± 0.13a	1.05 ± 0.15ab	0.88 ± 0.17ab	0.97 ± 0.2ab	0.96 ± 0.07ab	0.74 ± 0.12ab	0.8 ± 0.19ab	1.58 ± 0.42b
Glucarate	1 ± 0.34a	0.94 ± 0.27a	0.32 ± 0.1a	0.66 ± 0.2a	0.24 ± 0.1a	0.83 ± 0.29a	0.72 ± 0.19a	0.52 ± 0.12a	0.75 ± 0.15a	0.66 ± 0.21a	0.39 ± 0.26a	0.46 ± 0.08a
Glucose	1 ± 0.09ab	1.14 ± 0.13bc	0.91 ± 0.2ab	1.53 ± 0.25c	0.58 ± 0.11a	0.87 ± 0.05ab	1.01 ± 0.12ab	1.09 ± 0.09b	0.78 ± 0.14ab	0.75 ± 0.07ab	0.66 ± 0.18ab	0.93 ± 0.2ab
Glucose-6-P	1 ± 0.34a	1.07 ± 0.39a	0.65 ± 0.31a	1.11 ± 0.36a	0.57 ± 0.21a	0.95 ± 0.31a	0.92 ± 0.36a	0.91 ± 0.31a	1.51 ± 0.6a	0.8 ± 0.3a	0.45 ± 0.16a	0.92 ± 0.31a
Glutamate	1 ± 0.18a	1.27 ± 0.11a	0.91 ± 0.17a	1.19 ± 0.15a	0.88 ± 0.15a	1.29 ± 0.13a	1.59 ± 0.27ab	1.35 ± 0.14a	1.4 ± 0.27a	1.21 ± 0.21a	1.44 ± 0.12ab	2.05 ± 0.38b
Glutamine	1 ± 0.26a	1.35 ± 0.33a	1.1 ± 0.35a	0.87 ± 0.24a	0.93 ± 0.28a	0.87 ± 0.18a	1.49 ± 0.54a	1.11 ± 0.22a	1.55 ± 0.8a	1.35 ± 0.14a	1.07 ± 0.35a	1.78 ± 0.41a
Glycerate	1 ± 0.12c	0.72 ± 0.08abc	0.87 ± 0.21bc	1.62 ± 0.16d	0.41 ± 0.08a	0.76 ± 0.09abc	0.67 ± 0.04abc	0.87 ± 0.05bc	0.87 ± 0.15bc	0.95 ± 0.11bc	0.58 ± 0.07ab	1.08 ± 0.16c
Glycerol	1 ± 0.29ab	0.69 ± 0.08ba	1.29 ± 0.56ab	0.74 ± 0.15ab	0.6 ± 0.15a	0.81 ± 0.13ab	1.01 ± 0.1ab	0.73 ± 0.09ab	1.25 ± 0.64ab	0.81 ± 0.11ab	0.92 ± 0.33ab	1.72 ± 0.49b
Glycerol-3-P	1 ± 0.1a	1.16 ± 0.13a	0.93 ± 0.14a	1 ± 0.15a	0.94 ± 0.11a	1.24 ± 0.12a	1.24 ± 0.09a	1.04 ± 0.08a	1.12 ± 0.11a	1.14 ± 0.04a	0.96 ± 0.15a	0.94 ± 0.08a
Glycine	1 ± 0.16ab	1.22 ± 0.13ab	0.95 ± 0.2ab	0.94 ± 0.09ab	1.58 ± 0.37ab	1.2 ± 0.14ab	1.3 ± 0.23ab	1.41 ± 0.26b	1.33 ± 0.23a	1.07 ± 0.13ab	0.81 ± 0.23ab	1.05 ± 0.24ab
Histidine	1 ± 0.2a	2.82 ± 0.57c	2.35 ± 0.48abc	1.55 ± 0.36abc	0.75 ± 0.2a	0.89 ± 0.11a	1.5 ± 0.24abc	1.67 ± 0.23abc	2.03 ± 1.02abc	1.11 ± 0.3ab	1.15 ± 0.2abc	2.73 ± 0.73bc
Homoserine	1 ± 0.19a	1.22 ± 0.25a	1.09 ± 0.31a	0.67 ± 0.09a	0.84 ± 0.15a	1.12 ± 0.32a	0.7 ± 0.18a	0.66 ± 0.06a	0.77 ± 0.1a	1.09 ± 0.14a	1.01 ± 0.23a	0.91 ± 0.08a
Isocitrate	1 ± 0.09a	1.34 ± 0.07a	1.76 ± 0.16a	1.33 ± 0.11a	1.07 ± 0.18a	1.46 ± 0.33a	1.33 ± 0.1a	1.43 ± 0.09a	1.39 ± 0.01a	1 ± 0.04a	1.45 ± 0.27a	1.6 ± 0.07a
Isoleucine	1 ± 0.12a	1.92 ± 0.52b	0.94 ± 0.19a	1.06 ± 0.21ab	0.77 ± 0.23a	0.91 ± 0.05a	1.51 ± 0.5ab	0.89 ± 0.02a	1.58 ± 0.35ab	1.17 ± 0.22ab	0.89 ± 0.25a	1.15 ± 0.18ab
Isomaltose	1 ± 0.14a	1.47 ± 0.25a	0.54 ± 0.11a	1.2 ± 0.09a	0.74 ± 0.21a	1.21 ± 0.23a	1.53 ± 0.38a	1.17 ± 0.14a	1.35 ± 0.34a	0.95 ± 0.14a	1.16 ± 0.4a	1.08 ± 0.06a
Lysine	1 ± 0.05ab	0.92 ± 0.04ab	1.57 ± 0.23bc	1.12 ± 0.12abc	0.58 ± 0.05a	1.11 ± 0.18abc	1.46 ± 0.16bc	1.06 ± 0.16ab	1.26 ± 0.31abc	1.02 ± 0.2ab	0.94 ± 0ab	1.82 ± 0.17c
Malate	1 ± 0.13bc	1.24 ± 0.16c	1.12 ± 0.24bc	1.19 ± 0.19bc	0.36 ± 0.1a	0.72 ± 0.05ab	0.79 ± 0.11abc	0.82 ± 0.14abc	0.86 ± 0.17abc	0.79 ± 0.13abc	0.72 ± 0.2ab	1.74 ± 0.16d
Maltose	1 ± 0.16ab	0.99 ± 0.07ab	1.3 ± 0.28ab	1.79 ± 0.1b	0.62 ± 0.09a	1.21 ± 0.27ab	1.35 ± 0.29ab	1.26 ± 0.14ab	1.57 ± 0.34ab	0.96 ± 0.25ab	0.95 ± 0.23ab	1.25 ± 0.36ab
Methionine	1 ± 0.05ab	2.09 ± 0.32bc	1.6 ± 0.41abc	1.06 ± 0.16ab	1.4 ± 0.26abc	0.73 ± 0.06a	1.56 ± 0.31abc	0.97 ± 0.09ab	1.69 ± 0.46abc	1.15 ± 0.01ab	1.36 ± 0.14abc	2.49 ± 0.56c
myo-inositol	1 ± 0.07a	1.03 ± 0.06a	0.81 ± 0.16a	1.16 ± 0.13a	0.77 ± 0.19a	1.02 ± 0.07a	0.99 ± 0.08a	0.97 ± 0.09a	1.05 ± 0.19a	0.97 ± 0.08a	1.09 ± 0.07a	0.94 ± 0.1a
Nicotinate	1 ± 0.08ab	1.24 ± 0.07bc	1.23 ± 0.22bc	1.58 ± 0.19c	0.59 ± 0.12a	1.01 ± 0.1ab	1.12 ± 0.07bc	1.15 ± 0.11bc	0.95 ± 0.17ab	0.99 ± 0.06ab	1.12 ± 0.2bc	1.42 ± 0.18bc
Ornithine	1 ± 0.1a	1.08 ± 0.09ab	1.04 ± 0.11ab	0.94 ± 0.1ab	1.63 ± 0.62a	1.06 ± 0.08a	1.08 ± 0.11ab	1.18 ± 0.19ab	1.33 ± 0.18ab	1 ± 0.15ab	1.02 ± 0.17ab	1.66 ± 0.19b
Phenylalanine	1 ± 0.24ab	1.89 ± 0.4b	0.83 ± 0.22ab	0.65 ± 0.08a	0.91 ± 0.28ab	0.95 ± 0.05ab	1.49 ± 0.64ab	0.99 ± 0.25ab	1.26 ± 0.31ab	0.96 ± 0.26ab	0.95 ± 0.36ab	1 ± 0.18ab
Phosphoric acid	1 ± 0.08b	1.06 ± 0.07b	0.88 ± 0.12b	0.99 ± 0.04b	0.6 ± 0.13a	0.93 ± 0.04b	0.91 ± 0.04b	0.92 ± 0.04b	0.92 ± 0.11b	0.84 ± 0.06ab	0.84 ± 0.13ab	0.97 ± 0.03b
Proline	1 ± 0.17a	2.25 ± 0.53ab	1.12 ± 0.28ab	2.57 ± 0.79ab	4.14 ± 1.14ab	5.48 ± 0.76bc	8.7 ± 3.83c	3.42 ± 0.69ab	2.08 ± 0.48ab	2.05 ± 0.36ab	2.41 ± 0.66ab	2.39 ± 0.45ab
Putrescine	1 ± 0.09a	1.36 ± 0.09a	1.03 ± 0.25a	1.29 ± 0.26a	0.69 ± 0.1a	1 ± 0.12a	1.11 ± 0.13a	1.37 ± 0.26a	1.12 ± 0.3a	1.11 ± 0.19a	0.71 ± 0.2a	2.54 ± 0.27b
Pyruvate	1 ± 0.13abc	1.56 ± 0.24abcd	0.98 ± 0.23abc	1.63 ± 0.43abcd	0.91 ± 0.24ab	1.13 ± 0.16abcd	2.23 ± 0.59d	1.46 ± 0.2abcd	0.68 ± 0.08a	0.72 ± 0.15a	2.13 ± 0.62cd	1.94 ± 0.28bcd
Quinate	1 ± 0.07c	0.34 ± 0.02ab	0.45 ± 0.12ab	0.49 ± 0.11ab	0.79 ± 0.01bc	0.64 ± 0.16abc	0.36 ± 0.09ab	0.23 ± 0.04a	0.37 ± 0.06ab	0.55 ± 0abc	0.24 ± 0.03a	0.45 ± 0.07ab
Rhamnose	1 ± 0.07b	1.15 ± 0.11bc	1.02 ± 0.23b	1.31 ± 0.17bc	0.51 ± 0.11a	0.93 ± 0.03ab	1.08 ± 0.14bc	1.06 ± 0.12bc	1 ± 0.2b	0.85 ± 0.07ab	0.86 ± 0.26ab	1.53 ± 0.09c
Serine	1 ± 0.2ab	2.12 ± 0.45c	1.06 ± 0.21ab	1.84 ± 0.31bc	0.7 ± 0.13a	1.83 ± 0.31bc	2.28 ± 0.24c	3.22 ± 0.28d	1.61 ± 0.33abc	1.13 ± 0.15ab	1.08 ± 0.33ab	2.2 ± 0.37c
Spermidine	1 ± 0.13ab	1.24 ± 0.16abc	1.61 ± 0.15bc	1.04 ± 0.17ab	0.66 ± 0.1a	0.71 ± 0.09a	1.08 ± 0.06abc	0.93 ± 0.03a	1.62 ± 0.15bc	1.01 ± 0.02ab	1.31 ± 0.29abc	1.71 ± 0.13c
Succincate	1 ± 0.11a	0.7 ± 0.13a	0.78 ± 0.09a	0.75 ± 0.14a	0.76 ± 0.18a	0.75 ± 0.05a	0.53 ± 0.04a	0.57 ± 0.05a	0.72 ± 0.21a	1.02 ± 0.16a	0.55 ± 0.02a	0.92 ± 0.09a
Sucrose	1 ± 0.08ab	1.01 ± 0.09ab	0.67 ± 0.16a	1.57 ± 0.29bcd	0.64 ± 0.17a	1.77 ± 0.2cd	2.16 ± 0.49d	1.93 ± 0.1cd	0.91 ± 0.16ab	1.28 ± 0.13abc	0.97 ± 0.26ab	1.36 ± 0.15abc
Threonine	1 ± 0.14ab	2.16 ± 0.66c	0.95 ± 0.23a	0.85 ± 0.1a	0.53 ± 0.14a	0.74 ± 0.04a	1.02 ± 0.18ab	0.75 ± 0.05a	1.97 ± 0.57bc	1.34 ± 0.29abc	1.02 ± 0.29ab	1.1 ± 0.19ab
Trehalose	1 ± 0.13abc	1.52 ± 0.21bc	0.59 ± 0.14a	1.78 ± 0.33c	0.68 ± 0.02ab	1.24 ± 0.15bac	1.62 ± 0.37c	1.52 ± 0.22bc	1.63 ± 0.13c	1.03 ± 0.17abc	1.58 ± 0.27bc	1.33 ± 0.09abc
Tryptophan	1 ± 0.24abc	4.54 ± 0.42e	0.51 ± 0.17a	1.92 ± 0.45bc	0.32 ± 0.09a	0.69 ± 0.08a	1.38 ± 0.44abc	0.85 ± 0.17ab	1.23 ± 0.39abc	0.75 ± 0.17a	0.48 ± 0.18a	2.1 ± 0.18c
Tyramine	1 ± 0.14ab	1.28 ± 0.24abcd	0.74 ± 0.19a	1.63 ± 0.17bcde	0.71 ± 0.17a	2.29 ± 0.18e	1.9 ± 0.3de	1.83 ± 0.31cde	1.25 ± 0.28abcd	1.09 ± 0.06abc	1.11 ± 0.29abc	1.86 ± 0.19de
Tyrosine	1 ± 0.12ab	1.09 ± 0.21ab	1.16 ± 0.25ab	1.02 ± 0.29ab	0.42 ± 0.14a	0.95 ± 0.06ab	1.4 ± 0.4ab	0.73 ± 0.04b	1.26 ± 0.23ab	0.99 ± 0.26ab	0.41 ± 0.14a	0.94 ± 0.19ab
Urea	1 ± 0.15b	0.81 ± 0.05ab	0.85 ± 0.18ab	0.71 ± 0.09ab	0.53 ± 0.08a	0.81 ± 0.16ab	0.86 ± 0.09ab	0.72 ± 0.06ab	0.7 ± 0.09ab	0.59 ± 0.01ab	0.6 ± 0.08ab	0.71 ± 0.06ab
Valine	1 ± 0.16a	1.37 ± 0.24a	0.84 ± 0.19a	0.94 ± 0.2a	0.85 ± 0.25a	1.01 ± 0.11a	1.27 ± 0.22a	1.05 ± 0.07a	1.26 ± 0.24a	1.05 ± 0.17a	0.95 ± 0.25a	1.05 ± 0.37a
Xylose	1 ± 0.1ab	1.09 ± 0.09abc	1.2 ± 0.42abc	1.9 ± 0.18c	0.52 ± 0.1a	0.84 ± 0.03ab	1.24 ± 0.17abc	1.32 ± 0.15abc	0.88 ± 0.21ab	0.8 ± 0.11ab	1.13 ± 0.28abc	1.58 ± 0.35bc

Supplemental Table C4-4. Relative metabolite levels from MG to MG+3 detected by GC-MS in tomato WT and *aox1a* mutant fruits. Values were determined after normalization by the mean levels of WT pericarp samples at mature green (MG) stage. Levels correspond to the mean ± SE of n=4-6 independent replicates. Letters denote significant differences ($P < 0.05$).



Supplemental Figure C4-1. Relative expression levels of AOX-encoding genes in tomato (AOX1a, AOX1b, AOX1c, and AOX2) at different tissues and fruit developmental stages. From left to right: Unopened Flower Bud; Fully Opened Flower (Anthesis stage); Leaves; Root; 1 cm Fruit; 2 cm Fruit; 3 cm Fruit; Mature green fruit; Breaker fruit, and Breaker fruit + 10. The eFP browser expression data was downloaded from U bar Toronto (Winter et al., 2007).



Supplemental Figure C4-2. Representative image of MicroTom fruits infiltrated on vine with **A)** Norfluorazon, **B)** Water and DMSO and **C)** Non-infiltrated fruits.

```
setwd("YOUR/WORKING/DIRECTORY")

# Load necessary libraries
library(readxl)
library(dplyr)
library(tidyr)
library(ggplot2)
library(factoextra)
library(ComplexHeatmap)
library(ggrepel)
library(ggfortify)

# xls files
data <- read_excel("Dades_GCMS_Allmetabolites_WT_MG.xlsx", sheet = 1)

# Convert data into a long format
data_long <- pivot_longer(data, cols = -Metabolite,
             names_to = c("Condition", "Time", "Replicate"),
             names_pattern = "([a-zA-Z-1-3-.]+)_MG\\+?(\\d*)_(\\d)")
data_long$Time[data_long$Time == ''] <- 0

# Calculate averages again, checking for numeric conversion
data_avg <- data_long %>%
  mutate(value = as.numeric(value)) %>%
  group_by(Metabolite, Condition, Time) %>%
  summarise(Average = mean(value, na.rm = TRUE), .groups = 'drop')

############################  HEATMAP ##############################

# Construct the heatmap matrix
data_pca_avg <- pivot_wider(data_avg, id_cols = c("Condition",
"Time"), names_from = Metabolite, values_from = Average)
#row1 <- data_pca_avg[1,]
#row1$Condition <- "MG"#data_pca_avg <- data_pca_avg %>%
dplyr::filter(Time !="0") #data_pca_avg <- rbind(data_pca_avg, row1)
avg_matrix <- as.matrix(select(data_pca_avg, -c(Condition, Time)))

rownames(avg_matrix) <- paste(data_pca_avg$Condition,
as.character(data_pca_avg$Time), sep="_")

#samples$name <- factor(samples$name, levels = c("T0", "7 days", "30
days", "recovery")
# Heatmap plot
annotation_col = data.frame(
  Condition = data_pca_avg$Condition,
  Day = as.integer(data_pca_avg$Time)
)
annotation_col$Condition <- factor(annotation_col$Condition, levels =
c("WT","a1.1","a2.3"))
rownames(annotation_col) = rownames(avg_matrix)

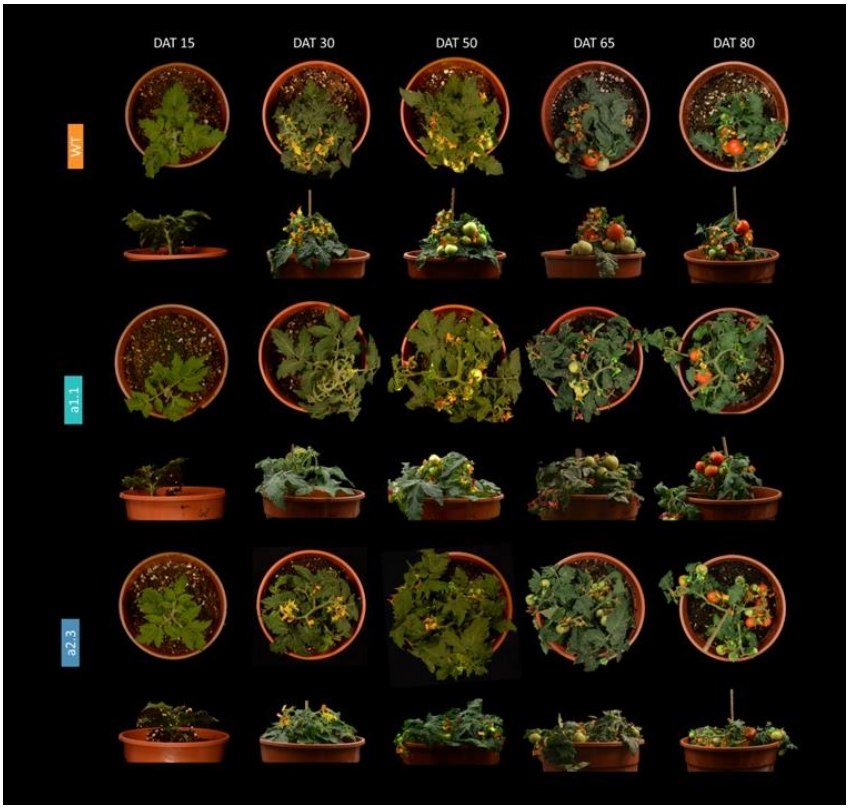
ann_colors = list(
  Day = c("white", "firebrick"),
  Condition = c("WT" = "#FF912B", "a1.1" = "#2BC2C2","a2.3" =
"#4C90BA")
)
ann_colors$Condition <- factor(ann_colors$Condition, levels = c("WT" =
"#FF912B", "a1.1" = "#2BC2C2","a2.3" = "#4C90BA"))

min_val <- min(log(t(avg_matrix)))
max_val <- max(log(t(avg_matrix)))
mid_val <- 0  # Setting zero as the middle value in your data after
log transformation

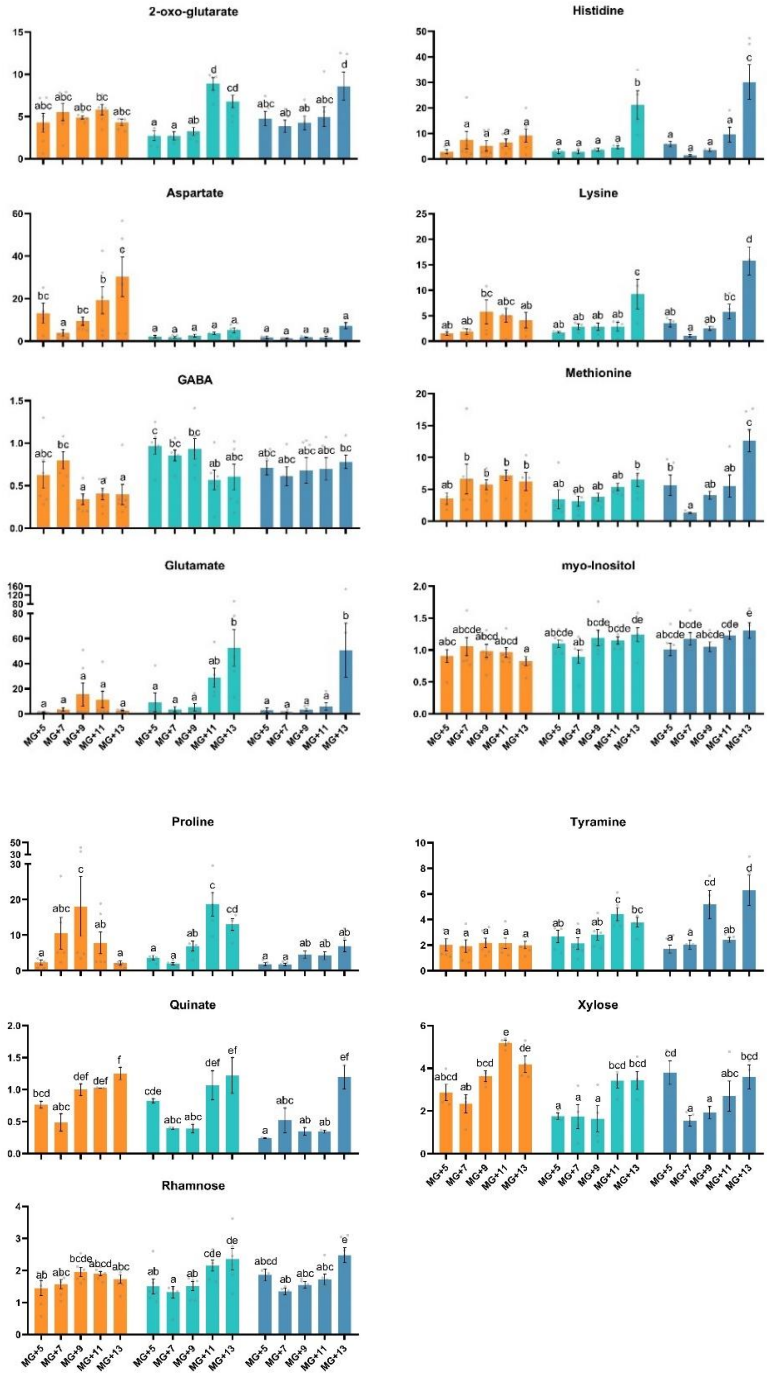
# Create a custom color function
color_function <- function(n) {
  # Generate a sequence of n colors from blue to white to red
  colors <- c(colorRampPalette(c("blue", "white"))(n * abs(min_val) /
(abs(min_val) + max_val) * n/2 + 1),
              colorRampPalette(c("white", "red"))(n * max_val /
(abs(min_val) + max_val) * n/2 + 1))
  colors <- colors[-(n/2 + 1)]  # Remove the duplicate white in the
middle
  return(colors)
}

# Generate the heatmap
pheatmap(log(t(avg_matrix)),
         scale = "none",
         border_color = "white",
         color = color_function(100),  # Apply the custom color
function
         annotation_col = annotation_col,
         annotation_colors = ann_colors)
```

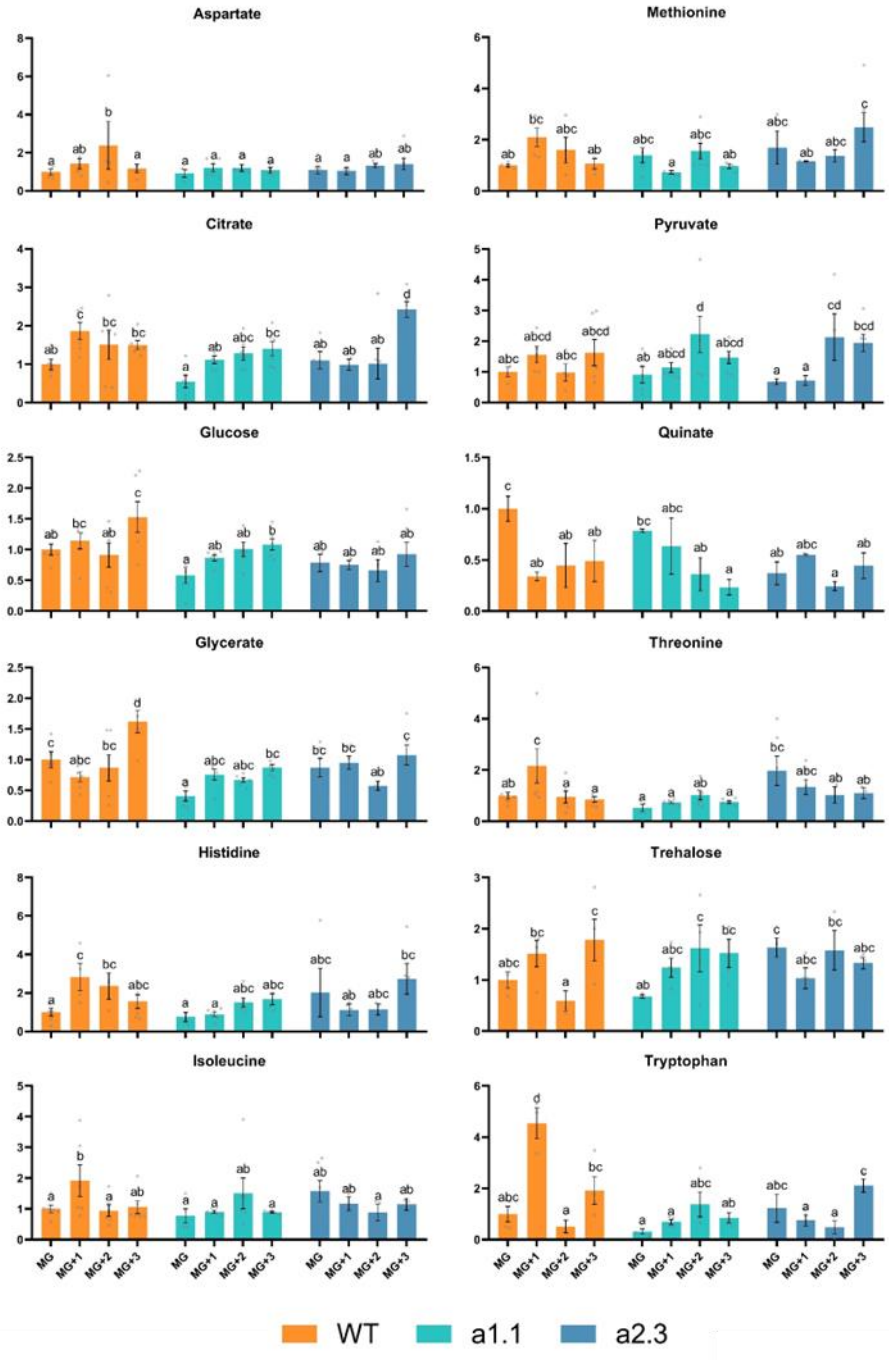
Supplemental Figure C4-3. Script used to perform Heatmap and clusters for R



Supplemental Figure C4-4. Representative images from top- and front-view pictures of WT and *aox1a* mutant lines (*a1.1* and *a2.3*) at 15, 30, 50, 65, and 80 days after transplanting to 0,5 L pots.



Supplemental Figure C4-5. Relative levels of individual metabolites that displayed statistically significant (P<0.05) differences between WT and *aox1a* mutant fruits during ripened stages. Values are means ± SE of four to six replicates and different letters represent statistically significant differences (P < 0.05).



Supplemental Figure C4-6. Relative levels of individual metabolites that displayed statistically significant (P<0.05) differences between WT and *aox1a* mutant fruits during non-ripened stages**.** Values are means ± SE of four to six replicates and different letters represent statistically significant differences (P < 0.05).

General Discussion

1. Ensuring supply of carotenoid precursors: a major challenge with multiple regulatory checkpoints

Plant carotenoids are essential for photosynthesis and photoprotection and they also play important roles as signals, both as pigments that attract pollinators and seed-dispersing animals and as precursors for bioactive molecules such as hormones (e.g., ABA and strigolactones). Consistent with this multiplicity of roles, they are produced in the plastids of most plant tissues. While the same biosynthetic pathway operates in all the cases, tissue-specific changes in the expression of biosynthetic genes can result in changes in the carotenoid profile. For example, the down-regulation of genes encoding lycopene cyclases during tomato fruit ripening results in the accumulation of lycopene, a carotenoid species that is not normally found in leaves as it is converted into downstream products. A crucial point that has been often overlooked is how the supply of metabolic precursors for carotenoid synthesis is regulated in different types of tissues. A major bottleneck is the activity of PSY, the first committed and main rate-determining step of the carotenoid pathway (Zhou et al., 2022). PSY converts MEP-derived GGPP into phytoene, the precursor of all carotenoids in all tissues. Regulation of PSY gene expression plays a major role in the control of PSY activity in different tissues. For example, the gene encoding the tomato PSY1 isoform is highly induced during fruit ripening, hence ensuring an enhanced flux metabolic flux into the carotenoid pathway. Additional forms of regulation of PSY activity take place at the post-translational level. In **Chapter 1** we investigated the role of Arabidopsis FIBRILLIN6 (FBN6) on the control of PSY activity and confirmed the importance of protein-protein interactions to ensure an appropriate PSY-mediated supply of carotenoid precursors when needed.

The GGPP substrate for PSY activity is provided by the MEP pathway in all plastid types. The MEP pathway is fueled by the Calvin cycle in the chloroplasts photosynthetic tissues (Pokhilko et al., 2015). The source of energy and carbon to feed the massive production of carotenoids that takes place in some non-photosynthetic systems such as the chromoplasts of ripening tomato fruit, however, remains little explored. We initially analyzed the relevance of the AOX pathway and the crosstalk between plastids and mitochondria for the exchange of energy and carbon between these endosymbiotic organelles in **Chapter 2** using Arabidopsis as a model. Then, in **Chapters 3 and 4** we

addressed the question in tomato and demonstrated the central relevance of mitochondrial respiration and the AOX pathway to support carotenoid and ethylene biosynthesis during the transition from chloroplasts to chromoplasts that takes place during fruit ripening.

2. FIBRILLIN6 (FBN6) modulates PSY activity and carotenoid biosynthesis.

The interaction between FBN proteins, stress responses, and carotenoid biosynthesis has become a critical area of study in plant biology. In the first chapter of this Thesis, we explored these relationships in detail, unveiling a new role of FBN proteins beyond the reported function of some members of the family in stabilizing carotenoid-containing plastoglobules (PGs), which are essential for carotenoid storage in chromoplasts and in response to stress conditions, when they help maintain plastid function and integrity.

In **Chapter 1** of this Thesis, our results demonstrate a role of Arabidopsis FIBRILLIN6 (FBN6) in promoting carotenoid biosynthesis by enhancing the activity of phytoene synthase (PSY), a key enzyme that controls the metabolic flux into the carotenoid pathway (Iglesias-Sanchez et al., 2024; Annex 1). FBN6, a fibrillin not associated to chloroplast PGs, was found to co-localize with PSY, facilitating PSY activity, especially under high light conditions (Iglesias-Sanchez et al., 2024; Annex 1). This interaction ensures the adequate synthesis of carotenoids, vital for plant photoprotection (Fraser and Bramley, 2004) and development. It is important to note that carotenoids play a critical role in mitigating oxidative stress by neutralizing ROS, which are harmful byproducts of various metabolic processes (Alscher et al., 2002). Additionally, carotenoids such as zeaxanthin and violaxanthin are involved in the xanthophyll cycle, a protective mechanism that dissipates excess light energy as heat, thereby protecting plants from photooxidative damage (Jahns and Holzwarth, 2012). This antioxidant function of carotenoids is particularly crucial under conditions of high light intensity, where ROS production is elevated (Jahns and Holzwarth, 2012).

Our findings concerning the role of FBN6 in PSY-driven carotenoid accumulation and light acclimation suggest that manipulating FBN6 levels in crops could improve their resilience to light-induced stress, thereby enhancing crop yield and stability under

stressful conditions. This is particularly relevant for plants grown in environments with fluctuating light intensity, such as greenhouses or vertical farms. Recent studies support the significance of manipulating the xanthophyll cycle for improving photosynthetic efficiency and crop yield (Kromdijk et al., 2016; De Souza et al., 2022). De Souza et al. (2022) demonstrated that bioengineering plants to accelerate the recovery from photoprotection enhances photosynthetic efficiency and biomass production in soybean. Their work showed that modifying the xanthophyll cycle components—violaxanthin de-epoxidase (VDE), PsbS, and zeaxanthin epoxidase (ZEP)—can lead to significant yield improvements in fluctuating light conditions. This aligns with our findings on FBN6, suggesting that enhancing key components involved in photoprotective mechanisms at chloroplast membranes can substantially improve crop performance under variable light environments (De Souza et al., 2022). Enhancing carotenoid biosynthesis pathways can improve plant resilience to environmental stressors, supporting the idea that manipulating these pathways in crops could lead to better stress tolerance and improved agricultural productivity (Garcia-Molina and Leister, 2020).

Carotenoids are precursors of important bioactive molecules, including vitamin A, which is essential for human health (Rodriguez-Concepcion et al., 2018). Therefore, enhancing carotenoid levels in crops through biotechnological approaches involving FBN6 can contribute to better nutrition and help combat vitamin A deficiency in human populations (Torres-Montilla and Rodriguez-Concepcion, 2021; Morelli and Rodriguez-Concepcion, 2023). The increased production of carotenoids in crops can lead to the development of functional foods with added health benefits, such as improved vision, enhanced immune response, and reduced risk of chronic diseases (Fraser and Bramley, 2004).

In summary, our research on Arabidopsis FBN6 opens up several avenues for future applications in agriculture and human health. By leveraging the role of FBN6 in carotenoid biosynthesis and stress response, it is possible to develop crops that are not only more nutritious but also more resilient to environmental stressors. This can contribute significantly to food security and public health, particularly in regions prone to nutritional deficiencies and agricultural challenges (Iglesias-Sanchez et al., 2024; Annex 1).

3. The role of alternative oxidase (AOX) pathway in primary metabolism during stress

The regulation of carotenoid profiles is just one of the mechanisms by which plants deal with environmental stresses. In this Thesis we also focused on the role of the mitochondrial AOX pathway and the communication with plastids on the metabolic responses to stress, a process that can directly impact the supply of energy and carbon precursors to the carotenoid pathway (**Figure D-1**). The AOX is a crucial component of the mitochondrial electron transport chain, providing an alternative pathway for electron flow, which is especially important for providing flexibility in cellular energy and carbon metabolism under stress conditions (Del-Saz et al., 2018). Most of the previous studies on AOX under stress have highlighted its role in cell redox balancing and preventing mitochondrial ROS formation (reviewed in Vanlerberghe, 2013). Moreover, the mitochondrial AOX pathway can dissipate energy and carbon excess from the chloroplast through different metabolic pathways, i.e. the malate vale and photorespiration, thus improving photosynthetic performance (reviewed in Del-Saz et al., 2018 and in Vanlerberghe et al., 2020). Our results from **Chapter 2** show that the *AOX1a* gene is crucial for maintaining *in vivo* respiratory activity under acute osmotic and salinity stresses (Del-Saz et al., 2022; Annex 3). In line with previous observations, decreased photosynthetic performance together with the higher levels of some oxidative stress related metabolites in the *aox1a* mutants highlighted the crucial role of the AOX in cell redox balancing and avoidance of excessive ROS accumulation under stress (**Figure D-2**). Nonetheless, substantial reductions in the accumulation of osmoregulatory metabolites in *aox1a* mutants overlapped with lower leaf relative water contents (**Figure D-2**). These novel observations suggested an important role of AOX for leaf osmoprotection, beyond its role in mitigating oxidative stress through cell redox balancing (i.e. NAD(P)H/ATP ratios).

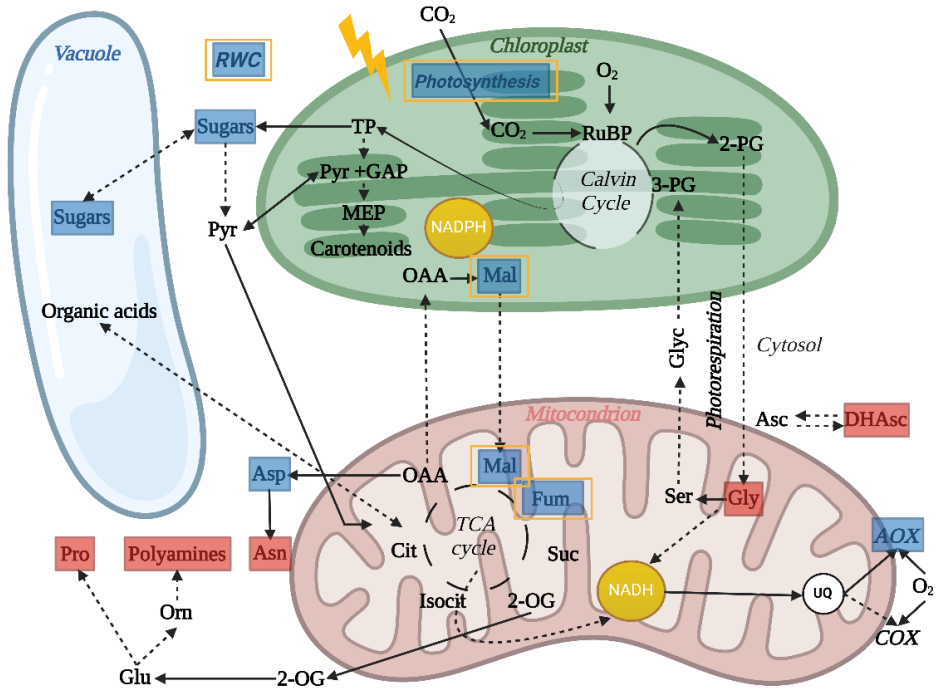


Figure D-1: Schematic overview illustrating the impact of AOX pathway restriction on leaf cell physiology and metabolism in *Arabidopsis thaliana* (**Chapter 2**; Del-Saz et al., 2022; Annex 3) and Medicago truncatula (Del-Saz et al., 2016) plants after 1 day of salt stress treatment. Blue and red boxes indicate significant ($P < 0.05$) reductions and increases, respectively, in physiological indicators and metabolite levels found in plants with lower AOX *in vivo* activity response, either in Arabidopsis *aox1a* mutant (as compared to wild-type) or in Medicago salt-sensitive genotype (as compared to salt-tolerant genotype). The orange boxes highlight changes co-occurring in the salt-sensitive genotype from Medicago plants and in Arabidopsis *aox1a* mutants (https://biorender.com).

In wild-type (WT) Arabidopsis plants, the *in vivo* activation of the AOX pathway sustained leaf mitochondrial respiration and the accumulation of stress-related metabolites (SRMs) (Del-Saz et al., 2022; Annex 3). The reduction in the accumulation of SRMs in *aox1a* mutants suggests an impairment of the TCA cycle activity due to limited NADH reoxidation in the absence of *in vivo* AOX activity response. Therefore, results from **Chapter 2** extend the concept about the important role of the AOX pathway in providing flexibility to carbon metabolism (Del-Saz et al., 2018), in this case, being crucial for ensuring the biosynthesis of SRMs for osmoprotection (**Figure D-2**). In close agreement, higher levels of osmoprotective metabolites and *in vivo* AOX activity were

found in a salt-tolerant genotype of *Medicago truncatula* plants, as compared to a salt-sensitive genotype (Figure 2 from Del-Saz et al., 2016). Furthermore, our study in Chapter 2 also provides new insights into the specific contribution of the AOX1a isoform and the compensatory role of AOX1d under salinity and osmotic stress conditions. While AOX1d could partially compensate for the absence of AOX1a, particularly under non-stress conditions, it is not sufficient to restore the metabolic role of the AOX pathway under salinity stress. In this context, our results complement other observations suggesting partial compensation by other AOX isoforms in *aox1a* mutants under salinity stress (Oh et al., 2022), and further extends the knowledge about the impact of AOX isoform changes over the role and regulation of the AOX pathway *in vivo*.

Given the observed differences in metabolic responses between *aox1a* mutants and WT plants, genetically engineered crops to enhance AOX capacity or activity could be a viable strategy for improving tolerance to abiotic stresses like drought and salinity. This approach could be particularly beneficial for salt-sensitive crops, where improving osmotic adjustment and reducing oxidative damage are critical for maintaining productivity under adverse conditions (Smith et al., 2009; Munns and Gilliham, 2015). Moreover, there is a need to investigate the exact mechanisms by which AOX1a and other AOX isoforms contribute to metabolic flexibility and stress tolerance in other types of abiotic stresses, as well as in biotic stress and their combinations. Insights from studying the role and regulation of the AOX pathway under the mentioned conditions can be applied to develop crops with enhanced stress tolerance in the context of multi-stress situations derived from climate change (Florez-Sarasa et al., 2020). Enhancing AOX expression may generate plants better equipped to withstand environmental stresses, leading to more stable agricultural production. Since most of the current information on the AOX-research field has been focused on model plants (i.e. Arabidopsis and tobacco), future research should focus on breeding or genetically engineering crops with optimized AOX activity to enhance their resilience to water and salt stress, potentially mitigating climate change impacts on agriculture. Improving stress tolerance could also reduce the need for chemical inputs, promoting more sustainable agricultural practices (González Guzmán et al., 2022).

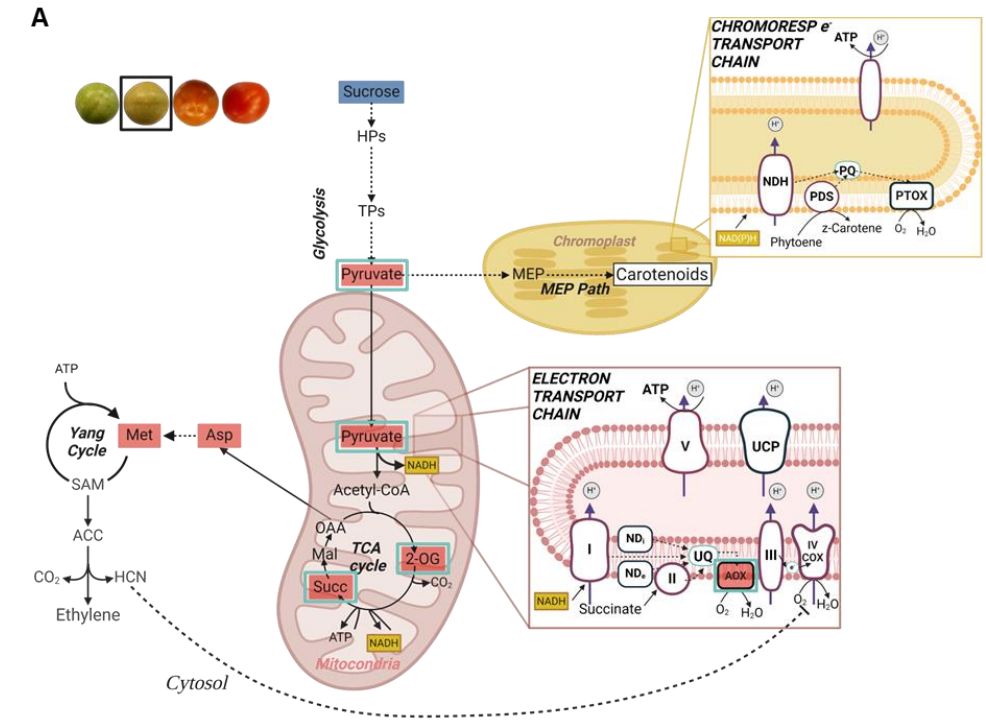
4. The role of AOX during fruit ripening

Our research from **Chapter 3** and **Chapter 4** has clarified the critical role of the AOX pathway in tomato fruit ripening and led to propose a new model about the contributions of the tomato mito- and chromo-respiratory pathways (**Figure D-2**). The *in vivo* activity of AOX pathway significantly increased at the breaker stage, becoming the main contributor to climacteric respiration (**Chapter 3** and **Figure D-2A**). The lack of correlation between AOX transcript levels and activity suggests that AOX regulation is primarily post-translational, influenced by the accumulation of pyruvate (Pyr, one of the substrates of the MEP pathway), 2-oxoglutarate (2-OG), and succinate (Succ) (**Chapter 3**, **Figure D-2A**). In previous *in vitro* studies, Pyr and 2-OG could allosterically activate the AOX1a isoform from Arabidopsis (Selinski et al., 2018a), while Succ specifically activated tomato AOX1b isoform (Holtzapffel et al., 2003). Further research will still be required to definitely unravel the precise contribution of each isoform to climacteric respiration *in vivo*, i.e. involving AOX1a, AOX1b and double mutants. However, our results from **Chapter 4** showed that altered expression of AOX1b partly restored respiration peaks and metabolic functions in *aox1a* mutant fruits. Overall, our results from **Chapter 3** and **4** denote that both AOX1a and AOX1b isoforms cooperate to achieve the climacteric AOX respiration required for fruit ripening metabolism (**Figure D-2A**). Conversely, the plastid terminal oxidase (PTOX) pathway showed minimal contribution to overall respiration during all ripening stages, as evidenced by our experiments of O_2 isotope discrimination with wild-type and PTOX-defective ghost mutants (**Chapter 3**). Our results contrast with a previous study reporting PTOX contribution of up to 26% of total oxygen uptake in ripe tomato fruits (Renato et al., 2014). The overlooked effects of OGAL over the AOX activity *in vivo* are behind these controversial results (**Chapter 3**). In addition, Renato et al. (2014) observations showing fewer energized (ATP-producing) mitochondria in red (R) tomato fruits are in line with our observations of a decrease in the *in vivo* activity of the ATP-coupled COX pathway, although not with their proposal of an increase in AOX activity at R stage (**Figure D-2B**).

Although different roles of AOX during fruit ripening have been proposed (Hewitt and Dhingra, 2020; Xu et al., 2012), its precise contribution to fruit primary and secondary

metabolism remained poorly understood. Indeed, the roles of AOX in secondary metabolism (including carotenoid biosynthesis) are far from being understood (McDonald, 2023). The combined decrease in sucrose and increase in Pyr levels suggest a high glycolytic flux at the BR stage (**Figure D-2A**). Pyr and other glycolytic intermediates can serve as precursors for the synthesis of secondary metabolites such as flavonoids and carotenoids (Aharoni and Galili, 2011; Enfissi et al., 2017; Rodríguez-Concepción and Boronat, 2015; Zhang et al., 2015). In this context, changes in the patterns of glucose, glycerate and Pyr accumulation together with altered respiration rates and carotenoid accumulation in *aox1a* mutants denote the role of AOX in providing carbon precursors for the MEP and carotenoid pathways. Previous studies in leaf and root tissues, including our **Chapter 2**, also suggest the relevance of the AOX pathway in providing metabolic flexibility, not only under high cell energy (ATP) charge, but also when there is a high carbon skeletons demand (**Figure D-1**; Del-Saz et al., 2018, 2022).

In addition, our results showing the coordinated increase of the *in vivo* AOX activity, aspartate (Asp) and methionine (Met) during the climacteric peak (**Chapter 3**) has uncovered a new metabolic link between AOX and the synthesis of Asp family amino acids (**Figure D-2**). Furthermore, impaired respiration and TCA metabolism in *aox1a* mutants resulted in a marked restriction of Asp (**Chapter 4**). Taken together, our results from **Chapter 3** and **4** strongly suggest that the AOX pathway mediates the supply of Asp and Met for the climacteric synthesis of ethylene, the most important hormone triggering fruit ripening. Although previous studies observed delayed ripening and reduced total respiration in tomato fruits of AOX-silenced plants (Xu et al., 2012), our results provide a clear mechanistic interaction between ethylene synthesis and AOX respiration. Despite the Yang cycle allows for the synthesis of ethylene precursors while recycling Met, there is evidence indicating that 'de novo' synthesis of Met becomes relevant when high rates of ethylene production occur in tomato fruits (Katz et al., 2006). Therefore, a high AOX respiratory flux at the climacteric peak is required to provide the carbon precursors (oxalacetate and Asp) needed for 'de novo' Met synthesis (**Figure D-2**). These observations have implications beyond fruit ripening, i.e. providing a plausible mechanistic link between AOX and ethylene hormone during plant stress responses, since both are among the most relevant factors highly induced by environmental perturbations.


A
Sucrose
HPs
TPs
Glycolysis
Pyruvate
MEP
Carotenoids
MEP Path
Chromoplast
CHROMORESP e⁻ TRANSPORT CHAIN
ATP
NDH
PQ
PDS
PTOX
z-Carotene
Phytoene
NAD(P)H
ELECTRON TRANSPORT CHAIN
V
UCP
I
II
III
IV COX
UQ
AOX
NADH
Succinate
Acetyl-CoA
OAA
Mal
TCA cycle
2-OG
Succ
ATP
NADH
Mitocondria
Yang Cycle
Met
Asp
SAM
ACC
CO2
HCN
Ethylene
Cytosol

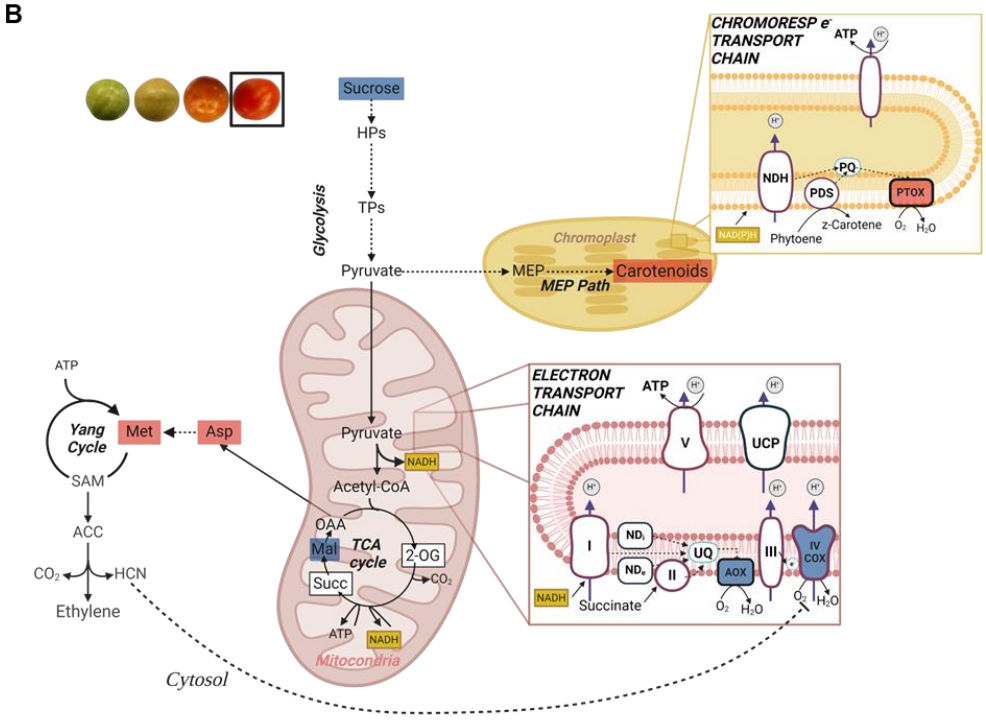

B
Sucrose
HPs
TPs
Glycolysis
Pyruvate
MEP
Carotenoids
MEP Path
Chromoplast
CHROMORESP e⁻ TRANSPORT CHAIN
ATP
NDH
PQ
PDS
PTOX
z-Carotene
Phytoene
NAD(P)H
ELECTRON TRANSPORT CHAIN
V
UCP
I
II
III
IV COX
UQ
AOX
NADH
Succinate
Acetyl-CoA
OAA
Mal
TCA cycle
2-OG
Succ
ATP
NADH
Mitocondria
Yang Cycle
Met
Asp
SAM
ACC
CO2
HCN
Ethylene
Cytosol

Figure D-2. Schematic overview illustrating the impact of in vivo AOP restriction on tomato fruit metabolism in **A)** breaker (BR) and **B)** red ripe (RR) stage. Blue and red boxes indicate significant ($P < 0.05$) reductions and increases, respectively, in physiological indicators and metabolite levels. Green boxes in (A) denote the AOX metabolic activators. (https://biorender.com).

A better understanding of climacteric respiration during fruit ripening, as provided in this Thesis, can serve as a foundation for developing new strategies to improve fruit quality across various crop species, thereby boosting their market value and increasing consumer satisfaction. A fine-tuned manipulation of AOX has the potential to become a new strategy in commercial postharvest practices through the control of respiration, as an alternative to ethylene. Future research could explore developing crop varieties with optimized AOX activity, ensuring adequate fruit development and ripening. Additionally, our research can be extended to explore the differences between climacteric and non-climacteric fruit ripening, with potential future applications in preserving fruit quality during storage and transportation, ultimately contributing to a reduction in food waste.

Conclusions

Chapter 1: Arabidopsis FIBRILLIN6 influences carotenoid biosynthesis by directly promoting phytoene synthase activity

1. Arabidopsis FBN6 co-immunoprecipitates and co-localizes with PSY, suggesting a direct interaction.
2. FBN6-PSY interaction enhances the activity of PSY, a key enzyme in the carotenoid biosynthesis pathway.
3. FBN6 is required to support the increase in carotenoid levels that occurs during seedling deetiolation and in response to high light.

Chapter 2: The lack of alternative oxidase 1a restricts *in vivo* respiratory activity and stress-related metabolism for leaf osmoprotection and redox balancing under sudden acute water and salt stress in *Arabidopsis thaliana*

1. The lack of Arabidopsis *AOX1a* does not impair the *in vivo* alternative oxidase (AOX) pathway activity (v_{alt}) under control conditions, probably due to the presence of other AOX isoforms, but restricted its response to stress.
2. Decreased photosynthetic performance together with higher levels of oxidative stress-related metabolites in the *aox1a* mutants denotes the crucial role of the AOX in cell redox balancing and avoidance of excessive ROS accumulation under acute water and salt stress.
3. The lack v_{alt} response in the *aox1a* mutants coincided with reduced accumulation of sugars (i.e. glucose, fructose) and TCA cycle intermediates (i.e. fumarate) which curtailed their osmoprotection under stress.
4. The AOX pathway provides metabolic flexibility allowing the biosynthesis of stress-related metabolites, in addition to its role in cell redox balancing and preventing mitochondrial ROS formation.

Chapter 3: The *in vivo* post-translational activation of alternative oxidase triggers climacteric respiration in tomato.

1. Mitochondrial respiration is the primary contributor to energy and metabolite supply during tomato fruit ripening, while the contribution of chromorespiration, mediated by plastid terminal oxidase (PTOX) activity, is limited to the very late stages of ripening when *in vivo* activities of both mitochondrial alternative (AOX) and cytochrome oxidase (COX) pathways decrease.
2. The AOX *in vivo* activity (ν_{alt}) significantly increases at the breaker stage, becoming the main contributor to climacteric respiration.
3. The lack of correlation between ν_{alt} and transcript levels of fruit-specific AOX isoforms together with changes in key organic acids (pyruvate, 2-oxoglutarate and succinate) suggests a post-translational regulation of fruit AOX through allosteric activation.
4. The climacteric activation of AOX allows for increased generation of glycolytic and TCA cycle intermediates to provide crucial ripening-related carbon precursors

Chapter 4: Lack of alternative oxidase 1a restricts carbon supply for ethylene and carotenoid biosynthesis during tomato fruit ripening

1. Tomato AOX1a is important for normal growth and development in tomato plants under non-stress conditions.
2. The absence of AOX1a leads to disrupted respiration patterns, with delayed or absent respiration peaks and ethylene-induced gene expression.
3. Lack of AOX1a restricts the supply of aspartate, fundamental for the synthesis of methionine which is the precursor for ethylene synthesis.
4. Despite early metabolic limitations, AOX1a-defective mutants partly restore metabolic functions and carotenoid levels by the end of ripening through altered expression of AOX1b.

References

Aharoni, A., and Galili, G. (2011). Metabolic engineering of the plant primary-secondary metabolism interface. *Curr Opin Biotechnol* 22, 239–244. doi: 10.1016/j.copbio.2010.11.004

Alcázar, R., Bueno, M., and Tiburcio, A. F. (2020). Polyamines: Small Amines with Large Effects on Plant Abiotic Stress Tolerance. *Cells* 9. doi: 10.3390/cells9112373

Almeida, A. M., Jarmuszkiewicz, W., Khomsi, H., Arruda, P., Vercesi, A. E., and Sluse, F. E. (1999). Cyanide-Resistant, ATP-Synthesis-Sustained, and Uncoupling-Protein-Sustained Respiration during Postharvest Ripening of Tomato Fruit. *Plant Physiol* 119, 1323–1329. doi: 10.1104/pp.119.4.1323

Alscher, R. G., Erturk, N., and Heath, L. S. (2002). Role of superoxide dismutases (SODs) in controlling oxidative stress in plants. *J Exp Bot* 53, 1331–1341. doi: 10.1093/jexbot/53.372.1331

Arnholdt-Schmitt, B., Costa, J. H., and de Melo, D. F. (2006). AOX - a functional marker for efficient cell reprogramming under stress? *Trends Plant Sci* 11, 281–287. doi: 10.1016/j.tplants.2006.05.001

Bandehagh, A., and Taylor, N. L. (2020). Can Alternative Metabolic Pathways and Shunts Overcome Salinity Induced Inhibition of Central Carbon Metabolism in Crops? *Front Plant Sci* 11. doi: 10.3389/fpls.2020.01072

Barja, M. V., Ezquerro, M., Beretta, S., Diretto, G., Florez-Sarasa, I., Feixes, E., et al. (2021). Several geranylgeranyl diphosphate synthase isoforms supply metabolic substrates for carotenoid biosynthesis in tomato. *New Phytologist* 231, 255–272. doi: 10.1111/nph.17283

Barr, J., White, W. S., Chen, L., Bae, H., and Rodermel, S. (2004). The GHOST terminal oxidase regulates developmental programming in tomato fruit. *Plant Cell Environ* 27, 840–852. doi: 10.1111/j.1365-3040.2004.01190.x

Barreto, P., Couñago, R. M., and Arruda, P. (2020). Mitochondrial uncoupling protein-dependent signaling in plant bioenergetics and stress response. *Mitochondrion* 53, 109–120. doi: 10.1016/j.mito.2020.05.001

Barreto, P., Koltun, A., Nonato, J., Yassitepe, J., Maia, I. de G., and Arruda, P. (2022). Metabolism and Signaling of Plant Mitochondria in Adaptation to Environmental Stresses. *Int J Mol Sci* 23. doi: 10.3390/ijms231911176

Barsan, C., Zouine, M., Maza, E., Bian, W., Egea, I., Rossignol, M., et al. (2012). Proteomic analysis of chloroplast-to-chromoplast transition in tomato reveals metabolic shifts coupled with disrupted thylakoid biogenesis machinery and

elevated energy-production components. *Plant Physiol* 160, 708–725. doi: 10.1104/pp.112.203679

Barsottini, M. R. O., Copsey, A., Young, L., Baroni, R. M., Cordeiro, A. T., Pereira, G. A. G., et al. (2020). Biochemical characterization and inhibition of the alternative oxidase enzyme from the fungal phytopathogen Moniliophthora perniciosa. *Commun Biol* 3, 263–272. doi: 10.1038/s42003-020-0981-6

Bartoli, C. G., Pastori, G. M., and Foyer, C. H. (2000). Ascorbate Biosynthesis in Mitochondria Is Linked to the Electron Transport Chain between Complexes III and IV. doi: 10.1104/pp.123.1.335

Batista-Silva, W., Heinemann, B., Rugen, N., Nunes-Nesi, A., Araújo, W. L., Braun, H. P., et al. (2019). The role of amino acid metabolism during abiotic stress release. *Plant Cell Environ* 42, 1630–1644. doi: 10.1111/pce.13518

Beauvoit, B., Belouah, I., Bertin, N., Cakpo, C. B., Colombié, S., Dai, Z., et al. (2018). Putting primary metabolism into perspective to obtain better fruits. *Ann Bot* 122, 1–21. doi: 10.1093/aob/mcy057

Bolhassani, A., Milani, A., Basirnejad, M., and Shahbazi, S. (2017). Carotenoids: biochemistry, pharmacology and treatment. *Br J Pharmacol* 174, 1290–1324. doi: 10.1111/bph.v174.11/issuetoc

Bouchnak, I., Brugière, S., Moyet, L., Le Gall, S., Salvi, D., Kuntz, M., et al. (2019). Unraveling hidden components of the chloroplast envelope proteome: Opportunities and limits of better MS sensitivity. *Molecular and Cellular Proteomics* 18, 1285–1306. doi: 10.1074/mcp.RA118.000988

Bouvier, F., and Camara, B. (2007). "The Role of Plastids in Ripening Fruits," in *Advances in Photosynthesis and Respiration The Structure and Function of Plastids*, 419–432. doi: 10.1007/978-1-4020-4061-0_21

Bréhélin, C., Kessler, F., and van Wijk, K. J. (2007). Plastoglobules: versatile lipoprotein particles in plastids. *Trends Plant Sci* 12, 260–266. doi: 10.1016/j.tplants.2007.04.003

Camara, B., Hugueney, P., Bouvier, F., Kuntz, M., and Monéger, R. (1995). Biochemistry and Molecular Biology of Chromoplast Development. *Int Rev Cytol* 163, 175–247. doi: 10.1016/S0074-7696(08)62211-1

Cao, H., Luo, H., Yuan, H., Eissa, M. A., Thannhauser, T. W., Welsch, R., et al. (2019). A neighboring aromatic-aromatic amino acid combination governs activity

divergence between tomato phytoene synthases. *Plant Physiol* 180, 1988–2003. doi: 10.1104/pp.19.00384

Carrari, F., and Fernie, A. R. (2006). Metabolic regulation underlying tomato fruit development. *J Exp Bot* 57, 1883–1897. doi: 10.1093/jxb/erj020

Chai, T. T., Simmonds, D., Day, D. A., Colmer, T. D., and Finnegan, P. M. (2012). A GmAOX2b antisense gene compromises vegetative growth and seed production in soybean. *Planta* 236, 199–207. doi: 10.1007/s00425-012-1601-6

Clifton, R., Millar, A. H., and Whelan, J. (2006). Alternative oxidases in Arabidopsis: A comparative analysis of differential expression in the gene family provides new insights into function of non-phosphorylating bypasses. *Biochim Biophys Acta Bioenerg* 1757, 730–741. doi: 10.1016/j.bbabio.2006.03.009

Colombié, S., Beauvoit, B., Nazaret, C., Bénard, C., Vercambre, G., Le Gall, S., et al. (2017). Respiration climacteric in tomato fruits elucidated by constraint-based modelling. *New Phytologist* 213, 1726–1739. doi: 10.1111/nph.14301

Dahal, K., Martyn, G. D., Alber, N. A., and Vanlerberghe, G. C. (2017). Coordinated regulation of photosynthetic and respiratory components is necessary to maintain chloroplast energy balance in varied growth conditions. *J Exp Bot* 68, 657–671. doi: 10.1093/jxb/erw469

Dahal, K., and Vanlerberghe, G. C. (2017). Alternative oxidase respiration maintains both mitochondrial and chloroplast function during drought. *New Phytologist* 213, 560–571. doi: 10.1111/nph.14169

Dahal, K., and Vanlerberghe, G. C. (2018). Improved chloroplast energy balance during water deficit enhances plant growth: More crop per drop. *J Exp Bot* 69, 1183–1197. doi: 10.1093/jxb/erx474

Dahal, K., Wang, J., Martyn, G. D., Rahimy, F., and Vanlerberghe, G. C. (2014). Mitochondrial alternative oxidasemaintains respiration and preserves photosynthetic capacity during moderate drought in nicotiana tabacum. *Plant Physiol* 166, 1560–1574. doi: 10.1104/pp.114.247866

Darko, E., Végh, B., Khalil, R., Marček, T., Szalai, G., Pál, M., et al. (2019). Metabolic responses of wheat seedlings to osmotic stress induced by various osmolytes under iso-osmotic conditions. *PLoS One* 14. doi: 10.1371/journal.pone.0226151

Davidi, L., Levin, Y., Ben-Dor, S., and Pick, U. (2015). Proteome analysis of cytoplasmatic and plastidic β-carotene lipid droplets in Dunaliella bardawil. *Plant Physiol* 167, 60–79. doi: 10.1104/pp.114.248450

Day, D. A., Krab, K., Lambers, H., Moore, A. L., Siedow, J. N., Wagner, A. M., et al. (1996). The Cyanide-Resistant Ocidase: To Inhibit or Not to Inhibit, That Is the Question. *Plant Physiol* 110, 1–2. doi: 10.1104/pp.110.1.1

De Souza, A. P., Burgess, S. J., Doran, L., Hansen, J., Manukyan, L., Maryn, N., et al. (2022). Soybean photosynthesis and crop yield are improved by accelerating recovery from photoprotection. *Science* 377, 851–854. doi: 10.1126/science.adc9831

Del-Saz, N. F., Florez-Sarasa, I., Clemente-Moreno, M. J., Mhadhbi, H., Flexas, J., Fernie, A. R., et al. (2016). Salinity tolerance is related to cyanide-resistant alternative respiration in Medicago truncatula under sudden severe stress. *Plant Cell Environ* 39, 2361–2369. doi: 10.1111/pce.12776

Del-Saz, N. F., Iglesias-Sanchez, A., Alonso-Forn, D., López-Gómez, M., Palma, F., Clemente-Moreno, M. J., et al. (2022). The Lack of Alternative Oxidase 1a Restricts in vivo Respiratory Activity and Stress-Related Metabolism for Leaf Osmoprotection and Redox Balancing Under Sudden Acute Water and Salt Stress in Arabidopsis thaliana. *Front Plant Sci* 13. doi: 10.3389/fpls.2022.833113

Del-Saz, N. F., Ribas-Carbo, M., Martorell, G., Fernie, A. R., and Florez-Sarasa, I. (2017). Measurements of electron partitioning between cytochrome and alternative oxidase pathways in plant tissues. *Methods in Molecular Biology*, 203–217. doi: 10.1007/978-1-4939-7292-0_17

Del-Saz, N. F., Ribas-Carbo, M., McDonald, A. E., Lambers, H., Fernie, A. R., and Florez-Sarasa, I. (2018). An In Vivo Perspective of the Role(s) of the Alternative Oxidase Pathway. *Trends Plant Sci* 23, 206–219. doi: 10.1016/j.tplants.2017.11.006

Deruère, J., Römer, S., d'Harlingue, A., Backhaus, R. A., Kuntz, M., and Camara, B. (1994). Fibril Assembly and Carotenoid Overaccumulation in Chromoplasts: A Model for Supramolecular Lipoprotein Structures. *Plant Cell* 6, 119–133. doi: 10.1105/tpc.6.1.119

Dinakar, C., Raghavendra, A. S., and Padmasree, K. (2010). Importance of AOX pathway in optimizing photosynthesis under high light stress: Role of pyruvate and malate in activating AOX. *Physiol Plant* 139, 13–26. doi: 10.1111/j.1399-3054.2010.01346.x

Egea, I., Barsan, C., Bian, W., Purgatto, E., Latché, A., Chervin, C., et al. (2010). Chromoplast differentiation: Current status and perspectives. *Plant Cell Physiol* 51, 1601–1611. doi: 10.1093/pcp/pcq136

Enfissi, E. M. A., Nogueira, M., Bramley, P. M., and Fraser, P. D. (2017). The regulation of carotenoid formation in tomato fruit. *Plant Journal* 89, 774–788. doi: 10.1111/tpj.13428

Epstein, E., Levin, D. L., Croft, J. D. Jr., and Lutzner, M. A. (1972). Mycosis Fungoides: Survival, Pronostic Features, Response to Therapy and Autopsy Findings. *Medicine* 15, 61–72.

Fàbregas, N., and Fernie, A. R. (2019). The metabolic response to drought. *J Exp Bot* 70, 1077–1085. doi: 10.1093/jxb/ery437

Fernandez, A. I., Viron, N., Alhagdow, M., Karimi, M., Jones, M., Amsellem, Z., et al. (2009). Flexible tools for gene expression and silencing in tomato. *Plant Physiol* 151, 1729–1740. doi: 10.1104/pp.109.147546

Fernández-Cancelo, P., Iglesias-Sanchez, A., Torres-Montilla, S., Ribas-Agustí, A., Teixidó, N., Rodriguez-Concepcion, M., et al. (2022). Environmentally driven transcriptomic and metabolic changes leading to color differences in "Golden Reinders" apples. *Front Plant Sci* 13. doi: 10.3389/fpls.2022.913433

Fernandez-Moreno, J.-P., Orzaez, D., and Granell, A. (2013). VIGS: A Tool to Study Fruit Development in Solanum lycopersicum. *Methods Molecular Biology*, 183–196. doi: 10.1007/978-1-62703-278-0_14

Fernie, A. R., Aharoni, A., Willmitzer, L., Stitt, M., Tohge, T., Kopka, J., et al. (2011). Recommendations for reporting metabolite data. *Plant Cell* 23, 2477–2482. doi: 10.1105/tpc.111.086272

Fernie, A. R., Carrari, F., and Sweetlove, L. J. (2004). Respiratory metabolism: Glycolysis, the TCA cycle and mitochondrial electron transport. *Curr Opin Plant Biol* 7, 254–261. doi: 10.1016/j.pbi.2004.03.007

Fernie, A. R., and Yan, J. (2019). De Novo Domestication: An Alternative Route toward New Crops for the Future. *Mol Plant* 12, 615–631. doi: 10.1016/j.molp.2019.03.016

Ferro, M., Brugière, S., Salvi, D., Seigneurin-Berny, D., Court, M., Moyet, L., et al. (2010). AT-CHLORO, a comprehensive chloroplast proteome database with subplastidial localization and curated information on envelope proteins. *Molecular and Cellular Proteomics* 9, 1063–1084. doi: 10.1074/mcp.M900325-MCP200

Florez-Sarasa, I., Fernie, A. R., and Gupta, K. J. (2020). Does the alternative respiratory pathway offer protection against the adverse effects resulting from climate change? *J Exp Bot* 71, 465–469. doi: 10.1093/jxb/erz428

Florez-Sarasa, I., Flexas, J., Rasmusson, A. G., Umbach, A. L., Siedow, J. N., and Ribas-Carbo, M. (2011). In vivo cytochrome and alternative pathway respiration in leaves of Arabidopsis thaliana plants with altered alternative oxidase under different light conditions. *Plant Cell Environ* 34, 1373–1383. doi: 10.1111/j.1365-3040.2011.02337.x

Florez-Sarasa, I., Noguchi, K., Araújo, W. L., Garcia-Nogales, A., Fernie, A. R., Flexas, J., et al. (2016). Impaired cyclic electron flow around photosystem I disturbs high-light respiratory metabolism. *Plant Physiol* 172, 2176–2189. doi: 10.1104/pp.16.01025

Florez-Sarasa, I., Obata, T., Del-Saz, N. F., Reichheld, J. P., Meyer, E. H., Rodriguez-Concepcion, M., et al. (2019). The Lack of Mitochondrial Thioredoxin TRXo1 Affects in Vivo Alternative Oxidase Activity and Carbon Metabolism under Different Light Conditions. *Plant Cell Physiol* 60, 2369–2381. doi: 10.1093/pcp/pcz123

Forde, B. G., and Lea, P. J. (2007). Glutamate in plants: Metabolism, regulation, and signalling. *J Exp Bot* 58, 2339–2358. doi: 10.1093/jxb/erm121

Foyer, C. H., Kyndt, T., and Hancock, R. D. (2020). Vitamin C in Plants: Novel Concepts, New Perspectives, and Outstanding Issues. *Antioxid Redox Signal* 32, 463–485. doi: 10.1089/ars.2019.7819

Fraser, P. D., and Bramley, P. M. (2004). The biosynthesis and nutritional uses of carotenoids. *Prog Lipid Res* 43, 228–265. doi: 10.1016/j.plipres.2003.10.002

Fraser, P. D., Schuch, W., and Bramley, P. M. (2000). Phytoene synthase from tomato (Lycopersicon esculentum) chloroplasts - partial purification and biochemical properties. *Planta* 211, 361–369. doi: 10.1007/s004250000293

Fukano, Y., and Tachiki, Y. (2021). Evolutionary ecology of climacteric and non-climacteric fruits. *Biol Lett* 17. doi: 10.1098/rsbl.2021.0352

Galle, A., Florez-Sarasa, I., Thameur, A., De Paepe, R., Flexas, J., and Ribas-Carbo, M. (2010). Effects of drought stress and subsequent rewatering on photosynthetic and respiratory pathways in Nicotiana sylvestris wild type and the mitochondrial complex I-deficient CMSII mutant. *J Exp Bot* 61, 765–775. doi: 10.1093/jxb/erp344

Gámez-Arjona, F. M., De La Concepción, J. C., Raynaud, S., and Mérida, Á. (2014). Arabidopsis thaliana plastoglobule-associated fibrillin 1a interacts with fibrillin 1b in vivo. *FEBS Lett* 588, 2800–2804. doi: 10.1016/j.febslet.2014.06.024

Garcia, A., Gaju, O., Bowerman, A. F., Buck, S. A., Evans, J. R., Furbank, R. T., et al. (2023). Enhancing crop yields through improvements in the efficiency of photosynthesis and respiration. *New Phytologist* 237, 60–77. doi: 10.1111/nph.18545

Garcia-Molina, A., and Leister, D. (2020). Accelerated relaxation of photoprotection impairs biomass accumulation in Arabidopsis. *Nat Plants* 6, 9–12. doi: 10.1038/s41477-019-0572-z

Garmash, E. V., Dymova, O. V., Silina, E. V., Malyshev, R. V., Belykh, E. S., Shelyakin, M. A., et al. (2022). AOX1a Expression in Arabidopsis thaliana Affects the State of Chloroplast Photoprotective Systems under Moderately High Light Conditions. *Plants* 11. doi: 10.3390/plants11223030

Garmash, E. V., Velegzhaninov, I. O., Ermolina, K. V., Rybak, A. V., and Malyshev, R. V. (2020). Altered levels of AOX1a expression result in changes in metabolic pathways in Arabidopsis thaliana plants acclimated to low dose rates of ultraviolet B radiation. *Plant Science* 291. doi: 10.1016/j.plantsci.2019.110332

Garrido, A., Conde, A., Serôdio, J., De Vos, R. C. H., and Cunha, A. (2023). Fruit Photosynthesis: More to Know about Where, How and Why. *Plants* 12. doi: 10.3390/plants12132393

Giovannoni, J. J. (2004). Genetic regulation of fruit development and ripening. *Plant Cell* 16. doi: 10.1105/tpc.019158

Giovannoni, J., Nguyen, C., Ampofo, B., Zhong, S., and Fei, Z. (2017). The Epigenome and Transcriptional Dynamics of Fruit Ripening. *Annu Rev. Plant Biol*. 6, 61-84. doi: 10.1146/annurev-arplant-042916-040906

Giraud, E., Ho, L. H. M., Clifton, R., Carroll, A., Estavillo, G., Tan, Y. F., et al. (2008). The absence of Alternative Oxidase1a in Arabidopsis results in acute sensitivity to combined light and drought stress. *Plant Physiol* 147, 595–610. doi: 10.1104/pp.107.115121

Gomez-Casanovas, N., Blanc-Betes, E., Gonzalez-Meler, M. A., and Azcon-Bieto, J. (2007). Changes in respiratory mitochondrial machinery and cytochrome and alternative pathway activities in response to energy demand underlie the acclimation of respiration to elevated CO2 in the invasive Opuntia ficus-indica. *Plant Physiol* 145, 49–61. doi: 10.1104/pp.107.103911

Gong, Q., Li, S., Zheng, Y., Duan, H., Xiao, F., Zhuang, Y., et al. (2020). SUMOylation of MYB30 enhances salt tolerance by elevating alternative respiration via

transcriptionally upregulating AOX1a in Arabidopsis. *Plant Journal* 102, 1157–1171. doi: 10.1111/tpj.14689

González Guzmán, M., Cellini, F., Fotopoulos, V., Balestrini, R., and Arbona, V. (2022). New approaches to improve crop tolerance to biotic and abiotic stresses. *Physiol Plant* 174. doi: 10.1111/ppl.13547

Grant, N., Onda, Y., Kakizaki, Y., Ito, K., Watling, J., and Robinson, S. (2009). Two Cys or not two Cys? That is the question; alternative oxidase in the thermogenic plant sacred lotus. *Plant Physiol* 150, 987–995. doi: 10.1104/pp.109.139394

Gurrieri, L., Merico, M., Trost, P., Forlani, G., and Sparla, F. (2020). Impact of drought on soluble sugars and free proline content in selected arabidopsis mutants. *Biology* 9, 1–14. doi: 10.3390/biology9110367

Guy, R. D., and Vanlerberghe, G. C. (2005). Partitioning of respiratory electrons in the dark in leaves of transgenic tobacco with modified levels of alternative oxidase. *Physiol Plant* 125, 171–180. doi: 10.1111/j.1399-3054.2005.00557.x

Hesse, H., Kreft, O., Maimann, S., Zeh, M., and Hoefgen, R. (2004). Current understanding of the regulation of methionine biosynthesis in plants., in *Journal of Experimental Botany*, 1799–1808. doi: 10.1093/jxb/erh139

Hewitt, S., and Dhingra, A. (2020). Beyond Ethylene: New Insights Regarding the Role of Alternative Oxidase in the Respiratory Climacteric. *Front Plant Sci* 11. doi: 10.3389/fpls.2020.543958

Hoefnagel, M. H. N., Millar, A. H., Wiskich, J. T., and Day, D. A. (1995). Cytochrome and Alternative Respiratory Pathways Compete for Electrons in the Presence of Pyruvate in Soybean Mitochondria. *Arch Biochem Biophys* 318, 394–400. doi: 10.1006/abbi.1995.1245

Holtzapffel, R. C., Castelli, J., Finnegan, P. M., Millar, A. H., Whelan, J., and Day, D. A. (2003). A tomato alternative oxidase protein with altered regulatory properties. *Biochim Biophys Acta* 1606, 153–162. doi: 10.1016/j.bbabio.2003.08.001

Holtzapffel, R. C., Finnegan, P. M., Millar, A. H., Badger, M. R., and Day, D. A. (2002). Mitochondrial protein expression in tomato fruit during on-vine ripening and cold storage. *Functional Plant Biology* 29, 827–834. doi: 10.1071/PP01245

Howitt, C. A., and Pogson, B. J. (2006). Carotenoid accumulation and function in seeds and non-green tissues. *Plant Cell Environ* 29, 435–445. doi: 10.1111/j.1365-3040.2005.01492.x

Hummel, I., Pantin, F., Sulpice, R., Piques, M., Rolland, G., Dauzat, M., et al. (2010). Arabidopsis plants acclimate to water deficit at low cost through changes of carbon usage: An integrated perspective using growth, metabolite, enzyme, and gene expression analysis. *Plant Physiol* 154, 357–372. doi: 10.1104/pp.110.157008

Igamberdiev, A. U., and Bykova, N. V. (2023). Mitochondria in photosynthetic cells: Coordinating redox control and energy balance. *Plant Physiol* 191, 2104–2119. doi: 10.1093/plphys/kiac541

Iglesias-Sanchez, A., Navarro-Carcelen, J., Morelli, L., and Rodriguez-Concepcion, M. (2024). Arabidopsis FIBRILLIN6 influences carotenoid biosynthesis by directly promoting phytoene synthase activity. *Plant Physiol* 194, 1662–1673. doi: 10.1093/plphys/kiad613

Jahns, P., and Holzwarth, A. R. (2012). The role of the xanthophyll cycle and of lutein in photoprotection of photosystem II. *Biochim Biophys Acta Bioenerg* 1817, 182–193. doi: 10.1016/j.bbabio.2011.04.012

Jarvis, P., and López-Juez, E. (2013). Biogenesis and homeostasis of chloroplasts and other plastids. *Nat Rev Mol Cell Biol* 14, 787–802. doi: 10.1038/nrm3702

Josse, E. M., Alcaraz, J. P., Labouré, A. M., and Kuntz, M. (2003). In vitro characterization of a plastid terminal oxidase (PTOX). *Eur J Biochem* 270, 3787–3794. doi: 10.1046/j.1432-1033.2003.03766.x

Just, D., Garcia, V., Fernandez, L., Bres, C., Mauxion, J. P., Petit, J., et al. (2013). Micro-Tom mutants for functional analysis of target genes and discovery of new alleles in tomato. *Plant Biotechnology* 30, 225–231. doi: 10.5511/plantbiotechnology.13.0622a

Katz, Y. S., Galili, G., and Amir, R. (2006). Regulatory role of cystathionine-γ-synthase and de novo synthesis of methionine in ethylene production during tomato fruit ripening. *Plant Mol Biol* 61, 255–268. doi: 10.1007/s11103-006-0009-8

Kaur, G., Abugu, M., and Tieman, D. (2023). The dissection of tomato flavor: biochemistry, genetics, and omics. *Front Plant Sci* 14. doi: 10.3389/fpls.2023.1144113

Kavi Kishor, P. B., Suravajhala, P., Rathnagiri, P., and Sreenivasulu, N. (2022). Intriguing Role of Proline in Redox Potential Conferring High Temperature Stress Tolerance. *Front Plant Sci* 13. doi: 10.3389/fpls.2022.867531

Kazachkova, Y., Eshel, G., Pantha, P., Cheeseman, J. M., Dassanayake, M., and Barak, S. (2018). Halophytism: What have we learnt from arabidopsis thaliana relative model systems? *Plant Physiol* 178, 972–988. doi: 10.1104/pp.18.00863

Keunen, E., Schellingen, K., Van Der Straeten, D., Remans, T., Colpaert, J., Vangronsveld, J., et al. (2015). ALTERNATIVE OXIDASE1a modulates the oxidative challenge during moderate Cd exposure in Arabidopsis thaliana leaves. *J Exp Bot* 66, 2967–2977. doi: 10.1093/jxb/erv035

Kim, E.-H., Lee, Y., and Kim, H. U. (2015). Fibrillin 5 is essential for plastoquinone-9 biosynthesis by binding to solanesyl diphosphate synthases in *Arabidopsis*. *Plant Cell* 27, 2956–71. doi: 10.1105/tpc.15.00707

Kim, I., and Kim, H. U. (2022). The mysterious role of fibrillin in plastid metabolism: current advances in understanding. *J Exp Bot* 73, 2751–2764. doi: 10.1093/jxb/erac087

Klee, H. J., and Giovannoni, J. J. (2011). Genetics and control of tomato fruit ripening and quality attributes. *Annu Rev Genet* 45, 41–59. doi: 10.1146/annurev-genet-110410-132507

Kopka, J., Schauer, N., Krueger, S., Birkemeyer, C., Usadel, B., Bergmüller, E., et al. (2005). GMD@CSB.DB: The Golm metabolome database. *Bioinformatics* 21, 1635–1638. doi: 10.1093/bioinformatics/bti236

Kreslavski, V. D., Khudyakova, A. Y., Strokina, V. V., Shirshikova, G. N., Pashkovskiy, P. P., Balakhnina, T. I., et al. (2021). Impact of high irradiance and UV-B on the photosynthetic activity, pro-/antioxidant balance and expression of light-activated genes in Arabidopsis thaliana hy4 mutants grown under blue light. *Plant Physiology and Biochemistry* 167, 153–162. doi: 10.1016/j.plaphy.2021.07.030

Kromdijk, J., Głowacka, K., Leonelli, L., Gabilly, S. T., Iwai, M., Niyogi, K. K., et al. (2016). Improving photosynthesis and crop productivity by accelerating recovery from photoprotection. *Science (1979)* 354, 857–861. doi: 10.1126/science.aaf9621

Kromer, S. (1995). Respiration during Photosynthesis. *Annu. Rev. Plant Physiol. Plant Mol. Bioi* 46, 45–70.

Kromer, S., Malmberg, G., Gardestrom, P., and Trygger Samfundet, C. (1993). Mitochondrial Contribution to Photosynthetic Metabolism(A Study with Barley (Hordeum vulgare L.) Leaf Protoplasts at Different Light lntensities and CO, Concentrations). *Plant Physiol* 1, 947–955. doi: 10.1104/pp.102.3.947

Laizet, Y., Pontier, D., Mache, R., and Kuntz, M. (2004). Subfamily Organization and Phylogenetic Origin of Genes Encoding Plastid Lipid-Associated Proteins of the Fibrillin Type. *Journal of Genome Science and Technology* 3, 19–28. doi: 10.1166/gl.2004.038

Lambers, H., and Oliveira, R. S. (2019). "Photosynthesis, Respiration, and Long-Distance Transport: Photosynthesis," in *Plant Physiological Ecology* 11, 114. doi: 10.1007/978-3-030-29639-1_2

Lee, K., Lehmann, M., Paul, M. V., Wang, L., Luckner, M., Wanner, G., et al. (2020). Lack of FIBRILLIN6 in Arabidopsis thaliana affects light acclimation and sulfate metabolism. *New Phytologist* 225, 1715–1731. doi: 10.1111/nph.16246

Leitner-Dagan, Y., Ovadis, M., Shklarman, E., Elad, Y., David, D. R., and Vainstein, A. (2006). Expression and functional analyses of the plastid lipid-associated protein CHRC suggest its role in chromoplastogenesis and stress. *Plant Physiol* 142, 233–244. doi: 10.1104/pp.106.082404

Li, J., Yang, S., Wu, Y., Wang, R., Liu, Y., Liu, J., et al. (2024). Alternative Oxidase: From Molecule and Function to Future Inhibitors. *ACS Omega* 9, 12478–12499. doi: 10.1021/acsomega.3c09339

Li, S., Chen, K., and Grierson, D. (2019). A critical evaluation of the role of ethylene and MADS transcription factors in the network controlling fleshy fruit ripening. *New Phytologist* 221, 1724–1741. doi: 10.1111/nph.15545

Li, Y. T., Liu, M. J., Li, Y., Liu, P., Zhao, S. J., Gao, H. Y., et al. (2020). Photoprotection by mitochondrial alternative pathway is enhanced at heat but disabled at chilling. *Plant Journal* 104, 403–415. doi: 10.1111/tpj.14931

Liang, M. H., Zhu, J., and Jiang, J. G. (2018). Carotenoids biosynthesis and cleavage related genes from bacteria to plants. *Crit Rev Food Sci Nutr* 58, 2314–2333. doi: 10.1080/10408398.2017.1322552

Lisec, J., Schauer, N., Kopka, J., Willmitzer, L., and Fernie, A. R. (2006). Gas chromatography mass spectrometry-based metabolite profiling in plants. *Nat Protoc* 1, 387–396. doi: 10.1038/nprot.2006.59

Liu, H., Ding, Y., Zhou, Y., Jin, W., Xie, K., and Chen, L. L. (2017). CRISPR-P 2.0: An Improved CRISPR-Cas9 Tool for Genome Editing in Plants. *Mol Plant* 10, 530–532. doi: 10.1016/j.molp.2017.01.003

Livak, K. J., and Schmittgen, T. D. (2001). Analysis of relative gene expression data using real-time quantitative PCR and the 2-ΔΔCT method. *Methods* 25, 402–408. doi: 10.1006/meth.2001.1262

Llorente, B., D'Andrea, L., and Rodríguez-Concepción, M. (2016). Evolutionary recycling of light signaling components in fleshy fruits: New insights on the role of pigments to monitor ripening. *Front Plant Sci* 7. doi: 10.3389/fpls.2016.00263

Loreto, F., Centritto, M., Barta, C., Calfapietra, C., Fares, S., and Monson, R. K. (2007). The relationship between isoprene emission rate and dark respiration rate in white poplar (Populus alba L.) leaves. *Plant Cell Environ* 30, 662–669. doi: 10.1111/j.1365-3040.2007.01648.x

Luedemann, A., Von Malotky, L., Erban, A., and Kopka, J. (2012). TagFinder: Preprocessing software for the fingerprinting and the profiling of gas chromatography-mass spectrometry based metabolome analyses. *Methods in Molecular Biology* 860, 255–286. doi: 10.1007/978-1-61779-594-7_16

Lundquist, P. K., Poliakov, A., Bhuiyan, N. H., Zybailov, B., Sun, Q., and van Wijk, K. J. (2012). The functional network of the arabidopsis plastoglobule proteome based on quantitative proteomics and genome-wide coexpression analysis. *Plant Physiol* 158, 1172–1192. doi: 10.1104/pp.111.193144

Lytovchenko, A., Eickmeier, I., Pons, C., Osorio, S., Szecowka, M., Lehmberg, K., et al. (2011). Tomato fruit photosynthesis is seemingly unimportant in primary metabolism and ripening but plays a considerable role in seed development. *Plant Physiol* 157, 1650–1663. doi: 10.1104/pp.111.186874

Maaroufi-Dguimi, H., Debouba, M., Gaufichon, L., Clément, G., Gouia, H., Hajjaji, A., et al. (2011). An Arabidopsis mutant disrupted in ASN2 encoding asparagine synthetase 2 exhibits low salt stress tolerance. *Plant Physiology and Biochemistry* 49, 623–628. doi: 10.1016/j.plaphy.2011.03.010

Margaria, P., and Palmano, S. (2011). Response of the Vitis vinifera L. cv. "Nebbiolo" proteome to Flavescence dorée phytoplasma infection. *Proteomics* 11, 212–224. doi: 10.1002/pmic.201000409

Martí, M. C., Florez-Sarasa, I., Camejo, D., Ribas-Carbó, M., Lázaro, J. J., Sevilla, F., et al. (2011). Response of mitochondrial thioredoxin PsTrxo1, antioxidant enzymes, and respiration to salinity in pea (Pisum sativum L.) leaves. *J Exp Bot* 62, 3863–3874. doi: 10.1093/jxb/err076

Matos, I. F., Morales, L. M. M., Santana, D. B., Silva, G. M. C., Gomes, M. M. de A., Ayub, R. A., et al. (2022). Ascorbate synthesis as an alternative electron source for

mitochondrial respiration: Possible implications for the plant performance. *Front Plant Sci* 13. doi: 10.3389/fpls.2022.987077

Mattoo, A. K., Sobolev, A. P., Neelam, A., Goyal, R. K., Handa, A. K., and Segre, A. L. (2006). Nuclear magnetic resonance spectroscopy-based metabolite profiling of transgenic tomato fruit engineered to accumulate spermidine and spermine reveals enhanced anabolic and nitrogen-carbon interactions. *Plant Physiol* 142, 1759–1770. doi: 10.1104/pp.106.084400

McDonald, A. E. (2023). Unique opportunities for future research on the alternative oxidase of plants. *Plant Physiol* 191, 2084–2092. doi: 10.1093/plphys/kiac555

Mcdonald, A. E., Sieger, S. M., and Vanlerberghe, G. C. (2002). Methods and approaches to study plant mitochondrial alternative oxidase. *Physiol Plant* 116, 135–243. doi: 10.1034/j.1399-3054.2002.1160201.x

Meléndez-Martínez, A. J. (2019). An Overview of Carotenoids, Apocarotenoids, and Vitamin A in Agro-Food, Nutrition, Health, and Disease. *Mol Nutr Food Res* 63. doi: 10.1002/mnfr.201801045

Millar, A. H., Mittova, V., Kiddle, G., Heazlewood, J. L., Bartoli, C. G., Theodoulou, F. L., et al. (2003). Control of Ascorbate Synthesis by Respiration and Its Implications for Stress Responses. *Plant Physiol* 133, 443–447. doi: 10.1104/pp.103.028399

Moller, I. M. (2001). Plant Mitochondria and Oxidative Stress: Electron Transport, NADPH Turnover, and Metabolism of Reactive Oxygen Species. *Annu. Rev. Plant Physiol. Plant Mol. Biol* 52, 561–91. doi: doi:10.1146/annurev.arplant.52.1.561

Moller, I. M., Bérczi, A., Van Der Plas, L. H. W., and Lambers, H. (1988). Measurement of the activity and capacity of the alternative pathway in intact plant tissues: Identification of problems and possible solutions. *Physiologia Plantarum* 72, 642–649. doi: 10.1111/j.1399-3054.1988.tb09176.x

Moller, I. M., Rasmusson, A. G., and Van Aken, O. (2021). Plant mitochondria – past, present and future. *Plant Journal* 108, 912–959. doi: 10.1111/tpj.15495

Morelli, L., Paulišić, S., Qin, W., Iglesias-Sanchez, A., Roig-Villanova, I., Florez-Sarasa, I., et al. (2021). Light signals generated by vegetation shade facilitate acclimation to low light in shade-avoider plants. *Plant Physiol* 186, 2137–2151. doi: 10.1093/plphys/kiab206

Morelli, L., and Rodriguez-Concepcion, M. (2023). Open avenues for carotenoid biofortification of plant tissues. *Plant Commun* 4. doi: 10.1016/j.xplc.2022.100466

Morelli, L., Torres-Montilla, S., Glauser, G., Shanmugabalaji, V., Kessler, F., and Rodriguez-Concepcion, M. (2023). Novel insights on the contribution of plastoglobules and reactive oxygen species to chromoplast differentiation. *New Phytol, 237: 1696-1710.* 237, 1696–1710. doi: https://doi.org/10.1111/nph.18585

Munns, R., Day, D. A., Fricke, W., Watt, M., Arsova, B., Barkla, B. J., et al. (2020). Energy costs of salt tolerance in crop plants. *New Phytologist* 225, 1072–1090. doi: 10.1111/nph.15864

Munns, R., and Gilliham, M. (2015). Salinity tolerance of crops - what is the cost? *New Phytologist* 208, 668–673. doi: 10.1111/nph.13519

Neelwarne (2015a). "Alternative respiratory pathways in higher plants," in *Alternative respiratory pathways in higher plants*, (John Wiley and Sons, Ltd), i–xv. doi: 10.1002/9781118789971.fmatter

Neelwarne, B. (2015b). Alternative respiratory pathway in ripening fruits. *Alternative respiratory pathways in higher plants*, 201–219.

Noguchi, K., and Yoshida, K. (2008). Interaction between photosynthesis and respiration in illuminated leaves. *Mitochondrion* 8, 87–99. doi: 10.1016/j.mito.2007.09.003

Nunes-Nesi, A., Carrari, F., Gibon, Y., Sulpice, R., Lytovchenko, A., Fisahn, J., et al. (2007). Deficiency of mitochondrial fumarase activity in tomato plants impairs photosynthesis via an effect on stomatal function. *Plant Journal* 50, 1093–1106. doi: 10.1111/j.1365-313X.2007.03115.x

Oh, G. G. K., O'Leary, B. M., Signorelli, S., and Harvey Millar, A. (2022). Alternative oxidase (AOX) 1a and 1d limit prolineinduced oxidative stress and aid salinity recovery in Arabidopsis. *Plant Physiol* 188, 1521–1536. doi: 10.1093/plphys/kiab578

O'Leary, B. M., Asao, S., Millar, A. H., and Atkin, O. K. (2019). Core principles which explain variation in respiration across biological scales. *New Phytologist* 222, 670–686. doi: 10.1111/nph.15576

Osorio, S., Alba, R., Damasceno, C. M. B., Lopez-Casado, G., Lohse, M., Zanor, M. I., et al. (2011). Systems biology of tomato fruit development: Combined transcript, protein, and metabolite analysis of tomato transcription factor (nor, rin) and ethylene receptor (Nr) mutants reveals novel regulatory interactions. *Plant Physiol* 157, 405–425. doi: 10.1104/pp.111.175463

Osorio, S., Carneiro, R. T., Lytovchenko, A., McQuinn, R., Sørensen, I., Vallarino, J. G., et al. (2020). Genetic and metabolic effects of ripening mutations and vine

detachment on tomato fruit quality. *Plant Biotechnol J* 18, 106–118. doi: 10.1111/pbi.13176

Paulišić, S., Qin, W., Arora Verasztó, H., Then, C., Alary, B., Nogue, F., et al. (2021). Adjustment of the PIF7-HFR1 transcriptional module activity controls plant shade adaptation. *EMBO J* 40, 1–16. doi: 10.15252/embj.2019104273

Pires, M. V., Pereira Júnior, A. A., Medeiros, D. B., Daloso, D. M., Pham, P. A., Barros, K. A., et al. (2016). The influence of alternative pathways of respiration that utilize branched-chain amino acids following water shortage in Arabidopsis. *Plant Cell Environ* 39, 1304–1319. doi: 10.1111/pce.12682

Podgórska, A., Mazur, R., Ostaszewska-Bugajska, M., Kryzheuskaya, K., Dziewit, K., Borysiuk, K., et al. (2020). Efficient Photosynthetic Functioning of Arabidopsis thaliana Through Electron Dissipation in Chloroplasts and Electron Export to Mitochondria Under Ammonium Nutrition. *Front Plant Sci* 11. doi: 10.3389/fpls.2020.00103

Pokhilko, A., Bou-Torrent, J., Pulido, P., Rodríguez-Concepción, M., and Ebenhöh, O. (2015). Mathematical modelling of the diurnal regulation of the MEP pathway in Arabidopsis. *New Phytologist* 206, 1075–1085. doi: 10.1111/nph.13258

Pott, D. M., Osorio, S., and Vallarino, J. G. (2019). From central to specialized metabolism: An overview of some secondary compounds derived from the primary metabolism for their role in conferring nutritional and organoleptic characteristics to fruit. *Front Plant Sci* 10, 835–854. doi: 10.3389/fpls.2019.00835

Quinet, M., Angosto, T., Yuste-Lisbona, F. J., Blanchard-Gros, R., Bigot, S., Martinez, J. P., et al. (2019). Tomato Fruit Development and Metabolism. *Front Plant Sci* 10. doi: 10.3389/fpls.2019.01554

Raghavendra, A. S., and Padmasree, K. (2003). Beneficial interactions of mitochondrial metabolism with photosynthetic carbon assimilation. *Trends Plant Sci* 8, 546–553. doi: 10.1016/j.tplants.2003.09.015

Ranocha, P., McNeil, S. D., Ziemak, M. J., Li, C., Tarczynski, M. C., and Hanson, A. D. (2001). The S-methylmethionine cycle in angiosperms: Ubiquity, antiquity and activity. *Plant Journal* 25, 575–584. doi: 10.1046/j.1365-313X.2001.00988.x

Rasmusson, A. G., Fernie, A. R., and Van Dongen, J. T. (2009). Alternative oxidase: A defence against metabolic fluctuations? *Physiol Plant* 137, 371–382. doi: 10.1111/j.1399-3054.2009.01252.x

Renato, M., Boronat, A., and Azcón-Bieto, J. (2015). Respiratory processes in non-photosynthetic plastids. *Front Plant Sci* 6. doi: 10.3389/fpls.2015.00496

Renato, M., Pateraki, I., Boronat, A., and Azcón-Bieto, J. (2014). Tomato fruit chromoplasts behave as respiratory bioenergetic organelles during ripening. *Plant Physiol* 166, 920–933. doi: 10.1104/pp.114.243931

Ribas-Carbo, M., Berry, J. A., Yakir, D., Giles, L., Robinson, S. A., Lennon, A. M., et al. (1995). Electron Partitioning between the Cytochrome and Alternative Pathways in Plant Mitochondria'. *Plant Physiol* 109, 829–837. doi: 10.1104/pp.109.3.829

Ribas-Carbo, M., Lennon, A. M., Robinson, S. A., Ciles, L., Berry, J. A., and Siedow, J. N. (1997). The Regulation of Electron Partitioning between the Cytochrome and Alternative Pathways in Soybean Cotyledon and Root Mitochondria. *Plant Physiol* 113, 903–91. doi: 10.1104/pp.113.3.903

Ribas-Carbo, M., Taylor, N. L., Giles, L., Busquets, S., Finnegan, P. M., Day, D. A., et al. (2005). Effects of water stress on respiration in soybean leaves. *Plant Physiol* 139, 466–473. doi: 10.1104/pp.105.065565

Rodriguez-Concepcion, M., Avalos, J., Bonet, M. L., Boronat, A., Gomez-Gomez, L., Hornero-Mendez, D., et al. (2018). A global perspective on carotenoids: Metabolism, biotechnology, and benefits for nutrition and health. *Prog Lipid Res* 70, 62–93. doi: 10.1016/j.plipres.2018.04.004

Rodríguez-Concepción, M., and Boronat, A. (2015). Breaking new ground in the regulation of the early steps of plant isoprenoid biosynthesis. *Curr Opin Plant Biol* 25, 17–22. doi: 10.1016/j.pbi.2015.04.001

Rodríguez-Villalón, A., Gas, E., and Rodríguez-Concepción, M. (2009). Phytoene synthase activity controls the biosynthesis of carotenoids and the supply of their metabolic precursors in dark-grown Arabidopsis seedlings. *Plant Journal* 60, 424–435. doi: 10.1111/j.1365-313X.2009.03966.x

Romero-Aguilar, L., Cárdenas-Monroy, C., Garrido-Bazán, V., Aguirre, J., Guerra-Sánchez, G., and Pardo, J. P. (2020). On the use of n-octyl gallate and salicylhydroxamic acid to study the alternative oxidase role. *Arch Biochem Biophys* 694. doi: 10.1016/j.abb.2020.108603

Sadali, N. M., Sowden, R. G., Ling, Q., and Jarvis, R. P. (2019). Differentiation of chromoplasts and other plastids in plants. *Plant Cell Rep* 38, 803–818. doi: 10.1007/s00299-019-02420-2

Saisho, D., Nambara, E., Naito, S., Tsutsumi, N., Hirai, A., and Nakazono, M. (1997). Characterization of the gene family for alternative oxidase from Arabidopsis thaliana. Kluwer Academic Publishers. doi: doi: 10.1023/A:1005818507743

Sanchez, D. H., Siahpoosh, M. R., Roessner, U., Udvardi, M., and Kopka, J. (2008). Plant metabolomics reveals conserved and divergent metabolic responses to salinity. *Physiol Plant* 132, 209–219. doi: 10.1111/j.1399-3054.2007.00993.x

Sánchez-Guerrero, A., Fernández del-Saz, N., Florez-Sarasa, I., Ribas-Carbó, M., Fernie, A. R., Jiménez, A., et al. (2019). Coordinated responses of mitochondrial antioxidative enzymes, respiratory pathways and metabolism in Arabidopsis thaliana thioredoxin trxo1 mutants under salinity. *Environ Exp Bot* 162, 212–222. doi: 10.1016/j.envexpbot.2019.02.026

Sanhueza, C., Bascunan-Godoy, L., Corcuera, L. J., and Turnbull, M. H. (2013). The response of leaf respiration to water stress in Nothofagus species. *New Zealand Journal of Botany* 51, 88–103. doi: 10.1080/0028825X.2012.759600

Schmidt, M., Geßner, G., Luff, M., Heiland, I., Wagner, V., Kaminski, M., et al. (2006). Proteomic analysis of the eyespot of Chlamydomonas reinhardtii provides novel insights into its components and tactic movements. *Plant Cell* 18, 1908–1930. doi: 10.1105/tpc.106.041749

Selinski, J., Hartmann, A., Deckers-Hebestreit, G., Day, D. A., Whelan, J., and Scheibe, R. (2018a). Alternative oxidase isoforms are differentially activated by tricarboxylic acid cycle intermediates. *Plant Physiol* 176, 1423–1432. doi: 10.1104/pp.17.01331

Selinski, J., Scheibe, R., Day, D. A., and Whelan, J. (2018b). Alternative Oxidase Is Positive for Plant Performance. *Trends Plant Sci* 23, 588–597. doi: 10.1016/j.tplants.2018.03.012

Shabala, S., and Shabala, L. (2011). Ion transport and osmotic adjustment in plants and bacteria. *Biomol Concepts* 2, 407–419. doi: 10.1515/BMC.2011.032

Shahbazi, M., Gilbert, M., Labouré, A. M., and Kuntz, M. (2007). Dual role of the plastid terminal oxidase in tomato. *Plant Physiol* 145, 691–702. doi: 10.1104/pp.107.106336

Shameer, S., Ratcliffe, R. G., and Sweetlove, L. J. (2019). Leaf energy balance requires mitochondrial respiration and export of chloroplast NADPH in the light. *Plant Physiol* 180, 1947–1961. doi: 10.1104/pp.19.00624

Shanmugabalaji, V., Besagni, C., Piller, L. E., Douet, V., Ruf, S., Bock, R., et al. (2013). Dual targeting of a mature plastoglobulin/fibrillin fusion protein to chloroplast

plastoglobules and thylakoids in transplastomic tobacco plants. *Plant Mol Biol* 81, 13–25. doi: 10.1007/s11103-012-9977-z

Shanmugabalaji, V., Zita, W., Collombat, J., and Kessler, F. (2022). "Plastoglobules: A hub of lipid metabolism in the chloroplast," in *Advances in Botanical Research*, (Academic Press Inc.), 91–119. doi: 10.1016/bs.abr.2021.09.002

Singh, D. K., Laremore, T. N., Smith, P. B., Maximova, S. N., and McNellis, T. W. (2012). Knockdown of FIBRILLIN4 Gene Expression in Apple Decreases Plastoglobule Plastoquinone Content. *PLoS One* 7, 1–10. doi: 10.1371/journal.pone.0047547

Singh, D. K., and McNellis, T. W. (2011). Fibrillin protein function: The tip of the iceberg? *Trends Plant Sci* 16, 432–441. doi: 10.1016/j.tplants.2011.03.014

Slama, I., Abdelly, C., Bouchereau, A., Flowers, T., and Savouré, A. (2015). Diversity, distribution and roles of osmoprotective compounds accumulated in halophytes under abiotic stress. *Ann Bot* 115, 433–447. doi: 10.1093/aob/mcu239

Smith, C. A., Melino, V. J., Sweetman, C., and Soole, K. L. (2009). Manipulation of alternative oxidase can influence salt tolerance in Arabidopsis thaliana. *Physiol Plant* 137, 459–472. doi: 10.1111/j.1399-3054.2009.01305.x

Strodtkötter, I., Padmasree, K., Dinakar, C., Speth, B., Niazi, P. S., Wojtera, J., et al. (2009). Induction of the AOX1D isoform of alternative oxidase in A. thaliana T-DNA insertion lines lacking isoform AOX1A is insufficient to optimize photosynthesis when treated with antimycin a. *Mol Plant* 2, 284–297. doi: 10.1093/mp/ssn089

Sun, H., Ren, M., and Zhang, J. (2022). Genome-wide identification and expression analysis of fibrillin (FBN) gene family in tomato (Solanum lycopersicum L.). *PeerJ* 10. doi: 10.7717/peerj.13414

Suzuki, M., Takahashi, S., Kondo, T., Dohra, H., Ito, Y., Kiriiwa, Y., et al. (2015). Plastid proteomic analysis in tomato fruit development. *PLoS One* 10. doi: 10.1371/journal.pone.0137266

Sweetlove, L. J., Beard, K. F. M., Nunes-Nesi, A., Fernie, A. R., and Ratcliffe, R. G. (2010). Not just a circle: Flux modes in the plant TCA cycle. *Trends Plant Sci* 15, 462–470. doi: 10.1016/j.tplants.2010.05.006

Szabados, L., and Savouré, A. (2010). Proline: a multifunctional amino acid. *Trends Plant Sci* 15, 89–97. doi: 10.1016/j.tplants.2009.11.009

Terry, L. I., Roemer, R. B., Booth, D. T., Moore, C. J., and Walter, G. H. (2016). Thermogenic respiratory processes drive the exponential increase of volatile organic compound emissions in Macrozamia cycad cones. *Plant Cell Environ* 39, 1588–1600. doi: 10.1111/pce.12730

Thalmann, M., and Santelia, D. (2017). Starch as a determinant of plant fitness under abiotic stress. *New Phytologist* 214, 943–951. doi: 10.1111/nph.14491

Theologis, A., and Laties, G. G. (1978). Respiratory Contribution of the Alternate Path during Various Stages of Ripening in Avocado and Banana Fruits. *Plant Physiol* 62, 249–255. doi: 10.1104/pp.62.2.249

Toledo-Ortiz, G., Huq, E., and Rodríguez-Concepción, M. (2010). Direct regulation of phytoene synthase gene expression and carotenoid biosynthesis by phytochrome-interacting factors. *Proc Natl Acad Sci U S A* 107, 11626–11631. doi: 10.1073/pnas.0914428107

Torres-Montilla, S., and Rodriguez-Concepcion, M. (2021). Making extra room for carotenoids in plant cells: New opportunities for biofortification. *Prog Lipid Res* 84. doi: 10.1016/j.plipres.2021.101128

Torres-Romero, D., Gomez-Zambrano, A., Serrato, A. J., Sahrawy, M., and Merida, A. (2022). Arabidopsis fibrillin 1-2 subfamily members exert their functions via specific protein-protein interactions. *J Exp Bot* 73, 903–914. doi: 10.1093/jxb/erab452

Trudel, M. J., and Ozbun, J. L. (1970). Relationship between Chlorophylls and Carotenoids of Ripening Tomato Fruit as Influenced by Potassium Nutrition. *J Exp Bot* 21, 8–9. doi: 10.1093/jxb/21.4.881

Tucker, G. A. (1993). *Biochemistry of fruit ripening*. Chapman and Hall 1, 1-51. doi: 10.1007/978-94-011-1584-1

Umbach, A. L., Fiorani, F., and Siedow, J. N. (2005). Characterization of transformed Arabidopsis with altered alternative oxidase levels and analysis of effects on reactive oxygen species in tissue. *Plant Physiol* 139, 1806–1820. doi: 10.1104/pp.105.070763

Vainstein, A., Halevy, A. H., Smirra, L., and Vishnevetsky, M. (1994). Chromoplast Biogenesis in Cucumis sativus Corollas' Rapid Effect of Gibberellin A3 on the Accumulation of a Chromoplast-Specific Carotenoid-Associated Protein. *Plant Physiol* 104, 321–326. doi: 10.1104/pp.104.2.321

Van Wijk, K. J., and Kessler, F. (2017). Plastoglobuli: Plastid Microcompartments with Integrated Functions in Metabolism, Plastid Developmental Transitions, and Environmental Adaptation. *Annu Rev Plant Biol* 68, 253–289. doi: 10.1146/annurev-arplant-043015-111737

Vanlerberghe, G. C. (2013). Alternative oxidase: A mitochondrial respiratory pathway to maintain metabolic and signaling homeostasis during abiotic and biotic stress in plants. *Int J Mol Sci* 14, 6805–6847. doi: 10.3390/ijms14046805

Vanlerberghe, G. C., Dahal, K., Alber, N. A., and Chadee, A. (2020). Photosynthesis, respiration and growth: A carbon and energy balancing act for alternative oxidase. *Mitochondrion* 52, 197–211. doi: 10.1016/j.mito.2020.04.001

Ventura, Y., Eshel, A., Pasternak, D., and Sagi, M. (2015). The development of halophyte-based agriculture: Past and present. *Ann Bot* 115, 529–540. doi: 10.1093/aob/mcu173

Vercesi, A. E., Borecký, J., De Godoy Maia, I., Arruda, P., Cuccovia, I. M., and Chaimovich, H. (2006). Plant uncoupling mitochondrial proteins. *Annu Rev Plant Biol* 57, 383–404. doi: 10.1146/annurev.arplant.57.032905.105335

Vishwakarma, A., Tetali, S. D., Selinski, J., Scheibe, R., and Padmasree, K. (2015). Importance of the alternative oxidase (AOX) pathway in regulating cellular redox and ROS homeostasis to optimize photosynthesis during restriction of the cytochrome oxidase pathway in Arabidopsis thaliana. *Ann Bot* 116, 555–569. doi: 10.1093/aob/mcv122

Watanabe, C. K., Hachiya, T., Takahara, K., Kawai-Yamada, M., Uchimiya, H., Uesono, Y., et al. (2010). Effects of aox1a deficiency on plant growth, gene expression of respiratory components and metabolic profile under low-nitrogen stress in arabidopsis thaliana. *Plant Cell Physiol* 51, 810–822. doi: 10.1093/pcp/pcq033

Watling, J. R., Robinson, S. A., and Seymour, R. S. (2006). Contribution of the alternative pathway to respiration during thermogenesis in flowers of the sacred lotus. *Plant Physiol* 140, 1367–1373. doi: 10.1104/pp.105.075523

Welchen, E., Canal, M. V., Gras, D. E., and Gonzalez, D. H. (2021). Cross-talk between mitochondrial function, growth, and stress signalling pathways in plants. *J Exp Bot* 72, 4102–4118. doi: 10.1093/jxb/eraa608

Welsch, R., Zhou, X., Yuan, H., Álvarez, D., Sun, T., Schlossarek, D., et al. (2018). Clp Protease and OR Directly Control the Proteostasis of Phytoene Synthase, the Crucial Enzyme for Carotenoid Biosynthesis in Arabidopsis. *Mol Plant* 11, 149–162. doi: 10.1016/j.molp.2017.11.003

Winkenbach, F., Falk, H., Liedvogel, B., and Sitte, P. (1976). Chromoplasts of Tropaeolum majus L.: Isolation and characterization of lipoprotein elements. *Planta* 128, 23–28. doi: 10.1007/BF00397174

Xu, F., Copsey, A. C., Young, L., Barsottini, M. R. O., Albury, Ma. S., and Moore, A. L. (2021). Comparison of the Kinetic Parameters of Alternative Oxidases From Trypanosoma brucei and Arabidopsis thaliana: A Tale of Two Cavities. *Front Plant Sci* 12. doi: 10.3389/fpls.2021.744218

Xu, F., Yuan, S., Zhang, D. W., Lv, X., and Lin, H. H. (2012). The role of alternative oxidase in tomato fruit ripening and its regulatory interaction with ethylene. *J Exp Bot* 63, 5705–5716. doi: 10.1093/jxb/ers226

Yang, S., and Hoffman, N. E. (1984). Ethylene Biosynthesis and its Regulation in Higher Plants. *Annu Rev Plant Biol* 35, 155–189. doi: 10.1146/annurev.pp.35.060184.001103

Yang, Y., Sulpice, R., Himmelbach, A., Meinhard, M., Christmann, A., and Grill, E. (2006). Fibrillin expression is regulated by abscisic acid response regulators and is involved in abscisic acid-mediated photoprotection. *Proceedings of the National Academy of Sciences* 103, 6061–6066. doi: 10.1073/pnas.0501720103

Yoshida, K., Terashima, I., and Noguchi, K. (2007). Up-regulation of mitochondrial alternative oxidase concomitant with chloroplast over-reduction by excess light. *Plant Cell Physiol* 48, 606–614. doi: 10.1093/pcp/pcm033

Ytterberg, A. J., Peltier, J. B., and Van Wijk, K. J. (2006). Protein profiling of plastoglobules in chloroplasts and chromoplasts. A surprising site for differential accumulation of metabolic enzymes. *Plant Physiol* 140, 984–997. doi: 10.1104/pp.105.076083

Zhang, D. W., Yuan, S., Xu, F., Zhu, F., Yuan, M., Ye, H. X., et al. (2016). Light intensity affects chlorophyll synthesis during greening process by metabolite signal from mitochondrial alternative oxidase in Arabidopsis. *Plant Cell Environ* 39, 12–25. doi: 10.1111/pce.12438

Zhang, Y., Butelli, E., Alseekh, S., Tohge, T., Rallapalli, G., Luo, J., et al. (2015). Multi-level engineering facilitates the production of phenylpropanoid compounds in tomato. *Nat Commun* 6. doi: 10.1038/ncomms9635

Zhang, Z. S., Liu, M. J., Scheibe, R., Selinski, J., Zhang, L. T., Yang, C., et al. (2017). Contribution of the Alternative Respiratory Pathway to PSII Photoprotection in C3 and C4 Plants. *Mol Plant* 10, 131–142. doi: 10.1016/j.molp.2016.10.004

Zhou, X., Rao, S., Wrightstone, E., Sun, T., Lui, A. C. W., Welsch, R., et al. (2022a). Phytoene Synthase: The Key Rate-Limiting Enzyme of Carotenoid Biosynthesis in Plants. *Front Plant Sci* 13. doi: 10.3389/fpls.2022.884720

Zhou, X., Rao, S., Wrightstone, E., Sun, T., Lui, A. C. W., Welsch, R., et al. (2022b). Phytoene Synthase: The Key Rate-Limiting Enzyme of Carotenoid Biosynthesis in Plants. *Front Plant Sci* 13. doi: 10.3389/fpls.2022.884720

Zhou, X., Sun, T., Owens, L., Yang, Y., Fish, T., Wrightstone, E., et al. (2023). Carotenoid sequestration protein FIBRILLIN participates in CmOR-regulated β-carotene accumulation in melon. *Plant Physiol* 193, 643–660. doi: 10.1093/plphys/kiad312

Zhu, T., Zou, L., Li, Y., Yao, X., Xu, F., Deng, X., et al. (2018). Mitochondrial alternative oxidase-dependent autophagy involved in ethylene-mediated drought tolerance in Solanum lycopersicum. *Plant Biotechnol J* 16, 2063–2076. doi: 10.1111/pbi.12939

Annex 1

https://doi.org/10.1093/plphys/kiad613 PLANT PHYSIOLOGY 2024: 194: 1662–1673

Plant Physiology®

ResearchArticle

Arabidopsis FIBRILLIN6 influences carotenoid biosynthesis by directly promoting phytoene synthase activity

Ariadna Iglesias-Sanchez [1,2,†], Juan Navarro-Carcelen [1,†], Luca Morelli [1,2,‡] and Manuel Rodriguez-Concepcion [1,*]

1 Institute for Plant Molecular and Cell Biology (IBMCP), CSIC-Universitat Politècnica de València, Valencia 46022, Spain
2 Centre for Research in Agricultural Genomics (CRAG) CSIC-IRTA-UAB-UB, Campus UAB Bellaterra, Barcelona 08193, Spain

*Author for correspondence: manuelrc@ibmcp.upv.es
†Equal contributors, in alphabetical order.
‡Present address: Department of Biology & CESAM & ECOMARE, Universidade de Aveiro, Aveiro 3810-193, Portugal.
The author responsible for distribution of materials integral to the findings presented in this article in accordance with the policy described in the Instructions for Authors (https://academic.oup.com/plphys/pages/General-Instructions) is Manuel Rodriguez-Concepción.

Abstract

Carotenoids are health-promoting plastidial isoprenoids with essential functions in plants as photoprotectants and photosynthetic pigments in chloroplasts. They also accumulate in specialized plastids named chromoplasts, providing color to non- photosynthetic tissues such as flower petals and ripe fruit. Carotenoid accumulation in chromoplasts requires specialized structures and proteins such as fibrillins (FBNs). The FBN family includes structural components of carotenoid sequestering structures in chromoplasts and members with metabolic roles in chloroplasts and other plastid types. However, the association of FBNs with carotenoids in plastids other than chromoplasts has remained unexplored. Here, we show that Arabidopsis (*Arabidopsis thaliana*) FBN6 interacts with phytoene synthase (PSY), the first enzyme of the carotenoid pathway. FBN6, but not FBN4 (a FBN that does not interact with PSY), enhances the activity of plant PSY (but not of the bacterial PSY crtB) in *Escherichia coli* cells. Overexpression of FBN6 in *Nicotiana benthamiana* leaves results in a higher production of phytoene, the product of PSY activity, whereas loss of FBN6 activity in Arabidopsis mutants dramatically reduces the production of carotenoids during seedling de-etiolation and after exposure to high light. Our work hence demonstrates that FBNs promote not only the accumulation of carotenoids in chromoplasts but also their biosynthesis in chloroplasts.

Received September 12, 2023. Accepted October 18, 2023. Advance access publication November 15, 2023

Open Access

© The Author(s) 2023. Published by Oxford University Press on behalf of American Society of Plant Biologists.
This is an Open Access article distributed under the terms of the Creative Commons Attribution-NonCommercial-NoDerivs licence (https://creativecommons.org/licenses/by-nc-nd/4.0/), which permits non- commercial reproduction and distribution of the work, in any medium, provided the original work is not altered or transformed in any way, and that the work is properly cited. For commercial re-use, please contact journals.permissions@oup.com

Introduction

Carotenoids are a family of plant isoprenoids with roles in photosynthesis and photoprotection in green tissues. They also function as pigments in non-photosynthetic tissues such as flower petals and ripe fruits to attract animals for pollination and seed dispersal. Carotenoids are also precursors of bioactive molecules in plants (including hormones such as abscisic acid and strigolactones) and animals (including retinoids such as vitamin A) (Rodriguez-Concepcion et al. 2018). Carotenoids accumulate at high levels in chloroplasts, where they are mostly associated with the photosynthetic apparatus. However, they are most abundant in chromoplasts, which are plastids specialized in the sequestration of these highly lipophilic compounds found in carotenoid- accumulating non-photosynthetic tissues (Rodriguez- Concepcion et al. 2018). Chromoplast ultrastructure changes depending on the species, organ, and carotenoid type they accumulate. For example, chromoplasts from carrot (*Daucus carota*) roots accumulate carotenoids as large crystals whereas those of red pepper (*Capsicum annuum*) contain a large number of plastoglobules (PG) with fibrillar extensions surrounded by an outer layer of proteins referred to as plastoglobulins or fibrillins (FBNs) (Egea et al. 2010).

FBNs are encoded by gene families in plants and algae that can be grouped into 12 clades (Singh and McNellis 2011; Kim and Kim 2022). They include members with diverse molecular masses, pI values, hydrophobicity profiles, and homology with lipocalins (small proteins involved in the binding and transport of small lipophilic compounds), suggesting that each FBN family member has specific biological function(s) (Singh and McNellis 2011; Lundquist et al. 2012; Kim and Kim 2022). In agreement, plastid types vary in their FBN composition, suggesting that specific FBNs might have specialized functions in different classes of plastids (Singh and McNellis 2011; Kim and Kim 2022). However, their mechanisms of action remain poorly understood in most cases. In tomato (*Solanum lycopersicum*), the PG-associated FBN1, FBN2, and FBN4 isoforms accumulate at high levels during fruit ripening, when carotenoids are actively produced and stored in chromoplasts (Barsan et al. 2012; Suzuki et al. 2015). FBN1 homologs from rapeseed (*Brassica juncea*) and melon (*Cucumis melo*) contribute to carotenoid accumulation in chromoplasts (Li et al. 2023; Zhou et al. 2023). By contrast, the Arabidopsis (*Arabidopsis thaliana*) homologs FBN1a, FBN1b, and FBN2 are involved in photoprotection and stress responses (Torres-Romero et al. 2022) whereas FBN4 is likely involved in the partitioning of metabolites between the PG and thylakoid membranes of chloroplasts (Singh et al. 2012). Arabidopsis FBN1a, FBN1b, and FBN2 interact with each other around the PG surface, but FBN2 also plays FBN1-independent roles through interaction with other proteins (Torres-Romero et al. 2022). Arabidopsis FBN5 is a stromal protein involved not only in the acclimation to photooxidative stress but also in plastoquinone-9 biosynthesis by binding to solanesyl diphosphate synthases (Kim et al. 2015). FBN6 is needed for plants to acclimate to light stress, and it contributes to reactive oxygen species (ROS) scavenging (Lee et al. 2020). The role of other FBNs remains poorly studied (Singh and McNellis 2011; Kim and Kim 2022).

Arabidopsis FBN6 was found to be among the proteins co-immunoprecipitated with a GFP-tagged version of phytoene synthase (PSY), the first and main rate-determining enzyme of the carotenoid pathway (Welsch et al. 2018). Furthermore, FBN6 is the only FBN enriched in purified envelope fractions where PSY is also found (Ferro et al. 2010; Bouchnak et al. 2019). Therefore, we questioned whether this particular isoform modulates PSY activity, thereby potentially impacting the metabolic flux of the carotenoid pathway in chloroplasts. Besides confirming binding and co-localization of Arabidopsis FBN6 and PSY, we demonstrate the functional relevance of such an interaction.

Results and discussion

Arabidopsis FBN6 and PSY physically interact in particular subplastidial locations

FBN6 was one of the proteins pulled down with a GFP antibody in Arabidopsis lines overexpressing the fusion protein PSY-GFP (Welsch et al. 2018), suggesting that FBN6 and PSY physically interact in vivo. To confirm this previously observed interaction and test its specificity, we performed co-immunoprecipitation experiments in *Nicotiana benthamiana* leaves. Constructs encoding C-terminal myc-tagged FBN6 and GFP-tagged PSY were co-agroinfiltrated in leaves, and 4 d later, protein extracts were used for immunoprecipitation using anti-myc antibodies (Fig. 1). As a negative control, we used a myc-tagged version of Arabidopsis phosphoribulokinase (PRK), a stromal enzyme of the Calvin cycle (Barja et al. 2021). Immunoblot analysis of immunoprecipitated proteins with anti-GFP antibodies detected PSY-GFP in FBN6-myc but not in PRK-myc samples (Fig. 1A). The specificity of the FBN6-PSY interaction was then tested by using a myc-tagged version of the FBN4 protein as a negative control (Torres-Romero et al. 2022). Results (Fig. 1B) showed that Arabidopsis FBN4 does not interact with PSY, and this confirmed the specificity of FBN6 and PSY interaction.

When analyzing the co-immunoprecipitation assays, we noticed that the PSY-GFP protein concentrated in fluorescent dots within chloroplasts (Fig. 2A). These dots are similar to those observed for PG-associated proteins (Lundquist et al. 2012; Gámez-Arjona et al. 2014; Morelli et al. 2023) and for PSY enzymes (Shumskaya et al. 2012) when fused to fluorescent protein tags. Interestingly, GFP-tagged Arabidopsis FBN6 shows a spotted distribution within chloroplasts despite the fact that the protein is not found in PG but localized in thylakoid and envelope membranes (Ferro et al. 2010; Lundquist et al. 2012; Bouchnak et al. 2019; Lee et al. 2020). To test whether the fluorescent dots observed in chloroplasts harboring FBN6-GFP and PSY-GFP proteins corresponded to the same or different subplastidial locations, we fused the red fluorescent protein (RFP) to FBN6 (FBN6-RFP construct) and co-agroinfiltrated it with the PSY-GFP construct. Confocal microscopy of the leaves 4 d after agroinfiltration showed a clear overlapping of RFP and GFP fluorescence signals (Fig. 2A), indicating that FBN6 and PSY co-localize within chloroplasts, as expected for interacting proteins.

Despite the fact that FBN6-GFP has been previously found to co-localize with PG

proteins fused to fluorescent tags in co-expression experiments similar to the results reported here, subsequent analysis of chloroplast membrane fractions argued against a localization of FBN6 in PG (Lee et al. 2020), a conclusion that is supported by proteomic data (Ferro et al. 2010; Lundquist et al. 2012; Bouchnak et al. 2019). While overexpression of FBNs and other PG-associated proteins typically results in PG proliferation (Shanmugabalaji et al. 2013; Van Wijk and Kessler 2017), overproduction of FBN6 or/and PSY proteins in agroinfiltrated leaf chloroplasts did not cause changes in PG core-associated proteins such as FBN1 or FBN2 homologs (Fig. 2B). These results provide further indirect evidence that FBN6 and PSY are not PG-associated proteins. Together, we conclude that Arabidopsis FBN6 and PSY interact and preferentially co- localize in particular locations of the chloroplast such as envelope or thylakoid membrane domains different from PG.

FBN6 promotes PSY activity

To test the possible relevance of FBN6 binding for PSY activity, we used a bacterial system free of other plant proteins that might influence the outcome of the interaction.

Specifically, we used an *Escherichia coli* strain carrying a synthetic operon that only lacks a gene encoding PSY to produce the orange carotenoid β-carotene from endogenous bacterial precursors (Ahrazem et al. 2019; Fig. 3A). Constructs to produce versions of plant proteins lacking their N-terminal plastid-targeting sequences were generated using appropriate gene-specific primers (Supplemental Table S1). Strains co-transformed with such constructs harboring Arabidopsis PSY and FBN6 sequences were found to produce significantly more β-carotene than those expressing only PSY or co-expressing PSY and FBN4 (Fig. 3, B and C), despite that PSY protein levels remained very similar in all the cases (Fig. 3D). By contrast, FBN6 had no effect when crtB, a PSY from the bacterium *Pantoea ananatis*, was used instead of PSY to produce carotenoids in the bacterial cells (Fig. 3E). These results strongly suggest that the presence of FBN6 specifically promotes the activity of the plant PSY enzyme in this bacterial system (i.e., in the absence of other plastid proteins that might indirectly improve PSY activity).

To verify whether FBN6 could also promote PSY activity in the chloroplasts of plant cells, we analyzed the production of phytoene (the direct product of PSY activity) and downstream carotenoids in *N. benthamiana* leaves agroinfiltrated with constructs to transiently express the Arabidopsis genes encoding FBN6, PSY, or both (Fig. 4 and Supplemental Tables S2 and S3). Control leaves were agroinfiltrated with a GFP construct. While phytoene was not detected in control or FBN6 samples, it was present in PSY samples, and it increased in samples agroinfiltrated with both FBN6 and PSY (Fig. 4A). To investigate whether overexpression of FBN6 could also impact the endogenous PSY enzymes in *N. benthamiana* leaves, we used norflurazon (NFZ). This inhibitor prevents phytoene conversion into downstream carotenoids, thereby allowing indirect estimation of PSY activity through quantifying the amount of phytoene accumulation in NFZ-treated tissues. As expected, phytoene was detected

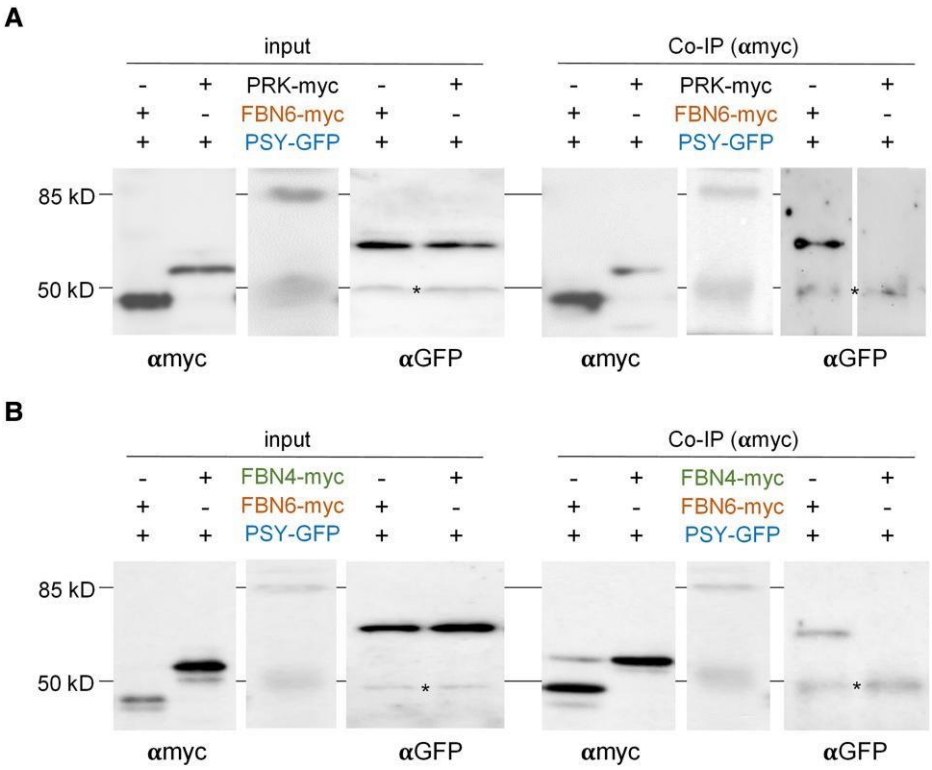


Figure 1. FBN6 and PSY can be immunoprecipitated together. *N. benthamiana* leaves were co-agroinfiltrated with the indicated combinations of proteins with C-terminal myc or GFP tags. Four days later, agroinfiltrated leaves were collected and used for protein extraction and analysis. Part of the protein extracts was used to test protein production (input) by immunoblot analyses with antibodies against myc (αmyc) or GFP (αGFP; asterisk marks the position of unspecific bands). The remaining protein extracts were used for co-immunoprecipitation (Co-IP) experiments using αmyc followed by immunoblot analyses with immunoblot analyses with αmyc (to confirm successful IP) and αGFP (to detect the presence of co-immunoprecipitated PSY-GFP protein). **A)** Experiment using the Calvin cycle enzyme PRK fused to the myc tag as a negative control. **B)** Experiment using the PG-associated FBN4 protein fused to the myc tag to test for the specificity of the FBN6-PSY interaction.

in all the samples treated with NFZ FBN6 samples showed a slight but statistically significant increase in phytoene compared with GFP controls, in agreement with the conclusion that FBN6 is a promoter of endogenous PSY activity. In *PSY*-overexpressing samples, the presence of FBN6 led to a much more obvious increase in phytoene content (Fig. 4A). In the case of total carotenoids, FBN6 alone did not lead to increased levels but a combination of FBN6 and PSY resulted in more carotenoids than PSY alone (Fig. 4B). Consistent with the results in bacterial systems, the effect of FBN6 in enhancing PSY-promoted carotenoid accumulation was not observed when crtB was used instead of the plant PSY enzyme (Fig. 4B).

While these results support a positive and specific effect of FBN6 on PSY activity, it is also possible that FBN6 might promote the accumulation of PSY-derived phytoene and other carotenoids in chloroplasts by playing other (additional) roles, e.g., by modulating

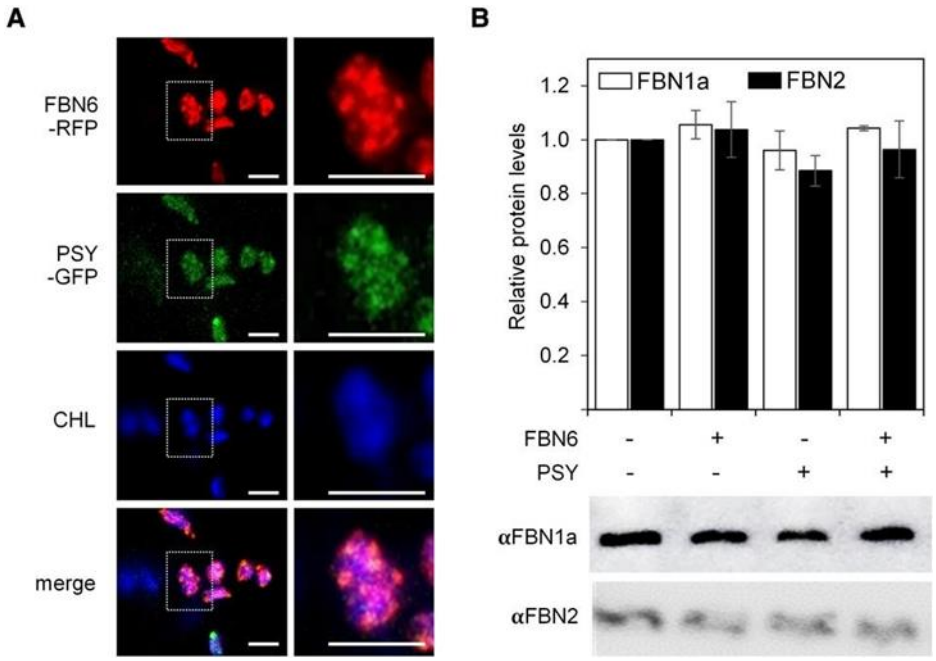


Figure 2. FBN6 and PSY co-localize in chloroplasts. N. benthamiana leaves were co-agroinfiltrated with constructs encoding FBN6-RFP and PSY-GFP, and 4 d later, samples were taken for confocal and immunoblot analyses. A) Representative confocal microscopy images of a leaf section transiently expressing the indicated fluorescent fusion proteins. All panels in the same column show the same field. RFP fluorescence is shown in the top panels, GFP fluorescence in the second row, and chlorophyll autofluorescence in the third row. Bottom panels show a merge of the 3 fluorescence channels. Right panels are a magnification of the area boxed in white in the left panels. Bars, 5 µm. B) Immunoblot analysis of the accumulation of FBNs identified using antibodies against Arabidopsis PG-associated FBN1a and FBN2 proteins in leaves expressing the indicated constructs or a GFP control (−/−). Quantification was made by relativizing each band intensity to the one obtained in the control. Representative results are shown in the lower panels. Barplot shows the mean ± SD values of quantitative data from n = 3 leaves

PSY folding or carotenoid stability. To test whether PSY folding or/and degradation rate could be altered by FBN6 *in planta*, we overexpressed the 2 Arabidopsis proteins in *N. benthamiana* leaves (or PSY and FBN4 as a control) and used total protein extracts in proteolytic assays (Fig. 5). Levels of PSY protein were similar in extracts from leaves co-expressing FBN6 or FBN4 constructs (Fig. 5A), arguing against a possible role for FBN6 in promoting PSY accumulation in chloroplasts. Next, PSY folding and aggregation status was estimated from accessibility to cleavage by proteinase K. Consistent with the conclusion that FBN6 does not change PSY protein structure, PSY degradation by proteinase K occurred similarly in extracts from leaves co-agroinfiltrated with FBN6 or FBN4 (Fig. 5, B and C). These results suggest that PSY folding or degradation rate is not altered by interaction with FBN6. We further investigated the possible influence of FBN6 on the stability of the carotenoid products by analyzing the rate of carotenoid removal during leaf senescence (Fig. 5D). In this case, *N. benthamiana* leaves were agroinfiltrated with constructs harboring either FBN6 or FBN4 as a control together with crtB to boost phytoene and downstream carotenoid

production (Morelli et al. 2023). Four days later, agroinfiltrated leaves were cut from the plant and incubated in the dark for up to 1 wk. Degradation of phytoene and downstream carotenoids was virtually identical in samples carrying FBN6 or FBN4 (Fig. 5D), indicating that these FBNs do not have a differential role in carotenoid storage or stability. Together, the results in bacterial and plant systems strongly support the conclusion that FBN6 interaction with PSY leads to a higher enzymatic activity.

Genetic evidence confirms the functional relevance of FBN6 for PSY activity

If FBN6 is a positive regulator of PSY activity, loss of FBN6 in mutants would be expected to prevent normal carotenoid synthesis. FBN6-defective Arabidopsis *fbn6-1* mutants were found to have reduced chlorophyll levels compared with wild-type (WT) controls, but no data on carotenoid levels were reported (Lee et al. 2020). In Arabidopsis, the most active production of carotenoids takes place during de-etiolation to protect the emerging photosynthetic apparatus against photooxidative damage caused by excess incoming light (Rodríguez-Villalón et al. 2009). The boost in carotenoid synthesis during de-etiolation is mediated in part by increased expression of the PSY-encoding gene in Arabidopsis (Rodríguez-Villalón et al. 2009; Toledo-Ortiz et al., 2010). Interestingly, the gene encoding FBN6 was also highly induced during this process (Fig. 6A). Because co- expression is only associative evidence of a possible common role, we next used genetics to test whether FBN6 activity was required for normal carotenoid production in etiolated and de-etiolating seedlings. Compared with the WT, the *fbn6-1* mutant contains similar levels of carotenoids in etiolated seedlings, but it shows a strongly attenuated production during de-etiolation (up to 24 h after illumination). As a result, greening (chlorophyll accumulation) was delayed (Fig. 6B and Supplemental Table S4).

After a few days under normal light (NL), the differences in carotenoid (and chlorophyll) levels between WT and *fbn6-1* plants were attenuated but still detectable (Fig. 6C and Supplemental Table S5). To test the putative influence of increased FBN6 on carotenoid biosynthesis in etiolated and de-etiolating seedlings, we transformed Arabidopsis plants with a construct to overexpress an Arabidopsis plants with a construct to overexpress an RFP-tagged FBN6 protein. Most transformants showed no RFP fluorescence, and the ones producing detectable levels of FBN6-RFP protein showed levels of total *FBN6* transcripts (endogenous and transgenic) that were similar or lower than those in untransformed controls (Supplemental Fig. S1). These results suggest that accumulation of FBN6-encoding transcripts is tightly regulated, perhaps to maintain a balanced ratio with *PSY* transcripts (Fig. 6A).RFP-tagged FBN6 protein. Most transformants showed no RFP fluorescence, and the ones producing detectable levels of FBN6-RFP protein showed levels of total *FBN6* transcripts (endogenous and transgenic) that were similar or lower than those in untransformed controls (Supplemental Fig. S1). These results suggest that accumulation of FBN6-encoding transcripts is tightly regulated, perhaps to maintain a balanced ratio with *PSY* transcripts (Fig. 6A).

Carotenoid levels, but not *PSY* expression, increase when Arabidopsis plants are

exposed to high light (HL), suggesting an up-regulation of PSY enzyme activity to increase the metabolic flux toward carotenoid synthesis (Kreslavski et al. 2021). Similar to *PSY*, transcripts encoding FBN6 also showed unchanged levels when 9-d-old Arabidopsis seedlings were exposed for 24 h to HL compared with controls left at NL for the same time (Fig. 6A). Most interestingly, the HL-triggered increase in carotenoid levels

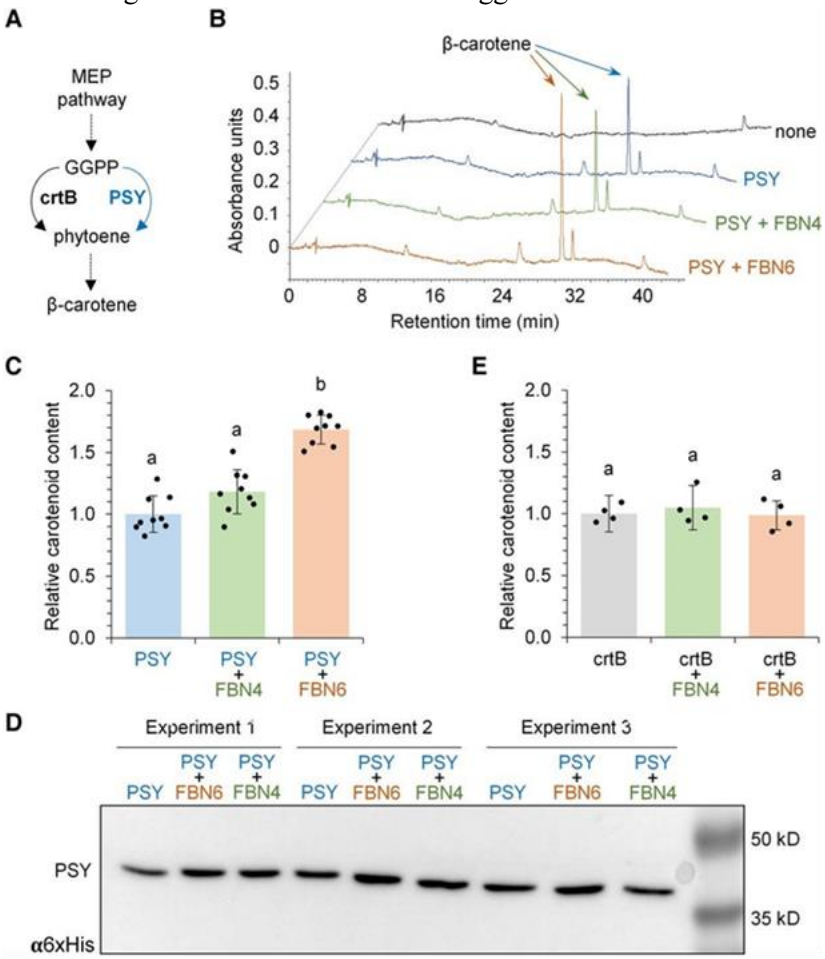


Figure 3. FBN6 enhances PSY activity. A) E. coli cells were transformed with constructs to produce β-carotene from precursors supplied by the endogenous methylerythritol 4-phosphate pathway when plant or bacterial (PSYs or crtB, respectively) were exogenously provided. GGPP, geranylgeranyl diphosphate. B) Representative HPLC chromatograms showing the carotenoids produced in cells co-transformed with constructs encoding PSY, FBN4 or/and FBN6. A control not expressing PSY or FBNs is also shown (marked as "none"). The main carotenoid product (β-carotene) is indicated. C) Total carotenoid levels in cells co-transformed with constructs encoding PSY, FBN4, or/and FBN6. D) Immunoblot analysis of the His-tagged PSY protein used in the assays. The blot shows the levels of the recombinant protein in 3 different experiments of the indicated combinations. E) Total carotenoid levels in cells expressing crtB instead of PSY together with FBN4 or FBN6. In C) and E), mean ± SD are represented relative to carotenoid levels in samples with PSY (C, n = 9) or crtB (E, n = 4) alone; dots represent individual data points and letters represent statistically significant differences ($P < 0.05$) among means according to one-way ANOVA followed by post hoc Tukey's tests.

was highly attenuated in FBN6-defective plants compared with the WT controls (Fig. 6C). By contrast, the reduction in chlorophylls associated with HL exposure was similar in WT and *fbn6-1* seedlings in absolute terms but seemingly stronger in the mutant in relative terms (Fig. 6C), likely because disrupted up-regulation of carotenoid contents in *fbn6-1* seedlings results in defective photoprotection and a higher chlorophyll degradation rate. We conclude that FBN6 is required to support the increase in carotenoid levels that takes place in response to HL, a role that is consistent with its proposed PSY-promoting activity.

An alternative connection between FBNs and carotenoids

FBN gene expression often parallels the carotenoid content of non-photosynthetic plant tissues, e.g. during fruit ripening, where their role is assumed to be mainly structural (Singh and McNellis 2011). Indeed, FBNs were initially identified as proteins specifically associated with carotenoid accumulation in fruit and petal chromoplasts, as components of "fibrils" and PG structures (Deruère et al. 1994; Vainstein et al. 1994). Similarly, green algae FBNs were also proposed to be involved in the formation and stabilization of the chloroplast eyespot, a carotenoid-rich light sensing system (Schmidt et al. 2006; Davidi et al. 2015). More recently, rapeseed and melon FBN1 homologs were shown to contribute to carotenoid accumulation by interacting with other proteins and promoting PG proliferation in flower and fruit chromoplasts (Li et al. 2023; Zhou et al. 2023). However, in plant chloroplasts, carotenoids are not normally concentrated in PG or any other lipid body but are distributed in thylakoids and, to a lower extent, envelope membranes (Morelli et al. 2023). Despite the fact that chloroplast FBNs are presumed to maintain

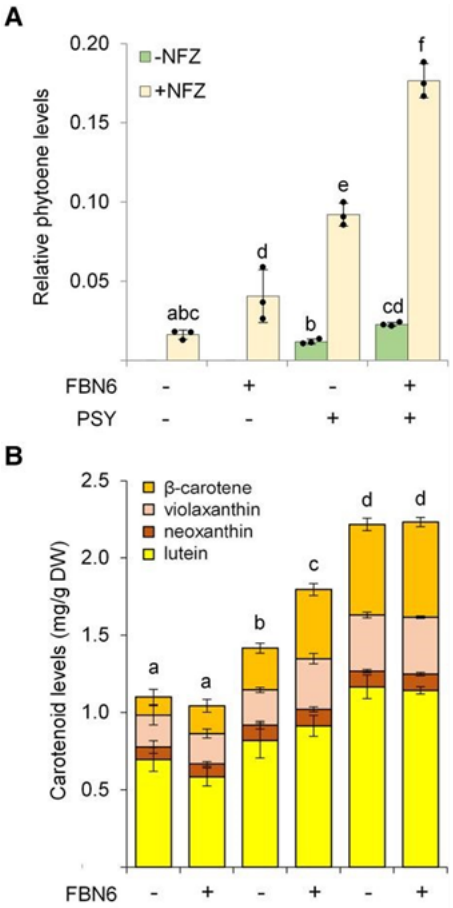


Figure 4. FBN6 promotes phytoene and downstream carotenoid production. *N. benthamiana* leaves were agroinfiltrated with the indicated constructs, and 4 d later, samples were taken for HPLC analysis of carotenoids. A GFP construct was used as a control. **A)** Phytoene levels in leaf samples either treated (+) or not (−) with NFZ 1 day after agroinfiltration with GFP, PSY, or/and FBN6 constructs. Values are represented relative to total carotenoid levels in untreated control leaves and they correspond to the mean ± SD of $n = 3$ leaf samples. **B)** Levels of downstream carotenoids in untreated samples. DW, dry weight. Values correspond to the mean ± SD of $n = 3$ leaf samples. In both plots, different letters represent statistically significant differences ($P < 0.05$) among means of total carotenoids according to one-way ANOVA followed by post hoc Tukey's tests. Supplemental Tables S2 and S3 show absolute values of carotenoid and chlorophyll levels

photosynthetic function and are present in all the compartments where carotenoids are synthesized and accumulated, a direct functional association between FBNs and carotenoid biosynthesis has remained unexplored.

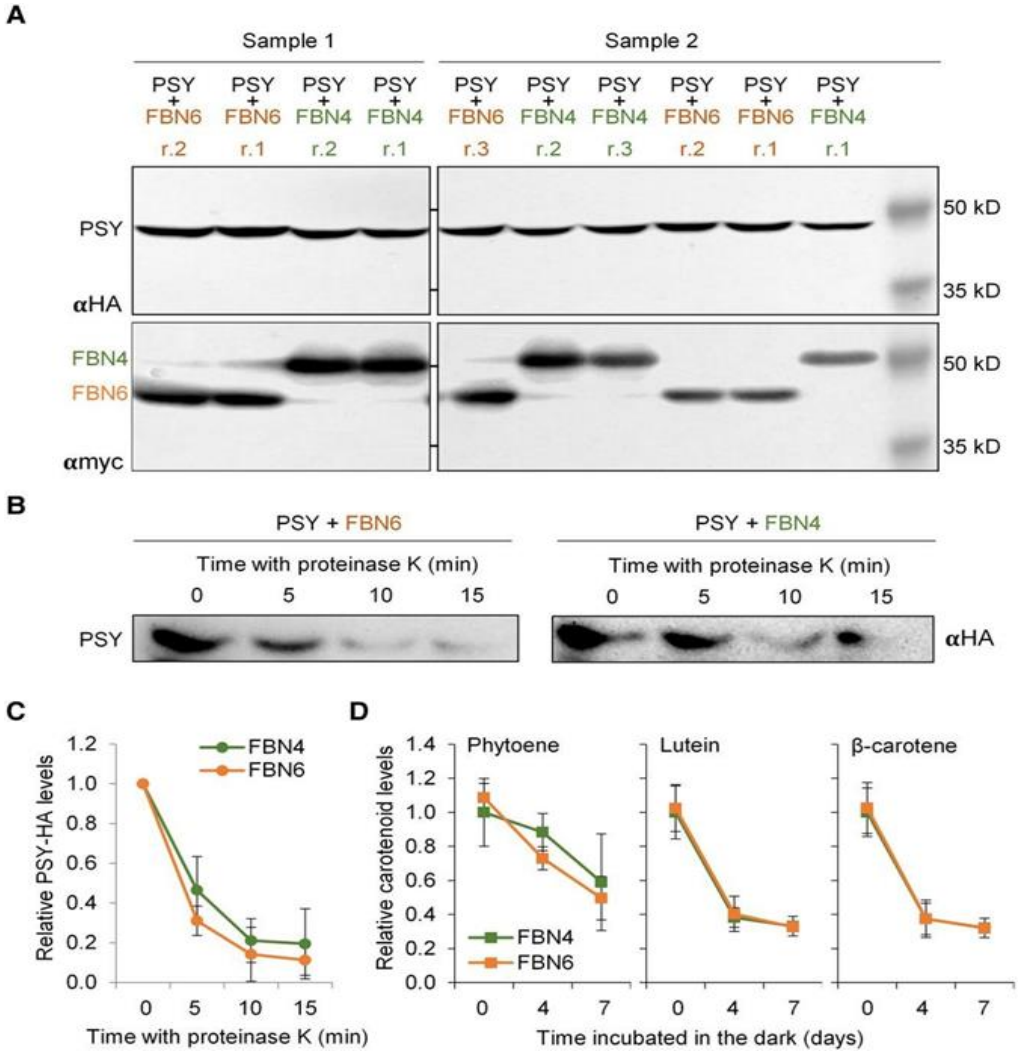


Figure 5. FBN6 does not influence PSY or carotenoid accumulation. *N. benthamiana* leaves were co-agroinfiltrated with constructs to express combinations of myc-tagged FBN6 (or FBN4 as a control) with HA-tagged PSY (or crtB as a control), and 4 days later, samples were collected to prepare protein or pigment extracts. **A)** Immunoblot analysis of PSY-HA, FBN4-myc and FBN6-myc protein levels in several replicates (i.e. plants) from 2 different samples (i.e., experiments). **B)** Immunoblot analysis of PSY-HA protein in extracts additionally containing either FBN6-myc or FBN4-myc after incubation with proteinase K for the indicated times (minutes). **C)** Quantification of PSY-HA protein abundance in extracts treated with proteinase K as described in **B)**. Mean ± SD values of $n = 3$ independent experiments are represented relative to the starting levels, i.e. before incubation with the protease (Time 0). **D)** Carotenoid levels in *N. benthamiana* leaves co-expressing crtB together with either FBN6 or FBN4, cut from the plant and incubated in the dark for the indicated times (days). Mean ± SD values of $n = 3$ independent experiments are represented relative to the starting levels, i.e. before placing the cut leaves in the dark (Day 0). The *y*-axis is the same for the 3 plots. Statistical analyses (2-way ANOVA) detected no significant differences (2-way ANOVA, $P > 0.05$) between FBN6 and FBN4 samples in the experiments shown in **C)** and **D)**

Studies on FBN-interacting proteins have substantially improved our understanding of the function of catalyzes one of the first steps of jasmonic acid (JA) biosynthesis. FBN2 also interacts with other proteins involved in different metabolic processes, including other (Gámez-Arjona et al. 2014). FBN4 interacts with the major ferredoxin protein in

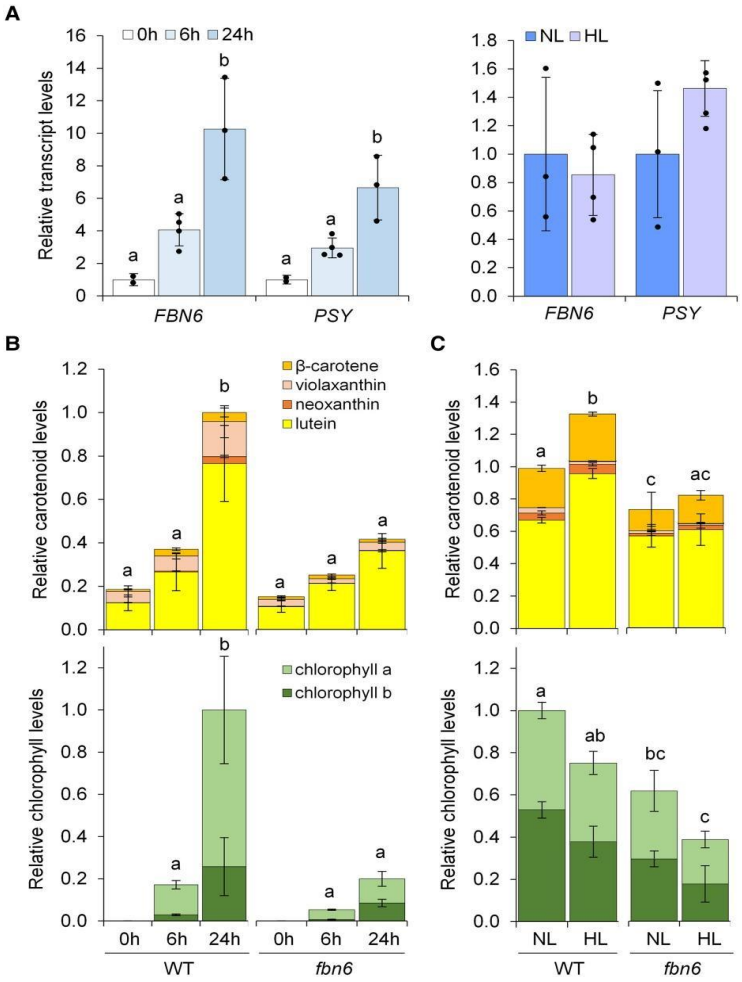


Figure 6. FBN6 is required for carotenoid production in Arabidopsis. De-etiolation experiments were carried out with Arabidopsis WT and FBN6-defective mutant seeds germinated in the dark for 3 d; the resulting etiolated seedlings were then exposed to white light for 6 and 24 h. For HL experiments, WT and *fbn6* seedlings germinated and grown under NL conditions for 9 d were exposed for 24 h to either NL (as a control) or HL. **A)** Expression profiles of genes encoding FBN6 and PSY during de-etiolation (left) or HL exposure (right) of WT seedlings. Transcript levels are normalized using the *UBC21* gene and shown relative to etiolated (0 h) or NL-exposed samples, respectively. **B)** Carotenoid and chlorophyll levels in de-etiolating WT and *fbn6* seedlings. Values are represented relative to total pigment levels in WT 24 h samples. **C)** Carotenoid and chlorophyll levels in HL-exposed WT and *fbn6* seedlings. Values are represented relative to total pigment levels in WT NL samples. In all plots, mean ± SD of $n \geq 3$ replicates are represented. Letters represent statistically significant differences ($P < 0.05$) among means of total carotenoids and chlorophylls according to one-way ANOVA followed by post hoc Tukey's tests. Supplemental Tables S4 and S5 show absolute values of carotenoid and chlorophyll levels

Arabidopsis (Fd2) and with harpin protein HrpN, an elicitor secreted by pathogenic bacteria that activates plant defense and resistance (Kim and Kim 2022). FBN5 participates in the production of the plastidial isoprenoid plastoquinone through interaction with solanesyl diphosphate synthase isoforms 1 and 2 (SPS1 and SPS2), which catalyze the first committed step in the production to increasing ing to and transporting of the prenyl chain of the molecule (Kim et al. 2015). Based on the presence of a lipocalin domain involved in bind- active site of the enzymes, thereby contributing small hydrophobic metabolites, it their enzymatic activity (Kim et al. 2015). was proposed that FBN5 might bind the solanesyl diphos- The lipocalin motif of FBN4 likely contributes to the role of phate product of SPS1 and SPS2 and remove it from the this isoform in the trafficking of plastoquinone and other small lipids between the thylakoids and the PG (Singh et al. 2012). Interestingly, FBN6 also contains a lipocalin motif (Singh and McNellis 2011). Based on that proposed for FBN5, a non-PG FBN protein, we speculate that direct interaction of FBN6 with PSY might result in improved activity of the enzyme by facilitating removal of the phytoene product from the active site. Regardless of the specific mechanism involved, our data support the conclusion that FBN6 plays a physiologically relevant role in carotenoid biosynthesis in Arabidopsis chloroplasts by physically binding to PSY to promote its enzymatic activity. Therefore, we demonstrate that FBNs promote not only the accumulation of carotenoids but also their biosynthesis. The unveiled role of FBN6 in carotenogenesis reported here can explain the phenotypes previously reported for the *fbn6-1* mutant, which were similar to those of mutants disrupted in ROS homeostasis (Lee et al. 2020). Because carotenoids are essential photoprotectants that dissipate excess light energy as heat and detoxify excess ROS in chloroplasts (Rodriguez-Concepcion et al. 2018), we conclude that the reduced acclimation to light stress and impaired ROS scavenging phenotypes observed in the *fbn6-1* mutant are likely a primary result of defective carotenoid biosynthesis. Lower growth, increased glutathione levels, or resistance to cadmium stress would be secondary effects of impaired ROS homeostasis.Similar to the up-regulation of PSY and FBN6 genes during Arabidopsis de-etiolation (Fig. 6A), the burst in carotenoid synthesis that takes place during tomato fruit ripening is also associated with increased expression of genes encoding the corresponding PSY and FBN6 homologs (Barja et al. 2021; Sun et al. 2022). This observation suggests that FBN6-dependent promotion of PSY activity and carotenoid biosynthesis might not be restricted to chloroplasts but can also occur in chromoplasts. Further experiments with FBN6-defective tomato plants should confirm this possibility and provide additional insights into the possible biotechnological use of this FBN isoform.

Materials and methods

Plant material and growth conditions

N. benthamiana and Arabidopsis (*A. thaliana*) plants were grown as described (Morelli et al. 2023). The *fbn6-1* mutant (GABI_159E10) (Lee et al. 2020) was obtained from the Nottingham Arabidopsis Stock Centre (NASC). Homozygous lines were identified by genomic PCR with T-DNA and gene-specific primers (Supplemental Table S1). Transgenic lines overexpressing an RFP-tagged version of Arabidopsis FBN6

were generated in the Columbia-0 background using construct pGWB454-FBN6-RFP. Lines with a single T-DNA insertion were identified based on the Mendelian segregation of the kanamycin resistance marker gene, and transformants showing different levels of FBN6-RFP protein (as deduced from RFP fluorescence intensity) were selected for analysis. For the de-etiolation experiments, seeds were surface-sterilized and sown on Petri dishes containing solid 0.5× MS medium without sucrose. After stratification for 3 d at 4°C in the dark, seeds were exposed to white light (50 μmol photons·m^{-2} s^{-1}, referred to as normal light or NL) for 3 h at 22°C to stimulate synchronized germination. Then, plates were covered in aluminum foil and incubated at 22°C in the dark for 3 d for seeds to germinate and produce etiolated seedlings. Such etiolated seedlings were either collected in the dark or exposed to NL to allow de-etiolation. For the intense light experiments, seedlings grown on plates for 9 d under NL were exposed for 24 h to 600 μmol photons·m^{-2} s^{-1} (referred to as high light or HL) or left under NL for the same time. *N. benthamiana* leaves were agroinfiltrated as described (Morelli et al. 2023). Some leaves were later treated with the commercial herbicide Zorial, containing 80% NFZ. The herbicide was diluted in a 0.05% (v/v) solution of Tween 20 in water to a final concentration of 2 μM NFZ. The solution was then infiltrated with a syringe on the leaf areas that had been agroinfiltrated with constructs of interest 24 h earlier (so the agroinfiltration halo was properly absorbed). For the carotenoid degradation experiment, agroinfiltrated leaves were left in the plant for 4 d and then cut and placed on top of solid 0.5× MS medium without sucrose in Petri dishes. Samples were taken before and after incubating the plates in the dark at 22°C for 4 or 7 d.

Gene constructs

The full coding region of the Arabidopsis FBN6 (AT5G19940) cDNA was PCR-amplified using primers AtFBN6-attB1-F and AtFBN6-attB2-R (Supplemental Table S1) and cloned into Gateway pDONR207 and subsequently pGWB420 (to create the FBN6-myc fusion) and pGWB454 (to create the FBN6-RFP fusion). Similarly, the FBN4-myc fusion was generated by PCR-mediated amplification of a cDNA sequence encoding full-length FBN4 (AT3G23400) with primers AtFBN4-attB1-F and AtFBN4-attB2-R (Supplemental Table S1) and cloned into Gateway pGWB420 via pDONR207. Similarly, the PSY-HA fusion was generated in pGWB414 following PCR amplification with primers AtPSY-attB1-F and AtPSY-attB2-R (Supplemental Table S1). Constructs encoding PRK-myc (Barja et al. 2021) and PSY-GFP (Welsch et al. 2018) were previously available in the lab. For the experiments in bacteria, plant cDNA sequences were PCR-amplified using gene-specific primers to remove their plastid transcript peptide (Supplemental Table S1). The Arabidopsis PSY sequence was cloned into a Gateway-compatible version of pET28 fused to an N-terminal 6× His tag, whereas the FBN-encoding cDNAs were cloned in pET23 (Novogen).

Activity assays in bacteria

Competent TOP10 cells were transformed with either plasmid pAC-BETA (with the *P. ananatis* genes *crtE*, *crtB*, *crtI*, and *crtY* required for β-carotene production in *E. coli*) or with the derived plasmid pAC-85b, which lacks the *crtB* gene encoding PSY

(Cunningham and Gantt 2007). As indicated, cells were also co-transformed with plasmids to produce His-tagged plant PSY either alone or in combination with FBN6 or FBN4 proteins lacking their N-terminal plastid-targeting domains. Transformants were selected on Luria broth (LB) solid medium supplemented with antibiotics to final concentrations of 30 μg/ml chloramphenicol (to select for the pAC plasmids), 25 μg/ml kanamycin (to select for the pET28-His-PSY construct), or/and 100 μg/ml carbenicillin (to select for the pET23 plasmids encoding FBNs). To assess carotenoid production, overnight-grown 5 ml precultures of positive transformants were used to inoculate 50 ml of fresh LB media supplemented with the indicated antibiotics. After growth at 20°C and 200 rpm for 3 d, cells were harvested by centrifugation (6,000 × *g*, 10 min) and resuspended in 4 ml of acetone. The mixture was shaken at 55°C in darkness for 15 min in a ThermoMixer (Eppendorf) and then spin at 4°C (13,000 × *g*, 10 min). The supernatant was transferred to a new tube and evaporated using a SpeedVac. The remaining residue was resuspended in 1 ml DMSO for spectrophotometric quantification of carotenoids by measuring absorbance at 472 nm. Some samples diluted in acetone were used for HPLC-DAD analysis of the carotenoid composition (Barja et al. 2021). Levels were normalized to optical density at 600 nm (OD600).

Protein degradation

For protease accessibility assays, *N. benthamiana* leaves agroinfiltrated with constructs to produce PSY-HA together with FBN6-myc or FBN4-myc were collected after 4 d. The tissue was flash-frozen and ground in liquid nitrogen to a fine powder. About 75 mg of the resulting powder was mixed with 0.3 ml of lysis buffer containing 50 mM Tris–HCl pH = 7.5, 150 mM NaCl, 1 mM DTT, 1 mM $MgCl_2$, 5% (v/v) glycerol, 1% (v/v) NP-40, and 2% (w/v) PVPP. The mixture was vortexed and centrifugated at 14,000 × *g*, 2 min. The supernatant was collected, and the amount of total protein content was quantified using a commercial Bradford assay (Pierce). Immediately after preparation, protein extracts were diluted with 50 mM Tris–HCl pH = 7.5 to a final concentration of 2 μg/μl of protein and incubated at 37°C with 0.1 μg/ml proteinase K (Invitrogen). After stopping the reaction with SDS-PAGE loading buffer, extracts were used for immunoblot analysis.

Microscopy

Fluorescent proteins transiently expressed in agroinfiltrated *N. benthamiana* leaves or stably produced in transgenic Arabidopsis lines were analyzed with a Leica TCS SP5 Confocal Laser Scanning Microscope using a 63× immersion objective. GFP fluorescence was detected using a PMT detector (gain 980) from 500 to 560 nm after argon laser excitation at 488 nm (29%), while RFP was excited by a Diode laser 561 (20%) and signal was detected using a PMT detector (gain 76) from 570 to 630 nm. Chlorophyll autofluorescence was detected using a PMT detector (gain 41) from 650 to 750 nm after argon laser exitation at 488 nm (29%).

Co-immunoprecipitation and immunoblot assays

N. benthamiana leaves were agroinfiltrated with the appropriate constructs and samples were collected after 4 d for co-immunoprecipitation experiments performed as described (Barja et al. 2021). Immunoblot analysis of plant protein extracts was carried

out as described (Paulišić et al. 2021). In the case of *E. coli*, extracts for immunoblot analysis were made by directly boiling pelleted cells in 12.5 mM Tris–HCl pH = 6.8, 4% (w/v) SDS. Blots were incubated with available antibodies against FBN1a and FBN2 (Morelli et al. 2023) diluted 1:5,000 or commercial antibodies against GFP (Invitrogen, 1:2,000), Myc (Calbiochem, 1:5,000), HA (Sigma, 1:1,000) and 6× His (Proteintech, 1:5,000) epitopes. Quantification of the signals was carried out as described (Morelli et al. 2023).

Gene expression and metabolite analysis

RNA isolation, cDNA synthesis, and reverse transcription quantitative PCR experiments were carried out as described (Barja et al. 2021) using the primers listed in Supplemental Table S1. Normalized transcript levels were calculated using Arabidopsis *UBC21* (At5g25760) as the reference gene. Carotenoids and chlorophylls were extracted from plant tissues, separated, identified, and quantified by HPLC-DAD (Barja et al. 2021).

Statistical analyses

One-way ANOVA followed by Tukey's multiple comparisons test and Student's *t*-test analyses were used to determine statistically significant differences.

Accession numbers

Sequence data from this article can be found under the following accession numbers: At5g17230 (PSY), At5g19940 (FBN6), At3g23400 (FBN4), Solyc09g090330 (SlFBN4), At1g32060 (PRK), At5g25760 (UBC21), and ADD79329 (crtB).

Acknowledgments

We thank Venkatasalam Shanmugabalaji and Felix Kessler (University of Neuchatel, Switzerland) for the kind gift of the fibrillin antibodies, Tsuyoshi Nakagawa (Shimane University, Japan) for the Gateway vectors, Lourdes Gómez Gómez for the pAC-85b plasmid, and the Nottingham Arabidopsis Stock Centre (NASC) for providing *fbn6-1* seeds. We also thank members of our laboratory for helpful discussions.

Author contributions

A.I.-S., J.N.-C., L.M., and M.R.-C. designed the research and analyzed data; A.I.-S., J.N.-C., and L.M. conducted the experiments; M.R.-C. wrote the paper.

Supplemental data

The following materials are available in the online version of this article.

Supplemental Figure S1.Characterization of *35S: FBN6-RFP* lines.

Supplemental Table S1. Primers used in this work.

Supplemental Table S2. Phytoene levels in control and NFZ-treated *N. benthamiana leaves* agroinfiltrated with FBN6 and/or PSY constructs.

Supplemental Table S3. Photosynthetic pigment levels in *N. benthamiana* leaves agroinfiltrated with FBN6, PSY, and/or crtB constructs.

Supplemental Table S4. Photosynthetic pigment levels in etiolated and de-etiolating WT and *fbn6* Arabidopsis seedlings.

Supplemental Table S5. Photosynthetic

pigment levels in WT and *fbn6* Arabidopsis seedlings exposed to HL.

Funding

This work was funded by grants from Spanish MCIN/AEI/ 10.13039/501100011033 and European NextGeneration EU/ PRTR and PRIMA programs to M.R.-C. (PID2020-115810GB-I00 and UToPIQ-PCI2021-121941). M.R.-C. is also supported by Generalitat Valenciana (PROMETEU/2021/056 and AGROALNEXT/2022/067). Our group is a member of CaRed (Spanish Carotenoid Network) funded by MCIN/ AEI (RED2022-134577-T). A.I.-S. and J.N.-C. received predoctoral fellowships from MCIN/AEI (PRE2018-083610 and PRE2021-098681, respectively).
Conflict of interest statement. None declared.

References

Ahrazem O, Diretto G, Argandoña Picazo J, Fiore A, Rubio-Moraga Á, Rial C, Varela RM, Macías FA, Castillo R, Romano E, et al. The specialized roles in carotenogenesis and apocarotenogenesis of the phytoene synthase gene family in saffron. Front Plant Sci. 2019:**10**: 249. https://doi.org/10.3389/fpls.2019.00249

Barja MV, Ezquerro M, Beretta S, Diretto G, Florez-Sarasa I, Feixes E, Fiore A, Karlova R, Fernie AR, Beekwilder J, et al. Several geranylgeranyl diphosphate synthase isoforms supply metabolic substrates for carotenoid biosynthesis in tomato. New Phytol. 2021:**231**(1): 255–272. https://doi.org/10.1111/nph.17283

Barsan C, Zouine M, Maza E, Bian W, Egea I, Rossignol M, Bouyssie D, Pichereaux C, Purgatto E, Bouzayen M, et al. Proteomic analysis of chloroplast-to-chromoplast transition in tomato reveals metabolic shifts coupled with disrupted thylakoid biogenesis machinery and elevated energy-production components. Plant Physiol. 2012:**160**(2):708–725. https://doi.org/10.1104/pp.112. 203679

Bouchnak I, Brugière S, Moyet L, Le Gall S, Salvi D, Kuntz M, Tardif M, Rolland N. Unraveling hidden components of the chloroplast envelope proteome: opportunities and limits of better MS sensitivity. Mol Cell Proteomics. 2019:**18**(7):1285–1306. https://doi.org/10. 1074/mcp.RA118.000988

Cunningham FX Jr, Gantt E. A portfolio of plasmids for identification and analysis of carotenoid pathway enzymes: adonis aestivalis as a case study. Photosynth Res. 2007:**92**(2):245–259. https://doi.org/10.1007/s11120-007-9210-0

Davidi L, Levin Y, Ben-Dor S, Pick U. Proteome analysis of cytoplasmatic and plastidic β-carotene lipid droplets in *Dunaliella bardawil*. Plant Physiol. 2015:**167**(1):60–79. https://doi.org/10.1104/pp.114.248450

Deruère J, Römer S, D'Harlingue A, Backhaus RA, Kuntz M, Camara B. Fibril assembly and carotenoid overaccumulation in chromoplasts: a model for supramolecular lipoprotein structures. Plant Cell. 1994:**6**(1):119–133. https://doi.org/10.1105/tpc.6.1.119

Egea I, Barsan C, Bian W, Purgatto E, Latché A, Chervin C, Bouzayen M, Pech JC. Chromoplast differentiation: current status and perspectives. Plant Cell Physiol. 2010:**51**(10):1601–1611. https://doi.org/10. 1093/pcp/pcq136

Ferro M, Brugière S, Salvi D, Seigneurin-Berny D, Court M, Moyet L, Ramus C, Miras S, Mellal M, Le Gall S, et al. AT-CHLORO, a comprehensive chloroplast proteome database with subplastidial localization and curated information on envelope proteins. Mol Cell Proteomics. 2010:**9**(6):1063–1084. https://doi.org/10.1074/mcp. M900325-MCP200

Gámez-Arjona FM, Raynaud S, Ragel P, Mérida Á. Starch synthase 4 is located in the thylakoid membrane and interacts with plastoglobule-associated proteins in Arabidopsis. Plant J. 2014:**80**(2):305–316. https://doi.org/10.1111/tpj.12633

Kim I, Kim HU. The mysterious role of fibrillin in plastid metabolism: current advances in understanding. J Exp Bot. 2022:**73**(9): 2751–2764. https://doi.org/10.1093/jxb/erac087

Kim EH, Lee Y, Kim HU. Fibrillin 5 is essential for plastoquinone-9 biosynthesis by binding to solanesyl diphosphate synthases in arabidopsis. Plant Cell. 2015:**27**(10):2956–2971. https://doi.org/10.1105/tpc.15.00707

Kreslavski VD, Khudyakova AY, Strokina VV, Shirshikova GN, Pashkovskiy PP, Balakhnina TI, Kosobryukhov AA, Kuznetsov VV, Allakhverdiev SI. Impact of high irradiance and UV-B on the photosynthetic activity, pro-/antioxidant balance and

expression of light-activated genes in *Arabidopsis thaliana* hy4 mutants grown under blue light. Plant Physiol Biochem. 2021:**167**:153–162. https://doi.org/10.1016/j.plaphy.2021.07.030

Lee K, Lehmann M, Paul MV, Wang L, Luckner M, Wanner G, Geigenberger P, Leister D, Kleine T. Lack of FIBRILLIN6 in *Arabidopsis thaliana* affects light acclimation and sulfate metabolism. New Phytol. 2020:**225**(4):1715–1731. https://doi.org/10.1111/nph.16246

Li R, Zeng Q, Zhang X, Jing J, Ge X, Zhao L, Yi B, Tu J, Fu T, Wen J, et al. Xanthophyll esterases in association with fibrillins control the stable storage of carotenoids in yellow flowers of rapeseed (*Brassica juncea*). New Phytol. 2023:**240**(1):285–301. https://doi.org/10.1111/nph.18970

Lundquist PK, Poliakov A, Bhuiyan NH, Zybailov B, Sun Q, van Wijk KJ. The functional network of the arabidopsis plastoglobule proteome based on quantitative proteomics and genome-wide coexpression analysis. Plant Physiol. 2012:**158**(3):1172–1192. https://doi.org/10.1104/pp.111.193144

Morelli L, Torres-Montilla S, Glauser G, Shanmugabalaji V, Kessler F, Rodriguez-Concepcion M. Novel insights on the contribution of plastoglobules and reactive oxygen species to chromoplast differentiation. New Phytol. 2023:**237**(5):1696–1710. https://doi.org/10.1111/ nph.18585

Paulišić S, Qin W, Arora Verasztó H, Then C, Alary B, Nogue F, Tsiantis M, Hothorn M, Martínez-García JF. Adjustment of the PIF7-HFR1 transcriptional module activity controls plant shade adaptation. EMBO J. 2021:**40**(1):e104273. https://doi.org/10.15252/embj.2019104273

Rodriguez-Concepcion M, Avalos J, Bonet ML, Boronat A, Gomez-Gomez L, Hornero-Mendez D, Limon MC, Meléndez-

Martínez AJ, Olmedilla-Alonso B, Palou A, et al. A global perspective on carotenoids: metabolism, biotechnology, and benefits for nutrition and health. Prog Lipid Res. 2018:**70**:62–93. https://doi.org/10.1016/j.plipres.2018.04.004

Rodríguez-Villalón A, Gas E, Rodríguez-Concepción M. Phytoene synthase activity controls the biosynthesis of carotenoids and the supply of their metabolic precursors in dark-grown Arabidopsis seedlings. Plant J. 2009:**60**(3):424–435. https://doi.org/10.1111/j.1365-313X.2009.03966.x

Schmidt M, Gessner G, Luff M, Heiland I, Wagner V, Kaminski M, Geimer S, Eitzinger N, Reissenweber T, Voytsekh O, et al. Proteomic analysis of the eyespot of Chlamydomonas reinhardtii provides novel insights into its components and tactic movements. Plant Cell. 2006:**18**(8):1908–1930. https://doi.org/10.1105/tpc.106.041749

Shanmugabalaji V, Besagni C, Piller LE, Douet V, Ruf S, Bock R, Kessler F. Dual targeting of a mature plastoglobulin/fibrillin fusion protein to chloroplast plastoglobules and thylakoids in transplastomic tobacco plants. Plant Mol Biol. 2013:**81**(1–2):13–25. https:// doi.org/10.1007/s11103-012-9977-z

Shumskaya M, Bradbury LMT, Monaco RR, Wurtzel ET. Plastid localization of the key carotenoid enzyme phytoene synthase is altered by isozyme, allelic variation, and activity. Plant Cell. 2012:**24**(9):3725–3741. https://doi.org/10.1105/tpc.112.104174

Singh DK, Laremore TN, Smith PB, Maximova SN, McNellis TW. Knockdown of FIBRILLIN4 gene expression in apple decreases plastoglobule plastoquinone content. PLoS One. 2012:**7**(10):1–10. https:// doi.org/10.1371/journal.pone.0047547

Singh DK, McNellis TW. Fibrillin protein function: the tip of the iceberg? Trends Plant Sci. 2011:**16**(8):432–441. https://doi.org/10.1016/ j.tplants.2011.03.014

Sun H, Ren M, Zhang J. Genome-wide identification and expression analysis of fibrillin (FBN) gene family in tomato (*Solanum lycopersicum* L.). PeerJ. 2022:**10**:e13414. https://doi.org/10.7717/peerj.13414

Suzuki M, Takahashi S, Kondo T, Dohra H, Ito Y, Kiriiwa Y, Hayashi M, Kamiya S, Kato M, Fujiwara M, et al. Plastid proteomic analysis in tomato fruit development. PLoS One. 2015:**10**(9):e0137266. https://doi.org/10.1371/journal.pone.0137266

Toledo-Ortiz G, Huq E, Rodríguez-Concepción M. Direct regulation of phytoene synthase gene expression and carotenoid biosynthesis by phytochrome-interacting factors. Proc Natl Acad Sci U S A. 2010: **107**(25):11626–11631. https://doi.org/10.1073/pnas.0914428107

Torres-Romero D, Gómez-Zambrano Á, Serrato AJ, Sahrawy M, Mérida Á. Arabidopsis fibrillin 1–2 subfamily members exert their functions via specific protein–protein interactions. J Exp Bot. 2022:**73**(3):903–914. https://doi.org/10.1093/jxb/erab452

Vainstein A, Halevy AH, Vishnevetsky M. Chromoplast biogenesis in Cucumis sativus corollas. Plant Physiol. 1994:**104**(2):321–326. https:// doi.org/10.1104/pp.104.2.321

Van Wijk KJ, Kessler F. Plastoglobuli: plastid microcompartments with integrated functions in metabolism, plastid developmental transitions, and environmental adaptation. Annu Rev Plant Biol. 2017: **68**(1):253–289.

https://doi.org/10.1146/annurev-arplant-043015-111737

Welsch R, Zhou X, Yuan H, Álvarez D, Sun T, Schlossarek D, Yang Y, Shen G, Zhang H, Rodriguez-Concepcion M, et al. Clp protease and OR directly control the proteostasis of phytoene synthase, the crucial enzyme for carotenoid biosynthesis in Arabidopsis. Mol Plant. 2018:**11**(1):149–162. https://doi.org/10.1016/j.molp.2017.11.003

Zhou X, Sun T, Owens L, Yang Y, Fish T, Wrightstone E, Lui A, Yuan H, Chayut N, Burger J, et al. Carotenoid sequestration protein FIBRILLIN participates in CmOR-regulated β-carotene accumulation in melon. Plant Physiol. 2023:**193**(1):643–660. https://doi.org/10.1093/plphys/kiad312

Annex 2

doi:10.1093/plphys/kiab206 PLANT PHYSIOLOGY 2021: 186: 2137–2151

Plant Physiology®

Light signals generated by vegetation shade facilitate acclimation to low light in shade-avoider plants

Luca Morelli[1,2], Sandi Paulisic[2], Wenting Qin[1,2], Ariadna Iglesias-Sanchez[2], Irma Roig-Villanova[2,†], Igor Florez-Sarasa[2], Manuel Rodriguez-Concepcion[1,2,‡] and Jaime F. Martinez-Garcia[1,2,3,*,‡]

1 Institute for Plant Molecular and Cell Biology (IBMCP), CSIC-UPV, Vale`ncia 46022, Spain
2 Centre for Research in Agricultural Genomics (CRAG) CSIC-IRTA-UAB-UB, Campus UAB Bellaterra, Barcelona 08193, Spain
3 Institucio´ Catalana de Recerca i Estudis Avançats (ICREA), Passeig Lluís Companys 23, Barcelona 08010, Spain
*Author for communication: jaume.martinez@ibmcp.upv.es
†Present address: Barcelona School of Agricultural Engineering (ESAB), Universitat Politècnica de Catalunya (UPC), Castelldefels, Barcelona 08860, Spain.
‡Senior authors.

M.R.-C. and J.F.M.-G. conceived the original research plan, directed, and coordinated the study. L.M., I.F.-S., A.I.-S., and M.R.-C. measured and analyzed photosynthetic parameters, respiration, and pigment levels; S.P., I.R.-V., and W.Q. performed all the other experiments. All authors analyzed their data and discussed the results. M.R.-C. and J.F.M.-G. wrote the paper with revisions and contributions or/and comments of all other authors. The author responsible for distribution of materials integral to the findings presented in this article in accordance with the policy described in the Instructions for Authors (https://academic.oup.com/plphys/pages/general-instructions) is: Jaime F. Martinez-Garcia (jaume.martinez@ibmcp.upv.es).

Abstract

When growing in search for light, plants can experience continuous or occasional shading by other plants. Plant proximity causes a decrease in the ratio of R to far-red light (low R:FR) due to the preferential absorbance of R light and reflection of FR light by photosynthetic tissues of neighboring plants. This signal is often perceived before actual shading causes a reduction in photosynthetically active radiation (low PAR). Here, we investigated how several Brassicaceae species from different habitats respond to low R:FR and low PAR in terms of elongation, photosynthesis, and photoacclimation. Shade-tolerant plants such as hairy bittercress (Cardamine hirsuta) displayed a good adaptation to low PAR but a poor or null response to low R:FR exposure. In contrast, shade-avoider species, such as Arabidopsis (Arabidopsis thaliana), showed a weak photosynthetic

Received September 23, 2020. Accepted April 08, 2021. Advance access publication May 7, 2021
© American Society of Plant Biologists 2021. All rights reserved. For permissions, please email: journals.permissions@oup.com

performance under low PAR but they strongly elongated when exposed to low R:FR. These responses could be genetically uncoupled. Most interestingly, exposure to low R:FR of shade-avoider (but not shade-tolerant) plants improved their photoacclimation to low PAR by triggering changes in photosynthesis-related gene expression, pigment accumulation, and chloroplast ultrastructure. These results indicate that low R:FR signaling unleashes molecular, metabolic, and developmental responses that allow shade-avoider plants (including most crops) to adjust their photosynthetic capacity in anticipation of eventual shading by nearby plants.

Introduction

Light is essential for plants as a source of energy and environmental information. Shading by nearby individuals can reduce light quantity (i.e. photon supply) and hence compromise photosynthetic activity and growth, a problematic situation in intensive cropping systems. To deal with the outcomes of mutual shading, plants have developed response mechanisms based on the perception of light quality, i.e. spectral information (Casal, 2013; Martinez-Garcia et al., 2010). The preferential absorbance of red (R) light and reflection of far-red (FR) light by photosynthetic tissues results in a decreased ratio of R to FR (R:FR) when light is reflected from or filtered through green stems and leaves. The low R:FR is a very reliable light signal that announces the close presence of nearby plants that may compete for resources.

Plants growing in ecosystems where access to light is restricted (e.g. in forest understories) show a shade-tolerant habit by adapting their light capture and utilization systems to low light intensity conditions. In contrast, plants growing in open habitats are shade-avoiders (also referred to as shade-intolerant or sun-loving). In shade-avoider plant species, such as Arabidopsis (Arabidopsis thaliana) and most sun-loving crops, perception of the low R:FR signal by the phytochrome photoreceptors activates a signaling pathway that eventually triggers a set of responses known as the shade-avoidance syndrome (SAS). The most prominent phenotype following exposure to low R:FR is elongation (e.g. of seedling hypocotyl, leaf petiole, and stem internode tissues), intended to overgrow neighboring competitors and outcompete them in the access to light. If the neighboring individuals overgrow and eventually shade the plant, the consequent reduction in light quantity (i.e. in the amount of radiation available for photosynthesis) results in additional and stronger SAS responses such as reduced leaf size, attenuated defense mechanisms, and early flowering (RoigVillanova and Martinez-Garcia, 2016).

The most extensively studied SAS response by far is hypocotyl elongation in A. thaliana (At). In this species, low R:FR inactivates phytochrome B (phyB), releasing PHYTOCHROME INTERACTING FACTORs (PIFs) that can then regulate gene expression and promote elongation growth. This response is also repressed by negative SAS regulators such as ELONGATED HYPOCOTYL 5 (HY5), amongst many others (Cifuentes-Esquivel et al., 2013; Ciolfi et al., 2013). Biological activity of these transcription factors can be modulated by additional components of the SAS regulatory network such as LONG HYPOCOTYL IN FAR-RED 1 (HFR1, which binds PIFs to

prevent their binding to target genes) and phytochrome A (phyA, which gets stabilized in shade and then promotes HY5 accumulation; Ciolfi et al., 2013; Martinez-Garcia et al., 2014; Yang et al., 2018). Both HFR1 and phyA hence act as additional SAS repressors that were recently found to be instrumental for the adaptation to shade. Indeed, the shade-tolerant hairy bittercress (Cardamine hirsuta), a close relative of At, does not elongate when exposed to low R:FR unless the function of phyA or HFR1 is genetically lost in mutant plants (Hay et al., 2014; Molina-Contreras et al., 2019; Paulisic et al., 2021).

Differences between shade-avoider and shade-tolerant species are not restricted to changes in elongation after exposure to low R:FR. Photoacclimation (i.e. the ability of plants to adjust photosynthesis to changes in the incident light with specific phenotypic changes) also diverges. Variation of photoacclimation responses among species on day-to-week time scale has been associated to two main strategies (Murchie and Horton, 1997; Ptushenko and Ptushenko, 2019). The first one consists of an alteration of photosynthetic pigment content, which positively corresponds with photosynthetic capacity. The second one involves changes in the photosynthetic machinery, which appears to be more important in plant species from environments where temporal and spatial variations in light irradiance are common, e.g. margins of woodlands. Combinations of these two main strategies give rise to the observed diversity in photoacclimation. In the case of At and C. hirsuta (Ch), a differential response to low R:FR in terms of photosynthetic pigment accumulation has been observed. Chlorophyll and carotenoid levels drop about 20% in At plants grown under low R:FR conditions, whereas the decrease is attenuated in Ch plants (Molina-Contreras et al., 2019). Whether photosynthetic capacity and/or chloroplast ultrastructure is differentially impacted by low R:FR in these species remains unknown. In terms of light quantity, the shade-avoider At showed a lower capacity to acclimate to reduced photosynthetically active radiation (low PAR) but a higher capacity to acclimate to intense light (high PAR) compared to the shade-tolerant Ch (Molina-Contreras et al., 2019). A similar physiological behavior has been described for shade-avoider and shade-tolerant species of the genus Tradescantia (Benkov et al., 2019), a model to study the ecology of photosynthesis and the mechanisms of photoacclimation in plants (Ptushenko and Ptushenko, 2019). The possible connections between low R:FR signaling and photoacclimation responses in plants remain, however, virtually unknown. Here, we explored natural and engineered genetic diversity to investigate this connection using different Brassicaceae species.

Results

Different Brassicaceae species present divergent photoacclimation responses

We previously showed that, compared to sun-loving At Col0, shade-tolerant Ch Ox exhibits a better ability to maintain photosynthesis after transfer to low PAR but a stronger chlorophyll loss when light intensity increases (Molina-Contreras et al., 2019). To better characterize the photoacclimation responses of these two Brassicaceae species, both At and Ch were germinated and grown for 7 d under control conditions of a photosynthetic photon flux density (PPFD) in the PAR region of 20–24 mmol m^2 s^1 (W_{20}). Then they were transferred

to either lower PAR (W_4, PPFD of 4 mmol m^2 s^1) or higher PAR (W_{200}, PPFD of 200 mmol m^2 s^1) for up to seven more days (Figure 1). Light curve analysis at day 3 after the transfer already showed clearly opposite responses of At and Ch, i.e. a better photosynthetic activity of Ch compared to At when transferred to W_4 and a better activity of At compared to Ch when transferred to W_{200} (Figure 1A). Derived parameters such as maximum electron transport rate (ETRm) and photosynthetic rate in light-limited region of the light curve (alpha) also illustrated that At performed better than Ch after transfer to higher light (W_{200}) but worst after transfer to lower light (W_4; Figure 1B). Other photosynthetic parameters such as maximum quantum efficiency of PSII (Fv/Fm) and light useefficiency of PSII (UPSII) also showed differences between At and Ch at day 3 after transfer, but these differences became clearer at longer times of exposure to either W_{200} or W_4 (Figure 1C). Specifically, Fv/Fm values were lower in Ch than in At after transfer to higher light, while the opposite was observed when transferred to lower light. A similar

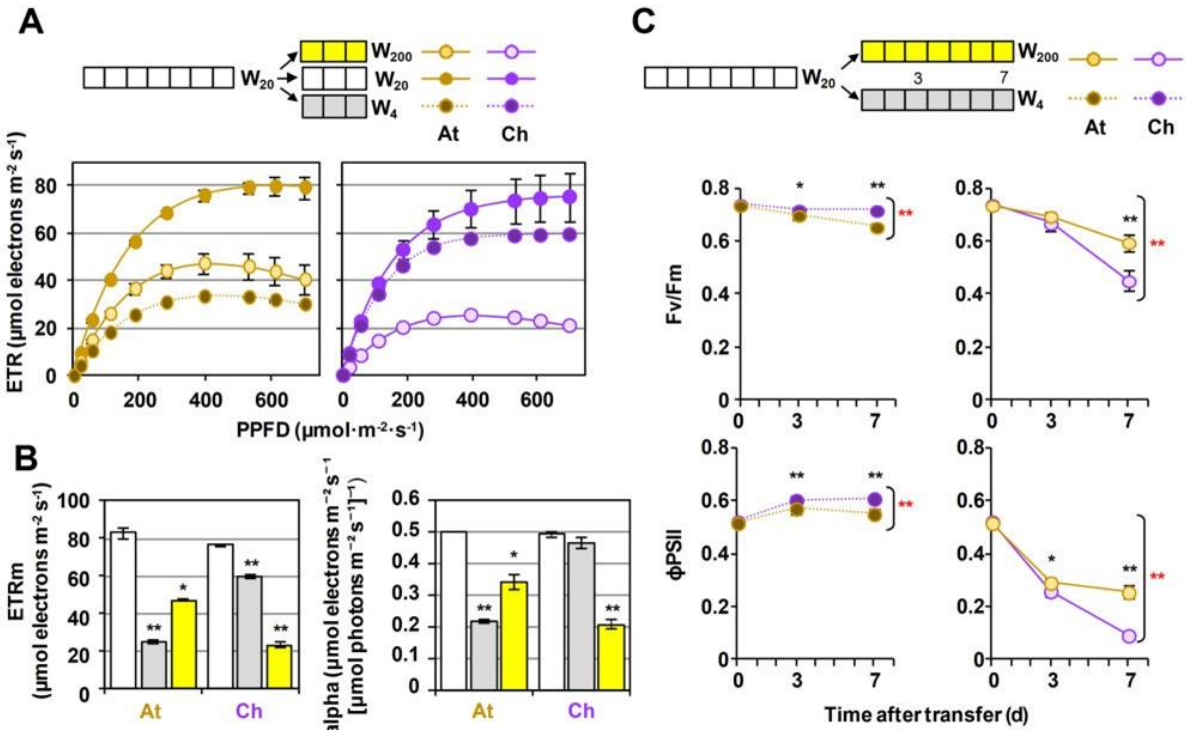


Figure 1. Arabidopsis thaliana and Cardamine hirsuta show antagonistic photoacclimation responses to higher and lower PAR. A, Light curves of At and Ch seedlings germinated and grown under white light of 20-mmolm2s1 PPFD (W20) for 7 d and then either kept under W20 or transferred to either 200 (W200) or 4 (W4) mmolm2s1 PPFD for 3 more days. Values represent the mean and standard error of n ¼ 3 plants for treatment. B, ETRm and photosynthetic rate in the light-limited region of the light curve (alpha) calculated from the curves shown in (A). Asterisks mark statistically significant changes (t test *P < 0.05, **P < 0.01) in W4 or W200 relative to W20. C, Maximum photochemical efficiency of PSII in the dark-adapted state (Fv/Fm) and effective quantum yield calculated at growth light (UPSII) of seedlings germinated and grown for 7 d under W20 and then transferred to either W200 or W4 for seven more days. Data were taken at 0, 3, and 7 d after the transfer. Values are mean and standard error of n ¼ 7 seedlings per treatment. Black asterisks mark statistically significant differences between At and Ch at each time point (t test *P < 0.05, **P < 0.01). Red asterisks indicate statistically significant differences between genotypes over time (two-way ANOVA, **P < 0.01).

trend was observed in the case of UPSII (Figure 1C). These results together indicate that Ch tolerates better the transfer to lower PAR (consistent with Ch being more tolerant to shade), while an increase in light irradiance compromises photosynthetic efficiency in Ch more than in shade-avoider At. Based on these results, we used light curve analysis at day 3 or earlier to estimate photoacclimation to lower PAR and Fv/Fm measurements at day 7 to estimate photoacclimation to higher PAR.

Besides At and Ch, the Brassicaceae family (mustards) includes many food crops (e.g. cauliflower, broccoli, radish, cabbage, kale, and similar green leafy vegetables) and a

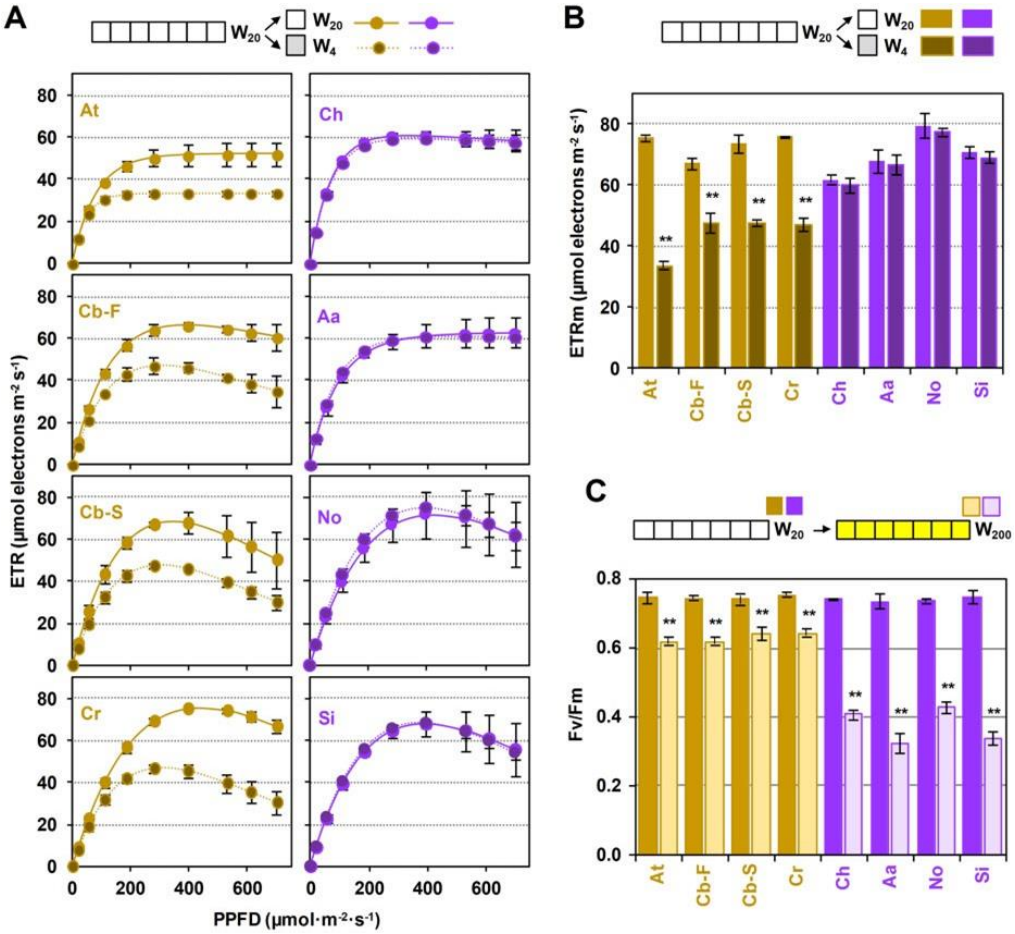


Figure 2. Brassicaceae plants can be grouped with either A. thaliana or C. hirsuta based on their photoacclimation responses. A, Light curves of Arabidopsis thaliana (At), Capsella bursa-pastoris (Cb-F and Cb-S), Capsella rubella (Cr), Cardamine hirsuta (Ch), Arabis alpina (Aa), Nasturtium officinale (No), and Sysimbrium irio (Si) seedlings germinated and grown under white light (W20) for 7 d and then either kept under W20 or transferred to lower PAR (W4) for one more day. Values represent the mean and standard error of n ¼ 3 plants for treatment. B, ETRm values calculated from the curves shown in (A). C, Fv/Fm values of seedlings grown for 7 d under W20 and then transferred to higher PAR (W200) for seven more days. Mean and standard error of n ¼ 9 seedlings per treatment are represented. Asterisks in (B) and (C) mark statistically significant changes t test, $P < 0.01$) relative to W20

diversity of wild species from forested and open habitats. As a first step to explore the possible connection between low PAR and low R:FR responses, we analyzed photoacclimation and hypocotyl elongation in six different Brassicaceae species or accessions, including At and Ch as controls. The selected wild mustards were alpine rock cress (Arabis alpina, Aa), two accessions of shepherd's purse (Capsella bursa-pastoris), Freiburg-1 (Cb-F) and Strasbourg-1 (Cb-S), pink shepherd'spurse (Capsella rubella, Cr), watercress (Nasturtium officinale, No), and London rocket (Sisymbrium irio, Si). Initially, we aimed to classify them as shade-avoider or shade-tolerant based on photoacclimation responses. After germination and growth for 7 d under W, seedlings were either kept under control W_{20} or transferred to lower light (W_4). Light curve analyses at day 1 after the transfer already showed differential responses that served to classify the accessions in two groups (Figure 2). Similar to the shade-avoider At, seedlings of Cb-F, Cb-S, and Cr showed a lowering of the curve under W_4 conditions, whereas those of Aa, No, and Si behaved as the shade-tolerant Ch and showed virtually identical light curves under W_{20} and W_4 (Figure 2A). ETRm and alpha values also illustrated that the W_4 treatment led to decreased photosynthetic performance in At, Cb-F, Cb-S, and Cr but not in Ch, Aa, No, and Si (Figure 2B; Supplemental Figure S1). We next analyzed photoacclimation to increased irradiation quantifying Fv/Fm before or after transferring 7-d-old W_{20}-grown seedlings to W_{200} for seven additional days. Again, At

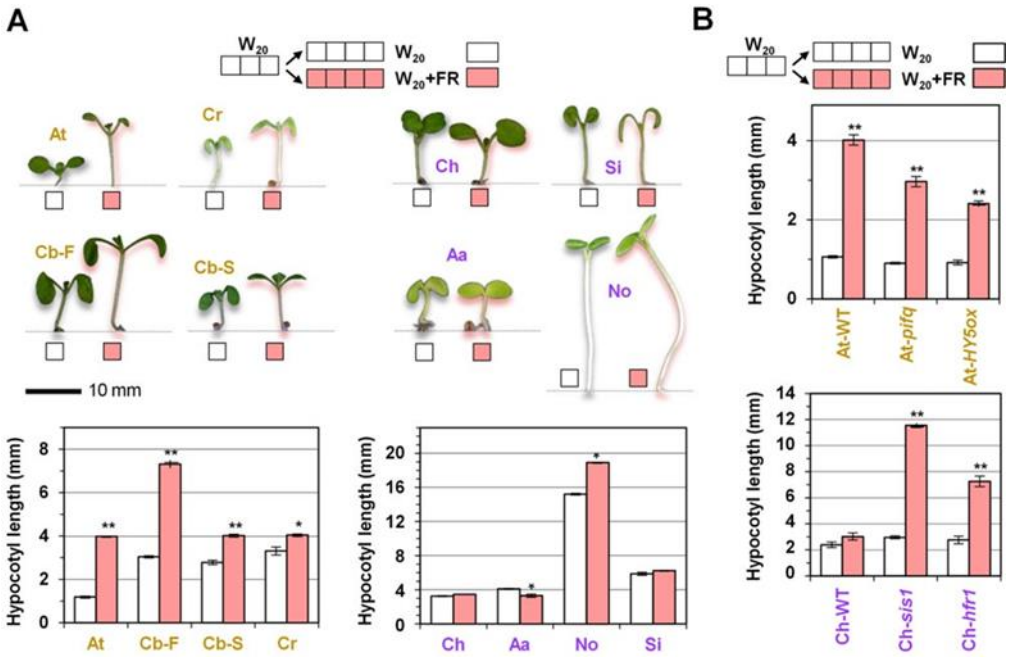


Figure 3. The hypocotyl elongation response to low R:FR is plastic in Brassicaceae plants. A, The indicated genotypes were germinated and grown under W20 for 3 d and then either kept under W20 or transferred to low R:FR (W20þFR) for four more days. Then, pictures were taken and hypocotyl length was measured. B, Hypocotyl length of the indicated mutants grown as indicated in (A). In both (A) and (B), mean and standard error of measurements from at least 20 seedlings in n ¼ 3 independent experiments per treatment are represented. Asterisks mark statistically signifi cant changes in W20þFR relative to W20 (t test, *P < 0.05, **P < 0.01).

grouped together with the two accessions of Cb and with Cr as they acclimated much better to high PAR compared to the group formed by Ch, Aa, No, and Si (Figure 2C). Together, these photoacclimation results led to classify the former group as shade-avoiders, and the latter as shade-tolerant species.

Photoacclimation responses can be uncoupled from shade-driven hypocotyl elongation

Next, we investigated whether the classification of the selected mustard species as shade-avoider or shade-tolerant based on their photoacclimation features corresponded with their elongation response to low R:FR. After germination and growth for 3 d under W_{20} (R:FR ¼ 1.5–3.3), seedlings were either kept under W_{20} or transferred to FR-supplemented W_{20} (W_{20}þFR, R:FR ¼ 0.02) for four additional days, and then hypocotyl length was measured (Figure 3). Similar to At, the Cb-F accession showed a strong hypocotyl elongation response, whereas Cb-S, Cr, and No elongated moderately in response to low R:FR. In contrast, Ch, Aa, and Si did not elongate in response to low R:FR (Figure 3A). These results confirm that the elongation response to low R:FR cannot be fully predicted based on the photoacclimation phenotype of a particular accession. Nonetheless, accessions classified as shade-avoider based on their photoacclimation behavior (i.e. poor photoacclimation to decreased PAR but good photoacclimation to increased PAR) exhibit a range of elongation responses to low R:FR (i.e. from moderate to strong elongation), whereas plant species with a shade-tolerant photoacclimation responses display either no elongation or a mild shade-avoider phenotype in terms of hypocotyl elongation when exposed to low R:FR (e.g. No).

The shade-avoider or shade-tolerant elongation phenotype in response to low R:FR can be reversed by manipulating the levels of specific SAS regulators. Previous results have shown that At lines overexpressing HY5 (At-HY5ox) display an attenuated hypocotyl response to low R:FR (Ortiz-Alcaide et al., 2019), whereas a similar but weaker response was observed in a quadruple mutant defective in all members of the photolabile PIF quartet (PIFQ), PIF1, PIF3, PIF4 and PIF5 (At-pifq; Figure 3B). Despite the different degrees of elongation response to low R:FR, these two lines showed photoacclimation responses to lower PAR very similar to those of wild-type (At-WT) controls (Figure 4). Both light curves (Figure 4A) and ETRm values (Figure 4B) were almost identical in At-WT plants and oximity shade hardly impacts their photoacclimation capacity, at least when plants are growing in the absence of the low R:FR signal. mutants hyposensitive to low R:FR. In the case of Ch, lines deficient in phyA (Ch-sis1) or HFR1 (Ch-hfr1) gain the ability to elongate when exposed to low R:FR (Molina-Contreras et al., 2019; Paulisic et al., 2021; Figure 3B). In contrast to the shade-hyposensitive At mutants, the hypersensitive Ch mutant lines appeared to gain a partial shade-avoider phenotype in terms of photoacclimation to low PAR, as lower values of light curves (Figure 4A) and ETRm (Figure 4B) were observed under W_4 compared to W_{20}. However, photoacclimation to increased PAR (W_{200}) estimated from Fv/Fm values and also from chlorophyll levels (MolinaContreras et al., 2019) was similar for Ch-WT, Ch-sis1, and Chhfr1 plants (Figure 4C). We therefore concluded that manipulation of the plant ability to elongate in response to

Activation of low R:FR signaling causes a decrease in pigment levels and photosynthetic activity

Low R:FR signals not only influence hypocotyl elongation but they are also known to reduce the contents of photosynthetic pigments (chlorophylls and carotenoids) in many plant species (Roig-Villanova et al., 2007; Cagnola et al., 2012; Patel et al., 2013; Bou-Torrent et al., 2015; MolinaContreras et al., 2019). The reduction is observed in both elongating (At-WT) and nonelongating (Ch-WT) seedlings, but it is stronger in the former (Figure 5). Cardamine hirsuta mutants that gained the ability to elongate in response to shade, such as Ch-sis1 and Ch-hfr1, also displayed stronger reductions in photosynthetic pigment contents relative to Ch-WT after low R:FR exposure (Figure 5A; MolinaContreras et al., 2019). Conversely, At mutants with a reduced ability to elongate in response to shade, such as Atpifq and At-HY5ox (Figure 3B), showed attenuated reduction of pigment contents relative to At-WT when exposed to low R:FR (Figure 5A).

To test whether decreases in photosynthetic pigment levels driven by simulated shade exposure might affect photosynthetic activity,

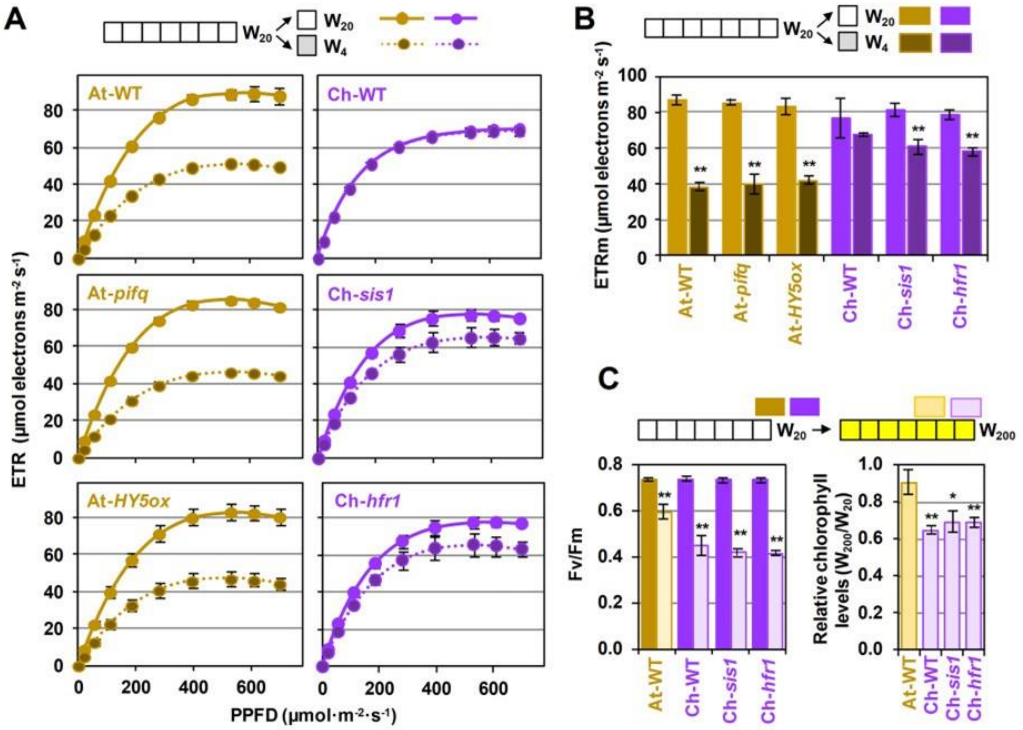


Figure 4. Mutations that alter sensitivity to low R:FR do not impact photoacclimation responses. A, Light curves of At and Ch wild-type and mutant seedlings germinated and grown under W20 for 7 d and then either kept under W20 or transferred to lower PAR (W4) for one more day. Values represent the mean and standard error of n ¼ 3 plants for treatment. B, ETRm values calculated from the curves shown in (A). C, Fv/Fm values and HPLC-determined relative chlorophyll levels of seedlings grown for 7 d under W20 and then transferred to higher PAR (W200) for seven more days. Mean and standard error of n ¼ 9 seedlings (Fv/Fm) or n ¼ 3 independent pools (HPLC) per treatment are represented. Asterisks in (B) and (C) mark statistically significant changes (t test, *P < 0.05, **P < 0.01) relative to W20.

we next measured Fv/Fm and UPSII in seedlings grown either under W_{20} or under W_{20}þFR (Figure 5B; Supplemental Figure S2A). Indeed, low R:FR was found to result in decreased photosynthetic activity in the lines with strong pigment loss responses independently on the species (At-WT, Ch-sis1, and Ch-hfr1). ETRm and alpha parameters also tended to be lower in WþFR-exposed AtWT, Ch-sis1, and Ch-hfr1 seedlings compared to W controls (Figure 5C; Supplemental Figure S2B). The effect of low R:FR on photosynthesis was much less dramatic in the rest of the lines (At-pifq, At-HY5ox, and Ch-WT), which consistently displayed a reduced impact of W_{20}þFR exposure on their photosynthetic pigment levels (Figure 5).

Proximity shade signals have also been found to impact photosynthesis at the level of gene expression. Analyses of low R:FR-triggered transcriptomic changes showed reduced levels of transcripts encoding photosynthesis-related proteins (e.g. enzymes involved in chlorophyll and carotenoid biosynthesis, components of the photosynthetic apparatus, and/or members of the carbon fixation process) in several species, including alfalfa (Lorenzo et al., 2019), maize (Shi et al., 2019), tomato (Cagnola et al., 2012), and At (Leivar et al., 2012). Interestingly, the changes in the expression of photosynthesis-related genes triggered by low R:FR are attenuated in the At-pifq mutant compared to At-WT seedlings (Figure 6). This is particularly evident in the case of low R:FR-repressed photosynthetic genes (Figure 6), suggesting that the PIF-mediated regulation of gene expression in response to low R:FR is instrumental for the observed changes in photosynthesis (Figure 5).

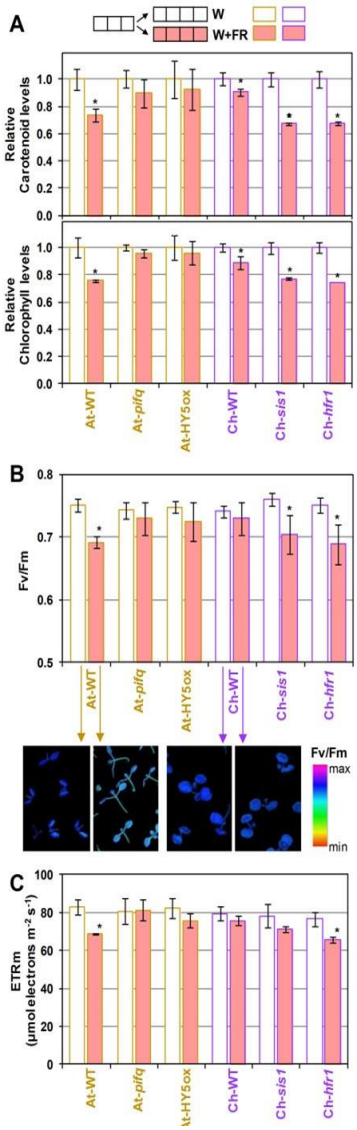


Figure 5. Activation of low R:FR signaling reduces photosynthetic pigment levels and activity. A, The indicated genotypes were germinated and grown under W_{20} for 3 d and then either kept under W_{20} or transferred to low R:FR (W_{20}þFR) for four more days. Then, the levels of photosynthetic pigments (carotenoids and chlorophylls) were quantified spectrophotometrically. B, Fv/Fm values of seedlings germinated and grown as indicated in (A). Lower pictures show false-color images in wild-type seedlings. (C) ETRm values of seedlings germinated and grown as indicated in (A). Mean and standard error of n ¼ 3 independent pools of seedlings (A) or n ¼ 9 seedlings (B and C) per treatment are represented. Asterisks mark statistically significant changes in W20þFR relative to W20 (t test, *P < 0.05).

Exposure of shade-avoider plants to low R:FR improves their photoacclimation to low PAR

The observation that exposure of low R:FR caused a decreased in photosynthetic activity of At-WT seedlings and shade-hypersensitive Ch mutants prompted us to analyze whether this light signal may also cause changes in chloroplast ultrastructure. Cotyledons from At-WT seedlings germinated and grown for 2 d under W_{20} and then either kept in W_{20} or transferred to W_{20}þFR for five additional days were collected and used for transmission electron microscopy (TEM). Chloroplasts from low R:FR-exposed samples were found to exhibit larger grana stacks and contain less and smaller plastoglobules compared to W-grown controls (Figure 7). Interestingly, similar changes are associated to low PAR photoacclimation (Rozak et al., 2002; Lichtenthaler, 2007; Wood et al., 2018).

We therefore reasoned that exposure to low R:FR in the absence of any light intensity change might trigger responses to anticipate a foreseeable shading involving a decrease in PAR. To test this hypothesis, we analyzed light curves of WT and mutant seedlings grown in either W_{20} or W_{20}þFR and then transferred to lower PAR (W_4) for 3 d (Figure 8). Pre-exposure of At-WT seedlings to low R:FR (W_{20}þFR) resulted in a strongly attenuated reduction in ETRm after their transfer to lower PAR (Figure 8A). In contrast, At mutants with reduced SAS elongation responses also lost the response to low R:FR in terms of improved photoacclimation to lower PAR (W_4; Figure 8A). Pretreatment with W_{20}þFR had virtually no effect on the photoacclimation of Ch-WT seedlings to lower PAR (W_4) but caused a slight but significant improvement of ETRm in shade-hypersensitive Ch mutants at day 1 after transfer to W_4 (Figure 8A). When When analyzing photoacclimation to higher PAR, pre-exposure of At-WT or Ch-WT seedlings to W20þFR resulted in no improvement compared to W20- grown controls (Figure 8B). If anything, Ch-WT seedlings grown under W20þFR photoacclimated worse than W20- grown seedlings when exposed to higher light intensity (Figure 8B).

The battery of mustards that grouped together with At in terms of photoacclimation responses (Cb-F, Cb-S, and Cr; Figure 2; Supplemental Figure S1) also showed improved photoacclimation to reduced PAR when pre-exposed to low R:FR, whereas the simulated shade signal did not have an effect on those clustered with Ch (Aa, No, and Si; Figure 8A). This low R:FR-dependent phenotype was independent of the growing light intensity and photoperiod, as it was also observed in At-WT seedlings growing under W_{200} or W_{200}þFR for 8 h or 16 h a day (i.e. under long day or short day conditions, respectively) and then transferred to W_{15} (Supplemental Figure S3). Because both the response of shade-avoider plants to low R:FR and the acclimation to low light involve a reduced respiration rate to cope with the limited generation of photoassimilates and hence contribute to carbon balance (Cagnola et al., 2012; Casal, 2013), we next measured changes in respiration in whole wild-type At and Ch seedlings exposed or not to low R:FR and then transferred to reduced PAR (Supplemental Figure S4). In W_{20} controls, respiration (estimated as total oxygen consumption in darkness) was reduced in At seedlings when they were moved to W_4. When exposed to W_{20}þFR, however, respiration was already lower and did not significantly change after transferring to lower PAR. In contrast, Ch seedlings showed similar respiration values in all conditions

(Supplemental Figure S4). Based on these data we conclude that detection and transduction of low R:FR signals not only allows shadeavoider plants to overgrow their neighbors but also to preadapt their photosynthetic and respiratory machinery to foreseeable conditions of actual shading involving reduced PAR. In contrast, shade-tolerant plants have a better adapted capacity to grow under reduce PAR and do not seem to use the low R:FR signal.

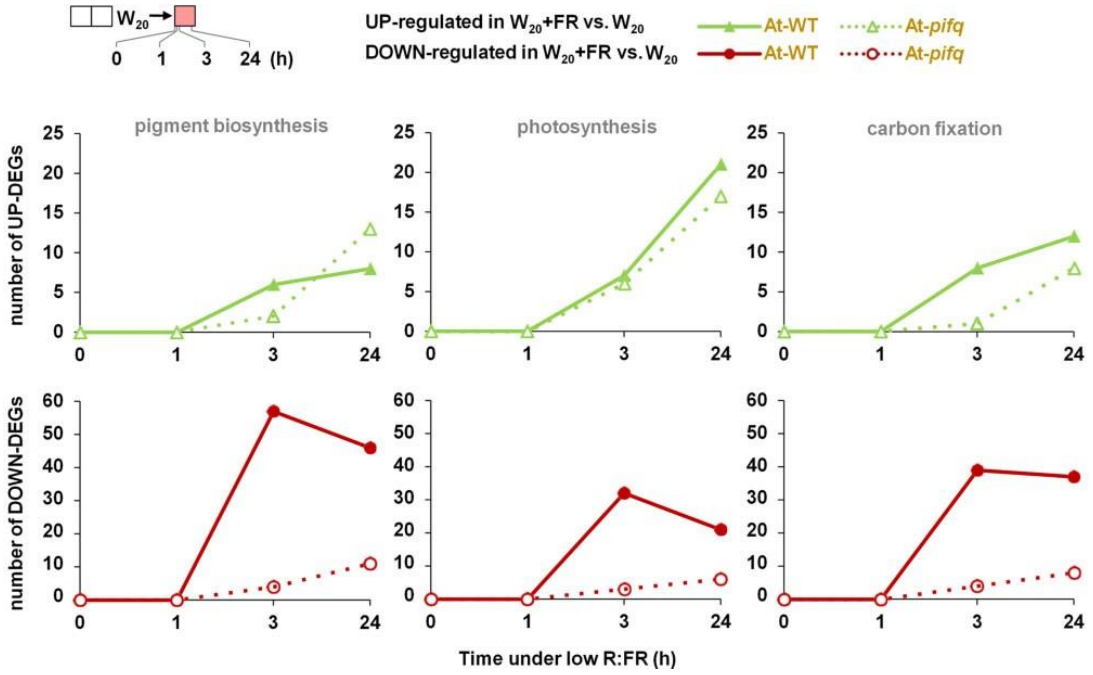


Figure 6. Exposure to low R/FR triggers changes in photosynthetic gene expression that are attenuated in the hyposensitive At-pifq mutant. Data were extracted from a publicly available experiment (Leivar et al., 2012). At-WT and At-pifq lines were germinated and grown under 19 mmolm2s1 PAR white light (W20, R:FR of 6.48) for 2 d and exposed to low R:FR (W20þFR, R:FR of 0.006) for 0, 1, 3, or 24 h. Plots represent the number of DEGs either up- or downregulated in W20þFR versus W20 that are involved in photosynthetic pigment biosynthesis (Kyoto Encyclopedia of Genes and Genomes pathways ath00906 and ath00860), photosynthesis (ath00195 and ath00196), and carbon fixation (ath00710)

Discussion

Plants have been traditionally classified as shade avoider and tolerant based mostly on their natural habitat, although virtually all plants are exposed to at least some degree of shade during their lifetime. As an ecological concept, shade tolerance refers to the capacity of a given plant to tolerate low light levels, but it is also associated with a wide range of traits, including phenotypic plasticity to optimize light capture (Valladares and Niinemets, 2008). Analyzing a range of caulescent herbs, it was suggested that the elongation response upon exposure to low R:FR was dependent on the shade habit, the shade-avoiders elongating the most and the shade-tolerant showing a mild or no elongation response (Smith, 1982). Indeed, elongation might not be the best solution for plants that spend all their lives under a canopy or permanently shaded by other plants. Another important parameter to

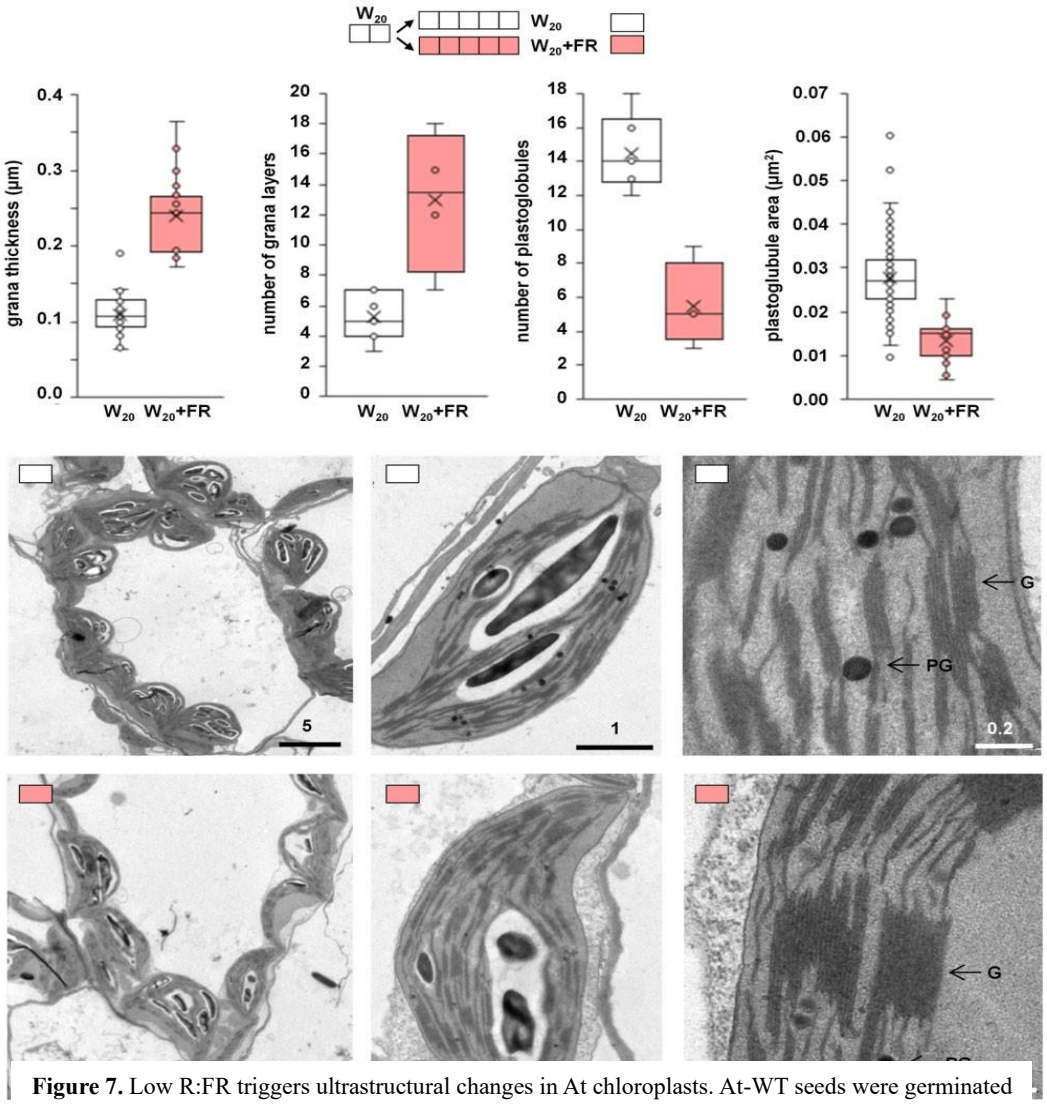


Figure 7. Low R:FR triggers ultrastructural changes in At chloroplasts. At-WT seeds were germinated and grown under W20 for 2 d and then either kept under W20 or transferred to low R:FR (W20þFR) for 5 more days. Cotyledons were then used for TEM analysis of chloroplast ultrastructure. Representative pictures at different scales (numbers indicate micrometer) are shown. Boxplots show quantification of the indicated parameters from the images. Boxes show the values between the upper and the lower quartile, the cross represents the mean and the horizontal line the median. Whiskers (the upper and lower extremes) and circles represent single data and the ones located outside of the whiskers limit are the outliers (data with the same numerical value are visualized as a single point). For quantifying grana thickness, all the distinguishable structures were used (W20 n ¼ 30, W20þFR n ¼ 20). For quantifying grana layers, four major grana complexes from higher magnifications were measured. For quantifying the number of plastoglobules, at least six individual chloroplasts for each treatment were used. Plastoglobule area was measured for all the plastoglobules (W20 n ¼ 87, W20þFR

ascertain the degree of shade tolerance of a plant is photoacclimation capacity, which is essential for plant fitness in environments with changing light input conditions (e.g. those where the growth of nearby plants may suddenly compromise access to light). By taking into account both parameters (the hypocotyl elongation response and the capacity to acclimate to low or high PAR), here we analyzed the shade tolerance of

several Brassicaceae species, including the closely related mustard model systems At and Ch. As a rule of thumb, we observed that Ch and other species showing a good photoacclimation response to lower PAR (and badly performing after transfer to higher PAR) showed a poor or null elongation response to low R:FR (Figures 2 and 3). Mustards such as At that photoacclimated poorly to lower PAR but better to higher PAR tended to more conspicuously elongate their hypocotyls in response to low R:FR, but there were exceptions of poorly elongating species such as No (Figures 2 and 3). Furthermore, mutation of genes encoding SAS regulators can dramatically change the elongation response to low R:FR without improving the photoacclimation phenotype (Figure 4). Together, these results confirm that the capacity for photosynthetic acclimation to changing irradiance is a species-specific trend (Bailey et al., 2001) and a reliable

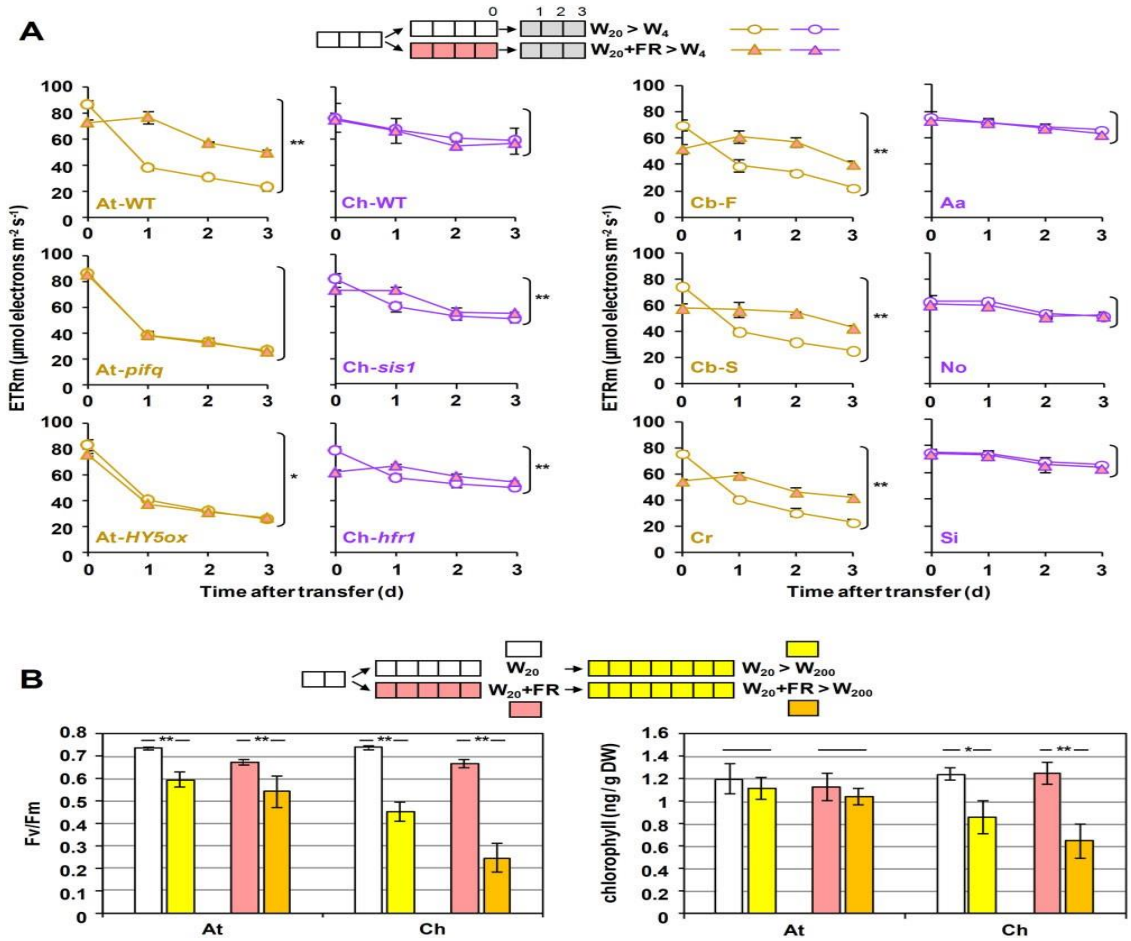


Figure 8. Pre-exposure to low R:FR improves the photoacclimation to low PAR in shade-avoider plants. A, The indicated genotypes were germinated and grown under W_{20} for 3 d, transferred to either W_{20} or W_{20}þFR for 4 d, and then exposed to W_4. Mean and standard error of ETRm values at 0, 1, 2, and 3 d after transfer to W_4 are shown (n ¼ 3 seedlings per treatment). Asterisks indicate statistically significant differences between treatments (W_{20} or W_{20}þFR) over time (two-way ANOVA, *P < 0.05, **P < 0.01). B, Wild-type At and Ch lines were germinated and grown under W_{20} for 2 d, transferred to either W_{20} or W_{20}þFR for 5 d, and then exposed to W_{200} for 7 more days. Fv/Fm values and HPLC-quantified chlorophyll levels were determined. Mean and standard error of n ¼ 7 seedlings (Fv/Fm) or n ¼ 3 independent pools (HPLC) per treatment are represented. Asterisks

indicator of shade tolerance. The shade-induced hypocotyl elongation response should only be used as a complementary phenotype to classify a plant as shade-tolerant (badly adapted to higher PAR exposure, well adapted to live under lower PAR and poorly responsive to low R:FR) or shade-avoider (well adapted to higher PAR, poor performers under lower PAR that elongate when exposed to low R:FR).Our results also unveiled that an activation of low R:FR signaling in shade-avoider species such as AtAt-WT and shade-tolerant Ch plants with mutations causing low R:FR hypersensitivity (Ch-sis1 and Ch-hfr1) regulated photosynthesis at multiple levels. We confirmed that exposure to WþFR caused a substantial decrease in the levels of photosynthetic pigments (chlorophylls and carotenoids) in these lines (Roig-Villanova et al., 2007; Bou-Torrent et al., 2015; Molina-Contreras et al., 2019; Paulisic et al., 2021) and proved that the changes had a direct impact on decreasing phytosynthetic activity (Figure 5). Low R:FR treatments are known to trigger changes in gene expression within minutes (Kohnen et al., 2016). These changes, which are often instrumental for altering rapid growth responses, such as hypocotyl or petiole elongation, are usually mediated by PIFs (Hornitschek et al., 2009; Galstyan et al., 2011; CifuentesEsquivel et al., 2013; de Wit et al., 2015; Gallemi et al, 2017). PIFs were also found to regulate longer-term changes in gene expression such as those affecting photosynthetic genes (Figure 6). Because loss of PIFQ function in the Atpifq mutant resulted in a much attenuated response to WþFR compared to At-WT in terms of photosynthetic gene expression (Figure 6) but it also prevented photosynthetic pigment and activity loss (Figure 5), we propose that stabilization of PIFQ proteins following low R:FR exposure triggers a reprogramming of photosynthesis-related gene expression that eventually results in lower pigment levels and reduced photosynthetic activity. Based on the results obtained with other mutants (Figure 5), we speculate that this signaling network is further influenced by factors such as HFR1 and HY5, which prevent PIF binding to target genes by heterodimerization (Hornitschek et al., 2009) or competition for promoter binding sites (Toledo-Ortiz et al., 2014), respectively.

Concomitant with the described molecular and physiological changes, we discovered that low R:FR treatment of AtWT seedlings triggered ultrastructural changes in the chloroplast endomembrane systems resembling those occurring after transfer to low PAR (Figure 7). Grana with more thylakoid layers and increased thickness were observed in the chloroplasts of At seedlings exposed to simulated shade. In contrast, chloroplasts from tobacco (Nicotiana tabacum) leaves that received end-of-day-FR treatments (considered to induce similar shade responses as low R:FR) showed fewer thylakoid layers per granum but more small grana spread throughout the chloroplast compared to end-of-day R controls (Kasperbauer and Hamilton, 1984). While these differences in chloroplast ultrastructure might derive from distinct treatments being applied to diverse species, both solutions likely contribute to optimize photosynthesis in the shade, when relatively less photons would strike a leaf. Indeed, leaves that develop under low PAR have chloroplasts with less plastoglobules (which are derived from thylakoid membranes) and more thylakoids per granum (Rozak et al., 2002; Lichtenthaler, 2007; Wood et al., 2018). Based on these results, we suggest that the chloroplast ultrastructural changes observed in At-WT plants grown under low R:FR are

most likely aimed to acclimate their photosynthetic machinery to perform better under low PAR by, for instance, allowing a more efficient energy transfer. In agreement, pretreatment with low R:FR improved photoacclimation to low PAR of At-WT seedlings but had no effect in At mutants defective in low R:FR signaling (Figure 8). Further experiments showed that the observed positive effect of low R:FR exposure for acclimation to low PAR can be observed in AtWT plants growing under different light conditions (Supplemental Figure S3) and in other shade-avoider Brassicaceae (Cb-F, Cb-S, and Cr), but not in shade-tolerant species such as Ch, Aa, No, and Si (Figure 8A).

At low irradiances, a proper balance between carbon allocation to growth and to respiration is important to meet the challenges associated with a shade environment. Wildtype At (shade-avoider) but not Ch (shade-tolerant) seedlings showed a drop in dark respiration when irradiation was reduced (Supplemental Figure S4), likely to reduce carbon loss for a better carbon balance. This adaptive mechanism might contribute to explain why shade-avoider and shade-tolerant species appear to show little or no differences in carbon balance under low light conditions (Sterck et al., 2013; Pons and Poorter, 2014). Similar to that observed for photosynthetic activity (Figure 8), the respiration drop observed in At-WT seedlings was attenuated by pre-exposure to low R:FR (Supplemental Figure S4). Interestingly, there is evidence for the specific activation/deactivation of respiratory pathways by the phytochrome system at different levels (Ribas-Carbo et al., 2008; Igamberdiev et al., 2014). Regardless of the signaling pathway connecting low R:FR perception to reduced photosynthesis and respiration, this is likely part of an anticipation mechanism for shade-avoider plants to prepare for the foreseeable reduction in PAR associated with shading. Indeed, low R:FR signals are perceived before actual shading takes place and light becomes limiting, and hence they are considered to act as a warning signal that shading might occur (Martinez-Garcia et al., 2010; Casal, 2013). When shade-avoider plants such as At and most crops (including tomato, cereals, or legumes) grow among taller plants or in a forest understory, they will use the low R:FR signals coming from a closing canopy to elongate (to overgrow its neighbors) but also to readapt its photosynthetic and respiratory machinery to low PAR before actual shading takes place. In contrast, shade-tolerant plants are adapted to grow under dim light and hence photoacclimation to low PAR is hardly improved even when hypersensitive mutants that show shade-avoider responses in terms of elongation (Figure 3) and photosynthesis (Figure 6) are pre-exposed to low R:FR (Figure 8).

While the observed decrease in respiration and photosynthetic pigment and activity levels in shade-avoider plants appears to be part of the anticipation mechanism to an eventual reduction in PAR, a too committed response might be detrimental if light conditions change (e.g. if shading does not occur or shade plants become exposed again to direct sunlight). We have previously shown that a compensation mechanism exist that represses the response to low R:FR when the photosynthetic capacity of chloroplasts is compromised (Ortiz-Alcaide et al., 2019). The retrograde (i.e. chloroplast-to-nucleus) pathway that adapts low R:FR perception and signaling to the photosynthetic status of the plant involves the antagonistic factors PIFs and HY5, which also participate in retrograde

signaling when underground seedlings are illuminated and start their photomorphogenic (i.e. photosynthetic) development (Ruckle et al., 2007; Martin et al., 2016; Xu et al., 2016; Ortiz-Alcaide et al., 2019). The balance of positive and negative regulators together with the chloroplast-mediated control of SAS likely contribute to prevent an excessive response to shade, hence preventing photooxidative damage (resulting from light intensity exceeding the photosynthetic capacity of the plant) and facilitating the return to high R:FR conditions if the low R:FR signal disappears (e.g. if a commitment to the shadeavoidance lifestyle is unnecessary). Together, our work demonstrates that regulation of photosynthetic (chloroplast) performance is both an output and an input of the response of plants to shade. Our results therefore contribute to a better understanding of how plants respond to shade, a knowledge that will contribute to optimally grow crop plants closer together or/and under canopies (e.g. in intercropping settings).

Materials and methods

Plant material and growth conditions

Alpine rock cress (Arabis alpina, pep1-1 mutant; Wang et al., 2009), Arabidopsis (Arabidopsis thaliana, Col-0 accession), hairy bittercress (Cardamine hirsuta, Oxford, Ox accession; Molina-Contreras et al., 2019), shepherd's purse (Capsella bursa-pastoris, accessions Strasbourg-1, Str-1 and Freiburg-1, Fre-1), pink shepherd's-purse (Capsella rubella), and London rocket (Sysimbrium irio) plants were grown in the greenhouse under long-day photoperiods (16-h light and 8-h dark) to produce seeds, as described (Gallemi et al., 2017). Seeds of C. bursa-pastoris were collected by Ruben Alcazar (University of Barcelona, Spain) from wild populations in Strasbourg (France, coordinates: 48.612436, 7.767881; Str-1) and Freiburg (Germany, coordinates: 47.994945, 7.861979; Fre-1). Seeds of C. rubella, collected from wild populations in Crete (Greece, coordinates 35.29, 24.42; accession 879) were previously described (Koenig et al., 2019). Seeds of S. irio were collected from wild populations in Bellaterra

(Barcelona, Spain, coordinates: 41.497731, 2.109558). Seeds of watercress (Nasturtium officinale) were provided by a seed company (www.semillasfito.es). Arabidopsis thaliana and Ch mutant and transgenic lines were previously available in our laboratories (Molina-Contreras et al., 2019; Ortiz-Alcaide et al., 2019; Paulisic et al., 2021).

For the light acclimation experiments seedlings were germinated and grown in Petri dishes containing solid medium without sucrose (0.5 MS): 2.2 gL^{1} MS basal salt mixture (Duchefa), 1% (w/v) agar, 0.25 gL^{1} 2-(N-morpholino)ethanesulfonic acid (MES; Sigma Aldrich), pH 5.7). Normal light conditions refer to white light (W) produced by cool-white vertical fluorescent tubes of a photosynthetic photon flux density in the PAR region (PPFD) of 20-24 mmol m^{2} s^{1} (W_{20}) with a R:FR of 1.5–3.3. Low light and high light conditions corresponded to W of PPFD of 4 (W_{4}) and 200 (W_{200}) mmol m^{2} s^{1}, respectively, produced by horizontal fluorescent tubes. Low R:FR treatment was produced by supplementing W_{20} with FR (W_{20}þFR). FR was emitted from a GreenPower LED module HF FR (Philips), providing a R:FR of 0.02 (Martinez-Garcia et al., 2014). For the light acclimation experiments shown in Supplemental Figure S3, seedlings were germinated and grown in

Petri dishes, as previously described, but exposed to long-day (16-h light/8-h darkness) or short-day (8-h light/16-h darkness) photoperiods. The light part of the photoperiod was produced by cool-white horizontal fluorescent tubes of 200–210 mmol m^2 s^1 of PPFD (W_{200}) with R:FR of 2–3.5). In that case, low light conditions corresponded to values of 15 mmol m^2 s^1 PPFD (W_{15}). In this set-up, low R:FR treatment was produced by supplementing W_{200} with the same FR lamps described above (W_{200}þFR), obtaining a R:FR of 0.2–0.25. Light fluence rates were measured with a Spectrosense2 meter (Skye Instruments Ltd), which provides PPFD (400–700 nm), and photon flux density in 10 nm windows of R (664–674 nm) and FR (725–735 nm) regions to calculate the R:FR (Martinez-Garcia et al., 2014). Full spectra photon distribution of W and WþFR treatments have been described elsewhere (Molina-Contreras et al., 2019).

Measurement of hypocotyl length

For hypocotyl measurement, about 30 seeds of each genotype were germinated and grown on plates containing 0.5 MS solid media. For quantification of hypocotyl length, at least 20 seedlings were analyzed with the FIJI-ImageJ software (Schindelin et al., 2012), as described (Roig-Villanova et al., 2019). All experiments were repeated at least three times with consistent results. Hypocotyl measurements from all the different experiments were averaged.

Photosynthetic measurements and pigment quantification

Whole seedlings were harvested, ground in liquid nitrogen, and the resulting powder was used for quantification of chlorophylls and carotenoids either spectrophotometrically or by high performance liquid chromatography (HPLC) as described (Bou-Torrent et al., 2015). Chlorophyll fluorescence measurements were carried out on seedlings using a MAXI-PAM fluorometer (Heinz Walz GmbH) as described (Molina-Contreras et al., 2019). Briefly, for every measurement the whole cotyledons of seven seedlings were considered. Effective quantum yield of photosystem II (PSII) under growth light, UPSII, was measured as DF/Fm^0, where DF corresponds to Fm^0F (the maximum minus the minimum fluorescence of light-exposed plants). Maximum quantum yield of PSII, Fv/Fm, was calculated as (FmFo)/Fm, where Fm and Fo are, respectively, the maximum and the minimum fluorescence of dark-adapted samples. For dark acclimation, plates were incubated for at least 30 min in darkness to allow the full relaxation of photosystems. Light curves were constructed with 10 incremental steps of actinic irradiance (E; 0, 20, 55, 110, 185, 280, 395, 530, 610, 700 lmol photons$m^2$$s^1$of PPFD). For each step, UPSII was monitored every minute and electron transport rate (ETR) was calculated as EUPSII0.84 0.5 (where 0.84 is the light absorptance by an average green leaf and 0.5 is the fraction of absorbed quanta available for PSII). The light response and associated parameters ETRm (maximum electron transport rate) and alpha (photosynthetic rate in lightlimited region of the light curve) were characterized by fitting iteratively the model of the rETR versus E curves using MS Excel Solver (Platt et al., 1980). The fit was very good in all the cases ($r > 0.98$).

Respiration measurements

Seedlings were germinated and grown on 0.5 MS plates, as described (Supplemental Figure S4). Before the measurements, seedlings were placed in the dark for about 30 min to avoid light-enhanced dark respiration. Five to 10 seedlings were then collected,

immediately weighed, and placed into the respiration cuvette containing the respiration buffer (30mM MES, pH 6.2, 0.2-mM $CaCl_2$). Oxygen uptake rates were measured in darkness using a liquid-phase Clark-type oxygen electrode (Rank Brothers Ltd.) as previously described (Florez-Sarasa et al., 2009) at a constant temperature of 23C.

Microarray data analyses

Microarray data corresponding to Col-0 At-WT and At-pifq seedlings exposed to low-R:FR for 0, 1, 3, and 24 h (Leivar et al., 2012) were analyzed to select for differentially expressed genes (DEGs) specifically related to photosynthesis. The reported list of DEGs was further filtered using cutoffs of FDR <0.05 and log2-transformed fold change higher than 0.585 for upregulated genes and lower than 0.599 for downregulated genes. Then, photosynthesis-related genes were identified by using the Kyoto Encyclopedia of Genes and Genomes Mapper tool (Kanehisa and Sato, 2020).

Transmission electron microscopy

TEM was carried out as described (Flores-Perez et al., 2008). Chloroplast features in the pictures were quantified by using the FIJI-ImageJ software (Schindelin et al., 2012).

Accession numbers

Sequence data from this article can be found in the EMBL/ Genbank and C. hirsuta genetic and genomic resource (http://chi.mpipz.mpg.de) data libraries under the following accession numbers:

AT1G02340 (AtHFR1), AT5G11260 (AtHY5), AT2G20180 (AtPIF1), AT1G09530 (AtPIF3), AT2G43010 (AtPIF4), AT3G59060 (AtPIF5), CARHR001660 (ChHFR1), and CARHR009540 (SIS1/ChPHYA).

Supplemental data

The following materials are available in the online version of this article.

Supplemental Figure S1. Alpha values calculated from the light curves shown in Figure 2A.

Supplemental Figure S2. Activation of low R:FR signaling reduces photosynthetic activity.

Supplemental Figure S3. Pre-exposure to low R:FR improves photoacclimation to lower PAR in A. thaliana plants grown under photoperiods.

Supplemental Figure S4. Exposure to low R:FR differentially impacts respiration rate of shade-avoider and shadetolerant plants.

Acknowledgments

We thank Mª Rosa Rodr´ıguez (CRAG) for technical support, and George Coupland (MPI for Plant Breeding Research, Cologne, Germany), Rube´n Alcazar (Universitat de Barcelona, Spain) and Ignacio Rubio (CRAG) for providing mustard seeds.

Funding

L.M. received a predoctoral fellowships from La Caixa Foundation (INPhINIT fellowship LCF/BQ/IN18/11660004). W.Q. is a recipient of a predoctoral Chinese Scholarship Council (CSC) fellowship. A.I.-S. is supported by a predoctoral fellowship from MICINN (PRE2018-083610). I.F.-S. has received funding from the European Union's Horizon 2020 research and

innovation programme under the Marie Skłodowska-Curie grant agreement no. 753301. Our research is supported by grants from MICINN-FEDER (BIO201785316-R, and BIO2017-84041-P) and AGAUR (2017-SGR1211, 2017-SGR710 and Xarba) to J.F.M.-G. and M.R.-C. We also acknowledge the support of the MINECO for the "Centro de Excelencia Severo Ochoa 2016-2019" award SEV-2015-0533 and by the CERCA Programme/Generalitat de Catalunya.

Conflict of interest statement. The authors declare no competing interests.

References

Bailey S, Walters RG, Jansson S, Horton P (2001) Acclimation of Arabidopsis thaliana to the light environment: the existence of separate low light and high light responses. Planta 213: 794–801

Benkov MA, Yatsenko AM, Tikhonov AN (2019) Light acclimation of shade-tolerant and sun-resistant Tradescantia species: photochemical activity of PSII and its sensitivity to heat treatment. Photosynth Res 139: 203–214

Bou-Torrent J, Toledo-Ortiz G, Ortiz-Alcaide M, CifuentesEsquivel N, Halliday KJ, Martinez-Garcia JF, RodriguezConcepcion M (2015) Regulation of carotenoid biosynthesis by shade relies on specific subsets of antagonistic transcription factors and cofactors. Plant Physiol 169: 1584–1594

Cagnola JI, Ploschuk E, Benech-Arnold T, Finlayson SA, Casal JJ (2012) Stem transcriptome reveals mechanisms to reduce the energetic cost of shade-avoidance responses in tomato. Plant Physiol 160: 1110–1119

Casal JJ (2013) Photoreceptor signaling networks in plant responses to shade. Annu Rev Plant Biol 64: 403–427

Cifuentes-Esquivel N, Bou-Torrent J, Galstyan A, Gallemi M, Sessa G, Salla Martret M, Roig-Villanova I, Ruberti I, Martinez-Garcia JF (2013) The bHLH proteins BEE and BIM positively modulate the shade avoidance syndrome in Arabidopsis seedlings. Plant J 75: 989–1002

Ciolfi A, Sessa G, Sassi M, Possenti M, Salvucci S, Carabelli M, Morelli G, Ruberti I (2013) Dynamics of the shade-avoidance response in Arabidopsis. Plant Physiol 163: 331–353

de Wit M, Ljung K, Fankhauser C (2015) Contrasting growth responses in lamina and petiole during neighbor detection depend on differential auxin responsiveness rather than different auxin levels. New Phytol 208: 198–209

Flores-Perez U, Sauret-Gueto S, Gas E, Jarvis P, RodriguezConcepcion M (2008) A mutant impaired in the production of plastome-encoded proteins uncovers a mechanism for the homeostasis of isoprenoid biosynthetic enzymes in Arabidopsis plastids. Plant Cell 20: 1303–1315

Florez-Sarasa I, Ostaszewska M, Galle A, Flexas J, Rychter AM, Ribas-Carbo M (2009) Changes of alternative oxidase activity, capacity and protein content in leaves of Cucumis sativus wild-type and MSC16 mutant grown under different light intensities. Physiol Plant 137: 419–426

Galstyan A, Cifuentes-Esquivel N, Bou-Torrent J, Martinez-Garcia JF (2011) The shade avoidance syndrome in Arabidopsis: a fundamental role for atypical basic helix-loop-helix proteins as transcriptional cofactors. Plant J 66: 258–267

Gallemi M, Molina-Contreras MJ, Paulisic S, Salla-Martret M, Sorin C, Godoy M, Franco-Zorrilla JM, Solano R, Martinez-Garcia JF (2017) A non-DNA-binding activity for the ATHB4 transcription factor in the control of vegetation proximity. New Phytol 216: 798–813

Hay AS, Pieper B, Cooke E, Mandakova T, Cartolano M, Tattersall AD, Ioio RD, McGowan SJ, Barkoulas M, Galinha C, et al. (2014) Cardamine hirsuta: a versatile genetic system for comparative studies. Plant J 78: 1–15

Hornitschek P, Lorrain S, Zoete V, Michielin O, Fankhauser C (2009) Inhibition of the shade avoidance response by formation of non-DNA binding bHLH heterodimers. EMBO J 28: 3893–3902

Igamberdiev AU, Eprintsev AT, Fedorin DN, Popov VN (2014) Phytochrome-mediated regulation of plant respiration and photorespiration. Plant Cell Environ 37: 290–299

Kanehisa M, Sato Y (2020) KEGG Mapper for inferring cellular functions from protein sequences. Protein Sci 29: 28–35

Kasperbauer MJ, Hamilton JL (1984) Chloroplast structure and starch grain accumulation in leaves that received different red and far-red levels during development. Plant Physiol 74: 967–970

Koenig D, Hagmann J, Li R, Bemm F, Slotte T, Neuffer B, Wright SI, Weigel D (2019) Long-term balancing selection drives evolution of immunity genes in Capsella. eLife 8

Kohnen MV, Schmid-Siegert E, Trevisan M, Petrolati LA, Senechal F, Muller-Moule P, Maloof J, Xenarios I, Fankhauser C (2016) Neighbor detection induces organ-specific transcriptomes, revealing patterns underlying hypocotyl-specific growth. Plant Cell 28: 2889–2904

Leivar P, Tepperman JM, Cohn MM, Monte E, Al-Sady B, Erickson E, Quail PH (2012) Dynamic antagonism between phytochromes and PIF family basic helix-loop-helix factors induces selective reciprocal responses to light and shade in a rapidly responsive transcriptional network in Arabidopsis. Plant Cell 24: 1398–1419

Lichtenthaler HK (2007) Biosynthesis, accumulation and emission of carotenoids, alpha-tocopherol, plastoquinone, and isoprene in leaves under high photosynthetic irradiance. Photosynth Res 92: 163–179

Lorenzo CD, Alonso Iserte J, Sanchez Lamas M, Antonietti MS, Garcia Gagliardi P, Hernando CE, Dezar CAA, Vazquez M, Casal JJ, Yanovsky MJ, et al. (2019) Shade delays flowering in Medicago sativa. Plant J 99: 7–22

Martin G, Leivar P, Ludevid D, Tepperman JM, Quail PH, Monte E (2016) Phytochrome and retrograde signalling pathways converge to antagonistically regulate a light-induced transcriptional network. Nat Commun 7: 11431

Martinez-Garcia JF, Galstyan A, Salla-Martret M, CifuentesEsquivel N, Gallem´ı M, Bou-Torrent J (2010) Regulatory components of shade avoidance syndrome. Adv Bot Res 53: 65–116

Martinez-Garcia JF, Gallemi M, Molina-Contreras MJ, Llorente B, Bevilaqua MR, Quail PH (2014) The shade avoidance syndrome in Arabidopsis: the antagonistic role of phytochrome a and B differentiates vegetation proximity and canopy shade. PLoS One 9: e109275

Molina-Contreras MJ, Paulisic S, Then C, Moreno-Romero J, Pastor-Andreu P, Morelli L, Roig-Villanova I, Jenkins H, Hallab A, Gan X, et al. (2019) Photoreceptor activity contributes to contrasting responses to shade in Cardamine and Arabidopsis seedlings. Plant Cell 31: 2649–2663

Murchie EH, Horton P (1997) Acclimation of photosynthesis to irradiance and spectral quality in British plant species: chlorophyll content, photosynthetic capacity and habitat preference Plant Cell Environ 20: 438–448

Ortiz-Alcaide M, Llamas E, Gomez-Cadenas A, Nagatani A, Martinez-Garcia JF, Rodriguez-Concepcion M (2019) Chloroplasts modulate elongation responses to canopy shade by retrograde pathways involving HY5 and ABA. Plant Cell

Patel D, Basu M, Hayes S, Majlath I, Hetherington FM, Tschaplinski TJ, Franklin KA (2013) Temperature-dependent shade avoidance involves the receptor-like kinase ERECTA. Plant J 73: 980–992

Paulisic S, Qin W, Arora Veraszto H, Then C, Alary B, Nogue F, Tsiantis M, Hothorn M, Martinez-Garcia JF (2021) Adjustment of the PIF7-HFR1 transcriptional module activity controls plant shade adaptation. EMBO J 40: e104273

Platt T, Gallegos CL, Harrison WG (1980) Photoinhibition of photosynthesis in natural assemblages of marine phytoplankton. J Mar Res 38: 687–701

Pons TL, Poorter H (2014) The effect of irradiance on the carbon balance and tissue characteristics of five herbaceous species differing in shade-tolerance. Front Plant Sci 5: 12

Ptushenko OS, Ptushenko VV (2019) Tradescantia-based models: a powerful looking glass for investigation of photoacclimation and photoadaptation in plants. Physiol Plant 166: 120–133

Ribas-Carbo M, Giles L, Flexas J, Briggs W, Berry JA (2008)Phytochrome-driven changes in respiratory electron transport partitioning in soybean (Glycine max. L.) cotyledons. Plant Biol (Stuttg) 10: 281–287

Roig-Villanova I, Bou-Torrent J, Galstyan A, Carretero-Paulet L, Portoles S, Rodriguez-Concepcion M, Martinez-Garcia JF (2007) Interaction of shade avoidance and auxin responses: a role for two novel atypical bHLH proteins. EMBO J 26: 4756–4767

Roig-Villanova I, Martinez-Garcia JF (2016) Plant responses to vegetation proximity: a whole life avoiding shade. Front Plant Sci 7: 236

Roig-Villanova I, Paulisic S, Martinez-Garcia JF (2019) Shade avoidance and neighbor detection. Methods Mol Biol 2026: 157–168

Rozak PR, Seiser RM, Wacholtz WF, Wise RR (2002) Rapid, reversible alterations in spinach thylakoid appression upon changes in light intensity. Plant Cell Environ 25: 421–429

Ruckle ME, DeMarco SM, Larkin RM (2007) Plastid signals remodel light signaling networks and are essential for efficient chloroplast biogenesis in Arabidopsis. Plant Cell 19: 3944–3960

Schindelin J, Arganda-Carreras I, Frise E, Kaynig V, Longair M, Pietzsch T, Preibisch S, Rueden C, Saalfeld S, Schmid B, et al. (2012) Fiji: an open-source platform for biological-image analysis. Nat Methods 9: 676–682

Shi Q, Kong F, Zhang H, Jiang Y, Heng S, Liang R, Ma L, Liu J, Lu X, Li P, et al. (2019) Molecular mechanisms governing shade responses in maize. Biochem Biophys Res Commun 516: 112–119

Smith H (1982) Light quality, photoperception, and plant strategy. Ann Rev Plant Physiol 33: 481–518

Sterck FJ, Duurrsma RA, Pearcy RW, Valladares F, Cieslak M, Weemstra M (2013) Plasticity influencing the light compensation point offsets the specialization for light niches across shrub species in a tropical forest understorey. J Ecol 101: 971–980

Toledo-Ortiz G, Johansson H, Lee KP, Bou-Torrent J, Stewart K, Steel G, Rodriguez-Concepcion M, Halliday KJ (2014) The HY5-PIF regulatory module coordinates light and temperature control of photosynthetic gene transcription. PLoS Genet 10: e1004416

Valladares F, Niinemets U (2008) Shade tolerance, a key plant feature of complex nature and consequences. Ann Rev Ecol Evol Syst 39: 237–257

Wang R, Farrona S, Vincent C, Joecker A, Schoof H, Turck F, Alonso-Blanco C, Coupland G, Albani MC (2009) PEP1 regulates perennial flowering in Arabis alpina. Nature 459: 423–427

Wood WHJ, MacGregor-Chatwin C, Barnett SFH, Mayneord GE, Huang X, Hobbs JK, Hunter CN, Johnson MP (2018) Dynamic thylakoid stacking regulates the balance between linear and cyclic photosynthetic electron transfer. Nat Plants 4: 116–127

Xu X, Chi W, Sun X, Feng P, Guo H, Li J, Lin R, Lu C, Wang H, Leister D, et al. (2016) Convergence of light and chloroplast signals for de-etiolation through ABI4-HY5 and COP1. Nat Plants 2: 16066

Yang C, Xie F, Jiang Y, Li Z, Huang X, Li L (2018) Phytochrome a negatively regulates the shade avoidance response by increasing auxin/indole acidic acid protein stability. Dev Cell 44: 29–41 e24

Annex 3

Edited by : *Miquel A. Gonzalez-Meler University of Illinois at Chicago, United States*

Reviewed by*:Brendan Michael O'Leary, Agriculture and Agri-Food Canada(AAFC), Canada Dinakar Challabathula, Central University of Tamil Nadu, India*

****Correspondence:*** *Nestor F. Del-Saz nesfernandez@udec.cl; Igor Florez-Sarasa gor.florez@cragenomica.es*

†These authors have contributed equally to this work Specialty section:
This article was submitted to Plant Physiology, a section of the journal Frontiers in Plant Science
Received: *10 December 2021*
Accepted: *19 April 2022*
Published: *17 May 2022*
Citation:
Del-Saz NF, Iglesias-Sanchez A, Alonso-Forn D, López-Gómez M, Palma F, Clemente-Moreno MJ, Fernie AR, Ribas-Carbo M and Florez-Sarasa I (2022) The Lack of Alternative Oxidase 1a Restricts in vivo Respiratory Activity and Stress-Related Metabolism for Leaf Osmoprotection and Redox Balancing Under Sudden Acute Water and Salt Stress in Arabidopsis thaliana. Front. Plant Sci. 13:833113. doi: 10.3389/fpls.2022.833113

The Lack of Alternative Oxidase 1aRestricts *in vivo* Respiratory Activity and Stress-Related Metabolism for Leaf Osmoprotection and Redox Balancing Under Sudden Acute Water and Salt Stress in *Arabidopsis thaliana*

Néstor F. Del-Saz[1]*†, **Ariadna Iglesias-Sanchez**[2]†, David Alonso-Forn[3], Miguel López-Gómez[4], Francisco Palma[4], María José Clemente-Moreno[5], Alisdair R. Fernie[6], Miquel Ribas-Carbo[5] and Igor Florez-Sarasa[2,7]

[1] Laboratorio de Fisiología Vegetal, Universidad de Concepción, Concepción, Chile, [2] Centre for Research in Agricultural Genomics CSIC-IRTA-UAB-UB, Barcelona, Spain, [3] Unidad de Recursos Forestales, Centro de Investigación y Tecnología Agroalimentaria de Aragón, Zaragoza, Spain, [4] Department of Plant Physiology, University of Granada, Granada, Spain, [5] Grup de Recerca en Biologia de les Plantes en Condicions Mediterranies, Departament de Biologia, Universitat de les Illes Balears, Palma, Spain, [6] Max Planck Institute of Molecular Plant Physiology, Potsdam, Germany, [7] Institut de Recerca i Tecnología Agroalimentàries (IRTA), Edifici CRAG, Barcelona, Spain

Keywords: water stress, salinity, alternative oxidase, oxygen-isotope fractionation, primary metabolism

frontiers | Frontiers in Plant Science

ORIGINALRESEARC H
published:17May202 2
doi:10.3389/fpls.2022.83311 3

Abstract:

In plants salt and water stress result in an induction of respiration and accumulation of stress-related metabolites (SRMs) with osmoregulation and osmoprotection functions that benefit photosynthesis. The synthesis of SRMs may depend on an active respiratory metabolism, which can be restricted under stress by the inhibition of the cytochrome oxidase pathway (COP), thus causing an increase in the reduction level of the ubiquinone pool. However, the activity of the alternative oxidase pathway (AOP) is thought to prevent this from occurring while at the same time, dissipates excess of reducing power from the chloroplast and thereby improves photosynthetic performance. The present research is based on the hypothesis that the accumulation of SRMs under osmotic stress will be affected by changes in folial AOP activity. To test this, the oxygen isotope-fractionation technique was used to study the in vivo respiratory activities of COP and AOP in leaves of wild-type Arabidopsis thaliana plants and of aox1a mutants under sudden acute stress conditions induced by mannitol and salt treatments. Levels of leaf primary metabolites and transcripts of respiratory-related proteins were also determined in parallel to photosynthetic analyses. The lack of in vivo AOP response in the aox1a mutants coincided with a lower leaf relative water content photosynthesis, Arabidopsis thaliana and a decreased accumulation of crucial osmoregulators. Additionally, levels of oxidative stress-related metabolites and transcripts encoding alternative respiratory components were increased. Coordinated changes in metabolite levels, respiratory activities and photosynthetic performance highlight the contribution of the AOP in providing flexibility to carbon metabolism for the accumulation of SRMs.

Introduction

Plants display several mechanisms for drought and salinity tolerance, however, these come with high energy and carbon demands that plant metabolism meets by adjusting photosynthesis and respiration (Munns et al., 2020; Vanlerberghe et al., 2020). An important tolerance mechanism to drought and salinity resides in the accumulation of metabolites that play multiple protective roles, including primary metabolites such as organic acids, sugars and polyols (Sanchez et al., 2008; Fàbregas and Fernie, 2019), as well as polyamines (Alcázar et al., 2020). These stress-related metabolites (SRMs) from primary metabolism, protect against osmotic and oxidative stress, serve as energy sources and/or are involved in stress-signalling pathways (Slama et al., 2015; Pires et al., 2016; Fàbregas and Fernie, 2019). At the same time, the synthesis and degradation of several SRMs involve metabolic pathways that are tightly linked to respiratory metabolism (Pires et al., 2016; Batista-Silva

et al., 2019; Bandehagh and Taylor, 2020). Thus, SRMs or their carbon precursors [i.e., glycolytic or tricarboxylic acid (TCA) cycle intermediates] are tightly associated to the generation of reducing equivalents (NADH and $FADH_2$), from which oxidation is coupled to the mitochondrial electron transport chain (mETC). A distinctive feature of the plant mETC is the presence of two terminal oxidases. In addition to the cyanide sensitive cytochrome oxidase (COX), the presence of a cyanide-resistant alternative oxidase (AOX) that couples the oxidation of ubiquinol with the reduction of O_2 to H_2O, confers to mETC the capacity to sustain O_2 consumption under COX restriction (Del-Saz et al., 2018; Vanlerberghe et al., 2020). Electron transport via the AOX pathway (AOP) is not coupled with energy conservation (Del-Saz et al., 2018; Vanlerberghe et al., 2020). Nonetheless, the AOP provides metabolic flexibility that helps plants acclimate to stress by allowing the oxidation of reducing equivalents coupled to TCA cycle and/or cytosolic reactions under conditions where the COX pathway (COP) is restricted (Del-Saz et al., 2018). In fact, the accumulation of SRMs has been reported to coincide with higher respiratory rates (Mattoo et al., 2006; Del-Saz et al., 2016; Pires et al., 2016; Bandehagh and Taylor, 2020), indicating an active mitochondrial metabolism under stress. Nevertheless, direct evidence about the influence of the AOP activity in modulating the synthesis of stress-related metabolites remains scarce.

The AOX protein is encoded by a multigene family which exhibits tissue-specific expression (Saisho et al., 1997; Clifton et al., 2006; Selinski et al., 2018a). AOX1 isoforms generally show the highest expression levels, being expressed in most tissues and induced by stress treatments in several species (Clifton et al., 2006; Vanlerberghe et al., 2020). Over the last two decades, reverse genetics has been used to decrease *AOX1* gene expression in order to test hypotheses regarding the role of the AOP. Following the suppression of *AOX1*, the amount of the AOX protein has been found to be markedly decreased concomitantly with a decrease in the AOP capacity (the maximum possible flux of electrons to AOX; Guy and Vanlerberghe, 2005; Umbach et al., 2005; Watanabe et al., 2010; Florez-Sarasa et al., 2011; Xu et al., 2012; Vishwakarma et al., 2015; Zhang et al., 2016; Garmash et al., 2020). In parallel, many studies have observed an increase in AOX protein or capacity under stress in wild-type plants (reviewed in Vanlerberghe, 2013; and in Vanlerberghe et al., 2020). In fact, a regulated overcapacity of AOP is thought to be required for ensuring an adequate activity under conditions inducing metabolic fluctuations (Rasmusson et al., 2009; Florez-Sarasa et al., 2011). By contrast to AOP capacity, *in vivo* AOP activity can be directly determined in the absence of added inhibitors by measuring the differential oxygen isotope discrimination during respiration (Day et al., 1996; Del-Saz et al., 2017). While there is substantial evidence on the molecular mechanisms regulating the AOX gene expression in response to drought and salinity stresses (Vanlerberghe, 2013; Dahal and Vanlerberghe, 2017; Zhu et al., 2018; Gong et al., 2020), only some studies have addressed when and to which extent the *in vivo* AOP activity is effectively responding. The *in vivo* AOP activity was reported to increase in response to severe drought and salt stress (Ribas-Carbo et al., 2005; Del-Saz et al., 2016), while unaltered activities were reported under milder or longer drought/salinity periods (Galle et al., 2010; Martí et al., 2011). These different responses denote, as previously highlighted (Munns et

al., 2020), that *in vivo* AOP activity determinations in combination with detailed metabolic and molecular analyses remain crucial for understanding the key changes in energy and carbon metabolism conferring drought (Vanlerberghe et al., 2020) and salt (Munns et al., 2020) tolerance.

In order to gain insight into the role of the AOP during stress-related metabolism, wild-type *Arabidopsis thaliana* plants and *aox1a* T-DNA insertional mutants, from which information regarding *in vivo* activity is still lacking, were treated with high concentrations (1 day, 300 mM) of mannitol and salt (NaCl), known to greatly induce the accumulation of several SRMs (Del-Saz et al., 2016; Darko et al., 2019). The *in vivo* activities of COP and AOP in leaves were measured using the oxygen-isotope discrimination technique and in parallel, leaf levels of primary metabolites and respiratory-related transcripts were also determined. In addition, leaf relative water content as well as photosynthetic performance, determined by chlorophyll fluorescence analysis in the dark and in the light, was also studied. We hypothesized that the lack of *AOX1a* will be associated with lower leaf rates of AOP respiration and less accumulation of SRMs under severe water and salt stress, with consequences for plant performance under stress.

Materials and Methods

Plant Material and Growth Conditions

Seeds of wild-type (WT) *A. thaliana* Columbia 0 (Col 0) and *aox1a* T-DNA insertion line (SALK_084897) were sown in pre-wetted pots with a mixture of peat-perlite (3:1). The T-DNA insertion within the *AtAOX1a* gene was confirmed by genomic PCR with T-DNA-specific primers and seeds from a homozygous line were used for the experiments. Pots were placed in plastic trays used for sub-irrigation. Plants were grown in a growth chamber for 32–35 days at 12 h/12 h photoperiod, 150 μmol quanta m^{-2} s^{-1} light intensity, 25°C/20°C day/night temperature and relative humidity above 50%. Plants were watered twice a week with half-strength Hoagland's solution (Epstein et al., 1972). On days 32–35, plants were divided in three groups, one was watered normally (control plants) while the other two were irrigated with watering solution containing 300 mM of sodium chloride (NaCl-treated plants) or 300 mM mannitol (Mannitol-treated plants). The analyses of control and treated plants were performed one day after the irrigation. All the experiments were repeated at least twice, and data is presented as a pool of at least two individual experiments (i.e., each consisting of two to four biological replicates/plants per genotype and treatment), since similar results were obtained in each individual experiment.

Respiration and Oxygen-Isotope Fractionation Measurements

Leaves were placed in the dark for 30 min to avoid lightenhanced dark respiration. The capacity of the alternative pathway (V_{alt}) was determined with an oxygen electrode as previously described (Del-Saz et al., 2016), and results were expressed in nmol O_2 g^{-1} dry weight s^{-1} as the mean ± SE of five or six biological replicates. Respiration and oxygen isotope fractionation measurements were performed as previously described (Del-Saz et al., 2016). Respiratory partitioning between the two respiratory pathways was calculated from the oxygen isotope

fractionation by the alternative oxidase (I_a) and the cytochrome oxidase (I_c). The I_a values, determined in the presence of 10 mM of KCN, were not significantly different between the genotypes and thus, the I_a mean value of calculations. Theh I_c, determined in presence of 25 mM of 30.8 ± 0.445 (six replicates) was used for all the partitioning Dry weights were obtained after drying leaves for 2 days at 60–h salicylhydroxamic acid (SHAM), was 20.5 (four replicates). Dry weights were obtained after drying leaves for 2 days at 60– Results were expressed in nmol O_2 g^{-1} dry weight s^{-1} as the mean ± SE of six or eight biological replicates.

Leaf Water Status

Leaf relative water content (RWC) was determined as follows:

$$RWC\ (\%) = (FW - DW)/(TW - DW) \times 100$$

where fresh (FW), turgid (TW) and dry (DW) weight of leaves were measured. FW was determined immediately after sampling; TW was obtained after incubating leaf discs in distilled water for 48 h in the dark at 4 °C (to minimize respiration losses) and DW was determined after drying for at least 2 days in an oven at 60– 70°C.

Photosynthetic Measurements

Chlorophyll fluorescence measurements were carried out on rosette leaves using a MAXI-PAM fluorometer (Heinz Walz GmbH) as previously described (Morelli et al., 2021; Annex 2). Briefly, for every measurement six rosette leaves from each plant were considered. The actual quantum efficiency of the photosystem II (PSII)-driven electron transport (δPSII) was determined under different light intensities (in µmol photons m^{-2} s^{-1} of photon flux density, PPFD): 800, 700, 600, 500, 400, 300, 200, 150, 100, 75, 50, 25 and 0. The chloroplast electron transport rate (ETR) was calculated as the product of δPSII x PPFD x 0.84 x 0.5, where 0.84 and 0.5 were assumed values for the leaf light absorptance and the fraction of absorbed quanta available for PSII. From the light response curves, the associated parameters ETR_m (maximum electron transport rate) and alpha (photosynthetic rate in light limited region of the light curve) were characterized by fitting iteratively the model of the rETR versus E curves using MS Excel Solver (Platt and Gallegos, 1980). The fit was very good in all the cases ($r > 0.98$). After the light curves, the maximum quantum efficiency of PSII, F_v/F_m, was calculated as $(F_m - F_o)/F_m$, where F_m and F_o are the maximum and the minimum fluorescence of dark-adapted samples, respectively. For dark acclimation, plants were incubated for at least 30 min in darkness to allow the full relaxation of photosystems.

Metabolite Profiling

Metabolite extractions were performed as described previously (Lisec et al., 2006) using approximately 50 mg of leaf tissue, previously frozen-powdered. Derivatization and GC–TOF–MS analyses were carried out as described previously (Lisec et al., 2006). Metabolites were identified manually by TagFinder software (Luedemann et al., 2012) using the reference library mass spectra and retention indices housed in the Golm Metabolome Database;[1] (Kopka et al., 2005). The parameters used for the peak annotation of the 46 metabolites can be found in Supplementary Table 1, which follows

previously reported recommendations (Fernie et al., 2011).

To process the GC-TOF-MS results, the intensity of a selected unique ion shown in Supplementary Table 1 was normalized to that of ribitol which was added to each sample as an internal standard, as well as to the fresh weight of the materials used for metabolite extraction. Fresh weight was then corrected by dry weight/fresh weight ratios used to determine the leaf RWC (see Section "Leaf Water Staus"). Thereafter, data were normalized to the mean value of Col-0 wild-type (WT) plants under control conditions (i.e., the value of all metabolites for WT at control conditions was set to 1). This normalization allowed the comparison of the relative metabolite levels among genotypes and treatments (Supplementary Table 2). In addition, leaf absolute metabolite levels (μmol gDW^{-1}) were also determined for all the metabolites detected and present in the authentic standards mixture (Supplementary Table 3). The experimental samples and standards mixtures containing 0, 100, 200, 500, and 1,000 ng of each compound were analysed in the same GC- MS runs, and the absolute metabolite amounts in the samples were calculated by extrapolation from standard curves using the peak intensity of a representative mass fragment. Values presented for both relative and absolute levels are means ± SE of four to six replicates corresponding to several fully expanded rosette leaves.

Western Blot Analysis

Protein extraction and western blot analysis was performed as previously described (Florez-Sarasa et al., 2016) with some modifications. Total plant protein extracts were obtained from 20 mg of frozen leaf powder resuspended in 100 μl SDS sample buffer [2% (w/v) SDS, 62.5mM Tris–HCl (pH 6.8), 10% (v/v) glycerol and 0.007% (w/v) bromophenol blue], 50 mM DTT and protease inhibitor cocktail (Roche Basel, Switzerland). Samples were incubated 30 min at 4°C to allow full reduction of the AOX protein and then boiled (95°C) for 5 min. The resuspended sample was centrifuged at 14,000 rpm for 10 min. After loading 25 μl on a 12% SDS-PAGE gel, proteins were transferred to a 0.45 μm Nitrocellulose membrane (Armersham Protan) using a semi-dry Trans-Blot ^{R} Turbo™ Transfer System of Bio-Rad. Membranes were incubated overnight at 4°C with diluted 1:500 polyclonal anti-AOX, AOX1 and 2 (AS04054, Agrisera, Sweden) or diluted 1:5,000 anti-Porin, voltage-dependent anion-selective channel protein 1–5 (AS07212, Agrisera, Sweden). Incubation with 1:20,000 horseradish peroxidase secondary antibodies (Cytiva) during 1h at room temperature. The detection of immunoreactive bands was performed using ECL SuperSignal™ West Femto Maximum Sensitivity Substrate (Thermo Fisher).

Chemiluminescent signals were collected by IQ 800 Armersham (Cytiva). The protein band quantifications were performed with ImageJ analysis software according to the manufacturer's instructions. The obtained band intensities for AOX were corrected for their corresponding porin band intensities and then normalized to the levels of the WT plants under control conditions (i.e., WT levels were set to 1). Three different immunoblot experiments per protein were performed and the image shown in Figure 1B belong to one of the three membranes obtained. Samples used in each of the three western blot experiments were a mixture of aliquots belonging to two biological replicates from

the same six biological replicates used for the gene expression analysis. The relative values presented in **Figure 1B** are means of the three western blot experiments.

Gene Expression Analysis

RNA was isolated from lyophilized leaves by using Maxwell ® RSC Plant RNA Kit (Promega Biotech Ibérica, Madrid, Spain) and automated system Maxwell ® RSC Instrument (Promega Biotech Ibérica, Madrid, Spain) according to the manufacturer's instructions, and was quantified using a NanoDrop 1000 spectrophotometer (Thermo Scientific,[1]). Afterward cDNA synthesis was performed following the recommendations of the Transcriptor First Strand cDNA Synthesis Kit (Roche Basel, Switzerland). Relative mRNA abundance was evaluated by quantitative PCR using LightCycler 480 SYBR Green I Master Mix (Roche Basel, Switzerland) on a LightCycler 480 realtime PCR system (Roche Basel, Switzerland). Primers used and the related information are detailed in the Supplementary Table 4. Two technical replicates of each biological replicate were performed, and the mean values were used for further calculations. Arabidopsis *AtUbqC* (At5g25760) was used as a reference gene to correct for differences in the total amount of transcripts and the $2^{-\Delta\Delta Ct}$ method (Livak and Schmittgen, 2001) was used to calculate the fold-change of gene expression. Finally, data were normalized to the mean value of plants under control conditions in each genotype (i.e., the level of all transcripts for WT and *aox1a* mutants at control was set to 1).

Statistical Analyses

For the statistical analyses in Figures 1–4 and 6, a oneway ANOVA with a level of significance of $P < 0.05$ was performed with SPSS statistical software package, version 25 (IBM Corp., 2016, Armonk, New York, NY, USA), and Duncan's posthoc test was used to determine statistically significant differences. In addition, Student's t tests were used for the statistical analyses in Figures 1B, 5, 6, Supplementary Figure 1, Supplementary Tables 2,3 in order to determine significant ($P < 0.05$) differences between genotypes under each experimental condition (**Figure 5**, **Supplementary Figure 1**, **Supplementary Tables 2,3**), or to determine significant ($P < 0.05$) differences between control and stress treatments in each genotype (Figures 1B, 6, Supplementary Tables 2,3).

[1] http://www.nanodrop.com/

Results

The Alternative Oxidase Capacity and Expression in *aox1a* and Wild-Type Plants Under Control and Stress Conditions

The capacity of the alternative oxidase pathway (V_{alt}), measured as the KCN-resistant respiration, was determined in both genotypes under control and stress treatments (Figure 1). As expected, V_{alt} was significantly ($P < 0.05$) lower in *aox1a* mutants than in WT plants (5.9 and 19.1 nmol O_2 g^{-1} DW s^{-1}, respectively) under control conditions. Under stress, V_{alt} increased in WT plants after salt treatment, while mannitol-treated plants displayed an intermediate V_{alt} (Figure 1A). On the other hand, V_{alt} remained similar in *aox1a* mutants under control and stress conditions, and it was much lower as compared to WT plants under stress conditions. Then, the AOX protein levels were determined in leaf crude extracts after immunoblotting analyses and quantified after normalization to mitochondrial porin levels (Figure 1B). In the line with respiratory capacity, the AOX protein levels were similarly increased after both stress treatments in WT plants. We did not detect any signal of AOX protein in the *aox1a* mutants as previously reported (Giraud et al., 2008; Strodtkötter et al., 2009). Thereafter, the expression profiles of the five genes encoding the AOX protein in *Arabidopsis* were determined by qPCR analyses in both genotypes under control and stress conditions (Figure 1C). Transcript levels of the *AOX1a* gene were not detected in the *aox1a* mutant,

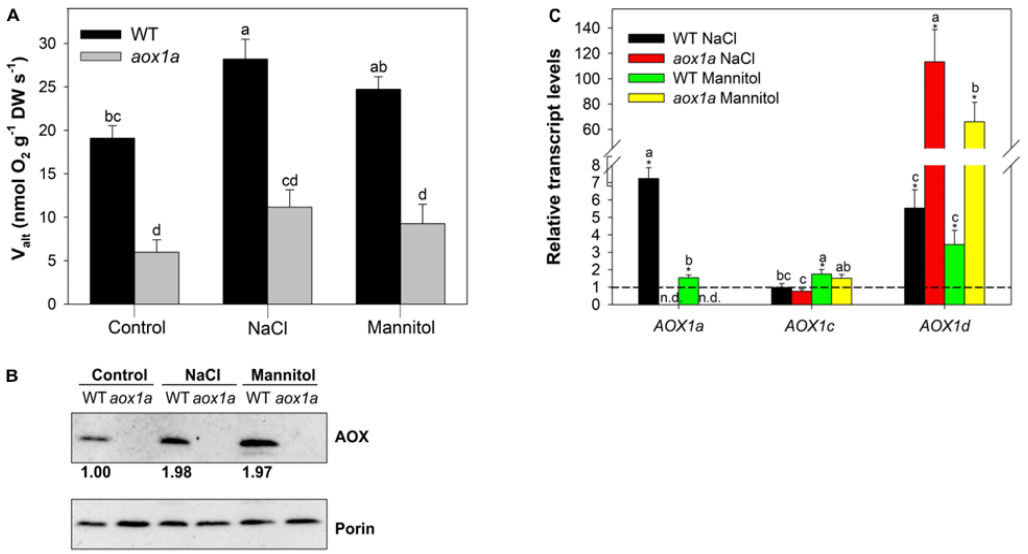


FIGURE 1 | Alternative oxidase (AOX) pathway capacity (Valt) and expression analysis. (A) Valt determined (see section "Materials and Methods") in leaves of wild-type Col 0 (WT) and aox1a Arabidopsis thaliana plants untreated with NaCl or Mannitol (Control), and after 1 day of severe NaCl or Mannitol treatments (300 mM). Values are means SE of 5–6 biological replicates. Significant differences ($P < 0.05$) are denoted by different letters. (B) Western blot analysis of AOX and porin (VDAC) protein levels from total leaf protein extracts (see section "Material and Methods" for details). The intensities of the signals from AOX were normalized to those from porin (VDAC) and are expressed relative to WT levels under control conditions. The normalized intensity values shown are averages of three independent blots. (C) Transcript levels of genes encoding AOX isoforms determined by qPCR analyses (see Materials and Methods for details) under control and stress conditions. Data are shown as fold-changes relative to control conditions (i.e., all control values were set to 1, which is denoted by the dashed line). Primers used and gene information can be found in Supplementary Table 4. Values are means SE of 5–6 replicates and asterisks denote significant differences ($P < 0.05$) to the control condition for each gene expression analysis. Letters denote significant differences ($P < 0.05$) among genotypes and stress conditions for each gene expression analysis. n.d. (not detected).

thus confirming the expected effect of the *aox1a* mutation, while the expression of this gene was induced in WT plants under both stress conditions (Figure 1C), particularly under salinity (7.2-fold increase). The transcript levels of *AOX1b* and *AOX2* were below the level of detection in all control and most of the stress-treated samples. The transcript levels of *AOX1c* were generally not responsive to stress, except for the slight significant ($P < 0.05$) increase in WT plants after mannitol treatment. On the other hand, the levels of *AOX1d* transcripts were highly responsive to both stress conditions, particularly in the *aox1a* mutants, which display a much higher response than in WT plants.

Leaf Phenotype and Water Status in *aox1a* and Wild-Type Plants Under Control and Stress Conditions

Wild-type (WT) and *aox1a* mutant plants did not show visual differences under control conditions, as previously observed in several other studies (Figure 2A). Acute salt and mannitol treatments caused minor leaf wilting in both WT and *aox1a* mutant plants after one day of stress (Figure 2A). Leaf relative water content (RWC) was determined as an indicator of water status in both genotypes after salt and mannitol treatments (Figure 2B). Salinity provoked a reduction of leaf RWC in both genotypes, while a significant ($P < 0.05$) reduction of leaf RWC after mannitol treatment was only observed in the *aox1a* mutants. Under both stress conditions, the leaf RWC was significantly ($P < 0.05$) lower in the *aox1a* mutants as compared to WT plants.

Respiration and Electron Partitioning to the Alternative Oxidase Pathway in *aox1a* and Wild-Type Plants Under Control and Stress Conditions

Both total respiration and the electron partitioning between the cytochrome oxidase pathway (COP) and the AOP were determined by using the oxygen isotope

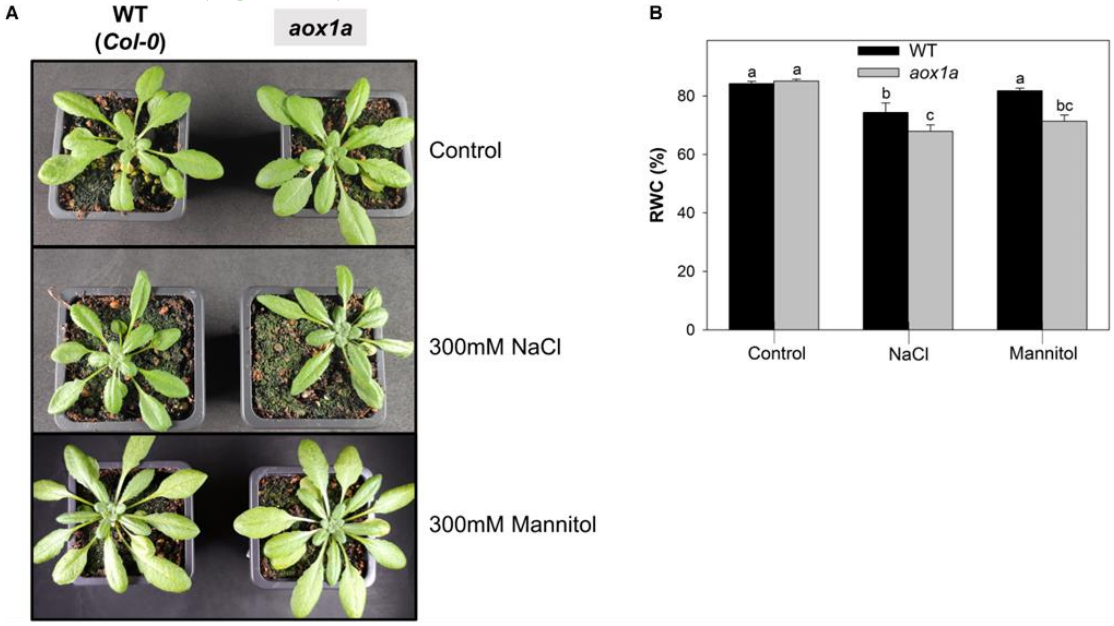


FIGURE 2 | Visual phenotype and relative water content. (A) Photographs representative of WT and aox1a plants untreated with NaCl or Mannitol (Control), and after 1 day of severe NaCl or Mannitol treatments (300 mM). (B) Leaf relative water content (RWC) in leaves of WT and aox1a plants under control and stress conditions. Values are means SE of 10–12 biological replicates. Significant differences ($P < 0.05$) are denoted by different letters.

discrimination technique (Figure 3). Total oxygen uptake (V_t) and electron partitioning to the alternative pathway (τ_a) were similar in WT and *aox1a* mutants under control conditions. Salt and mannitol treatments significantly ($P < 0.05$) increased respiration only in WT plants from 23.9 to 36.6 and 32.9 nmol O_2 g^{-1} DW s^{-1}, respectively. Similarly, τ_a significantly increased after salt and mannitol treatments in WT plants from 0.17 to 0.33 and 0.28, respectively. On the other hand, no significant ($P < 0.05$) change in τ_a was observed in *aox1a* mutants after salt and mannitol treatments. The *in vivo* AOP activity (v_{alt}) was similar in both lines under control conditions and increased significantly in WT plants after salt (1.94-fold) and mannitol (1.27-fold) treatments, whilst it was unaltered in *aox1a* mutants. The activity of the COP (v_{cyt}) was similar without significant ($P < 0.05$) differences between control and treated plants in both genotypes.

Photosynthetic Parameters in *aox1a* and Wild-Type Plants Under Control and Stress Conditions

The chloroplast electron transport rate (ETR) was determined at different light intensities in *aox1a* and WT plants under control and stress conditions (Figure 4A). While similar light-response curves were obtained in both genotypes under control conditions, some differences were observed under stress (Figure 4A). Light curves were modelled to obtain photosynthetic parameters (see section "Materials and Methods" for details) such as alpha, which indicates the photosynthetic rate in the light-limited region of the light curve, and the maximum electron transport rate (ETR_{max}; Figure 4B). Both parameters were similar among genotypes under control conditions. Regarding alpha, only *aox1a* mutants displayed a significant ($P < 0.05$) reduction after salt treatment as compared to control conditions, and this parameter became significantly ($P < 0.05$) lower in *aox1a* as compared to WT under salinity. On the other hand, the ETR_{max} was clearly reduced under both stress conditions and in both genotypes but notably, this parameter was significantly lower in the *aox1a* mutants as compared to WT plants under mannitol stress. In addition, the maximum efficiency of PSII (F_v/F_m) was determined by measuring chlorophyll fluorescence after dark adaptation, in order to evaluate the level of photoinhibitory stress after salt and mannitol treatments (Figure 4B). The F_v/F_m was also reduced in both genotypes under both stress conditions, and salinity was the condition inducing higher photoinhibition in both genotypes (Figure 4B). Notably, the aox1a mutants displayed significantly lower Fv/Fm after both stress treatments as compared to WT plants (Figure 4B). Overall, these results indicate a similar photosynthetic performance among genotypes under control conditions, however, the aox1a mutants displayed higher photoinhibition and lower photosynthetic activity under stress conditions.

Metabolite Profiling in *aox1a* and Wild-Type Plants Under Control and Stress Conditions

In order to further investigate the metabolic changes underlying the different physiological responses observed in the *aox1a* mutants, gas chromatography-time of flight-mass spectrometry (GC–TOF–MS) metabolite

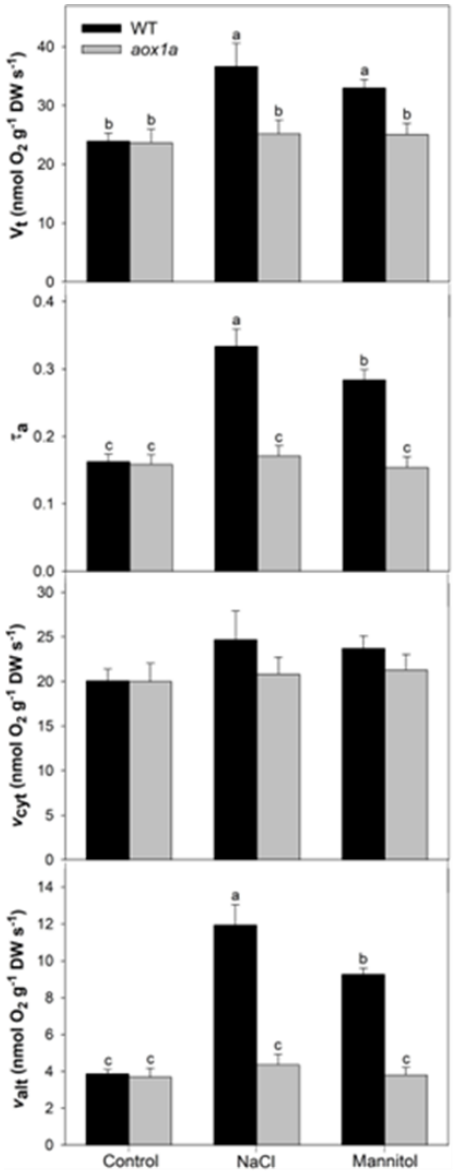


FIGURE 3 | Respiration and electron partitioning between the cytochrome and the alternative oxidase pathways (COP and AOP). Total respiration (Vt), electron partitioning to the AOP (ta), COP activity (vcyt) and AOP activity (valt) in leaves of Col 0 (WT) and aox1a A. thaliana plants untreated with NaCl or Mannitol (Control), and after 1 day of severe NaCl or Mannitol treatments (300 mM). Values are means SE of 6–8 biological replicates. Significant differences ($P < 0.05$) are denoted by different letters.

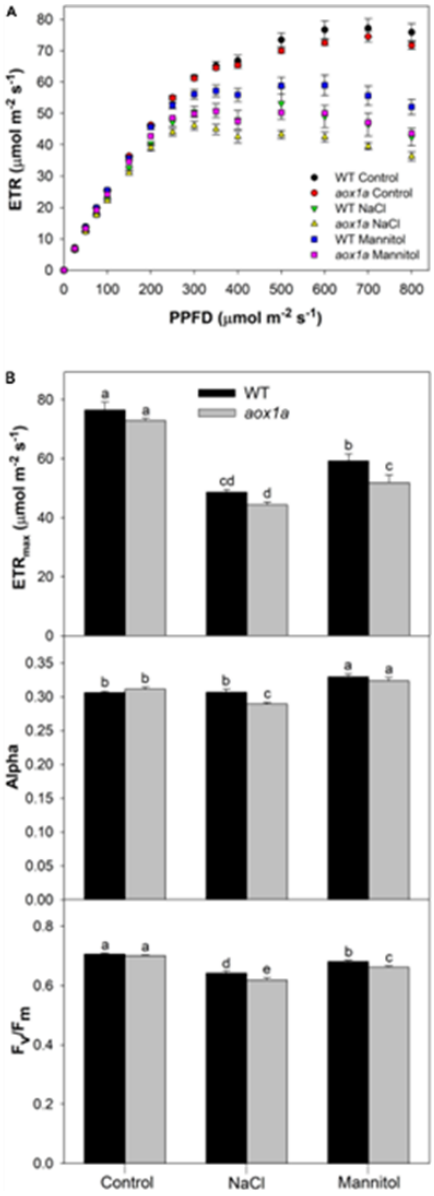


FIGURE 4 | Photosynthetic activity and capacity under different light intensities. (A) Light curves showing light dependent response (see Materials and Methods for details) of the chloroplast electron transport rate (ETR) in leaves of wild-type Col 0 (WT) and aox1a A. thaliana plants untreated with NaCl or Mannitol (Control), and after 1 day of severe NaCl or Mannitol treatments (300 mM). Values are means SE of 5–6 biological replicates. (B) Maximum electron transport rate (ETRmax) and photosynthetic rate in light limited region (alpha) were derived from light curves (see Materials and Methods for details) performed under control and stress conditions. The maximum quantum efficiency of PSII (Fv/Fm) was determined after 30 min in darkness (see Materials and Methods for details) under control and stress conditions. Values are means SE of 5–6 biological replicates. Significant differences ($P < 0.05$) are denoted by different letters.

profiling analysis was performed on rosette leaves from plants grown under control and stress conditions (Figure 5 and Supplementary Table 2). A total of 45 metabolites were identified using gas chromatography-mass spectrometry (GC-MS), including several amino acids, organic acids, sugars and sugar alcohols (Supplementary Tables 1,2; Figure 5). Relative metabolite levels were normalized to the mean levels of WT plants under control conditions (Supplementary Table 1 and Figure 5). Under control conditions, the *aox1a* mutants displayed higher levels of putrescine (2.31-fold), glycine (1.37-fold), erythritol (2.59-fold) and maltose (1.69-fold) as well as of the TCA cycle intermediates, citrate (1.62-fold), fumarate (1.30-fold) and malate (1.55-fold). Under stress, leaves of WT plants displayed significant increases in 31 metabolites after salt and mannitol treatments (Figure 5 and Supplementary Table2). While many of the metabolites increasing after mannitol treatment were the same as those increasing under salinity, there were several exceptions: alanine, glutamate, ornithine, citrate, glycerol and urea, which did not significantly ($P < 0.05$) increase after mannitol treatment; and glutamine, fumarate, erythritol, galactinol, xylose and trehalose, which increased only after mannitol treatment (Figure 5 and Supplementary Table 2). On the other hand, only glycerate and pyruvate displayed decreased levels after both stress treatments, and dehydroascorbate was reduced only after salt treatment (Figure 5 and Supplementary Table 2).

Metabolite levels in the *aox1a* mutants displayed similar patterns after both stress treatments as compared with WT plants (Figure 5). Nevertheless, the levels of asparagine, glycine, proline, malate and spermidine, although following similar stress-induced patterns in both genotypes,

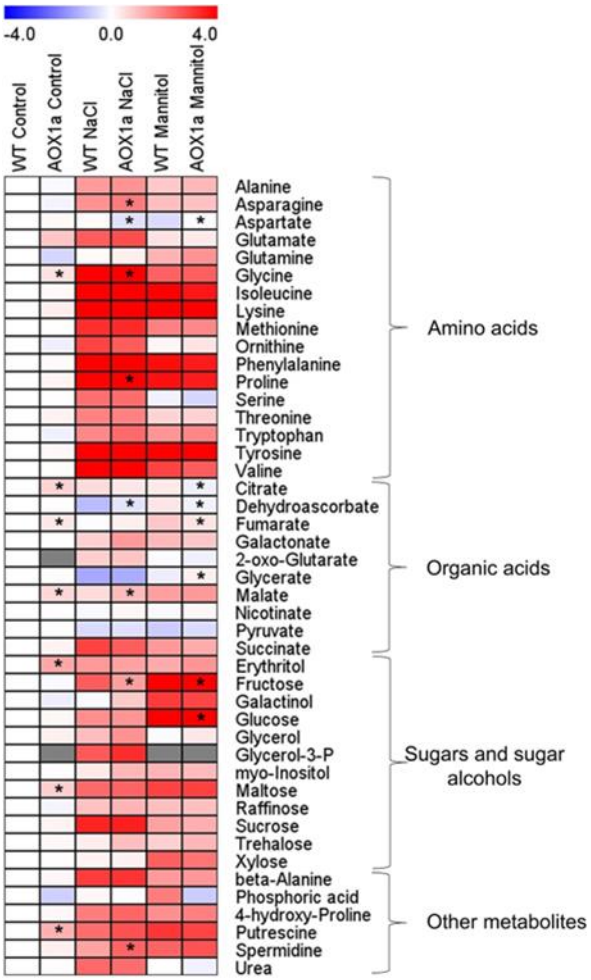


FIGURE 5 | Metabolite profiles showing relative changes in primary metabolism. Heat map showing the relative levels of the GC-MS-analysed metabolites in leaves of wild-type Col 0 (WT) and aox1a A. thaliana plants untreated with NaCl or Mannitol (Control), and after 1 day of severe NaCl or Mannitol treatments (300 mM). Metabolites were clustered per class into amino acids, organic acids, sugars and sugar alcohols, and other metabolites. Relative metabolite levels were normalized to the mean level of the WT plants under control conditions and fold-change values were log2 transformed (i.e., the level of all metabolites of WT plants under control conditions is 0). In this heat map, red and blue colours represent log2 fold-increased and –decreased metabolites, respectively. Gray colours indicate the metabolites not detected in some experimental conditions. Values are means SE of 4–6 replicates and asterisks denote significant differences ($P < 0.05$) to the WT plants in each experimental condition. The statistical differences between control and stress treatments in each genotype are presented in **Supplementary Table 2**.

were significantly ($P < 0.05$) higher in *aox1a* mutants than in WT plants under salinity

(Figure 5). On the other hand, aspartate, dehydroascorbate and fructose were significantly ($P < 0.05$) lower in *aox1a* mutants than in WT plants after salt treatment. Regarding mannitol stress, only aspartate and glycerate levels were significantly ($P < 0.05$) higher in *aox1a* mutants than in WT plants. On the other hand, fumarate, citrate, fructose and glucose were significantly ($P < 0.05$) lower in *aox1a* mutants than in WT plants after mannitol treatment.

Additionally, absolute levels of metabolites were determined to evaluate the physiological relevance for the accumulation of the stress-related metabolites with protective functions.

The absolute levels of 37 metabolites, present in our standard mixture, were determined for all conditions in both genotypes (Supplementary Figure 2 and Supplementary Table 3). Metabolites in order of absolute abundance under salinity conditions are shown in Supplementary Figure 3. Among the metabolites observed as significantly different between WT or *aox1a* mutants under salinity (Figure 5 and Supplementary Table 2), glycine and proline were above 2 μmol gDW^{-1} in either WT or *aox1a* mutants, while malate, fructose and asparagine displayed lower amounts in the range of 0.3–0.8 μmol gDW^{-1} (Supplementary Figure 2 and Supplementary Table 3). With respect to mannitol treatment, glucose was by far the most abundant metabolite (56.5 and 34.1 μmol gDW^{-1} in WT and *aox1a* mutant, respectively) that was significantly lower in the *aox1a* mutants, followed by fumarate (10.4 and 7.6 μmol gDW^{-1}) and fructose (4.1 and 2.0 μmol gDW^{-1}; Supplementary Figure 2 and Supplementary Table 3).

Gene Expression of Other Alternative Respiratory Components in *aox1a* and Wild-Type Plants Under Control and Stress Conditions

The relative levels of transcripts encoding mitochondrial proteins of the alternative respiratory pathways, other than AOX, were determined by qPCR in both WT and *aox1a* mutants (Supplementary Figure 1 and Figure 6). The aim of these gene expression analysis was to evaluate possible compensations from other alternative respiratory pathways for the lack of the *AOX1a* gene expression as well as the degree of mitochondrial stress perturbation. Regarding genes encoding alternative NAD(P)H dehydrogenases, transcript levels of *NDB3* were under the limit of detection while *NDB2* expression displayed a higher stress-response in the *aox1a* mutants as compared to WT (**Figure 6**), a similar trend as the observed for the *AOX1d* (**Figure 1C**). On the other hand, genes encoding *NDA1* and *NDA2* proteins were not responsive to stress conditions. Finally, the transcript levels of genes encoding uncoupling proteins (UCPs) were also evaluated (Supplementary Figure 1 and Figure 6); *UCP2* transcript levels were under the limit of detection while *UCP1* transcripts did not display any significant change under stress in both genotypes (Figure 6).

Discussion

Responses of plant respiration to abiotic stresses are largely variable (Lambers and Oliveira, 2019; O'Leary et al., 2019). This variability can be partly explained by plants' ability to adjust respiratory energy and carbon demands through changes in the partitioning of electrons between the cytochrome and alternative oxidase pathways (COP and AOP; Del-Saz et al., 2018; Lambers and Oliveira, 2019; O'Leary et al., 2019), without necessarily involve a major change in total respiration rate. In particular, the responses of the *in vivo* AOP and COP activities to salt

(Martí et al., 2011; Del-Saz et al., 2016; Sánchez-Guerrero et al.,2019) and water stress (Guy and Vanlerberghe, 2005; RibasCarbo et al., 2005; Galle et al., 2010; Sanhueza et al., 2013) are variable, however, a common pattern emerge with the electron partitioning to AOX usually increasing, either by a decrease in COP activity, increase in AOP activity or both (Del-Saz et al., 2018). Notably, a specific increase in the *in vivo* AOP activity (i.e., in the absence of COP changes), was observed in leaves of *Medicago truncatula* genotypes after a sudden severe salt stress (Del-Saz et al., 2016). Such a particular AOP activation *in vivo* is in line with its proposed role in providing metabolic flexibility to carbon and energy metabolism under short-term environmental perturbations (Del-Saz et al., 2018), as well as its role as a first line of defence against oxidative stress (Møller, 2001). Following previous evidence, we have here investigated the role of the AOP under sudden acute salt stress in more detail. Our hypothesis was that *in vivo* AOP response in *aox1a* mutants will be curtailed under acute stress, which would impair stress-related metabolism as compared to WT plants. In addition, we also applied a high mannitol concentration to both genotypes for exploring whether similar effects on the respiration and stress-related metabolism were observed after an acute osmotic stress in the absence of ionic toxicity. We are aware that osmotic stress conditions applied here were not fully controlled by our experimental approach with plants grown in soil, however, our previous observations (Del-Saz et al., 2016) and those presented here show and track typical physiological (Figures 2,4) and molecular (Figure 5) responses to salt and water stress, thus allowing the establishment of relationships between the degree of water and (photo)oxidative stress with the metaboli changes studied. changes studied.

The Lack of AOX1a Does Not Impair Alternative Oxidase Pathway *in vivo* Activity Under Control Conditions but Restricted Its Response to Stress

As expected, the capacity of the AOP was significantly lower in the *aox1a* mutant than in WT plants (Figure 1A), although it was not completely abolished in agreement with previous observations (Watanabe et al., 2010; Vishwakarma et al., 2015; Zhang et al., 2016). In the present study, the oxygen isotope provides additional evidence supporting that remaining Oh2

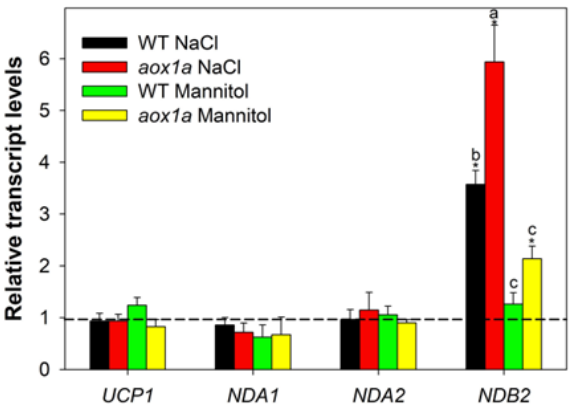


FIGURE 5 | Metabolite profiles showing relative changes in primary metabolism. Heat map showing the relative levels of the GC-MS-analysed metabolites in leaves of wild-type Col 0 (WT) and aox1a A. thaliana plants untreated with NaCl or Mannitol (Control), and after 1 day of severe NaCl or Mannitol treatments (300 mM). Metabolites were clustered per class into amino acids, organic acids, sugars and sugar alcohols, and other metabolites. Relative metabolite levels were normalized to the mean level of the WT plants under control conditions and fold-change values were log2 transformed (i.e., the level of all metabolites of WT plants under control conditions is 0). In this heat map, red and blue colours represent log2 fold-increased and –decreased metabolites, respectively. Gray colours indicate the metabolites not detected in some experimental conditions. Values are means SE of 4–6 replicates and asterisks denote significant differences ($P < 0.05$) to the WT plants in each experimental condition. The statistical differences between control and stress treatments in each genotype are presented in **Supplementary Table 2**.

discrimination in the presence of KCN (l_a of approx. 31) consumption after KCN treatment was mainly due to leaf AOX (maximum) activity. Indeed, *aox1a* mutants displayed similar total respiration, electron partitioning and *in vivo* AOP activity as WT plants under control conditions (Figure 3). These results are very similar to those reported in *AtAOX1a* anti-sense plants, previously obtained at the laboratory of the honourable Prof. James Siedow, grown under different light intensities (Florez-Sarasa et al., 2011). Our previous (Figure 1 from Florez-Sarasa et al., 2011) and current data (compare V_{alt} at Figure 1A with v_{alt} at Figure 3) show that AOX is almost fully engaged (v_{alt} to V_{alt} ratio close to 1) in *aox1a* impaired plants. Therefore, results presented here confirm that *AOX1a* isoform is not essential for maintaining leaf *in vivo* AOX activity under non-stress conditions. On the other hand, AOX protein signal could not be detected in the *aox1a* mutants under control conditions (Figure 1B) as in previous reports (Giraud et al., 2008; Strodtkötter et al., 2009; Oh et al., 2022). However, it is likely that samples after mitochondrial isolation or enrichment in mitochondrial membranes are required for the detection of low abundance AOX proteins (Oh et al., 2022). Indeed, AOX1D protein was detected in enriched mitochondrial membrane samples from *aox1a* mutants after proline incubation (Oh et al., 2022). Furthermore, evidence for the involvement in AOX capacity of isoforms other than AOX1a has recently been provided (Oh et al., 2022). To this respect, while single *aox1a* and *aox1d* mutants displayed lower AOX capacity as compared to WT plants, the reduction in AOX capacity was clearly more pronounced

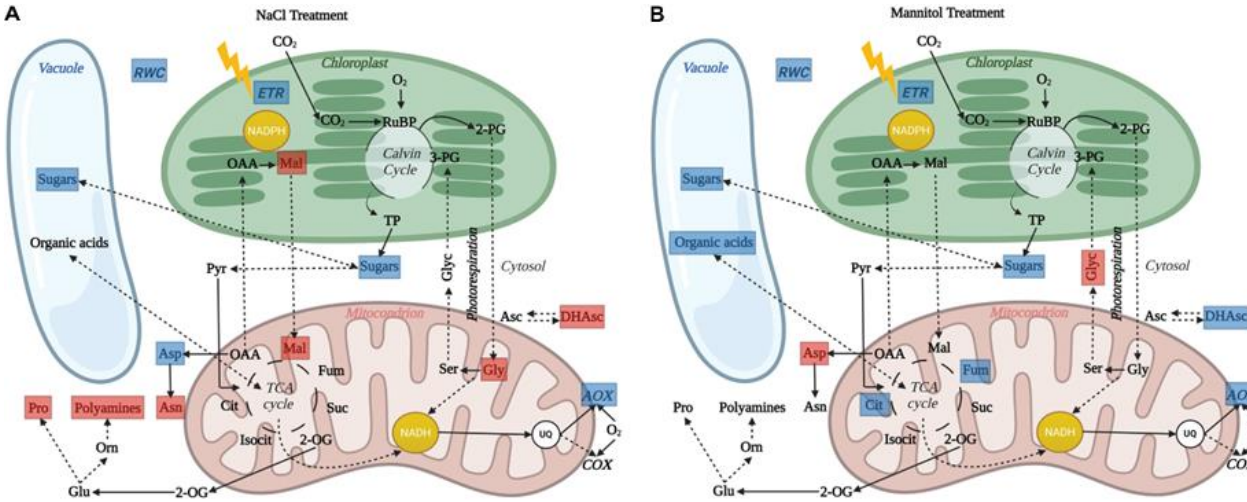


FIGURE 7 | Schematic overview illustrating the impact of in vivo AOP restriction on leaf cell physiology and metabolism in aox1a plants after (A) salt and (B) mannitol treatments. Blue and red boxes indicate significant ($P < 0.05$) reductions and increases, respectively, in physiological indicators and metabolite levels in aox1a mutants as compared to WT plants. After both stress treatments, the lack of in vivo AOP response was associated to reduced sugars (glucose, fructose or both) accumulation in aox1a mutants, which can be partially explained by their lower photosynthetic activity. Reduced accumulation of sugars in aox1a mutants could affect their osmotic adjustment as reflected by their lower relative water content (RWC). The reduction of fumarate and citrate accumulation in aox1a plants, the former likely contributing the decreased osmotic adjustment, may be explained by a TCA activity impairment triggered by the lack of response on the in vivo AOP activity, which allows matrix NADH re-oxidation without energy demand (i.e., ATP for growth) constrains. This limitation in NADH reoxidation can also explain the accumulation of photorespiratory cycle intermediates glycine (A) and glycerate (B). In addition, ion toxicity effects imposed by salinity could be aggravated by the lack of AOP response and, according to its role in avoiding ROS formation, thus trigger additional oxidative stress that was reflected in the alteration of other metabolic pathways involved in redox balancing and ROS detoxification (A), as denoted by the accumulation of malate, dehydroascorbate, proline, polyamines (spermidine) and asparagine. Image created with BioRender (https://biorender.com).

in double mutants *aox1a-aox1d* (Oh et al., 2022). While the relationship between protein levels and cyanide-resistant respiration may not be linear (Gonzalez-Meler et al., 1999) our and previous results (Oh et al., 2022) suggest that both AOX1a and AOX1d proteins can be responsible for AOX capacity in Arabidopsis plants. Notably, transcript levels of other AOX isoforms or alternative components of the mitochondrial respiratory chain in *aox1a* mutants were not higher than in WT plants (Supplementary Figure 1). Therefore, our and previous results in transcript and protein amounts suggest that *in vivo* AOP activity under non-stress conditions could be achieved without any additional induction of other AOX isoforms (i.e., AOX1c or AOX1d proteins). However, post-translational activation of the remaining AOX isoforms in *aox1a* mutants could also contribute to the observed *in vivo* AOP activity. To this respect, while moderate increases in the levels of some TCA cycle intermediates (citrate, malate and fumarate) were observed in *aox1a* mutants under control conditions (Figure 5), none of them have been shown to act as allosteric activators of any AOX isoform (Selinski et al., 2018b). However, analysis of AOX allosteric activators at the subcellular (mitochondrial) level would be required to attribute their effects on AOX activation *in vivo*.

Both stress treatments, significantly increased transcript levels of *AOX1a* and *AOX1d* in WT plants (Figure 1B), thus both isoforms could potentially contribute to the observed increase in AOP capacity (Figure 1A) and *in vivo* activity (Figure 3). On the other hand, the absence of *AOX1a* expression in the *aox1a* mutants coincided with a much higher induction of the *AOX1d* transcript levels (approx. 20 times higher) under both stress conditions, as compared to WT plants (Figure 1B). However, this response was not coupled to a significant ($P < 0.05$) increase in the AOX capacity or protein level under our experimental conditions (Figure 1). Moreover, the lack of *in vivo* AOP activity response observed in *aox1a* mutant leaves (Figure 3) clearly suggests that the absence of *AOX1a* was not compensated by other AOX isoforms (i.e., AOX1d) under stress conditions. These results are in line with previous observations suggesting no functional compensation for the lack of *AOX1a* under stress via high induction of *AOX1d* after respiratory inhibitor (Strodtkötter et al., 2009) and metal stress treatments (Keunen et al., 2015). In here, the *aox1a* mutants did not show respiratory response to acute salt and water stress, since AOP was the main contributor to this respiratory response in our experimental conditions (Figure 3). This AOP-specific response to acute salt stress was previously observed in a *Medicago truncatula* sensitive genotype (Del-Saz et al., 2016), which fits with the Arabidopsis behaviour, as a salt-sensitive species (Kazachkova et al., 2018). In addition, we here show that mannitol treatment induces a similar *in vivo* respiratory response as salt stress treatment (Figure 3), which suggests that the osmotic stress generated after both treatments is likely the main responsible for the observed *in vivo* AOP specific response. In fact, the lack of *in vivo* AOP response in *aox1a* mutants coincided with a more pronounced reduction in leaf RWC under both stress conditions, as compared to WT plants (Figure 2), which could be related to a reduced osmotic adjustment. Osmotic adjustment is an essential trait that plants use to maintain turgor by balancing the osmotic pressure imposed during salt or water stresses (Munns and Gilliham, 2015). While osmotic adjustment using inorganic ions is energetically "cheaper" than using organic solutes, salt-sensitive species usually rely in

ion exclusion (particularly in leaves) and accumulation of organic solutes (Munns and Gilliham, 2015). In the present study, salt and mannitol treatments induced a large accumulation of several stress-related metabolites (SRMs; Figure 5), many of them being well-known for their roles in osmoregulation and osmoprotection (Slama et al., 2015).

The Lack *in vivo* Alternative Oxidase Pathway Response Under Stress Altered the Accumulation of Stress-Related Metabolites Involved in Leaf Osmoregulation and Redox Balance

Osmotic stress has immediate effects on plant growth, and the accumulation of osmolytes is part of the typical plant responses involved in osmotic adjustment (Munns and Gilliham, 2015). The accumulation of osmolytes is favoured under conditions when plant growth declines before photosynthesis, which can result in a relatively favourable carbon status allowing the use of photosynthates for osmolyte production at low cost (Hummel et al., 2010). In our short-term stress study, photosynthesis was not strongly affected, particularly at growth light intensity (Figure 4), which suggests minor limitations on C availability. In agreement, a large accumulation of sugars, sugar alcohols and amino acids was observed in both genotypes after stress treatments (Figure 5). Previous reports suggest that accumulation of sugars in leaves of Arabidopsis and other species after mannitol and salt treatments have a prominent role on osmotic adjustment (Thalmann and Santelia, 2017; Gurrieri et al., 2020). On the other hand, the accumulation of amino acids (i.e., proline) is a well-known mechanism contributing to osmoprotection and osmoregulation in different species (Slama et al., 2015). The relatively low concentrations of amino acids as typically observed in Arabidopsis leaves suggest their roles as osmoprotectants of subcellular structures, in scavenging reactive oxygen species or counteracting redox imbalances, rather than contributing to osmotic adjustment (Shabala and Shabala, 2011; Slama et al., 2015; Gurrieri et al., 2020). Our results are in line with these observations since the levels of sucrose, glucose and fructose were not only highly accumulated, but also reached the highest absolute amounts, as compared to highly accumulated amino acids such as proline and glycine (Supplementary Figure 2). Importantly, the accumulation of glucose and fructose in the *aox1a* mutants was lower as compared with WT plants (Figure 5), and together with their lower relative water content (RWC), suggests a decreased osmotic adjustment in the *aox1a* mutants (Figure 7). In this line, the *aox1a* mutants after mannitol treatment also displayed lower levels of fumarate, which was among the top three most abundant metabolites under stress (Supplementary Figure 2), and this metabolite was previously suggested to have a high contribution to osmotic adjustment in Arabidopsis under severe drought (Hummel et al., 2010). The lower photosynthetic performance of *aox1a* mutants could partly explain their lower sugar levels, which in turn could slow down the carbon flow through glycolysis and consequently the TCA cycle activity for the fumarate production (Figure 7). Nevertheless, fumarate can also be produced from malate which levels could be altered by the redox imbalances in *aox1a* plants. Furthermore, the accumulation of osmolytes is thought to be the result of the coordinated regulation of biosynthetic and catabolic pathways (Slama et al., 2015), many of which are tightly linked to respiratory pathways (Bandehagh and Taylor, 2020). Therefore, we cannot discard that the lower accumulation of fumarate and citrate observed in *aox1a*

mutants after mannitol treatment could be partly due to a reduced TCA cycle activity as a direct consequence of a reduction in matrix NADH reoxidation by the AOP. Future experiments determining carbon fluxes (i.e., with ^{13}C labelled substrates under control and osmotic stress conditions) could unveil the precise nature of the observed altered accumulation of TCA cycle intermediates.

Impairment of photosynthetic performance and higher photoinhibition have been observed in other *aox1a* suppressed plants under drought (Giraud et al., 2008; Dahal et al., 2014, 2017; Dahal and Vanlerberghe, 2017, 2018) high light (FlorezSarasa et al., 2011) and temperature (Watanabe et al., 2010; Li et al., 2020) stress, which have been attributed to the role of the AOP in providing flexibility to carbon and energy metabolism in photosynthetic tissues, particularly under stress (Del-Saz et al., 2018; Vanlerberghe et al., 2020). In our study, while both stress conditions induced photoinhibition in both genotypes (Figure 3), the decrease in Fv/Fm was higher under salinity as compared to mannitol stress (Figure 3), thus suggesting that ion toxicity probably led to higher oxidative stress at the chloroplast level. In line with a higher oxidative stress after salt treatment, as compared to mannitol treatment, both genotypes displayed higher levels of different metabolites with known functions on protecting against oxidative stress themselves (i.e., dehydroascorbate, proline, asparagine; Figure 5 and Supplementary Table 2) or as precursors of oxidative stressrelated specialized metabolites (i.e., phenylalanine and tyrosine for phenylpropanoids synthesis; Figure 5 and Supplementary Table 2), as well as higher levels of transcripts encoding oxidative stress-responsive genes (*AOX1a* and *NDB2*; Figure 6). In agreement, the AOP activity in WT plants was significantly higher after salt than after mannitol stress (Figure 3). Importantly, the *aox1a* mutants, lacking stress response of the *in vivo* AOP activity, displayed higher levels of proline, asparagine, spemidine, and dehydroascorbate when compared to WT plants (Figures 5, 7). Increased levels of all these metabolites indicate a higher induction of metabolic pathways involved in redox balancing and avoidance of excessive ROS accumulation under stress (Szabados and Savouré, 2010; Maaroufi-Dguimi et al., 2011; Alcázar et al., 2020; Foyer et al., 2020). Moreover, higher glycine levels in *aox1a* mutants under salinity denotes a restriction in photorespiration due to reduction of glycine decarboxylation (Figure 7), as has been previously reported in *aox1a* mutants (Strodtkötter et al., 2009; Zhang et al., 2017; Li et al., 2020). Finally, higher malate levels in *aox1a* mutants could indicate an impairment in the reductant export from the chloroplast via the malate valve (Figure 7), as previously suggested (Yoshida et al., 2007; Dinakar et al., 2010; Vishwakarma et al., 2015).

Conclusions

Mitochondrial function has been suggested to be essential for drought and salinity tolerance in plants as it can have roles in signal transduction, ion exclusion and homeostasis, ROS detoxification, the generation of ATP, and carbon balance (Bandehagh and Taylor, 2020; Munns et al., 2020; Vanlerberghe et al., 2020). However, information about the *in vivo* AOP and COP activity and their metabolic roles under water and salt stress remain scarce. The different metabolic responses in *aox1a* mutants lacking *in vivo* AOP response under stress (Figure 7) reinforce the relevant roles of the AOX previously suggested in redox balancing, avoidance of excessive ROS accumulation

and photosynthetic performance. Furthermore, we here provide new evidence on the *in vivo* regulation and metabolic role of the AOP in the accumulation of stress-related metabolites associated to osmoregulation. While further experiments would be required to unravel the precise direction of subcellular carbon fluxes and its direct relationship with the *in vivo* AOP response, our results provide evidence on the contribution of the AOP in providing flexibility to carbon metabolism for biosynthesis, in addition to its role in cell redox balancing and preventing mitochondrial ROS formation (Smith et al., 2009; Vanlerberghe et al., 2020). Metabolites including TCA cycle intermediates (malate, citrate and fumarate), proline and hexoses, which were altered by the absence of *in vivo* AOP activity in this study, are similar to those typically altered when comparing salt-sensitive species *A. thaliana* with its relatives exhibiting salt-tolerance (Kazachkova et al., 2018). Therefore, our results provide important additional evidence reinforcing previous suggestions for AOX manipulation as a reasonable strategy for improving salt-tolerance in salt-sensitive crops (Smith et al., 2009), notwithstanding other important strategies involving salttolerant crops (Ventura et al., 2015; Fernie and Yan, 2019). Whether a higher AOP capacity or activity is primed for a better performance in case of salinity exposure remains to be investigated in a wider range of salt-tolerant crops. In addition, the relevance of AOP and its coordinated regulation with other alternative respiratory pathways under longer exposure to salt and/or water stress remains to be investigated in depth.

Data availability statement

The original contributions presented in the study are included in the article/**Supplementary Material**, further inquiries can be directed to the corresponding authors.

Author contributions

ND-S, MR-C, and IF-S conceived and designed the idea of this experiment. ND-S, AI-S, and DA-F carried out oxygen electrode and mass spectrometry measurements of respiration as well as leaf relative water content determinations. AI-S performed photosynthetic and gene expression analyses. ML-G, FP, and MC-M performed samples preparation, metabolite extractions and analyses. IF-S and AF performed the metabolite data analysis. IF-S and ND-S performed the statistical analysis. ND-S and IF-S wrote the first draft of the manuscript with subsequent inputs from all co-authors. All authors have read and agreed to the published version of the manuscript.

Funding

This work was financed by the MICINN–project CTM2014-53902-C2-1-P and FONDECYT No. 1191118 from National Agency for Research and Development (ANID). AI-S was supported by a predoctoral fellowship from MICINN (PRE2018083610). IF-S has received funding the “Ramon y Cajal” contract RYC2019-027244-I/AEI/10.13039/501100011033 and the European Social Fund.

Acknowledgments

We would like to thank Biel Martorell, Yunuen Avalos-Padilla and Javier Hidalgo for their technical help as well as Miquel Truyols and collaborators of the UIB Experimental Field and Greenhouses which are supported by the UIBGrant 15/2015.

References

Alcázar, R., Bueno, M., and Tiburcio, A. F. (2020). Polyamines: small amines with large effects on plant abiotic stress tolerance. *Cells* 9:2373. doi: 10.3390/cells9112373

Bandehagh, A., and Taylor, N. L. (2020). Can alternative metabolic pathways and shunts overcome salinity induced inhibition of central carbon metabolism in crops? *Front. Plant Sci.* 11:1072. doi: 10.3389/fpls.2020.01072

Batista-Silva, W., Heinemann, B., Rugen, N., Nunes-Nesi, A., Araújo, W. L., Braun, H. P., et al. (2019). The role of amino acid metabolism during abiotic stress release. *Plant Cell Environ.* 42, 1630–1644. doi: 10.1111/pce.13518

Clifton, R., Millar, A. H., and Whelan, J. (2006). Alternative oxidases in *Arabidopsis*: a comparative analysis of differential expression in the gene family provides new insights into function of non-phosphorylating bypasses. *Biochim. Biophys. Acta Bioenerget.* 1757, 730–741. doi: 10.1016/j.bbabio.2006.03.009

Dahal, K., Martyn, G. D., Alber, N. A., and Vanlerberghe, G. C. (2017). Coordinated regulation of photosynthetic and respiratory components is necessary to maintain chloroplast energy balance in varied growth conditions. *J. Exp. Bot.* 68, 657–671. doi: 10.1093/jxb/erw469

Dahal, K., and Vanlerberghe, G. C. (2017). Alternative oxidase respiration maintains both mitochondrial and chloroplast function during drought. *New Phytol.* 213, 560–571. doi: 10.1111/nph.14169

Dahal, K., and Vanlerberghe, G. C. (2018). Improved chloroplast energy balance during water deficit enhances plant growth: more crop per drop. *J. Exp. Bot.* 69, 1183–1197. doi: 10.1093/jxb/erx474

Dahal, K., Wang, J., Martyn, G. D., Rahimy, F., and Vanlerberghe, G. C. (2014). Mitochondrial alternative oxidasemaintains respiration and preserves photosynthetic capacity during moderate drought in *Nicotiana tabacum*. *Plant Physiol.* 166, 1560–1574. doi: 10.1104/pp.114.247866

Darko, E., Végh, B., Khalil, R., Marcek, T., Szalai, G., Pál, M., et al. (2019). Metabolicˇ responses of wheat seedlings to osmotic stress induced by various osmolytes under iso-osmotic conditions. *PLoS One* 14:e0226151. doi: 10.1371/journal. pone.0226151

Day, D. A., Krab, K., Lambers, H., Moore, A. L., Siedow, J. N., Wagner, A. M., et al. (1996). The cyanide-resistant ocidase: to inhibit or not to inhibit, that is the question. *Plant Physiol.* 110, 1–2. doi: 10.1104/pp.110.1.1

Del-Saz, N. F., Florez-Sarasa, I., Clemente-Moreno, M. J., Mhadhbi, H., Flexas, J., Fernie, A. R., et al. (2016). Salinity tolerance is related to cyanide-resistant alternative respiration in *Medicago truncatula* under sudden severe stress. *Plant Cell Environ.* 39, 2361–2369. doi: 10.1111/pce.12776

Del-Saz, N. F., Ribas-Carbo, M., Martorell, G., Fernie, A. R., and Florez-Sarasa, I. (2017). "Measurements of electron partitioning between cytochrome and alternative oxidase pathways in plant tissues," in *Methods in Molecular Biology*, ed. K. Jagadis Gupta (New York, NY: Humana Press Inc), 203–217. doi: 10.1007/ 978-1-4939-7292-0_17

Del-Saz, N. F., Ribas-Carbo, M., McDonald, A. E., Lambers, H., Fernie, A. R., and Florez-Sarasa, I. (2018). An in vivo perspective of the role(s) of the alternative oxidase pathway. *Trends Plant Sci.* 23, 206–219. doi: 10.1016/j.tplants.2017.11. 006

Dinakar, C., Raghavendra, A. S., and Padmasree, K. (2010). Importance of AOX pathway in optimizing photosynthesis under high light stress: role of pyruvate and malate in activating AOX. *Physiol. Plant.* 139, 13–26. doi: 10.1111/j.1399-3054.2010.01346.x

Epstein, E. H. Jr., Levin, D. L., Croft, J. D. Jr., and Lutzner, M. A. (1972). MYCOSIS FUNGOIDES. *Medicine* 51, 61–72.

Fàbregas, N., and Fernie, A. R. (2019). The metabolic response to drought. *J. Exp. Bot.* 70, 1077–1085. doi: 10.1093/jxb/ery437

Fernie, A. R., Aharoni, A., Willmitzer, L., Stitt, M., Tohge, T., Kopka, J., et al. (2011). Recommendations for reporting metabolite data. *Plant Cell* 23, 2477–2482. doi: 10.1105/tpc.111.086272

Fernie, A. R., and Yan, J. (2019). De novo domestication: an alternative route toward new crops for the future. *Mol. Plant* 12, 615–631. doi: 10.1016/j.molp. 2019.03.016

Florez-Sarasa, I., Flexas, J., Rasmusson, A. G., Umbach, A. L., Siedow, J. N., and Ribas-Carbo, M. (2011). In vivo cytochrome and alternative pathway respiration in leaves of *Arabidopsis thaliana* plants with altered alternative oxidase under different light conditions. *Plant, Cell Environ.* 34, 1373–1383. doi: 10.1111/j.1365-3040.2011.02337.x

Florez-Sarasa, I., Noguchi, K., Araújo, W. L., Garcia-Nogales, A., Fernie, A. R., Flexas, J., et al. (2016). Impaired cyclic electron flow around photosystem I disturbs high-light respiratory metabolism. *Plant Physiol.* 172, 2176–2189. doi: 10.1104/pp.16.01025

Foyer, C. H., Kyndt, T., and Hancock, R. D. (2020). Vitamin C in plants: novel concepts, new perspectives, and outstanding issues. *Antioxidants Redox Signal.* 32, 463–485. doi: 10.1089/ars.2019.7819

Galle, A., Florez-Sarasa, I., Thameur, A., de Paepe, R., Flexas, J., and Ribas-Carbo, M. (2010). Effects of drought stress and subsequent rewatering on

photosynthetic and respiratory pathways in *Nicotiana sylvestris* wild type and the mitochondrial complex I-deficient CMSII mutant. *J. Exp. Bot.* 61, 765–775. doi: 10.1093/jxb/ erp344

Garmash, E. V., Velegzhaninov, I. O., Ermolina, K. V., Rybak, A. V., and Malyshev, R. V. (2020). Altered levels of AOX1a expression result in changes in metabolic pathways in *Arabidopsis thaliana* plants acclimated to low dose rates of ultraviolet B radiation. *Plant Sci.* 291:110332. doi: 10.1016/j.plantsci. 2019.110332

Giraud, E., Ho, L. H. M., Clifton, R., Carroll, A., Estavillo, G., Tan, Y. F., et al. (2008). The absence of Alternative Oxidase1a in *Arabidopsis* results in acute sensitivity to combined light and drought stress. *Plant Physiol.* 147, 595–610. doi: 10.1104/pp.107.115121

Gong, Q., Li, S., Zheng, Y., Duan, H., Xiao, F., Zhuang, Y., et al. (2020). SUMOylation of MYB30 enhances salt tolerance by elevating alternative respiration via transcriptionally upregulating AOX1a in *Arabidopsis*. *Plant J.* 102, 1157–1171. doi: 10.1111/tpj.14689

Gonzalez-Meler, M. A., Ribas-Carbo, M., Giles, L., and Siedow, J. N. (1999). The effect of growth and measurement temperature on the activity of the alternative respiratory pathway. *Plant Physiol.* 120, 765–772. doi: 10.1104/pp.120. 3.765

Gurrieri, L., Merico, M., Trost, P., Forlani, G., and Sparla, F. (2020). Impact of drought on soluble sugars and free proline content in selected *Arabidopsis mutants*. *Biology (Basel)* 9, 1–14. doi: 10.3390/biology9110367

Guy, R. D., and Vanlerberghe, G. C. (2005). Partitioning of respiratory electrons in the dark in leaves of transgenic tobacco with modified levels of alternative oxidase. *Physiol. Plant.* 125, 171–180. doi: 10.1111/j.1399-3054.2005.00557.x

Hummel, I., Pantin, F., Sulpice, R., Piques, M., Rolland, G., Dauzat, M., et al. (2010). *Arabidopsis* plants acclimate to water deficit at low cost through changes of carbon usage: an integrated perspective using growth, metabolite, enzyme, and gene expression analysis. *Plant Physiol.* 154, 357–372. doi: 10.1104/pp.110. 157008

Kazachkova, Y., Eshel, G., Pantha, P., Cheeseman, J. M., Dassanayake, M., and Barak, S. (2018). Halophytism: what have we learnt from *Arabidopsis thaliana* relative model systems? *Plant Physiol.* 178, 972–988. doi: 10.1104/pp.18.00863

Keunen, E., Schellingen, K., van der Straeten, D., Remans, T., Colpaert, J., Vangronsveld, J., et al. (2015). ALTERNATIVE OXIDASE1a modulates the oxidative challenge during moderate Cd exposure in *Arabidopsis thaliana* leaves. *J. Exp. Bot.* 66, 2967–2977. doi: 10.1093/jxb/erv035

Kopka, J., Schauer, N., Krueger, S., Birkemeyer, C., Usadel, B., Bergmüller, E., et al. (2005). GMD@CSB.DB: the Golm metabolome database. *Bioinformatics* 21, 1635–1638. doi: 10.1093/bioinformatics/bti236

Lambers, H., and Oliveira, R. S. (2019). "Photosynthesis, respiration, and longdistance transport: photosynthesis," in *Plant Physiological Ecology*, eds H. Lambers and R. S. Oliveira (Cham: Springer), 11–114. doi: 10.1007/978-3-030-29639-1_2

Lisec, J., Schauer, N., Kopka, J., Willmitzer, L., and Fernie, A. R. (2006). Gas chromatography mass spectrometry-based metabolite profiling in plants. *Nat. Protoc.* 1, 387–396. doi: 10.1038/nprot.2006.59

Livak, K. J., and Schmittgen, T. D. (2001). Analysis of relative gene expression data using real-time quantitative PCR and the 2-*11*CT method. *Methods* 25, 402–408. doi: 10.1006/meth.2001.1262

Li, Y. T., Liu, M. J., Li, Y., Liu, P., Zhao, S. J., Gao, H. Y., et al. (2020). Photoprotection by mitochondrial alternative pathway is enhanced at heat but disabled at chilling. *Plant J.* 104, 403–415. doi: 10.1111/tpj.14931

Luedemann, A., von Malotky, L., Erban, A., and Kopka, J. (2012). TagFinder: preprocessing software for the fingerprinting and the profiling of gas chromatography-mass spectrometry based metabolome analyses. *Methods Mol. Biol.* 860, 255–286. doi: 10.1007/978-1-61779-594-7_16

Maaroufi-Dguimi, H., Debouba, M., Gaufichon, L., Clément, G., Gouia, H., Hajjaji, A., et al. (2011). An *Arabidopsis mutant* disrupted in ASN2 encoding asparagine synthetase 2 exhibits low salt stress tolerance. *Plant Physiol. Biochem.* 49, 623–628. doi: 10.1016/j.plaphy.2011.03.010

Martí, M. C., Florez-Sarasa, I., Camejo, D., Ribas-Carbó, M., Lázaro, J. J., Sevilla, F., et al. (2011). Response of mitochondrial thioredoxin PsTrxo1, antioxidant enzymes, and respiration to salinity in pea (*Pisum sativum* L.) leaves. *J. Exp. Bot.* 62, 3863–3874. doi: 10.1093/jxb/err076

Mattoo, A. K., Sobolev, A. P., Neelam, A., Goyal, R. K., Handa, A. K., and Segre, A. L. (2006). Nuclear magnetic resonance spectroscopy-based metabolite profiling of transgenic tomato fruit engineered to accumulate spermidine and spermine reveals enhanced anabolic and nitrogen-carbon interactions. *Plant Physiol.* 142, 1759–1770. doi: 10.1104/pp.106.084400

Møller, I. M. (2001). Plant mitochondria and oxidative stress: electron transport, nadph turnover, and metabolism of reactive Oxygen Species. *Annu. Rev. Plant Physiol. Plant Mol. Biol.* 52, 561–591. doi: 10.1146/annurev.arplant.52.1.561

Morelli, L., Paulišic, S., Qin, W., Iglesias-Sanchez, A., Roig-Villanova, I., Florez-´ Sarasa, I., et al. (2021). Light signals generated by vegetation shade facilitate acclimation to low light in shade-avoider plants. *Plant Physiol.* 186, 2137–2151. doi: 10.1093/plphys/kiab206

Munns, R., Day, D. A., Fricke, W., Watt, M., Arsova, B., Barkla, B. J., et al. (2020). Energy costs of salt tolerance in crop plants. *New Phytol.* 225, 1072–1090. doi: 10.1111/nph.15864

Munns, R., and Gilliham, M. (2015). Salinity tolerance of crops – what is the cost? *New Phytol.* 208, 668–673. doi: 10.1111/nph.13519

Oh, G. G. K., O'Leary, B. M., Signorelli, S., and Millar, A. H. (2022). Alternative oxidase (AOX) 1a and 1d limit proline-induced oxidative stress and aid salinity recovery in *Arabidopsis*. *Plant Physiol.* 188, 1521–1536. doi: 10.1093/plphys/ kiab578

O'Leary, B. M., Asao, S., Millar, A. H., and Atkin, O. K. (2019). Core principles which explain variation in respiration across biological scales. *New Phytol.* 222, 670–686. doi: 10.1111/nph.15576

Pires, M. V., Pereira Júnior, A. A., Medeiros, D. B., Daloso, D. M., Pham, P. A., Barros, K. A., et al. (2016). The influence of alternative pathways of respiration that utilize branched-chain amino acids following water shortage in *Arabidopsis*. *Plant Cell Environ.* 39, 1304–1319. doi: 10.1111/pce.12682

Platt, T., and Gallegos, C. L. (1980). "Modelling primary production," in *Primary Productivity in the Sea*, ed. P. G. Falkowski (Boston, MA: Springer), 339–362. doi: 10.1007/978-1-4684-3890-1_19

Rasmusson, A. G., Fernie, A. R., and van Dongen, J. T. (2009). Alternative oxidase: a defence against metabolic fluctuations? *Physiol. Plant.* 137, 371–382. doi: 10.1111/j.1399-3054.2009.01252.x

Ribas-Carbo, M., Taylor, N. L., Giles, L., Busquets, S., Finnegan, P. M., Day, D. A., et al. (2005). Effects of water stress on respiration in soybean leaves. *Plant Physiol.* 139, 466–473. doi: 10.1104/pp.105.065565

Saisho, D., Nambara, E., Naito, S., Tsutsumi, N., Hirai, A., and Nakazono, M. (1997). *Characterization of the Gene Family for Alternative Oxidase From Arabidopsis thaliana*. Alphen aan den Rijn: Kluwer Academic Publishers, doi: 10.1023/A:1005818507743

Sanchez, D. H., Siahpoosh, M. R., Roessner, U., Udvardi, M., and Kopka, J. (2008). Plant metabolomics reveals conserved and divergent metabolic responses to salinity. *Physiol. Plant.* 132, 209–219. doi: 10.1111/j.1399-3054.2007.00993.x

Sánchez-Guerrero, A., Fernández del-Saz, N., Florez-Sarasa, I., Ribas-Carbó, M., Fernie, A. R., Jiménez, A., et al. (2019). Coordinated responses of mitochondrial antioxidative enzymes, respiratory pathways and metabolism in *Arabidopsis thaliana* thioredoxin trxo1 mutants under salinity. *Environ. Exp. Bot.* 162, 212–222. doi: 10.1016/j.envexpbot.2019.02.026

Sanhueza, C., Bascunan-Godoy, L., Corcuera, L. J., and Turnbull, M. H. (2013). The response of leaf respiration to water stress in *Nothofagus* species. *N. Z. J. Bot.* 51, 88–103. doi: 10.1080/0028825X.2012.759600

Selinski, J., Scheibe, R., Day, D. A., and Whelan, J. (2018a). Alternative oxidase is positive for plant performance. *Trends Plant Sci.* 23, 588–597. doi: 10.1016/j. tplants.2018.03.012

Selinski, J., Hartmann, A., Deckers-Hebestreit, G., Day, D. A., Whelan, J., and Scheibe, R. (2018b). Alternative oxidase isoforms are differentially activated by tricarboxylic acid cycle intermediates. *Plant Physiol.* 176, 1423–1432. doi: 10.1104/pp.17.01331

Shabala, S., and Shabala, L. (2011). Ion transport and osmotic adjustment in plants and bacteria. *Biomol. Concepts* 2, 407–419. doi: 10.1515/BMC.2011.032

Slama, I., Abdelly, C., Bouchereau, A., Flowers, T., and Savouré, A. (2015). Diversity, distribution and roles of osmoprotective compounds accumulated in halophytes under abiotic stress. *Ann. Bot.* 115, 433–447. doi: 10.1093/aob/ mcu239

Smith, C. A., Melino, V. J., Sweetman, C., and Soole, K. L. (2009). Manipulation of alternative oxidase can influence salt tolerance in *Arabidopsis thaliana*. *Physiol. Plant.* 137, 459–472. doi: 10.1111/j.1399-3054.2009.01305.x

Strodtkötter, I., Padmasree, K., Dinakar, C., Speth, B., Niazi, P. S., Wojtera, J., et al. (2009). Induction of the AOX1D isoform of alternative oxidase in *A. thaliana* T-DNA insertion lines lacking isoform AOX1A is insufficient to optimize photosynthesis when treated with antimycin a. *Mol. Plant* 2, 284–297. doi: 10.1093/mp/ssn089

Szabados, L., and Savouré, A. (2010). Proline: a multifunctional amino acid. *Trends Plant Sci.* 15, 89–97. doi: 10.1016/j.tplants.2009.11.009

Thalmann, M., and Santelia, D. (2017). Starch as a determinant of plant fitness under abiotic stress. *New Phytol.* 214, 943–951. doi: 10.1111/nph.14491

Umbach, A. L., Fiorani, F., and Siedow, J. N. (2005). Characterization of transformed *Arabidopsis* with altered alternative oxidase levels and analysis of effects on reactive oxygen species in tissue. *Plant Physiol.* 139, 1806–1820. doi: 10.1104/pp.105.070763

Vanlerberghe, G. C. (2013). Alternative oxidase: a mitochondrial respiratory pathway to maintain metabolic and signaling homeostasis during abiotic and biotic stress in plants. *Int. J. Mol. Sci.* 14, 6805–6847. doi: 10.3390/ijms14046805

Vanlerberghe, G. C., Dahal, K., Alber, N. A., and Chadee, A. (2020). Photosynthesis, respiration and growth: a carbon and energy balancing act for

alternative oxidase. *Mitochondrion* 52, 197–211. doi: 10.1016/j.mito.2020. 04.001

Ventura, Y., Eshel, A., Pasternak, D., and Sagi, M. (2015). The development of halophyte-based agriculture: past and present. *Ann. Bot.* 115, 529–540. doi: 10.1093/aob/mcu173

Vishwakarma, A., Tetali, S. D., Selinski, J., Scheibe, R., and Padmasree, K. (2015). Importance of the alternative oxidase (AOX) pathway in regulating cellular redox and ROS homeostasis to optimize photosynthesis during restriction of the cytochrome oxidase pathway in *Arabidopsis thaliana*. *Ann. Bot.* 116, 555–569. doi: 10.1093/aob/mcv122

Watanabe, C. K., Hachiya, T., Takahara, K., Kawai-Yamada, M., Uchimiya, H., Uesono, Y., et al. (2010). Effects of aox1a deficiency on plant growth, gene expression of respiratory components and metabolic profile under low-nitrogen stress in *Arabidopsis thaliana*. *Plant Cell Physiol.* 51, 810–822. doi: 10.1093/pcp/ pcq033

Xu, F., Yuan, S., Zhang, D. W., Lv, X., and Lin, H. H. (2012). The role of alternative oxidase in tomato fruit ripening and its regulatory interaction with ethylene. *J. Exp. Bot.* 63, 5705–5716. doi: 10.1093/jxb/er s226

Yoshida, K., Terashima, I., and Noguchi, K. (2007). Up-regulation of mitochondrial alternative oxidase concomitant with chloroplast overreduction by excess light. *Plant Cell Physiol.* 48, 606–614. doi: 10.1093/pcp/p cm033

Zhang, D. W., Yuan, S., Xu, F., Zhu, F., Yuan, M., Ye, H. X., et al. (2016). Light intensity affects chlorophyll synthesis during greening process by metabolite signal from mitochondrial alternative oxidase in *Arabidopsis*. *Plant Cell Environ.* 39, 12–25. doi: 10.1111/pce.12438

Zhang, Z. S., Liu, M. J., Scheibe, R., Selinski, J., Zhang, L. T., Yang, C., et al. (2017). Contribution of the alternative respiratory pathway to PSII photoprotection in C3 and C4 plants. *Mol. Plant* 10, 131–142. doi: 10.1016/j.molp.2016.10.004

Zhu, T., Zou, L., Li, Y., Yao, X., Xu, F., Deng, X., et al. (2018). Mitochondrial alternative oxidase-dependent autophagy involved in ethylene-mediated drought tolerance in *Solanum lycopersicum*. *Plant Biotechnol. J.* 16, 2063–2076. doi: 10.1111/pbi.12939

Conflict of Interest: The authors declare that the research was conducted in the absence of any commercial or financial relationships that could be construed as a potential conflict of interest.

Publisher's Note: All claims expressed in this article are solely those of the authors and do not necessarily represent those of their affiliated organizations, or those of the publisher, the editors and the reviewers. Any product that may be evaluated in this article, or claim that may be made by its manufacturer, is not guaranteed or endorsed by the publisher.

Copyright © 2022 Del-Saz, Iglesias-Sanchez, Alonso-Forn, López-Gómez, Palma, Clemente-Moreno, Fernie, Ribas-Carbo and Florez-Sarasa. This is an open-access article distributed under the terms of the Creative Commons Attribution License (CC BY). The use, distribution or reproduction in other forums is permitted, provided the original author(s) and the copyright owner(s) are credited and that the original publication in this journal is cited, in accordance with accepted academic practice. No use, distribution or reproduction is permitted which does not comply with these terms

Annex 4

PEN ACCESS

EDITED BY
Claudio Bonghi,
University of Padua, Italy

REVIEWED BY
Jinwook Lee,
Chung-Ang University, South Korea
Joanna Lado,
National Institute for Agricultural Research (INIA), Uruguay

*CORRESPONDENCE Manuel Rodriguez-Concepcion
manuelrc@ibmcp.upv.es Jordi Giné-Bordonaba
jordi.gine@irta.cat

SPECIALTY SECTION
This article was submitted to Crop and Product Physiology, a section of the journal Frontiers in Plant Science

RECEIVED 05 April 2022
ACCEPTED 13 July 2022
PUBLISHED 01 August 2022

CITATION
Fernández-Cancelo P, Iglesias-Sanchez A, Torres-Montilla S, Ribas-Agustí A, Teixidó N, Rodriguez-Concepcion M and Giné-Bordonaba J (2022) Environmentally driven transcriptomic and metabolic changes leading to color differences in "Golden Reinders" apples. *Front. Plant Sci.* 13:913433. doi: 10.3389/fpls.2022.913433

COPYRIGHT
© 2022 Fernández-Cancelo, Iglesias-Sanchez, Torres-Montilla, RibasAgustí, Teixidó, Rodriguez-Concepcion and Giné-Bordonaba. This is an open-access article distributed under the terms of the Creative Commons Attribution License (CC BY). The use, distribution or reproduction in other forums is permitted, provided the original author(s) and the copyright owner(s) are credited and that the original publication in this journal is cited, in accordance with accepted academic practice. No use, distribution or reproduction is permitted which does not comply with these terms.

DOI 10.3389/fpls.2022.913433

Environmentally driven transcriptomic and metabolic changes leading to color differences in "Golden Reinders" apples

Pablo Fernández-Cancelo [1], **Ariadna Iglesias-Sanchez** [2,3], Salvador Torres-Montilla [2,3], Albert Ribas-Agustí [4], Neus Teixidó [1], Manuel Rodriguez-Concepcion [2,3]* and Jordi Giné-Bordonaba [1]*

[1]Postharvest Programme, Institute of Agrifood Research and Technology (IRTA), Lleida, Spain, [2]Centre for Research in Agricultural Genomics (CRAG) CSIC-IRTA-UAB-UB, Barcelona, Spain, [3]Institute for Plant Molecular and Cell Biology (IBMCP), CSIC-Universitat Politècnica de Valencia, Valencia, Spain, [4] Food Safety and Functionality Programme, IRTA, Monells, Spain

Abstract

Apple is characterized by its high adaptation to diverse growing environments. However, little is still known about how different environments can regulate at the metabolic or molecular level specific apple quality traits such as the yellow fruit peel color. In this study, changes in carotenoids and chlorophylls, antioxidants as well as differences in the transcriptome were investigated by comparing the peel of "Golden Reinders" apples grown at different valley and mountain orchards. Mountain environment favored the development of yellow color, which was not caused by an enhanced accumulation of carotenoids but rather by a decrease in the chlorophyll content. The yellow phenotype was also associated to higher expression of genes related to chloroplast functions and oxidative stress. Time-course analysis over the last stages of apple development and ripening, in fruit from both locations, further revealed that the environment differentially modulated isoprenoids and phenylpropanoid metabolism and pointed out a key role for

H_2O_2 in triggering apple peel degreening. Overall, the results presented herein provide new insights into how different environmental conditions regulate pigment and antioxidant metabolism in apple leading to noticeable differences in the apple peel color.

KEYWORDS

antioxidant metabolism, color, environment, isoprenoids, oxidative stress, phenylpropanoids, Malus domestica (Bork.)

Introduction

Fruit peel color is an attribute highly appreciated by consumers (Iglesias et al., 2008) which is controlled by the relative concentrations of pigments, including isoprenoids (chlorophylls and carotenoids) and phenylpropanoids (anthocyanins; Merzlyak et al., 2003). Chlorophylls and carotenoids are both photosynthetic pigments associated with light-harvesting proteins which are involved in light absorption processes within the thylakoids (Polívka and Frank, 2010). While chlorophylls are responsible for the green color in unripe apples (Reay et al., 1998), carotenoids are the major pigments in yellow peel apples such as "Golden Delicious" (Delgado-Pelayo et al., 2014). During ripening, but also as a response to stress, chlorophyll levels decrease accompanying the perceived fruit color changes (Yin et al., 2016). Carotenoids are synthetized and stored in plastids, including chloroplasts, where they are required for the assembly of the photosynthetic apparatus and are essential for photoprotection by scavenging reactive oxygen species (ROS) and by dissipating excess light energy as heat (Rodriguez-Concepcion et al., 2018). Carotenoids also act together with tocopherols (another group of plastidial isoprenoids) as thylakoid antioxidants (Ramel et al., 2012). In addition, carotenoids are the precursors of abscisic acid (ABA), a hormone involved in the regulation of fruit ripening (Leng et al., 2013) and in the fruit or plant adaptation to environmental conditions (Wang et al., 2020). As an example, ABA is able to orchestrate the fruit tolerance to abiotic stresses by regulating the accumulation of ROS (Zhang et al., 2019) and the expression of antioxidant enzymes (Mou et al., 2015), such as superoxide dismutase (SOD), catalase (CAT), and peroxidases (APX and POX; Meitha et al., 2020). Indeed, antioxidant enzymes in combination with non-enzymatic antioxidants, such as phenolic compounds, tocopherols, carotenoids, ascorbic acid, and glutathione (Shao et al., 2008), are able to limit the accumulation of damaging ROS produced either during aerobic metabolism (Venditti et al., 2013) or under stress conditions (Choudhury et al., 2017). ROS (i.e., H_2O_2) not only act as damaging but also as signaling molecules participating in transduction cascades (Saxena et al., 2016), interacting with plant hormones (Chen et al., 2016), and regulating physiological processes such as fruit development (Khandaker et al., 2012). Some studies suggest that H_2O_2 may regulate, for instance, the chloroplast-to-chromoplast transition in carotenoid-rich fruit during ripening (Bouvier et al., 1998), favoring carotenoids

accumulation and color changes (Sadali et al., 2019). However, in "Golden" apples, carotenoid levels do not appear to increase but to decrease during fruit growth (Gross et al., 1978), suggesting that other mechanisms are likely involved in color development within this particular apple cultivar.

The fruit pigment content is strongly influenced by the environment, mainly temperature (Lin-Wang et al., 2011) and light (Llorente et al., 2016). For example, it has been observed that growing "Fuji" apples at high altitudes, where temperatures are low and sunlight incidence is high, promotes the accumulation of anthocyanins (Karagiannis et al., 2020). Anthocyanins own different roles within the fruit, including the protection against photo-oxidative stress induced by high light incidence (Zheng et al., 2020) and contributing, as non-photosynthetic pigments, to the red fruit color. Nowadays, and as a result of climate change, the environmental conditions in certain production areas are no longer suitable for developing fruit with optimal peel color (Lin-Wang et al., 2011), or other optimum quality traits (Sugiura et al., 2013). For instance, a recent study demonstrated that "Golden Reinders" apples grown in the Ebro valley never attained the yellow phenotype as observed in fruit grown in mountain regions, even if the fruit was left on the tree far beyond the commercial harvest date (Fernández-Cancelo et al., 2022). This said, no information is currently available on how the environment influences, at the metabolic and transcriptomic level, yellow peel color in "Golden" apples, despite being one of the most widely cultivated and consumed varieties worldwide (Bonany et al., 2013).

Accordingly, our study aimed to decipher the biochemical and transcriptomic shifts leading to color differences in the peel of "Golden Reinders" apples grown in different environments (mountain vs. valley) as well as to elucidate if color changes were only caused by differences in pigments content or rather to other metabolic shifts driven by environmental signals able to alter peel ripening. Special emphasis was also given to clarify how pigment content and antioxidant metabolism of the apple peel change during the last stages of fruit development and ripening in response to diverse growing environments.

Materials and methods

Plant material and experimental design

In 2018, four different orchards located in the province of Lleida (Catalonia, North-East Spain) were used to assess the influence of the environment on apple color at the commercial harvest date (CHD): two orchards from valley areas, Alcanó (214 meters above sea level, masl) and Vilanova (195 masl), and two from mountain areas, Llesp (989 masl) and Gotarta (1,191 masl). "Golden Reinders" apples were harvested at the CHD based on flesh firmness (71 ± 2.5 N) and starch index values (6 ± 0.8) from trees of similar age and grown under the same rootstock (M9) as well as similar agronomical practices. Further characterization of the fruit maturity at the time of harvest (focused on ethylene biosynthesis) is available from FernándezCancelo et al. (2021). A set of 45 fruit were harvested at the same canopy height from 10 random trees in each location at CHD. Thirty fruit were used for quality

evaluations (color, firmness, and starch index), whereas the peel from 15 fruit (5 apples per replicate and 3 replicates per location) were grinded and frozen in liquid nitrogen and kept at −80°C until further biochemical determinations.

Based on the color differences found in 2018, the next year fruit development and ripening were monitored in Vilanova (valley) and Gotarta (mountain) orchards at 4 sampling points, including the CHD (165 and 167 days after full bloom [DAFB] in valley and mountain orchards, respectively), based on the percentage of final fruit size (S1: 60% final fruit size, S2: 80% final fruit size, S3: 90% final fruit size, and S4: 100% final fruit size). Samplings started at 89 DAFB (corresponding with S1) and were performed approximately every 25–30 days differing less than 5 days between locations for each sampling point. The final fruit size (equivalent to CHD) also corresponded to 1,388 and 848 growing degree days (GDD) for apples from Vilanova and Gotarta, respectively, within the studied period. At each harvest, 50 fruit per location and sampling point were harvested at the same canopy height from 10 random trees and immediately transported to the laboratory for quality evaluations (30 fruit per location or sampling point). In parallel, peel from 20 fruit (5 apples per replicate and 4 replicates per location and sampling point) were ground and frozen in liquid nitrogen and kept at −80°C until further biochemical analysis.

Meteorological data including temperature, relative humidity (HR), evapotranspiration, and solar radiation were recorded at Vilanova and Gotarta orchards by portable meteorological stations (Decagon Devices, Pullman, WA, United States) equipped with a pyranometer (Apogee Instruments, Logan, UT, United States).

Fruit quality evaluation

On arrival to the laboratory, fruit weight, diameter, color, firmness, and starch index were measured on 30 individual fruit per orchard and sampling point. In the particular case of color and firmness determinations, measurements were made on two opposite sides of each examined fruit using a portable colorimeter (CM-2600d; Konica Minolta Sensing, Osaka, Japan) and a GÜSS FTA penetrometer (FR Turoni, Forlì, Italy), respectively. Starch index was evaluated by dipping equatorial fruit slices in an iodine solution (I_2-KI) for 10 min. The starch index was assigned to each fruit using the starch scale from 1 to 10 developed by the Centre Technique Interprofessionnel des Fruits et Légumes (CTIFL, Paris, France). Further quality measurements were earlier reported by Fernández-Cancelo et al. (2021).

RNA extraction and sequencing

RNA was extracted from lyophilized peel samples, using the Spectrum™ Plant Total RNA Kit (Sigma-Aldrich, St Louis, MO, United States) following the manufacturer's recommendation. Electrophoresis on an agarose gel by staining with GelRed™ Nucleic Acid Gel Stain (Biotium, Hayward, CA, United States) was used for the evaluation of RNA integrity and the absence of contaminant DNA. RNA-seq service was performed by Sequentia Biotech SL (Barcelona, Spain). Assessment of RNA quality and indexed library preparation was carried out as described (Llorente et al.,

2020). Sequencing was performed using the NovaSeq6000 System (Illumina) 2×150 bp, 30 M paired reads per sample. Data analysis was performed with the online platform AIR[2] using the *Malus* × *domestica* "Golden Delicious" GDDH13 v1.1 reference genome (Daccord et al., 2017) deposited in the Genome Database from Rosacea (GDR[3]). Differentially expressed genes (DEGs) were identified with the DESeq2 statistical method in the AIR platform. The resulting lists were filtered using cut-offs of false discovery rate < 0.05 and log2-transformed fold change (log2FC) >0.585 for upregulated genes and < −0.599 for downregulated genes. GO enrichment analyses were performed using default parameters with AppleMDO[3] automatically followed by AgriGO[4]. Enriched GO terms and *p*-values were then loaded into REVIGO[5] to identify and visualize non-redundant GO terms using a cutoff value of 0.5.

cDNA and qPCR analysis

The cDNA synthesis was performed on 1 µg of RNA using the SuperScript IV First-Strand Synthesis System (Invitrogen, Carlsbad, CA, United States). The gene expression analysis was performed by mixing KAPA SYBR® Fast qPCR Master Mix (Kapa Biosystems, Inc., Wilmington, MA, United States), 100 nM of each primer, and the corresponding diluted cDNA. The reaction was performed on a 7,500 Real-Time PCR System (Applied Biosystems, Waltham, MA, United States) under the following conditions: 10 s at 95°C followed by 40 cycles of 95°C during 15 s and 60°C for 1 min. A non-template control (NTC) was included by using DNA-free water instead of cDNA. A melt curve analysis was performed to check primer specific by including a final amplification cycle at 95°C for 15 s, 60°C for 1 min, 95°C for 30 s, and 60°C for 15 s. Primers used in this study were retrieved from the literature or designed *de novo* when indicated (Supplementary Table S1). Relative gene expression was expressed as Mean Normalized Expression (MNE) according to previous studies (Muller et al., 2002) using *Md8283* as a reference gene.

Photosynthetic pigments and tocopherols analysis

Carotenoids, chlorophylls, and tocopherols were extracted from lyophilized apple peel tissue as described for tomato leaves (Barja et al., 2021). An Agilent 1,200 series HPLC system (Agilent Technologies, Santa Clara, CA, United States) was used for the separation and detection of individual species with a photodiode array for (chlorophylls and carotenoids) or a fluorescence detector (for tocopherols). Quantification was performed by comparison of peak areas with commercial standards.

ABA quantification

ABA was extracted from lyophilized apple peel tissue as described elsewhere (Torres et al., 2017). The extract (5 µl) was injected on a Waters ACQUITY UPLC chromatograph

[2] https://www.transcriptomics.cloud

[3] https://www.rosaceae.org/ 3

[4] https://systemsbiology.cau.edu.cn/agriGOv2 5 https://revigo.irb.hr

(Waters Corporation, Milford, MA, United States) fitted with a Waters ACQUITY UPLC HSS T3 1.8 µm 100×2.1 mm column (Waters Corporation, Milford, MA, United States). Separation was carried out at a flow rate of 0.40 ml/min using a mobile phase consisting in a mixture of 0.1% formic acid and 2% of acetonitrile in water (A) and 0.1% formic acid in acetonitrile (B). The gradient program was held for the first 1 min at 5% B, increased linearly to 100% B in 1.5 min, and then maintained at 100% B for 1 min. The temperature of the column was kept at 35°C and the sample compartment was refrigerated at 10°C. Quantification was performed by comparison of peak areas with the commercial standard.

Quantification of hydrogen peroxide and malondialdehyde

Hydrogen peroxide concentration expressed in mmol kg−1 was determined using the PeroxiDetect Kit (Sigma-Aldrich, Saint Louis, MO, United States) after the extraction of 2.5 g of frozen peel in 10 ml of 5% trichloroacetic acid (TCA) based on the protocol described elsewhere (Giné-Bordonaba et al., 2019). Malondialdehyde (MDA) was analyzed as an index of lipid peroxidation using the thiobarbituric acid reactive substrates (TBARS) based on the protocol previously described (MartínezSolano et al., 2005) using 0.5 g of frozen tissue mixed with 4 ml of 0.1% trichloroacetic acid (TCA) solution.

Ascorbic acid and dehydroascorbic acid content

Based on previous protocols (Rassam and Laing, 2005), the extraction of ascorbic acid was carried out mixing 2.5 g of frozen peel tissue with 5 ml of metaphosphoric acid suspension (3% metaphosphoric acid, 8% acetic acid) and centrifuging at 24,000 × g for 22 min at 4°C. Quantification of ascorbic acid (AsA) and total ascorbic acid was performed as previously described (Fernández-Cancelo et al., 2021). Dehydroascorbic acid (DHA) was calculated by subtracting the ascorbic acid content from that of total ascorbic acid.

Determination of phenolic compounds and the peel antioxidant capacity

Total phenolic compounds (TPC) and antioxidant capacity of the apple peel were determined using frozen tissue as previously described (Giné Bordonaba and Terry, 2008) by mixing 3 g of apple frozen peel tissue with 10 ml of 79.5% (v/v) methanol and 0.5% (v/v) HCl in Milli-Q water. Sample extraction was held at 20°C with constant shaking for 2 h and mixing the samples every 30 min. The extract was centrifuged at 24,000 × *g* for 30 min at 20°C. From the same extract, total phenolic compounds were measured by means of the Folin–Ciocalteu method and total antioxidant capacity was measured by the Ferric Reducing Antioxidant Power (FRAP) assay as described in previous works (Giné-Bordonaba et al., 2016). Individual phenolic compounds from peel tissue were quantified from the same extracts used for antioxidant capacity determination. The methanolic extract was filtered through a 0.22 µm filter and injected (5 µl) on an Agilent 1,260 Infinity II liquid chromatograph UHPLC (Agilent Technologies, Santa Clara, CA, United States) fitted with a Waters XSelect HSS T3 (4.6×100 mm, 2.5 µm; Waters Corporation, Milford, MA, United

States) and a guard column Waters XSelect HSS T3 VanGuard (3.9×5 µm, 3.5 µm; Waters Corporation, Milford, MA, United States). Separation was carried out at a flow rate of 0.75 ml/min using a mobile phase consisting of 0.1% acetic acid in water (A) and 0.1% acetic acid in acetonitrile (B). The gradient program was held for the first 2 min at 6% B, increased linearly to 12% B in 3 min, then raised to 30% B in 29 min, and finally elevated to 100% B in 6 min and maintained at 100% B for 5 min. The temperature of the column was kept at 40°C and the sample compartment was refrigerated at 10°C. Detection was performed at 280, 320, and 520 nm, yet the online spectra were acquired in the 220–650 nm wavelength range with a resolution of 0.5 nm. Phenolic compounds were identified according to their retention time, spectral features, and ratios of maximum absorption peaks (λ). When no commercial standard was available, compounds were tentatively identified in an Acquity UPLC system equipped with diode array (DAD) and triple quadrupole mass spectrometer (MS) detectors using electrospray ionization interface (Waters, Milford, MA, USA). MS scan mode was used to obtain parent molecular ions and MS/MS daughters mode was used to obtain their fragmentation patterns, with argon as collision gas and 20–30 V as collision energies. Quantification was performed using calibration curves prepared with standard stock solutions of chlorogenic acid, catechin, and quercetin-3-O-glucoside, and their concentrations were expressed as g kg^{-1} FW. Detected phenolic acids and quercetin-derivatives were quantified using chlorogenic acid and quercetin-3-O-glucoside standard curves.

Antioxidant enzymes activity

Peroxidase (POX, EC 1.11.1.7) was extracted by mixing 5 g of frozen peel with 10 ml of phosphate buffer (100 mM, pH 6) with 0.5 mM cysteine and 0.5 g of PVPP and centrifuged at 20,000 *g* for 15 min at 4°C. A 2.5 ml of supernatant was loaded into a Sephadex G-25 column (PD 10; Pharmacia, Madrid, Spain) that had previously been equilibrated with 10 ml phosphate buffer (100 mM, pH 6), and the enzyme was eluted with 3.5 ml of the same buffer. POX activity was determined as described elsewhere (Giné-Bordonaba et al., 2017).

Ascorbate peroxidase (APX; EC 1.11.1.11) extraction, 5 g of frozen peel was mixed with 15 ml of 100 mM base phosphate buffer (pH 7.5) containing 0.8 mM ascorbic acid and 1 mM EDTA. The mixture was centrifuged at 10000 *g* for 15 min at 4°C (Collazo et al., 2018). APX activity was determined at 290 nm for 10 min by monitoring the H_2O_2-dependent decomposition of ascorbate in a mixture containing 20 µl of supernatant and 280 µl of a reaction solution containing 0.22 mM ascorbic acid, 1 mM EDTA, and 1 mM H_2O_2 (Nakano and Asada, 1981).

Extraction of superoxide dismutase (SOD, EC 1.15.1.1) and catalase (CAT, EC 1.11.1.6) was carried out at the same time by homogenizing 5 g of peel tissue in 15 ml potassium phosphate buffer (100 mM, pH 7.8) containing 2 mM DTT, 5% (w/v) PVPP, 0.1 mM EDTA, and 1.25 mM polyethylene glycol (Chiriboga et al., 2013). The homogenate was centrifuged at 20000 *g* for 15 min at 4°C and then a 2.5 ml aliquot was loaded into a Sephadex G-25 column (PD 10; Pharmacia, Madrid, Spain) equilibrated with 10 ml 100 mM phosphate buffer (pH 7.8). The enzyme was eluted with 3.5 ml of the same buffer. The resulting supernatant was

used as an enzyme extract to determine SOD and CAT activity. SOD activity was assayed by measuring its ability to inhibit the photochemical reduction of nitroblue tetrazolium (NBT) using the method described elsewhere (Giannopolitis and Ries, 1977). One unit of SOD (Unit of activity; UA) was considered the amount of enzyme required to inhibit NBT reduction by 50%. CAT activity was measured by the Claiborne method (Claiborne, 1986) following the disappearance of H_2O_2 at 240 nm. Except for SOD, enzymatic activity was expressed in UA per milligram of protein, with one UA representing the quantity of enzyme responsible for a change in 1 absorbance unit per minute. Protein was quantified by the method of Bradford (Bradford, 1976).

Statistical data analysis

Data were subjected to analysis of variance (ANOVA) tests using JMP 13.1.0 SAS Institute. When the analysis was statistically significant, Tukey's HSD test at the level $p \leq 0.05$ was performed for comparison of means for the interaction location and development stage. A principal component analysis (PCA) was also performed to characterize the samples harvested at CHD in the four orchards studied. Data were centered and weighted using the inverse of the standard deviation of each variable in order to avoid the influence of the different scales used for the variables. Spearman's rank correlation matrix ($p \leq 0.05$) was done using the R corplot package.

Results

Orchard location influences peel color and composition

"Golden Reinders" apples grown in four different locations (two valleys – Alcanó and Vilanova and two mountains - Llesp and Gotarta - orchards) and picked at the CHD showed significant differences in peel color (determined both visually and as changes in Hue angle, H°) among locations, but only apples harvested in Gotarta mountain orchard exhibited an optimal yellow peel color (H° = 96 ± 0.8) if compared with fruit from valley locations—Alcanó (H° = 107 ± 0.5) and Vilanova (H° = 108 ± 0.4)—and even with apples harvested in the mountain orchard of Llesp (H° = 104 ± 0.7). A principal component analysis (PCA; Figure 1A) using individual isoprenoids (chlorophylls, carotenoids, and tocopherols), H°, MDA, TPC, and antioxidant capacity as variables was used to differentiate the apple peel from fruit grown at the four different locations (two valley vs. two mountain orchards). The first two principal components captured 90.2% of the total variability and were sufficient to clearly differentiate the samples. The bidimensional plot illustrated that greenish peel apples were clustered together in the PC1-positive part of the plot, while yellow apples were plotted in the negative part. Enhanced yellow coloration of Gotarta apples was accompanied by a distinct pigment and antioxidant profile as depicted in Figure 1A. Interestingly, no statistically significant differences on carotenoid content were found between the four orchards studied, being its levels ca. 0.03 ± 0.003 mg kg^{-1} DW (Figure 1B). However, chlorophyll levels on apples from Gotarta were around 2.5-fold lower if compared to fruit from the other orchards (Figure 1C), hence owning a higher carotenoid/chlorophyll ratio (ca. 1.8 in Gotarta vs. 1.2 in the green apples). Gotarta apples also presented higher levels of oxidative stress markers such as MDA (20 ± 1.7 µmol kg^{-1}) if compared with valley apples (17 ± 2.3 µmol kg^{-1} and 16 ± 1.0 µmol kg^{-1} for

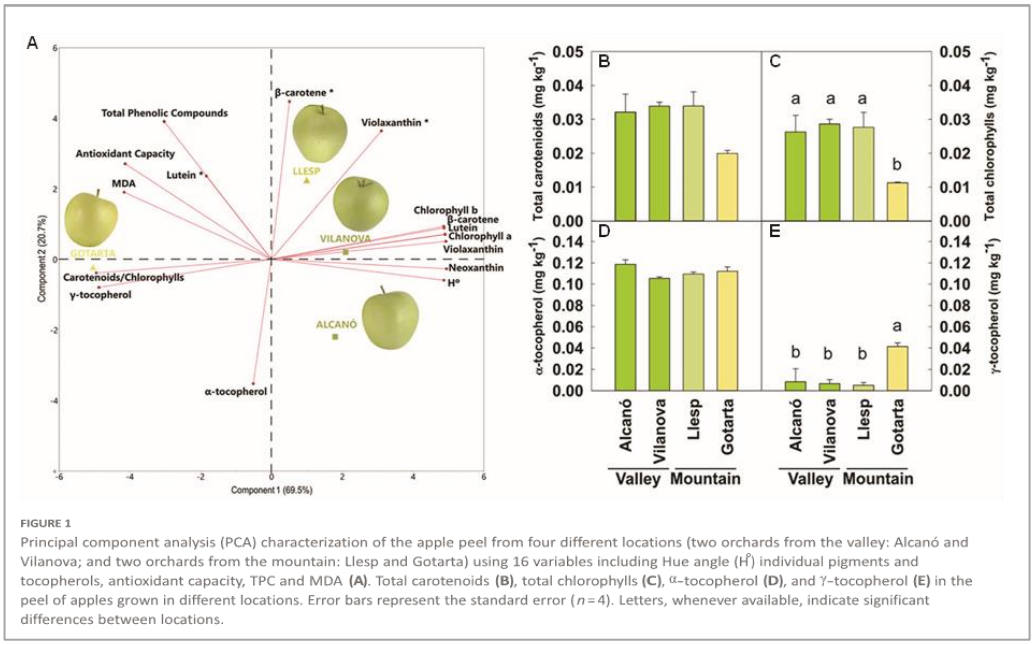


FIGURE 1
Principal component analysis (PCA) characterization of the apple peel from four different locations (two orchards from the valley: Alcanó and Vilanova; and two orchards from the mountain: Llesp and Gotarta) using 16 variables including Hue angle (H^0) individual pigments and tocopherols, antioxidant capacity, TPC and MDA **(A)**. Total carotenoids **(B)**, total chlorophylls **(C)**, α–tocopherol **(D)**, and γ–tocopherol **(E)** in the peel of apples grown in different locations. Error bars represent the standard error ($n = 4$). Letters, whenever available, indicate significant differences between locations.

Alcanó and Vilanova apples, respectively) and higher content of antioxidants, specifically γ-tocopherol (Figures 1D,E).

Transcriptome reprograming in response to orchard location

To study whether the expression of genes for enzymes in metabolic pathways involved in plastidial isoprenoid (chlorophyll, carotenoid, and tocopherol) biosynthesis and degradation was altered by the orchard location, a RNA-seq analysis of the peel from apples grown at the four different locations was performed (Figure 2; Supplementary Figure S1). Comparison of Gotarta (yellow phenotype) with the other three locations (green phenotype) showed that most genes of the carotenoid biosynthetic pathway were downregulated in Gotarta, whereas those involved in carotenoid degradation were upregulated, consistent with the observed trend toward lower levels of carotenoids in Gotarta apples (Supplementary Figure S1). By contrast, gene-encoding enzymes involved in chlorophyll degradation and tocopherol biosynthesis were strongly upregulated in "Gotarta" apples (Supplementary Figure S1).

To further identify other potential processes associated to color differences among orchards, a more detailed analysis of the RNA-seq data was performed (Figure 2). Comparison of Gotarta with the other three locations identified a common set of 797 genes that were upregulated in Gotarta and 693 genes that were downregulated ifcompared to all three locations leading to green apples (Figure 2A). GO term analysis of the whole set of differentially expressed genes (1,490 genes) showed an enrichment in processes related to photosynthesis, metabolism (including pigment and isoprenoid biosynthesis), plastid organization, and response to environmental cues (Figures 2B,C). Many terms within metabolism and cellular responses were actually related to photosynthesis, carbon fixation, and carbohydrate metabolic processes (Figure 2C), whereas another important group of GO terms was linked to

response to oxidative stress, including genes involved in the regulation of ROS and H_2O_2 metabolism (Figure 2C). We also observed that pathways regulating nitrogen and phosphorus metabolic process as well as general organic substance metabolism were overrepresented among the set of differentially expressed genes. In terms of biological quality, protein metabolic process,cellular responses, the regulation of and molecular function was the most represented (Figure 2C).

Pigment metabolism during fruit development is differentially affected by the environment

Based on the major differences on peel color, pigment composition, and gene expression,

Gotarta (mountain) and Vilanova (valley) orchards were selected to further monitor major metabolic and transcriptomic shifts

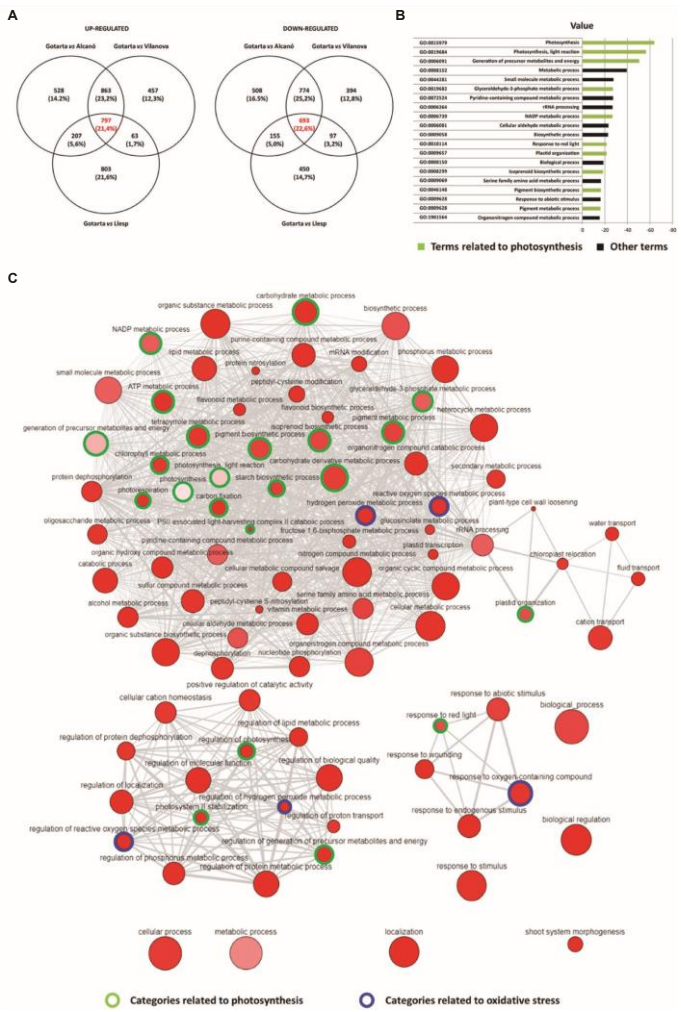


FIGURE 2
Number of genes upregulated and down-regulated **(A)** in Gotarta apples (yellow phenotype) compared with the other 3 orchards (green phenotypes). The 20 most frequent GO upregulated in Gotarta were displayed as % Total GO counted **(B)**. Gene functional categories enriched in Gotarta apples **(C)** provided by REVIGO's "Scatterplot view" (http://revigo.irb.hr/). Disc color indicates enrichment value of p (the softer the color the highest the value) and size represents the frequency of the category. Thickness of grey lines represent semantic similarity between categories while spatial arrangement of discs corresponds to grouping of categories by semantic similarity. Those related to photosynthesis are circled in green, and terms associated with oxidative stress are circled in blue.

associated to fruit color changes along fruit development (four developmental stages: S1 to S4, the latter being the CHD). Differences in carotenoid levels were observed between locations and developmental stages, yet the carotenoid profile, understood as the individual carotenoids identified among samples, remains relatively unchanged (Figure 3). Lutein was the main carotenoid found in the apple peel, accounting for 60% of total carotenoids. β-carotene and violaxanthin each contributed to 15% of the total carotenoids blend, while neoxanthin accounted only for the 8% of total carotenoids. In both locations, carotenoids content decreased as the fruit ripened on-tree, yet the reduction rate was 2-fold higher in mountain than in valley fruit. In consequence, although carotenoid levels were *ca.* 30% higher in Gotarta at the two initial samplings (S1 and S2), carotenoid content in mountain apples reached similar levels to those observed in valley apples in the last two samplings (S3 and S4) (Supplementary Figure S2A). The global decrease in carotenoid content during fruit development in both locations only translated into an increase of ABA from 27 ± 2.9 to 59 ± 2.5 μg kg^{-1} in valley fruit from S1 to S3 (Figure 3). In contrast, ABA levels in mountain fruit remained around 23 ± 2.2 μg kg^{-1} DW until S4, when it reached similar levels to those found in valley apples (49 ± 0.4 μg kg^{-1} DW). Chlorophyll levels followed the same pattern as carotenoids in both locations (Supplementary Figure S2B). Mountain apples accumulated a 40% more chlorophyll in the first two stages of development (S1 and S2) and then its levels matched with those from the valley at S3 and S4 (0.02 ± 0.001 and 0.01 ± 0.001 mg kg^{-1} DW, respectively). Carotenogenic gene expression (*MdPSY*, *MdVDE,* and *MdZEP*) progressively increased during fruit development for both studied locations (Supplementary Figures S3A–C). In the last stage, MdPSY expression was 1.4-fold higher in Vilanova whereas MdZEP and MdVDE showed a 30% greater expression in Gotarta. Regarding gene-encoding apocarotenoid production, MdCCD4 expression remained constant along fruit development in the valley, while it

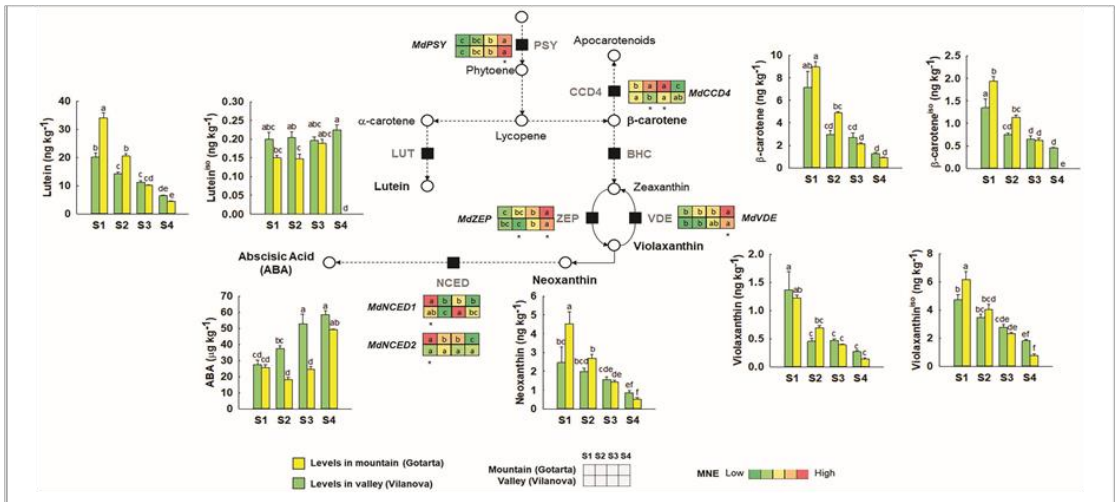


FIGURE 3
Comparison of carotenoid metabolism in "Golden Reinders" apples grown in mountain (Gotarta-) or valley (Vilanova-) orchards during fruit development/ripening. Dashed lines indicate that some steps have been omitted. Quantified carotenoid compounds are represented in bar plots, including minor carotenoid isomers marked with the superscript "iso." Error bars represent the standard error ($n = 4$). Letters, whenever available, indicate significant differences for the interaction location*developmental stage according to Tukey test ($p \leq 0.05$). The corresponding transcript levels of the main genes are represented as heatmaps. Letters within the heatmaps indicate significant differences ($p \leq 0.05$) between development stages, while asterisk denote differences among locations at each specific development stage.

increased from S1 to S2 and significantly declined at S4 in mountain apples (Supplementary Figure S3D). The expression of MdNCED1 and MdNCED2 was similar between locations and remained unchanged during fruit development except at the first stage (S1), where mountain apples showed 3-fold higher expression of both genes in comparison to fruit from the valley (Supplementary Figures S3E,F).

The levels of tocopherols and phenolic compounds are greater in mountain apples

Mountain apples showed 10-fold higher levels of γ-tocopherol at S4 if compared with valley apples (Supplementary Figure S2C), whereas during earlier stages (S1–S3), γ-tocopherol content remained below 0.004 mg kg−1 DW and constant in both locations. In contrast, α-tocopherol remained unchanged (0.03 ± 0.003 mg kg−1 DW) in both locations during fruit development and ripening on-tree (Supplementary Figure S2D). Eleven phenolic compounds were identified in both locations during fruit development, including phenolic acids (chlorogenic acid), dihydrochalcones (phloretin glycosides), flavanols (catechin, epicatechin, and procyanidin B2), and flavonols (quercetin glycosides; Figure 4). In general, the peel from mountain apples showed higher levels of phenolic compounds in the two first development stages (S1 and S2), except for phloretin2'-O-glucoside and procyanidin-B2 whose levels were not affected by the orchard location. All phenolic compounds identified followed a downward trend in both location as the fruit developed, being the decrease rate between 1.2 and 2.0-fold higher in mountains than in valley apples yet depending on the phenolic compound (Figure 4). At the CHD, despite most differences between locations levelled off, the peel from mountain apples showed generally higher levels of phenolic compounds than those from the valley. Analysis of MdPAL1 and MdPAL2 showed expression differences between locations mainly at S4, being significantly higher and lower the expression of MdPAL1 and MdPAL2 in mountain apples than in fruit from the valley.

The environment strongly influences ROS-scavenging enzymes in the apple peel

A completely different pattern of H_2O_2 accumulation was observed when comparing apples grown in mountain or valley orchards. Levels of H_2O_2 remained unchanged in valley apples from S2 to S4 (around 54 ± 4.2 mmol kg^{-1}), whereas in mountain apples, H_2O_2 raised from 77 ± 2.0 to 110 ± 8.1 mmol kg^{-1} within the same period (Figure 5). Enhanced H_2O_2 accumulation in the peel from mountain apples was not associated to higher levels of SOD, the enzyme responsible for the dismutation of $O_2^{\cdot-}$ into H_2O_2, since the activity of this enzyme remained relatively unchanged throughout fruit development/ripening in both loca tions. In contrast, the activities of enzymes involved in the decomposition of H_2O_2 into water and oxygen were location and developmental stage dependent. The activity of APX, the enzyme responsible to catalyze the H_2O_2-dependent oxidation of ascorbate was nearly 2-fold greater in mountain apples at S1, but it decreased in the rest of developmental stages to 13 ± 1.5 UA mg^{-1} protein, matching then the activity levels found in valley apples. Ascorbic acid levels in the valley remained unchanged with values below 75 mg kg^{-1}, whereas AsA levels massively increased from 92 ± 8.0 to 252 ± 30.0 mg kg^{-1} in mountain apple peel during fruit development and on-

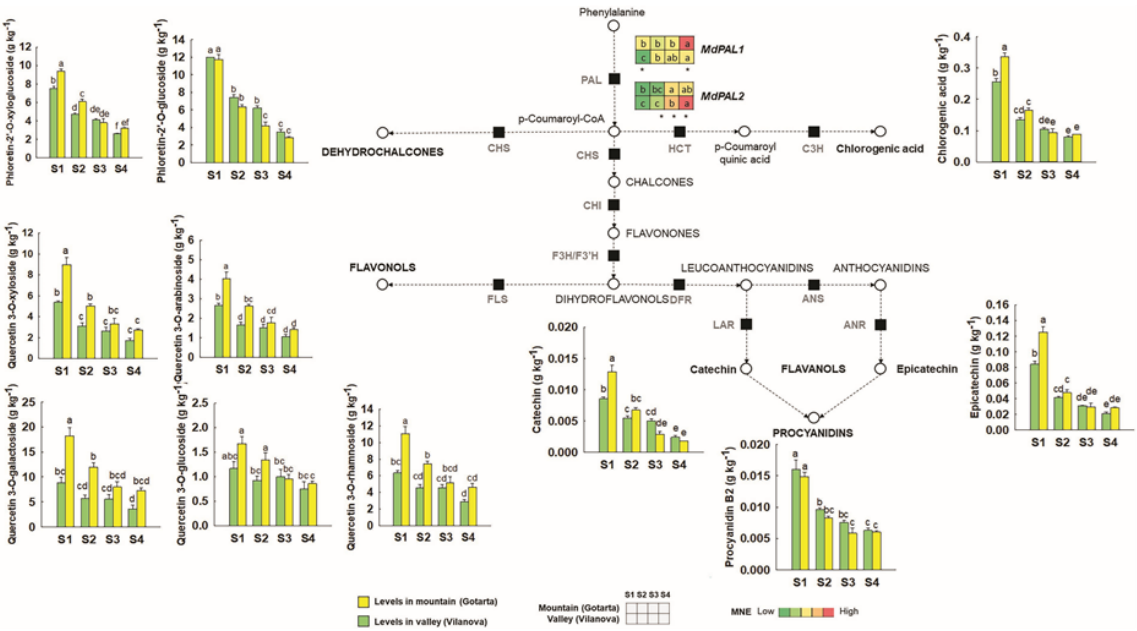


FIGURE 4
Comparison of phenolic compounds metabolism in "Golden Reinders" apples grown in (Gotarta- ●) or valley (Vilanova -●) orchards during fruit development/ripening. Dashed lines indicate that some steps have been omitted. Phenolic compounds are represented in plots. Error bars represent the standard error ($n = 4$). Letters, whenever available, indicate significant differences for the interaction location*developmental stage according to Tukey's test ($p \leq 0.05$). The corresponding transcript levels of the main genes are represented as heatmaps. Letters within the heatmaps indicate significant differences ($p \leq 0.05$) between development stages, while asterisk denote differences among locations at each specific development stage.

tree ripening. A similar pattern was observed for POX, whose activity was significantly higher in mountain apples at S1 and S2 (Figure 5). In the last two samplings (S3 and S4), POX activity from mountain apples decreased and matched the levels observed in fruit from the valley (134 ± 4.5 UA mg^{-1} protein). In contrast, no differences in CAT activity were observed between valley and mountain apples except at S4, when CAT activity in fruit from the valley increased until reaching values of 1.7 ± 0.07 UA mg^{-1} protein. Significant differences were found for the expression of all genes encoding for antioxidant enzymes along the different fruit development stages and locations except for *MdDHAR3* and *MdMDHAR2* that showed no changing pattern along fruit development/ripening (Supplementary Figure S5). Copper superoxide dismutase encoding genes (*MdCSD1* and *MdCSD2*) showed the same downward pattern in both locations along fruit development/ripening. However, the expression of *MdCSD2*, which encodes for chloroplastic SOD, was around 40-fold higher than its cytosolic counterpart *MdCSD1* (Supplementary Figures S5A,B). In turn, *MdFSD2* showed the opposite trend, reaching maximum expression levels at S4 for both locations (Supplementary Figure S5C). In the case of *MdAPX1,* encoding for cytosolic APX, only mountain apples showed an increase of gene expression from 30 to 60 MNE during development/ripening (Supplementary Figure S5D). The expression of *MdAPX6* and *MdMDHAR*1 increased during fruit development/ripening and significant differences were found for the expression of these genes at the CHD (Supplementary Figures S5F,G).

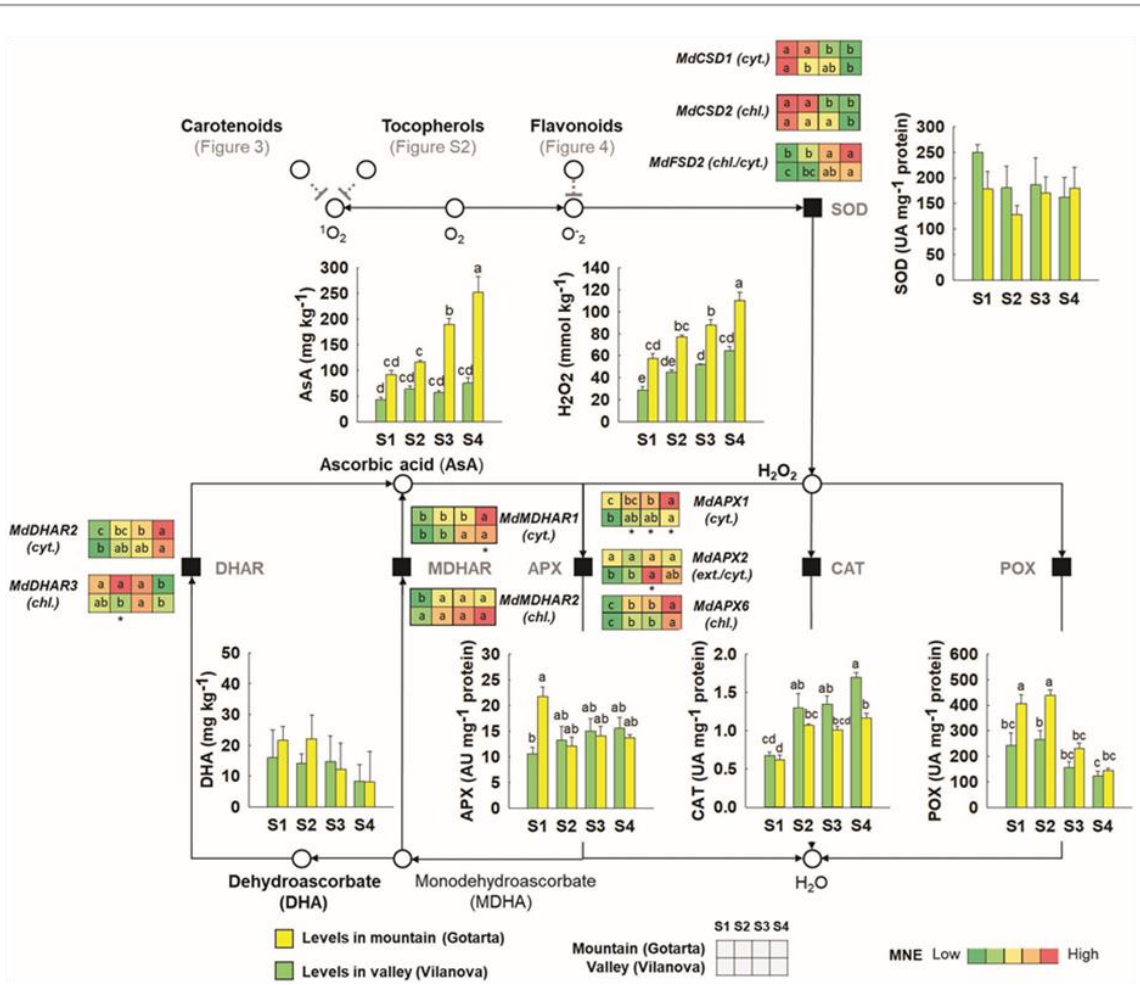


FIGURE 5
Comparative overview of the ROS-scavenging metabolism and ascorbate recycling pathway of "Golden Reinders" apples grown in mountain (Gotarta-●) or valley (Vilanova-●) orchards during fruit development/ripening. The activity of the main antioxidant enzymes, as well as the content of ascorbic acid and H_2O_2, is represented in bar plots. Error bars represent the standard error ($n = 4$). Letters, whenever available, indicate significant differences for the interaction location*stage according to Tukey test ($p \leq 0.05$). The corresponding transcript levels of the main genes are represented as heatmaps. Letters indicate significant differences ($p \leq 0.05$) between development stages, while asterisk denote differences among locations at each specific development stage.

Discussion

Optimal yellow peel color in "Golden Reinders" apples is associated to oxidative stress

"Golden Reinders" apples were grown under similar agronomical practices in four orchards of Lleida Province (two from the valley and two from the mountains) and harvested at the same ripening status in terms of fruit size (75 ± 0.4 mm), firmness (71 ± 0.5 N) and other ripening-related traits (Fernández-Cancelo et al., 2021) showed different peel color phenotype (Figure 1). Notably, fruit from mountain orchards, and especially those from Gotarta, showed enhanced yellow color, as desired by consumers, but also higher antioxidant capacity and elevated levels of MDA, a marker of lipid peroxidation (Hodges et al., 1999). Since the apples were harvested at a

similar maturity stage (Fernández-Cancelo et al., 2021), climatic differences between orchards may have influenced peel metabolism (McTavish et al., 2020) leading to different color phenotypes. Indeed, in our previous study, we demonstrated that optimal fruit color in "'Golden Reinders" apples was not associated to the fruit maturity stage and that fruit grown in the Ebro valley never attain the optimal yellow color desired by the consumer, even if left to ripen on-tree far beyond the CHD (Fernández-Cancelo et al., 2021). Among the wide variety of environmental factors that can influence fruit color (temperature, solar radiation, hours of sun, precipitations, and relative humidity), the low temperatures and solar radiation reached days before harvest in Gotarta (Supplementary Figures S8, S9) in combination with a probable higher accumulation of UV radiation due to the high altitude (data not measured; Blumthaler et al., 1997) may have favored chlorophyll degradation (LeónChan et al., 2017) and color changes in Gotarta apples.

Given the difficulties to evaluate the specific environmental factors affecting apple color, we decided to focus our study in investigating the metabolic or transcriptomic shifts capable to explain the color phenotype differences observed between growing locations, with a special emphasis on pigment and antioxidant metabolism. The pigment profiling presented herein revealed that yellow apples had similar levels of carotenoids but significant lower levels of chlorophylls than apples grown at other locations and showing greenish coloration (Figure 1). These observations strongly suggest that higher chlorophylls levels in greenish "Golden Reinders" apples may be shielding the carotenoid contribution to peel color as it was described in pepper (Filyushin et al., 2020). Hence, it may be that chlorophyll levels in apple peel must fall below a certain threshold for achieving an optimal yellow color as previously observed during olive ripening (Mínguez-Mosquera and GallardoGuerrero, 1995). Besides, our data demonstrated that enhanced yellow color was not due to enhanced content of carotenoids, as it may be deduced from available literature (Delgado-Pelayo et al., 2014) but rather associated to higher carotenoids/chlorophyll ratios triggered by environmental cues. Yellow peel apples showed also significantly higher levels of tocopherols which are antioxidant molecules involved in the protection of thylakoid membranes against lipid peroxidation (Piller et al., 2014). These observations, together with the results of the RNA-seq analyses showing an overrepresentation of gene categories related to photosynthesis and oxidative stress responses (Figure 2), strongly suggest that the yellow peel of Gotarta apples may be the result of higher exposure to oxidative damage.

Pigments and phenolic compounds decrease during fruit development and ripening

Based on the intense color differences observed between Vilanova and Gotarta apples, both locations were chosen as the most suitable to better understand the metabolic and transcriptomic differences underlying different apple phenotypes. To elucidate the point when color changes and pigment differences occur, apple development was followed at four different stages (S1 to S4) based on fruit size in both valley (Vilanova) and mountain (Gotarta) orchards. The optimal yellow color was only perceived in Gotarta apples at the last developmental stage (S4; equivalent to the

CHD), while in Vilanova, the apple peel remained green (Table 1). Color changes in fruit are generally associated to the transition from Pigments and phenolic compounds decrease during fruit development and ripening

Based on the intense color differences observed between Vilanova and Gotarta apples, both locations were chosen as the most suitable to better understand the metabolic and transcriptomic differences underlying different apple phenotypes. To elucidate the point when color changes and pigment differences occur, apple development was followed at four different stages (S1 to S4) based on fruit size in both valley (Vilanova) and mountain (Gotarta) orchards. The optimal yellow color was only perceived in Gotarta apples at the last developmental stage (S4; equivalent to the CHD), while in Vilanova, the apple peel remained green (Table 1). Color changes in fruit are generally associated to the transition from chloroplast to the chromoplast and the accumulation of carotenoids (Sadali et al., 2019). However, the observed differences in "Golden Reinders" peel color were again not due to enhanced accumulation of carotenoids but rather to a more intense degradation of chlorophylls (Supplementary Figure S2A). The characteristic decrease of chlorophyll and carotenoids in yellow peel apples (Solovchenko et al., 2005) was observed in both locations, yet the final carotenoid/chlorophyll ratio was higher in the mountain (Gotarta) location (Table 1). This accelerated degradation of chlorophylls not only explains the more yellowish color of these apples but also the increased levels of tocopherols (Figure 1), which in many fruits are made from phytol recycled from the chlorophylls degraded during ripening (Muñoz and Munné-Bosch, 2019). Differences in the chlorophyll and tocopherol levels may be driven, in turn, by differences in temperature and solar radiation among the studied locations (Karagiannis et al., 2020). In fact, a higher exposure to sunlight is known to favor the accumulation of chlorophyll and carotenoids in apple (Jing et al., 2020), while an excess of it can also induce apple ripening and accelerate chlorophyll loss (Solovchenko et al., 2006). Higher solar radiation combined with milder temperatures during the early development stages may have favored the accumulation of photosynthetic pigments (chlorophylls and carotenoids) in mountain locations at S1 and S2 (Supplementary Figures S2, S8, S9). As summer progressed, the pronounced decrease in solar radiation and temperatures in mountains possibly favored, to some extent, the inhibition of pigment biosynthesis (Nagata et al., 2007) and, hence, a more pronounced decline in the chlorophyll and carotenoids content in mountain apples if compared with those from the valley (Supplementary Figures S2, S8, S9).

The differences in the temporal changes of carotenoids along fruit development between locations were not a consequence of differences on the expression of *MdPSY*, the main regulator of carotenoid synthesis (Cazzonelli and Pogson, 2010). The upward trend in *MdPSY* expression in both locations did not lead to an accumulation of carotenoids, suggesting the possibility that degradation pathways were more active and rather responsible for the final levels of carotenoids observed in apples at the time of

TABLE 1 Peel color evolution during the four developmental stages studied in Vilanova (valley) and Gotarta (mountain) orchards.

	S1 (60% final fruit size)	S2 (80% final fruit size)	S3 (90% final fruit size)	S4 (100%final fruit size)
Vilanova (Valley Orchard)				
H°	104.5 ± 0.14 ab	104.2 ± 0.16 bc	103.6 ± 0.27 bc	100.5 ± 0.32 e
Carotenoids/ Chlorophylls	1.05 ± 0.023 a	0.95 ± 0.024 bc	0.98 ± 0.021 abc	0.94 ± 0.016 c
Gotarta (Mountain Orchard)				
H°	105.1 ± 0.12 a	103.3 ± 0.21 c	102.2 ± 0.24 d	95.8 ± 0.38 f
Carotenoids/ Chlorophylls	1.03 ± 0.005 ab	1.03 ± 0.017 abc	0.96 ± 0.027 abc	1.03 ± 0.018 abc

Hue angles (H°) were determined by measuring both sides of 30 fruits ($n = 60$), while the ratio carotenoids/chlorophylls were determined from four replicates ($n = 4$). Data are represented as the means of replicates ± standard error. Letters indicate significant differences for the interaction location*developmental stage according to Tukey's test ($p \leq 0.05$).

harvest (Figure 3). Nonetheless, carotenoid catabolism seemed to be strongly influenced by the orchard location. The upregulation of *MdCCD4* in S2 and S3 combined with the absence of correlation between carotenoids and ABA observed in mountain apples, suggest that high-altitude environments may favor alternative degradation pathways than those mediated by NCED, hence in agreement with available literature for other organisms (Liang et al., 2021). Indeed, the accumulation of ROS in mountain apples (Figure 5) may favor the synthesis of stress response apocarotenoids through the CCD4 pathway (Felemban et al., 2019). The pattern of ABA accumulation may be, in turn, influenced by temperature differences between locations since ABA is considered a stress response hormone involved in thermotolerance (Iqbal et al., 2021). In this regard, apple is a crop adapted to moderate climates (Funes et al., 2016); hence, the high temperatures reached in Vilanova during fruit development may activate the accumulation of ABA for better coping with heat stress (Torres et al., 2017). Likewise, the moderate temperatures in mountain during the three first stages (Supplementary Figure S8) likely kept ABA levels low until the last stage, when ABA may be induced not by warm but rather by cold temperatures (Lee et al., 2021). Indeed, evidence suggesting that ABA accumulates in response to high- or low-temperature stress is abundant for other species (Daie and Campbell, 1981), yet no data are currently available for apples. Future studies are encouraged to better understand the actual relationship between ABA content and environmental temperatures during apple growth.

Besides carotenoids, tocopherols play an important role in maintaining chloroplast integrity. In our study, α-tocopherol levels in the apple peel remained stable during fruit ripening in both locations, whereas a burst in γ-tocopherol was observed in mountain apples at the latest stage (S4). Given that

tocopherol synthesis utilizes phytyl-PP released during chlorophyll breakdown, it is plausible to hypothesize that the drop of night temperatures observed in high-altitude orchards days before harvest (Supplementary Figure S8) may strongly activate phytol recycling mechanisms and promote the accumulation of γ-tocopherol (Vom Dorp et al., 2015), thereby enhancing stress tolerance (Abbasi et al., 2007). The decrease in chlorophyll content and the accumulation of oxidative stress markers observed in Gotarta apples (Figures 3, 5) are signs compatible with senescence (Muñoz and Munné-Bosch, 2018). Senescence can be activated by environmental cues such as the low temperatures and low solar radiation reached in Gotarta just before harvest (Supplementary Figures S8, S9), or also by an accumulation of ROS (Figure 5) able to cause a potential oxidative damage in the peel of Gotarta apples (Thakur et al., 2016). Hence, the development of yellow color in mountain apples may be interpreted as the result of an activation of a peel senescence-like process driven by environmental stresses. However, the RNA-seq analysis did not show a differential expression of senescence-associated genes (SAGs) between locations able to support this hypothesis, and therefore further studies are warranted.

Although carotenoids and tocopherols play a key role as antioxidants in chloroplasts, the total antioxidant capacity in apple mainly depends on phenolic compounds (Lee et al., 2003). Phenolic compounds can be subdivided into different classes including hydroxycinnamic acid derivatives, chalcones, flavanols, flavonols, and anthocyanins (Haminiuk et al., 2012). The main phenolic compounds detected in "Golden Reinders" peel were chlorogenic acid and quercetin-3-O-glycosides (Figure 4), which followed the same trend as carotenoids, decreasing as the fruit developed and ripened, in accordance with previous studies made on apple (Wojdyło and Oszmiański, 2020). The higher levels of flavanols, flavonols, and hydroxycinnamic acid derivatives found at early development stages in mountain fruit may also be a consequence of the higher solar radiation received by apple peel at high altitudes in the first months of fruit growth (Awad et al., 2000).

The first step of the phenolic compound synthesis pathway is catalyzed by Phenylalanine Ammonia-Lyase (PAL), an enzyme encoded by several gene isoforms regulated by the environment (Huang et al., 2010). Extensive evidence has shown that PAL gene expression in model species (i.e., *Arabidopsis thaliana*) is responsive to a variety of environmental stimuli, including pathogen infection, wounding, nutrient depletion, UV irradiation, and extreme temperatures, among others (Huang et al., 2010). Accordingly, the PAL gene isoforms analyzed in our study (*MdPAL1* and *MdPAL2*) showed different expression patterns (Supplementary Figure S4) not only along fruit growth but also in response to the growing location, suggesting that each isoform may be differentially regulated by environmental stimuli.

In this sense, the observed *MdPAL1* gene expression pattern and the high correlation with γ-tocopherol (Supplementary Figure S7) suggest that both *MdPAL1* gene expression and γ-tocopherol may be regulated by similar environmental cues, being in this particular case, likely low temperatures prior to the time of harvest (Maeda et al., 2006; Olsen et al., 2008). *MdPAL2* gene expression, in contrast,

seemed to mainly change along fruit developmental, showing an upward trend as the fruit developed and ripened yet with more pronounced and significant higher expression levels in fruit grown in the valley at S4. In this particular case, and based on our metereological data, enhanced UV or solar radiation at this particular phenological stage may account for the higher *MdPAL2* gene expression in valley fruit. Overall, our results are in agreement with previous studies showing a differential expression of *PbPAL* genes among different tissues, phenological stages or even in response to exogenous hormonal treatments in other pome fruit species (i.e., pears; Li et al., 2019). Nonetheless, further studies are encouraged to elucidate the possible specialization or environmentally driven regulation of *MdPAL* genes in apple fruit.

The accumulation of H_2O_2 favored by the mountain environment may trigger apple peel degreening

In addition to the antioxidant molecules described above, fruit has enzymatic mechanisms able to neutralize toxic ROS species generated by aerobic metabolism and stress (Apel and Hirt, 2004). The RNA-seq data showed that a large number of genes related to oxidative stress were differentially expressed when comparing yellow and green peel "Golden Reinders" apples (Figure 2C). In this sense, we further investigated changes in the activity of enzymes involved in ROS-homeostasis during the last stages of apple development/ripening in both locations (mountain vs. valley; Figure 5). The enzyme SOD is present in the cytoplasm, mitochondrion, and the chloroplast (Feng et al., 2016), and is able to convert oxygen radicals produced in the processes of photosynthesis and respiration into a less reactive compound such as H_2O_2 (Meitha et al., 2020), which can be reduced by peroxidases present in cytosol and chloroplast (Maruta et al., 2016) and by catalase in peroxisome (Corpas, 2015). Although orchard location and developmental stages influenced SOD gene expression levels, SOD activity remained unchanged regardless of the environment. In contrast, peroxidase activities tended to be higher in the peel of mountain apples for POX in S1 and S2 and for ascorbic acid-dependent peroxidase (APX) in S1 (Figure 5). In general, the expression of genes involved in ascorbate metabolism or the antioxidant enzymes detailed above was poorly correlated with the equivalent enzymatic activity but well correlated with the concentration of the corresponding metabolite (Supplementary Figure S7). Based on the absence of correlation between APX activity, ascorbic acid (AsA), and the gene expression of ascorbate recycling enzymes *MdMDHAR* and *MdDHAR* (Supplementary Figure S7), it is possible to speculate that the differential accumulation pattern of ascorbic acid found between locations may be a mere consequence of a higher biosynthetic activity driven by environmental cues (Zhang et al., 2011). Furthermore, the high correlation between AsA and H_2O_2 (Supplementary Figure S7) suggests that AsA may play an important role in modulating the protection against ROS (Akram et al., 2017). In this sense, the increase of H_2O_2 levels observed in the peel of mountain-grown apples may be favored by the reduction of peroxidase activities during fruit development combined with the low catalase activity (Figure 5). Since during the early development stages (90 days before harvest) climatic differences were not appreciable between valley and mountain orchards, we would like to point out that other

environmental stresses such as higher UV radiation incidence on mountain apples may induce the accumulation of H_2O_2 (Nawkar et al., 2013). Given that fruit ripening is considered an oxidative process by itself (Steelheart et al., 2019), it is reasonable to hypothesize that the accumulation of H_2O_2 in mountain apples may trigger peel ripening associated processes such as color changes (Kumar et al., 2016) without affecting pulp ripening parameters such as firmness or starch index (Fernández-Cancelo et al., 2021). These results would further reinforce the results from recent studies suggesting that apple peel and flesh ripening are independent processes (Karagiannis et al., 2020).

The phenotypic differences observed between locations may be regulated epigenetically through DNA methylation and specific histone modifications driven by the environment (Baulcombe and Dean, 2014). Moreover, recent studies have shown that the DNA methylation can regulate pigment accumulation in apple (Jiang et al., 2019) but little is known about the involvement of histone modifications in apple color. Given that some deacetylases seem to have a key role in the modulation of color development in tomato (Guo et al., 2017) and since environmental stress may also alter the epigenetic regulation (Baulcombe and Dean, 2014), we decided to perform a gene expression analysis of a class of histone deacetylases known as sirtuins (*MdSRT1* and *MdSRT2*). Sirtuins are suggested to be involved in the epigenetic regulation of fruit ripening in other Rosaceae spp. (Vall-llaura et al., 2021) and well known for their association to several antioxidant and oxidative stress-related processes and functions (Singh et al., 2018). Indeed, the fact that sirtuins deacetylase activity is dependent on NAD^+, a key redox signaling molecule, sustains the idea that these molecules may be integral players in regulating cellular antioxidant and redox signaling pathways (Singh et al., 2018). In our study, the high correlation between the expression of *MdSRT2* and ripening associated traits such as Hue angle (H°), H_2O_2, and AsA levels (Supplementary Figure S7) suggests that fruit ripening and color changes may be induced epigenetically through the action of histone deacetylases as described in tomato (Guo et al., 2017). On the other hand, the analysis of *MdSRT1* gene expression, a sirtuin involved in abiotic stress responses in *A. thaliana* (Liu et al., 2017), showed a consistently higher expression in mountain apples at all ripening stages (Supplementary Figure S6). Overall, the expression analysis of sirtuins may point out that mountain apples suffer an additional stress during fruit growth able to induce epigenetic changes that lead to an acceleration of ripening processes including color changes. However, further studies should be performed to analyze which specific epigenetic modifications regulate peel color in "Golden Reinders" apples.

Conclusion

The results from this study demonstrate that differences in apple peel color among valley and mountain orchards at the time of harvest are explained by the influence of environmental conditions on antioxidant and pigment metabolism occurring earlier during fruit development. Optimal yellow coloration in "Golden Reinders" apples, as exclusively observed in mountain environments, was mainly a consequence of enhanced chlorophyll degradation instead of enhanced carotenoid levels as well as alterations in the expression of genes involved in chloroplasts functions. Likewise, the yellow phenotype

observed in mountain apples seems also to be regulated through epigenetic modifications driven by the environment and may be related, to some extent, to oxidative stress and to the specific action of H_2O_2 during fruit growth/ripening. In this sense, H_2O_2 seemed to play a key role triggering some peel ripening events, including those involved in peel degreening in fruit grown in the mountains. Further studies may be required to dissect how specific environmental cues (solar radiation, temperature and so on) can trigger or inhibit pigment and antioxidant metabolism in different apple varieties hence leading to fruit with different phenotypes. Besides, the results from this study may assist in selecting specific compounds that when applied exogenously are capable to trigger color changes in fruit grown under specific environments.

Data availability statement

RNA-seq raw data are freely available in SRA database with the Bioproject ID PRJNA839574. Other data supporting the findings of this study are available within the paper and within its Supplementary material published online.

Author contributions

PF-C: methodology, writing—original draft preparation, and writing—review and editing. AI-S, AR-A and ST-M: methodology and writing—review and editing. NT: supervision and writing—review and editing. MR-C and JG-B: conceptualization, methodology, supervision, funding acquisition, project administration, and writing—review and editing. All authors contributed to the article and approved the submitted version.

Funding

This work has been financially supported by the Spanish Agencia Estatal de Investigación (AEI) and European Regional Development Fund (ERDF) through the national projects

RTA2015-00037-CO2-01, BIO2017-84041-P, BIO2017-90877REDT and PID2020-115810GB-I00. Funding was also provided by the internal CRAG project "Green2Gold" in the context of the Severo Ochoa Programme for Centres of Excellence in R&D 2016–2019 (SEV-2015-0533). This work has been also supported by the CERCA Programme from the "Generalitat de Catalunya." Thanks are also given to AEI and ERDF for the predoctoral fellowships awarded to PF-C (BES-2017-080741) and AI-S (PRE2018-083610). ST-M is supported by a PhD fellowship from the Spanish Ministry of Education, Culture and Sports (FPU16/04054).

Acknowledgments

We are grateful to Dolors Ubach and Mª Rosa Rodriguez for their technical support and to Dr. Núria Vall-Llaura for her help with RT-qPCR analysis.

Conflict of interest

The authors declare that the research was conducted in the absence of any commercial

or financial relationships that could be construed as a potential conflict of interest.

Publisher's note

All claims expressed in this article are solely those of the authors and do not necessarily represent those of their affiliated organizations, or those of the publisher, the editors and the reviewers. Any product that may be evaluated in this article, or claim that may be made by its manufacturer, is not guaranteed or endorsed by the publisher.

Supplementary material

The Supplementary Material for this article can be found online at: https://www.frontiersin.org/articles/10.3389/fpls.2022.913433/ full#supplementary-material

References

Abbasi, A.-R., Hajirezaei, M., Hofius, D., Sonnewald, U., and Voll, L. M. (2007). Specific roles of α - and γ -tocopherol in abiotic stress responses of transgenic tobacco. *Plant Physiol.* 143, 1720–1738. doi: 10.1104/pp.106.094771

Akram, N. A., Shafiq, F., and Ashraf, M. (2017). Ascorbic acid-a potential oxidant scavenger and its role in plant development and abiotic stress tolerance. *Front. Plant Sci.* 8:613. doi: 10.3389/fpls.2017.00613

Apel, K., and Hirt, H. (2004). Reactive oxygen species: metabolism, oxidative stress, and signal transduction. *Annu. Rev. Plant Biol.* 55, 373–399. doi: 10.1146/ annurev.arplant.55.031903.141701

Awad, M. A., de Jager, A., and van Westing, L. M. (2000). Flavonoid and chlorogenic acid levels in apple fruit: characterisation of variation. *Sci. Hortic.* 83, 249–263. doi: 10.1016/S0304-4238(99)00124-7

Barja, M. V., Ezquerro, M., Beretta, S., Diretto, G., Florez-Sarasa, I., Feixes, E., et al. (2021). Several geranylgeranyl diphosphate synthase isoforms supply metabolic substrates for carotenoid biosynthesis in tomato. *New Phytol.* 231, 255–272. doi: 10.1111/nph.17283

Baulcombe, D. C., and Dean, C. (2014). Epigenetic regulation in plant responses to the environment. *Cold Spring Harb. Perspect. Biol.* 6:a019471. doi: 10.1101/ cshperspect.a019471

Blumthaler, M., Ambach, W., and Ellinger, R. (1997). Increase in solar UV radiation with altitude. *J. Photochem. Photobiol. B Biol.* 39, 130–134. doi: 10.1016/ S1011-1344(96)00018-8

Bonany, J., Buehler, A., Carbó, J., Codarin, S., Donati, F., Echeverria, G., et al. (2013). Consumer eating quality acceptance of new apple varieties in different European countries. *Food Qual. Prefer.* 30, 250–259. doi: 10.1016/j. foodqual.2013.06.004

Bouvier, F., Backhaus, R. A., and Camara, B. (1998). Induction and control of chromoplast-specific carotenoid genes by oxidative stress. *J. Biol. Chem.* 273, 30651–30659. doi: 10.1074/jbc.273.46.30651

Bradford, M. (1976). A rapid and sensitive method for the quantitation of microgram quantities of protein utilizing the principle of protein-dye binding. *Anal. Biochem.* 72, 248–254. doi: 10.1006/abio.1976.9999

Cazzonelli, C. I., and Pogson, B. J. (2010). Source to sink: regulation of carotenoid biosynthesis in plants. *Trends Plant Sci.* 15, 266–274. doi: 10.1016/j. tplants.2010.02.003

Chen, X., Xia, X., Guo, X., Zhou, Y., Shi, K., Zhou, J., et al. (2016). Apoplastic H_2O_2 plays a critical role in axillary bud outgrowth by altering auxin and cytokinin homeostasis in tomato plants. *New Phytol.* 211, 1266–1278. doi: 10.1111/ nph.14015

Chiriboga, M. A., Giné Bordonaba, J., Schotsmans, W. C., Larrigaudière, C., and Recasens, I. (2013). Antioxidant potential of "conference" pears during cold storage and shelf life in response to 1-methylcyclopropene. *LWT-Food Sci. Technol.* 51, 170–176. doi: 10.1016/j.lwt.2012.10.023

Choudhury, F. K., Rivero, R. M., Blumwald, E., and Mittler, R. (2017). Reactive oxygen species, abiotic stress and stress combination. *Plant J.* 90, 856–867. doi: 10.1111/tpj.13299

Claiborne, A. (1986). "Catalase activity," in *CRC Handbook of Methods for Oxygen Radical Research*. ed. R. A. Greenwald (Boca Raton, FL: CRC Press)

Collazo, C., Giné-Bordonaba, J., Aguiló-Aguayo, I., Povedano, I., Bademunt, A., and Viñas, I. (2018). *Pseudomonas graminis* strain CPA-7 differentially modulates the oxidative response in fresh-cut 'Golden delicious' apple depending on the storage conditions. *Postharvest Biol. Technol.* 138, 46–55. doi: 10.1016/j.postharvbio.2017.12.013

Corpas, F. J. (2015). What is the role of hydrogen peroxide in plant peroxisomes? *Plant Biol.* 17, 1099–1103. doi: 10.1111/plb.12376

Daccord, N., Celton, J.-M., Linsmith, G., Becker, C., Choisne, N., Schijlen, E., et al. (2017). High-quality *de novo* assembly of the apple genome and methylome dynamics of early fruit development. *Nat. Genet.* 49, 1099–1106. doi: 10.1038/ ng.3886

Daie, J., and Campbell, W. F. (1981). Response of tomato plants to stressful temperatures. *Plant Physiol.* 67, 26–29. doi: 10.1104/pp.67.1.26

Delgado-Pelayo, R., Gallardo-Guerrero, L., and Hornero-Méndez, D. (2014). Chlorophyll and carotenoid pigments in the peel and flesh of commercial apple fruit varieties. *Food Res. Int.* 65, 272–281. doi: 10.1016/j.foodres.2014. 03.025

Felemban, A., Braguy, J., Zurbriggen, M. D., and Al-Babili, S. (2019). Apocarotenoids involved in plant development and stress response. *Front. Plant Sci.* 10:1168. doi: 10.3389/fpls.2019.01168

Feng, K., Yu, J., Cheng, Y., Ruan, M., Wang, R., Ye, Q., et al. (2016). The SOD gene family in tomato: identification, phylogenetic relationships, and expression patterns. *Front. Plant Sci.* 7:1279. doi: 10.3389/fpls.2016.01279

Fernández-Cancelo, P., Muñoz, P., Echeverría, G., Larrigaudière, C., Teixidó, N., Munné-Bosch, S., et al. (2022). Ethylene and abscisic acid

play a key role in modulating apple ripening after harvest and after cold-storage. *Postharvest Biol. Technol.* 188:111902. doi: 10.1016/j.postharvbio.2022. 111902

Fernández-Cancelo, P., Teixidó, N., Echeverría, G., Torres, R., Larrigaudière, C., and Giné-Bordonaba, J. (2021). Dissecting the influence of the orchard location and the maturity at harvest on apple quality, physiology and susceptibility to major postharvest pathogens. *Sci. Hortic.* 285:110159. doi: 10.1016/j.scienta.2021.110159

Filyushin, M. A., Dzhos, E. A., Shchennikova, A. V., and Kochieva, E. Z. (2020). Dependence of pepper fruit colour on basic pigments ratio and expression pattern of carotenoid and anthocyanin biosynthesis genes. *Russ. J. Plant Physiol.* 67, 1054–1062. doi: 10.1134/S1021443720050040

Funes, I., Aranda, X., Biel, C., Carbó, J., Camps, F., Molina, A. J., et al. (2016). Future climate change impacts on apple flowering date in a Mediterranean subbasin. *Agric. Water Manag.* 164, 19–27. doi: 10.1016/j.agwat.2015.06.013

Giannopolitis, C. N., and Ries, S. K. (1977). Superoxide dismutases. *Plant Physiol.* 59, 309–314. doi: 10.1104/pp.59.2.309

Giné Bordonaba, J., and Terry, L. A. (2008). Biochemical profiling and chemometric analysis of seventeen UK-grown black currant cultivars. *J. Agric. Food Chem.* 56, 7422–7430. doi: 10.1021/jf8009377

Giné-Bordonaba, J., Cantín, C. M., Echeverría, G., Ubach, D., and Larrigaudière, C. (2016). The effect of chilling injury-inducing storage conditions on quality and consumer acceptance of different *Prunus persica* cultivars. *Postharvest Biol. Technol.* 115, 38–47. doi: 10.1016/j.postharvbio.2015.12.006

Giné-Bordonaba, J., Echeverria, G., Duaigües, E., Bobo, G., and Larrigaudière, C. (2019). A comprehensive study on the main physiological and biochemical changes occurring during growth and on-tree ripening of two apple varieties with different postharvest behaviour. *Plant Physiol. Biochem.* 135, 601–610. doi: 10.1016/j.plaphy.2018.10.035

Giné-Bordonaba, J., Echeverria, G., Ubach, D., Aguiló-Aguayo, I., López, M. L., and Larrigaudière, C. (2017). Biochemical and physiological changes during fruit development and ripening of two sweet cherry varieties with different levels of cracking tolerance. *Plant Physiol. Biochem.* 111, 216–225. doi: 10.1016/j. plaphy.2016.12.002

Gross, J., Zachariae, A., Lenz, F., and Eckhardt, G. (1978). Carotenoid changes in the peel of the «Golden delicious» apple during ripening and storage. *Z. Pflanzenphysiol.* 89, 321–332. doi: 10.1016/S0044-328X(78)80005-1

Guo, J.-E., Hu, Z., Li, F., Zhang, L., Yu, X., Tang, B., et al. (2017). Silencing of histone deacetylase SlHDT3 delays fruit ripening and suppresses carotenoid accumulation in tomato. *Plant Sci.* 265, 29–38. doi: 10.1016/j.plantsci.2017.09.013

Haminiuk, C. W. I., Maciel, G. M., Plata-Oviedo, M. S. V., and Peralta, R. M. (2012). Phenolic compounds in fruits – an overview. *Int. J. Food Sci. Technol.* 47, 2023–2044. doi: 10.1111/j.1365-2621.2012.03067.x

Hodges, D. M., DeLong, J. M., Forney, C. F., and Prange, R. K. (1999). Improving the thiobarbituric acid-reactive-substances assay for estimating lipid peroxidation in plant tissues containing anthocyanin and other interfering compounds. *Planta* 207, 604–611. doi: 10.1007/s004250050524

Huang, J., Gu, M., Lai, Z., Fan, B., Shi, K., Zhou, Y.-H., et al. (2010). Functional analysis of the *Arabidopsis* PAL gene family in plant growth, development, and response to environmental stress. *Plant Physiol.* 153, 1526–1538. doi: 10.1104/ pp.110.157370

Iglesias, I., Echeverría, G., and Soria, Y. (2008). Differences in fruit colour development, anthocyanin content, fruit quality and consumer acceptability of eight 'gala' apple strains. *Sci. Hortic.* 119, 32–40. doi: 10.1016/j.scienta.2008.07.004

Iqbal, N., Umar, S., Khan, N. A., and Corpas, F. J. (2021). Crosstalk between abscisic acid and nitric oxide under heat stress: exploring new vantage points. *Plant Cell Rep.* 40, 1429–1450. doi: 10.1007/s00299-021-02695-4

Jiang, S.-H., Sun, Q.-G., Chen, M., Wang, N., Xu, H.-F., Fang, H.-C., et al. (2019). Methylome and transcriptome analyses of apple fruit somatic mutations reveal the difference of red phenotype. *BMC Genomics* 20:117. doi: 10.1186/s12864-019-5499-2

Jing, C., Feng, D., Zhao, Z., Wu, X., and Chen, X. (2020). Effect of environmental factors on skin pigmentation and taste in three apple cultivars. *Acta Physiol. Plant.* 42:69. doi: 10.1007/s11738-020-03039-7

Karagiannis, E., Michailidis, M., Tanou, G., Scossa, F., Sarrou, E., Stamatakis, G., et al. (2020). Decoding altitude-activated regulatory mechanisms occurring during apple peel ripening. *Horticult. Res.* 7:120. doi: 10.1038/s41438-020-00340-x

Khandaker, M. M., Boyce, A. N., and Osman, N. (2012). The influence of hydrogen peroxide on the growth, development and quality of wax apple (*Syzygium samarangense*, [Blume] Merrill & L.M. Perry var. jambu madu) fruits. *Plant Physiol. Biochem.* 53, 101–110. doi: 10.1016/j.plaphy.2012.01.016

Kumar, V., Irfan, M., Ghosh, S., Chakraborty, N., Chakraborty, S., and Datta, A. (2016). Fruit ripening mutants reveal cell metabolism and redox state during ripening. *Protoplasma* 253, 581–594. doi: 10.1007/s00709-015-0836-z

Lee, Y., Do, V. G., Kim, S., Kweon, H., and McGhie, T. K. (2021). Cold stress triggers premature fruit abscission through ABA-dependent signal transduction in early developing apple. *PLoS One* 16:e0249975. doi: 10.1371/journal.pone.0249975

Lee, K. W., Kim, Y. J., Kim, D.-O., Lee, H. J., and Lee, C. Y. (2003). Major phenolics in apple and their contribution to the total antioxidant capacity. *J. Agric. Food Chem.* 51, 6516–6520. doi: 10.1021/jf034475w

Leng, P., Yuan, B., and Guo, Y. (2013). The role of abscisic acid in fruit ripening and responses to abiotic stress. *J. Exp. Bot.* 65, 4577–4588. doi: 10.1093/jxb/eru204

León-Chan, R. G., López-Meyer, M., Osuna-Enciso, T., Sañudo-Barajas, J. A., Heredia, J. B., and León-Félix, J. (2017). Low temperature and ultraviolet-B radiation affect chlorophyll content and induce the accumulation of UV-B-absorbing and antioxidant compounds in bell pepper (*Capsicum annuum*) plants. *Environ. Exp. Bot.* 139, 143–151. doi: 10.1016/j.envexpbot.2017.05.006

Li, G., Wan, H., Cheng, X., Su, X., Zhao, Y., Jiang, T., et al. (2019). Comparative genomic analysis of the PAL genes in five Rosaceae species and functional identification of Chinese white pear. *PeerJ* 7:e8064. doi: 10.7717/peerj.8064

Liang, M.-H., He, Y.-J., Liu, D.-M., and Jiang, J.-G. (2021). Regulation of carotenoid degradation and production of apocarotenoids in natural and engineered organisms. *Crit. Rev. Biotechnol.* 41, 513–534. doi: 10.1080/07388551.2021.1873242

Lin-Wang, K., Micheletti, D., Palmer, J., Volz, R., Lozano, L., Espley, R., et al. (2011). High temperature reduces apple fruit colour via modulation of the anthocyanin regulatory complex. *Plant Cell Environ.* 34, 1176–1190. doi: 10.1111/j. 1365-3040.2011.02316.x

Liu, X., Wei, W., Zhu, W., Su, L., Xiong, Z., Zhou, M., et al. (2017). Histone deacetylase AtSRT1 links metabolic flux and stress response in

Arabidopsis. *Mol. Plant* 10, 1510–1522. doi: 10.1016/j.molp.2017.10.010

Llorente, B., D'Andrea, L., Ruiz-Sola, M. A., Botterweg, E., Pulido, P., Andilla, J., et al. (2016). Tomato fruit carotenoid biosynthesis is adjusted to actual ripening progression by a light-dependent mechanism. *Plant J.* 85, 107–119. doi: 10.1111/ tpj.13094

Llorente, B., Torres-Montilla, S., Morelli, L., Florez-Sarasa, I., Matus, J. T., Ezquerro, M., et al. (2020). Synthetic conversion of leaf chloroplasts into carotenoidrich plastids reveals mechanistic basis of natural chromoplast development. *Proc. Natl. Acad. Sci. U. S. A.* 117, 21796–21803. doi: 10.1073/pnas.2004405117

Maeda, H., Song, W., Sage, T. L., and DellaPenna, D. (2006). Tocopherols play a crucial role in low-temperature adaptation and phloem loading in *Arabidopsis*. *Plant Cell* 18, 2710–2732. doi: 10.1105/tpc.105.039404

Martínez-Solano, J. R., Sánchez-Bel, P., Egea, I., Olmos, E., Hellin, E., and Romojaro, F. (2005). Electron beam ionization induced oxidative enzymatic activities in pepper (*Capsicum annuum L.*), associated with ultrastructure cellular damages. *J. Agric. Food Chem.* 53, 8593–8599. doi: 10.1021/jf050994i

Maruta, T., Sawa, Y., Shigeoka, S., and Ishikawa, T. (2016). Diversity and evolution of ascorbate peroxidase functions in chloroplasts: more than just a classical antioxidant enzyme? *Plant Cell Physiol.* 57, 1377–1386. doi: 10.1093/pcp/pcv203

McTavish, C. K., Poirier, B. C., Torres, C. A., Mattheis, J. P., and Rudell, D. R. (2020). A convergence of sunlight and cold chain: the influence of sun exposure on postharvest apple peel metabolism. *Postharvest Biol. Technol.* 164:111164. doi: 10.1016/j.postharvbio.2020.111164

Meitha, K., Pramesti, Y., and Suhandono, S. (2020). Reactive oxygen species and antioxidants in postharvest vegetables and fruits. *Int. J. Food Sci.* 2020, 1–11. doi: 10.1155/2020/8817778

Merzlyak, M. N., Solovchenko, A. E., and Gitelson, A. A. (2003). Reflectance spectral features and non-destructive estimation of chlorophyll, carotenoid and anthocyanin content in apple fruit. *Postharvest Biol. Technol.* 27, 197–211. doi: 10.1016/S0925-5214(02)00066-2

Mínguez-Mosquera, I., and Gallardo-Guerrero, L. (1995). Disappearance of chlorophylls and carotenoids during the ripening of the olive. *J. Sci. Food Agric.* 69, 1–6. doi: 10.1002/jsfa.2740690102

Mou, W., Li, D., Luo, Z., Mao, L., and Ying, T. (2015). Transcriptomic analysis reveals possible influences of aba on secondary metabolism of pigments, flavonoids and antioxidants in tomato fruit during ripening. *PLoS One* 10:e0129598. doi: 10.1371/JOURNAL.PONE.0129598

Muller, P. Y., Janovjak, H., Miserez, A. R., and Dobbie, Z. (2002). Processing of gene expression data generated by quantitative real-time RT-PCR. *BioTechniques* 32:1372–1374, 1376, 1378–1379.

Muñoz, P., and Munné-Bosch, S. (2018). Photo-oxidative stress during leaf, flower and fruit development. *Plant Physiol.* 176, 1004–1014. doi: 10.1104/ pp.17.01127

Muñoz, P., and Munné-Bosch, S. (2019). Vitamin E in plants: biosynthesis, transport, and function. *Trends Plant Sci.* 24, 1040–1051. doi: 10.1016/j.tplants.2019.08.006

Nagata, N., Tanaka, R., and Tanaka, A. (2007). The major route for chlorophyll synthesis includes [3,8-divinyl]-chlorophyllide a reduction in *Arabidopsis thaliana*. *Plant Cell Physiol.* 48, 1803–1808. doi: 10.1093/pcp/pcm153

Nakano, Y., and Asada, K. (1981). Hydrogen peroxide is scavenged by ascorbatespecific peroxidase in spinach chloroplasts. *Plant Cell Physiol.* 22, 867–880. doi: 10.1093/oxfordjournals.pcp.a076232

Nawkar, G. M., Maibam, P., Park, J. H., Sahi, V. P., Lee, S. Y., and Kang, C. H. (2013). UV-induced cell death in plants. *Int. J. Mol. Sci.* 14, 1608–1628. doi: 10.3390/ ijms14011608

Olsen, K. M., Lea, U. S., Slimestad, R., Verheul, M., and Lillo, C. (2008). Differential expression of four *Arabidopsis* PAL genes; PAL1 and PAL2 have functional specialization in abiotic environmental-triggered flavonoid synthesis. *J. Plant Physiol.* 165, 1491–1499. doi: 10.1016/j.jplph.2007.11.005

Piller, L. E., Glauser, G., Kessler, F., and Besagni, C. (2014). Role of plastoglobules in metabolite repair in the tocopherol redox cycle. *Front. Plant Sci.* 5:298. doi: 10.3389/fpls.2014.00298

Polívka, T., and Frank, H. A. (2010). Molecular factors controlling photosynthetic light harvesting by carotenoids. *Acc. Chem. Res.* 43, 1125–1134. doi: 10.1021/ar100030m

Ramel, F., Birtic, S., Ginies, C., Soubigou-Taconnat, L., Triantaphylides, C., and Havaux, M. (2012). Carotenoid oxidation products are stress signals that mediate gene responses to singlet oxygen in plants. *Proc. Natl. Acad. Sci. U. S. A.* 109, 5535–5540. doi: 10.1073/pnas.1115982109

Rassam, M., and Laing, W. (2005). Variation in ascorbic acid and oxalate levels in the fruit of *Actinidia chinensis* tissues and genotypes. *J. Agric. Food Chem.* 53, 2322–2326. doi: 10.1021/jf048197s

Reay, P. F., Fletcher, R. H., and Thomas, V. J. (1998). Chlorophylls, carotenoids and anthocyanin concentrations in the skin of 'Gala' apples during maturation and the influence of foliar applications of nitrogen and magnesium. *J. Sci. Food Agric.* 76, 63–71. doi: 10.1002/(SICI)1097-0010(199801)76:1<63::AID-JSFA908>3.0.CO;2-K

Rodriguez-Concepcion, M., Avalos, J., Bonet, M. L., Boronat, A., Gomez-Gomez, L., Hornero-Mendez, D., et al. (2018). A global perspective on carotenoids: metabolism, biotechnology, and benefits for nutrition and health. *Prog. Lipid Res.* 70, 62–93. doi: 10.1016/j.plipres.2018.04.004

Sadali, N. M., Sowden, R. G., Ling, Q., and Jarvis, R. P. (2019). Differentiation of chromoplasts and other plastids in plants. *Plant Cell Rep.* 38, 803–818. doi: 10.1007/ s00299-019-02420-2

Saxena, I., Srikanth, S., and Chen, Z. (2016). Cross talk between H_2O_2 and interacting signal molecules under plant stress response. *Front. Plant Sci.* 7:570. doi: 10.3389/fpls.2016.00570

Shao, H., Chu, L., Shao, M., Jaleel, C. A., and Hong-mei, M. (2008). Higher plant antioxidants and redox signaling under environmental stresses. *C. R. Biol.* 331, 433–441. doi: 10.1016/j.crvi.2008.03.011

Singh, C. K., Chhabra, G., Ndiaye, M. A., Garcia-Peterson, L. M., Mack, N. J., and Ahmad, N. (2018). The role of sirtuins in antioxidant and redox signaling. *Antioxid. Redox Signal.* 28, 643–661. doi: 10.1089/ars.2017.7290

Solovchenko, A. E., Avertcheva, O. V., and Merzlyak, M. N. (2006). Elevated sunlight promotes ripening-associated pigment changes in apple fruit. *Postharvest Biol. Technol.* 40, 183–189. doi: 10.1016/j.postharvbio.2006.01.013

Solovchenko, A. E., Chivkunova, O. B., Merzlyak, M. N., and Gudkovsky, V. A. (2005). Relationships between chlorophyll and carotenoid pigments during on- and off-tree ripening of apple fruit as revealed non-destructively with reflectance spectroscopy. *Postharvest Biol. Technol.* 38, 9–17. doi: 10.1016/j.postharvbio.2005.05.004

Steelheart, C., Galatro, A., Bartoli, C. G., and Gergoff Grozeff, G. E. (2019). "Nitric oxide and hydrogen peroxide: signals in fruit ripening," in *Nitric Oxide and Hydrogen Peroxide Signaling in Higher Plants*. (eds) D. Gupta, J. Palma and F. Corpas (Cham: Springer International Publishing), 175–199.

Sugiura, T., Ogawa, H., Fukuda, N., and Moriguchi, T. (2013). Changes in the taste and textural attributes of apples in response to climate change. *Sci. Rep.* 3:2418. doi: 10.1038/srep02418

Thakur, N., Sharma, V., and Kishore, K. (2016). Leaf senescence: an overview. *Indian J. Plant Physiol.* 21, 225–238. doi: 10.1007/s40502-016-0234-3

Torres, C. A., Sepúlveda, G., and Kahlaoui, B. (2017). Phytohormone interaction modulating fruit responses to photooxidative and heat stress on apple (*Malus domestica Borkh.*). *Front. Plant Sci.* 8:2129. doi: 10.3389/fpls.2017.02129

Vall-llaura, N., Torres, R., Lindo-García, V., Muñoz, P., Munné-Bosch, S., Larrigaudière, C., et al. (2021). PbSRT1 and PbSRT2 regulate pear growth and ripening yet displaying a species-specific regulation in comparison to other *Rosaceae* spp. *Plant Sci.* 308:110925. doi: 10.1016/j.plantsci.2021.110925

Venditti, P., Di Stefano, L., and Di Meo, S. (2013). Mitochondrial metabolism of reactive oxygen species. *Mitochondrion* 13, 71–82. doi: 10.1016/j.mito. 2013.01.008

Vom Dorp, K., Hölzl, G., Plohmann, C., Eisenhut, M., Abraham, M., Weber, A. P. M., et al. (2015). Remobilization of phytol from chlorophyll degradation is essential for tocopherol synthesis and growth of *Arabidopsis*. *Plant Cell* 27, 2846–2859. doi: 10.1105/tpc.15.00395

Wang, Q., Yu, F., and Xie, Q. (2020). Balancing growth and adaptation to stress: crosstalk between brassinosteroid and abscisic acid signaling. *Plant Cell Environ.* 43, 2325–2335. doi: 10.1111/pce.13846

Wojdyło, A., and Oszmiański, J. (2020). Antioxidant activity modulated by polyphenol contents in apple and leaves during fruit development and ripening. *Antioxidants* 9:567. doi: 10.3390/antiox9070567

Yin, X., Xie, X., Xia, X., Yu, J., Ferguson, I. B., Giovannoni, J. J., et al. (2016). Involvement of an ethylene response factor in chlorophyll degradation during citrus fruit degreening. *Plant J.* 86, 403–412. doi: 10.1111/tpj.13178

Zhang, C., Liu, J., Zhang, Y., Cai, X., Gong, P., Zhang, J., et al. (2011). Overexpression of SlGMEs leads to ascorbate accumulation with enhanced oxidative stress, cold, and salt tolerance in tomato. *Plant Cell Rep.* 30, 389–398. doi: 10.1007/s00299-010-0939-0

Zhang, Q., Zhang, L., Geng, B., Feng, J., and Zhu, S. (2019). Interactive effects of abscisic acid and nitric oxide on chilling resistance and active oxygen metabolism in peach fruit during cold storage. *J. Sci. Food Agric.* 99, 3367–3380. doi: 10.1002/ JSFA.9554

Zheng, X.-T., Yu, Z.-C., Tang, J.-W., Cai, M.-L., Chen, Y.-L., Yang, C.-W., et al. (2020). The major photoprotective role of anthocyanins in leaves of *Arabidopsis thaliana* under long-term high light treatment: antioxidant or light attenuator? *Photosynth. Res.* 149, 25–40. doi: 10.1007/s11120-020-00761-8